

Extracts from plants and other natural sources: application, characterization, optimization, and their use

Edited by

Tomislav Tosti, Saša Đurović and Yulia Smyatskaya

Published in

Frontiers in Nutrition

Frontiers in Pharmacology



FRONTIERS EBOOK COPYRIGHT STATEMENT

The copyright in the text of individual articles in this ebook is the property of their respective authors or their respective institutions or funders. The copyright in graphics and images within each article may be subject to copyright of other parties. In both cases this is subject to a license granted to Frontiers.

The compilation of articles constituting this ebook is the property of Frontiers.

Each article within this ebook, and the ebook itself, are published under the most recent version of the Creative Commons CC-BY licence. The version current at the date of publication of this ebook is CC-BY 4.0. If the CC-BY licence is updated, the licence granted by Frontiers is automatically updated to the new version.

When exercising any right under the CC-BY licence, Frontiers must be attributed as the original publisher of the article or ebook, as applicable.

Authors have the responsibility of ensuring that any graphics or other materials which are the property of others may be included in the CC-BY licence, but this should be checked before relying on the CC-BY licence to reproduce those materials. Any copyright notices relating to those materials must be complied with.

Copyright and source acknowledgement notices may not be removed and must be displayed in any copy, derivative work or partial copy which includes the elements in question.

All copyright, and all rights therein, are protected by national and international copyright laws. The above represents a summary only. For further information please read Frontiers' Conditions for Website Use and Copyright Statement, and the applicable CC-BY licence.

ISSN 1664-8714
ISBN 978-2-8325-5948-2
DOI 10.3389/978-2-8325-5948-2

About Frontiers

Frontiers is more than just an open access publisher of scholarly articles: it is a pioneering approach to the world of academia, radically improving the way scholarly research is managed. The grand vision of Frontiers is a world where all people have an equal opportunity to seek, share and generate knowledge. Frontiers provides immediate and permanent online open access to all its publications, but this alone is not enough to realize our grand goals.

Frontiers journal series

The Frontiers journal series is a multi-tier and interdisciplinary set of open-access, online journals, promising a paradigm shift from the current review, selection and dissemination processes in academic publishing. All Frontiers journals are driven by researchers for researchers; therefore, they constitute a service to the scholarly community. At the same time, the *Frontiers journal series* operates on a revolutionary invention, the tiered publishing system, initially addressing specific communities of scholars, and gradually climbing up to broader public understanding, thus serving the interests of the lay society, too.

Dedication to quality

Each Frontiers article is a landmark of the highest quality, thanks to genuinely collaborative interactions between authors and review editors, who include some of the world's best academicians. Research must be certified by peers before entering a stream of knowledge that may eventually reach the public - and shape society; therefore, Frontiers only applies the most rigorous and unbiased reviews. Frontiers revolutionizes research publishing by freely delivering the most outstanding research, evaluated with no bias from both the academic and social point of view. By applying the most advanced information technologies, Frontiers is catapulting scholarly publishing into a new generation.

What are Frontiers Research Topics?

Frontiers Research Topics are very popular trademarks of the *Frontiers journals series*: they are collections of at least ten articles, all centered on a particular subject. With their unique mix of varied contributions from Original Research to Review Articles, Frontiers Research Topics unify the most influential researchers, the latest key findings and historical advances in a hot research area.

Find out more on how to host your own Frontiers Research Topic or contribute to one as an author by contacting the Frontiers editorial office: frontiersin.org/about/contact

Extracts from plants and other natural sources: application, characterization, optimization, and their use

Topic editors

Tomislav Tosti — University of Belgrade, Serbia

Saša Đurović — Institute of General and Physical Chemistry, Serbia

Yulia Smyatskaya — Peter the Great St.Petersburg Polytechnic University, Russia

Citation

Tosti, T., Đurović, S., Smyatskaya, Y., eds. (2025). *Extracts from plants and other natural sources: application, characterization, optimization, and their use*.

Lausanne: Frontiers Media SA. doi: 10.3389/978-2-8325-5948-2

Table of contents

- 04 Editorial: Extracts from plants and other natural sources: application, characterization, optimization, and their use
Saša D. Đurović, Yulia A. Smyatskaya and Tomislav Tosti
- 06 Protocol for a randomized controlled trial evaluating the effect of *Hibiscus syriacus* L. flower extract on sleep quality
Yujin Choi, Yu Hwa Park, Changsop Yang, Do Hoon Kim, Kye Wan Lee and Mi Young Lee
- 13 Extraction, characterization and anti-oxidant activity of polysaccharide from red *Panax ginseng* and *Ophiopogon japonicus* waste
Jia Kang, Jue Zhao, Lan-Fang He, Li-Xia Li, Zhong-Kai Zhu and Meng-Liang Tian
- 28 Effects and action mechanisms of lotus leaf (*Nelumbo nucifera*) ethanol extract on gut microbes and obesity in high-fat diet-fed rats
Zhang Yanan, Ma Lu, Zhang Lu, Huo Jinhai and Wang Weiming
- 38 Structural characterization and antioxidant activity of pectic polysaccharides from *Veronica peregrina* L.
Su Yan, Xianbin Liu, Yuwen Wang, Xiaomin Yang, Lu Bai, Lin Sun, Yifa Zhou and Sisi Cui
- 51 Polyphenols and extracts from *Zingiber roseum* (Roxb.) Roscoe leaf mitigate pain, inflammation and pyrexia by inhibiting cyclooxygenase-2: an *in vivo* and *in silico* studies
Shakhawat Ahmed, Khondoker Shahin Ahmed, Md. Naiemur Rahman, Hemayet Hossain, Aixia Han, Peiwu Geng, A. F. M. Shahid Ud Daula and Abdullah Al Mamun
- 66 Recent trends in extraction, purification, structural characterization, and biological activities evaluation of *Perilla frutescens* (L.) Britton polysaccharide
Ling Zhu, Lijun Guan, Kunlun Wang, Chuanying Ren, Yang Gao, Jialei Li, Song Yan, Xindi Zhang, Xinmiao Yao, Ye Zhou, Bo Li and Shuwen Lu
- 85 Phyto-pharmacological evaluation and characterization of the methanolic extract of the *Baccaurea motleyana* Müll. Arg. seed: promising insights into its therapeutic uses
Suriya Akter Shompa, Hasin Hasnat, Saima Jahan Riti, Md. Mirazul Islam, Farjahan Nur, Safaet Alam, Chuxiao Shao, Shuanghu Wang, Peiwu Geng and Abdullah Al Mamun
- 111 Chemico-pharmacological evaluation of the methanolic leaf extract of *Catharanthus ovalis*: GC–MS/MS, *in vivo*, *in vitro*, and *in silico* approaches
Saimon Shahriar, Samia Akter Shermin, Hasin Hasnat, Faisal Hossain, Aixia Han, Peiwu Geng, Safaet Alam and Abdullah Al Mamun
- 131 Targeting bone homeostasis regulation: potential of traditional Chinese medicine flavonoids in the treatment of osteoporosis
Jiazhe Du, Yincang Wang, Chengliang Wu, Xinyu Zhang, Xiaofeng Zhang and Xilin Xu



OPEN ACCESS

EDITED AND REVIEWED BY
Michael Rychlik,
Technical University of Munich, Germany

*CORRESPONDENCE
Saša D. Đurović
✉ sasatfns@uns.ac.rs

RECEIVED 05 October 2024
ACCEPTED 11 October 2024
PUBLISHED 25 October 2024

CITATION
Đurović SD, Smyatskaya YA and Tosti T (2024)
Editorial: Extracts from plants and other
natural sources: application, characterization,
optimization, and their use.
Front. Nutr. 11:1506537.
doi: 10.3389/fnut.2024.1506537

COPYRIGHT
© 2024 Đurović, Smyatskaya and Tosti. This is
an open-access article distributed under the
terms of the [Creative Commons Attribution
License \(CC BY\)](#). The use, distribution or
reproduction in other forums is permitted,
provided the original author(s) and the
copyright owner(s) are credited and that the
original publication in this journal is cited, in
accordance with accepted academic practice.
No use, distribution or reproduction is
permitted which does not comply with these
terms.

Editorial: Extracts from plants and other natural sources: application, characterization, optimization, and their use

Saša D. Đurović^{1,2*}, Yulia A. Smyatskaya² and Tomislav Tosti³

¹Institute of General and Physical Chemistry, Belgrade, Serbia, ²Peter the Great Saint-Petersburg Polytechnic University, Graduate School of Biotechnology and Food Industries, Saint-Petersburg, Russia, ³Institute of Chemistry, Technology and Metallurgy - National Institute of the Republic of Serbia, University of Belgrade, Belgrade, Serbia

KEYWORDS

extraction, natural compounds, extracts, application, characterization, optimization

Editorial on the Research Topic

Extracts from plants and other natural sources: application, characterization, optimization, and their use

Natural compounds have attracted much of the scientific community's attention in the last decades because of a wide range of biological activity. The possibility of changing the synthetic compounds for natural ones in food products was and still is one of the main goals of many studies in this field. For this purpose, different extraction techniques have been developed, followed by the development of many analytical instruments and methods for detecting, identifying, and quantifying isolated natural compounds. Isolation of the natural compounds became a challenging problem of great importance since the natural matrix is a highly complex mixture of different compounds. Besides this, natural compounds, extracts, and their sources are the subject of many studies for their possible application in the food industry and agronomy. Natural compounds are used more often to substitute synthetic antioxidants and other compounds. Moreover, applications in phytotherapy are also very attractive and widely explored these days.

Acquiring the natural compounds from their source implies the application of extraction techniques. Nowadays, these techniques are in two major groups: conventional (maceration, hydrodistillation, and Soxhlet extraction) and nonconventional extraction (ultrasound-assisted, microwave-assisted, subcritical water, supercritical fluid extraction) techniques. The selection of the extraction techniques, conditions, and solvents depends on the nature of the desired compounds. The most recent trends include combining several techniques with different solvents to isolate as many bioactive compounds as possible. [Zhu et al.](#) presented in their review article extraction methods for extraction and purification of the polysaccharides from *Perilla frutescens* L. Reviewed approaches are based on the combination of different extraction techniques, conditions, and solvents for isolation of polysaccharides following by multi-step purification to obtain purified products. By contrast, [Yan et al.](#) used simple maceration with hot deionized water to isolate pectic polysaccharides from *Veronica peregrina* L., whose extracts were subsequently submitted to purification steps to prepare cleaner products. Optimizing the extraction process is an essential step for achieving the maximal yield of desired compounds. Several mathematical

tools are used for this purpose, but response surface methodology (RSM) is the most common one. Kang et al. applied RSM in combination with single-factor experiments and Box-Behnken (BBD) design to optimize the extraction of polysaccharides from red *Panax ginseng* and *Ophiopogon japonicus* waste.

After the isolation and purification of the extracts, the next step is chemical characterization, i.e., the determination of the composition and structures of the isolated compounds and the establishment of qualitative and quantitative profiles of the prepared samples. Many different analytical techniques and methods are used. Chromatographic techniques have become standard techniques for analysis of the extracts and isolated compounds. Shompa et al. reported the application of gas chromatography coupled with mass spectrometry (GC-MS) to evaluate the methanolic extract of the *Baccaurea motleyana* Müll. Arg. seeds, while Shahriar et al. used gas chromatography with tandem mass spectrometry (GC-MS/MS) to evaluate the methanolic leaf extract of *Catharanthus ovalis*. Liquid chromatography is widely used to analyze polyphenolic compounds, which is also confirmed by Ahmed et al., who used the HPLC-DAD technique to evaluate the extracts from *Zingiber roseum* (Roxb.) Roscoe leaf. Moreover, other analytical techniques, such as Fourier transform infrared spectroscopy (FTIR) and nuclear magnetic resonance (NMR), were also reported to be used for this purpose (Yan et al.; Kang et al.).

It is not important only to isolate compounds from their natural sources and to characterize them. It is pretty significant to determine the possible application of obtained extracts and evaluate the biological activity of crude extracts and purified compounds. Numerous techniques and methods have been developed for this purpose, while assessments could be done *in vitro* and *in vivo*. Many spectrophotometric methods have been reported for the evaluation of the antioxidant activity. Among them are the DPPH test, hydroxyl radical scavenging activity, ABTS radical scavenging activity, and many others (Yan et al.). Other *in vitro* methods for assessment of antimicrobial, cytotoxic activity, thrombolytic activity, and membrane-stabilizing activity were also reported and applied (Shompa et al.; Shahriar et al.). Polyphenolic compounds are considered the leading carriers of different biological activities in plants and are widely studied. Hence, Du et al. reviewed the potential of traditional Chinese medicine flavonoids in the treatment of osteoporosis. *In vivo* experiments include the investigation of living subjects such as laboratory animals. Yanan et al. reported the effects of lotus leaf (*Nelumbo nucifera*) ethanol extract on gut microbes and obesity in high-fat diet-fed rats and investigated the mechanism of action. They found that extracts regulate blood lipids and relieve chronic inflammation. Choi et al. reported a protocol for a randomized controlled trial evaluating the effect of *Hibiscus syriacus* L. flower extract on sleep quality, evaluating its effect on human subjects. Besides *in vitro* and *in vivo* studies, the rapid development of information technologies opened the door for computational studies of molecules and prediction of their action. Molecular docking studies become significant tools for evaluating

compounds' activity, binding energy for investigated enzymes, and other properties. This method relies on applying existing data about the enzyme structures and structures of natural and synthetic molecules. Using different physico-chemical models and computational simulations, programs predict interaction between investigated structures. Ahmed et al., Shompa et al., and Shahriar et al. used different programs to evaluate the interaction between small molecules of interest and enzymes whose structures were collected from an existing protein data bank.

The quality of the articles presented in this Research Topic illustrates the significance and the value of the subject of this Research Topic: *Extracts from plants and other natural sources: application, characterization, optimization, and their use*. The diversity of the article types, methods, starting materials, and approaches demonstrated the importance of studying compounds from natural sources and the possibility of their wide application in the food, pharmaceutical, and cosmetics industries. The presented articles also showed the necessity of further studies to fill existing gaps and expand our knowledge, which still needs to be completed. This fact opens the door for new studies and Research Topics to overcome these problems and answer all challenges.

Author contributions

SD: Writing – original draft, Writing – review & editing. YS: Writing – original draft, Writing – review & editing. TT: Writing – original draft, Writing – review & editing.

Funding

The author(s) declare financial support was received for the research, authorship, and/or publication of this article. This work was supported by the Ministry of Science, Technological Development and Innovation of the Republic of Serbia (Contracts Nos. 451-03-66/2024-03/200051 and 451-03-66/2024-03/200026).

Conflict of interest

The authors declare that the research was conducted in the absence of any commercial or financial relationships that could be construed as a potential conflict of interest.

Publisher's note

All claims expressed in this article are solely those of the authors and do not necessarily represent those of their affiliated organizations, or those of the publisher, the editors and the reviewers. Any product that may be evaluated in this article, or claim that may be made by its manufacturer, is not guaranteed or endorsed by the publisher.



OPEN ACCESS

EDITED BY

Tomislav Tosti,
University of Belgrade,
Serbia

REVIEWED BY

Nebojsa Ilija Jasnic,
Faculty of Biology,
University of Belgrade,
Serbia
Ivana Damnajnović,
University of Niš,
Serbia

*CORRESPONDENCE

Mi Young Lee
✉ mylee@kiom.re.kr

SPECIALTY SECTION

This article was submitted to
Clinical Nutrition,
a section of the journal
Frontiers in Nutrition

RECEIVED 19 February 2023

ACCEPTED 27 March 2023

PUBLISHED 20 April 2023

CITATION

Choi Y, Park YH, Yang C, Kim DH, Lee KW and
Lee MY (2023) Protocol for a randomized
controlled trial evaluating the effect of *Hibiscus*
syriacus L. flower extract on sleep quality.
Front. Nutr. 10:1169193.
doi: 10.3389/fnut.2023.1169193

COPYRIGHT

© 2023 Choi, Park, Yang, Kim, Lee and Lee.
This is an open-access article distributed under
the terms of the [Creative Commons Attribution
License \(CC BY\)](#). The use, distribution or
reproduction in other forums is permitted,
provided the original author(s) and the
copyright owner(s) are credited and that the
original publication in this journal is cited, in
accordance with accepted academic practice.
No use, distribution or reproduction is
permitted which does not comply with these
terms.

Protocol for a randomized controlled trial evaluating the effect of *Hibiscus syriacus* L. flower extract on sleep quality

Yujin Choi¹, Yu Hwa Park², Changsop Yang¹, Do Hoon Kim²,
Kye Wan Lee² and Mi Young Lee^{3*}

¹KM Science Research Division, Korea Institute of Oriental Medicine, Daejeon, Republic of Korea, ²R&D Center, Dongkook Pharm. Co., Ltd., Suwon, Republic of Korea, ³KM Convergence Research Division, Korea Institute of Oriental Medicine, Daejeon, Republic of Korea

Introduction: *Hibiscus syriacus* L. flower (HSF) is a food ingredient commonly used for tea, and previous animal studies have reported its sleep-promoting effect. This study aims to test the potential of HSF extract as functional food that improves sleep in humans.

Methods and analysis: Eighty participants with sleep disturbances who meet the inclusion/exclusion criteria will be enrolled in this study. Since the effect of HSF extract on sleep is considered to be that of a functional food rather than a medicine, participants with severe insomnia will be excluded from the study. The enrolled participants will be randomly assigned to the HSF extract or placebo groups in a 1:1 ratio. The HSF extract and placebo capsules will look identical, and participants, investigators, and outcome assessors will be blinded to the allocation. Four capsules of HSF extract or placebo will be orally administered 30–60min before bedtime for 4weeks. The primary outcome of this study will be the change in the Pittsburgh Sleep Quality Index (PSQI) global score from the baseline after 4weeks. The subjective and objective changes in the participants' sleep will be evaluated using the Insomnia Severity Index (ISI), Epworth Sleep Scale (ESS), sleep diary, and polysomnography (PSG). The occurrence of adverse events will be closely monitored.

Discussion: The results of this trial will provide data on the efficacy and safety of HSF extract in enhancing sleep quality. Based on the results, the potential of HSF extract as a functional food that improves sleep in humans will be evaluated, and the findings of the trial will be submitted to the Korean Ministry of Food and Drug Safety for consideration as a new functional ingredient that may help to improve sleep quality.

Clinical trial registration: Clinical Research Information Service: KCT0007314; Registered 19 May 2022, <https://cris.nih.go.kr/cris/search/detailSearch.do/21497>.

KEYWORDS

Hibiscus syriacus L. flower, sleep quality, functional food, dietary supplement, clinical protocol, randomized controlled trial

1. Introduction

Sleep is essential factor for maintaining physical and psychological well-being (1). Poor sleep has been found to be associated with reduced productivity and impaired work performance (2, 3), and insufficient sleep has been linked to an increased risk of cognitive decline (4). Despite the importance of sleep, dissatisfaction with sleep quantity or quality is prevalent among the general population, with up to 41.7% of individuals reporting insufficient sleep and 30–48% reporting difficulties with sleep initiation or maintenance (5, 6). Although medication may be effective for treating severe insomnia, there is still an unmet need for safe and accessible sleep aids for individuals with suboptimal sleep quality (7). One potential solution is the use of functional foods, which contain bioactive compounds that offer health-promoting properties (7, 8).

Several functional foods have been suggested as potential aids for improving sleep quality (7, 9, 10). For example, valerian, one of the botanical dietary supplements sold in the United States as sleep aids (11, 12), and chamomile, which is commonly consumed as a tea, have been reported to have beneficial effects on sleep quality (13, 14). In Korea, five functional food ingredients have been granted health claims for “may help to improve sleep quality” (15), including Ecklonia cava ethanol extract (16, 17), milk protein hydrolysate (Lactium) (18), rice bran ethanol extract (19), fermented L-glutamate GABA powder (20), and ashwagandha extract (21). The health functionality of these ingredients was established based on their sleep-promoting effects demonstrated in human and animal studies.

Hibiscus syriacus L. flower (HSF) is a food ingredient (22) that has been widely used to make flower tea. The root of *Hibiscus syriacus* L. is used as a medicine, and its effects on wound healing (23), depression-like behaviors, and neuroprotection (24) have been reported. Meanwhile, HSF has shown a sleep-promoting effect in three sleep-related animal models (25). The HSF extract and its active component (saponarin) increased the rapid-eye-movement sleep time in an electric foot shock-induced sleep disturbance model, restored sleep duration in a restraint-induced sleep disturbance model, and increased sleep maintenance time in a pentobarbital-induced sleep model (25). Based on the results of previous animal studies, the effect of HSF extract on sleep improvement needs be tested in humans.

The objective of this randomized, double-blind, placebo-controlled, parallel-group clinical trial is to evaluate the efficacy and safety of HSF extract on sleep improvement in adults with sleep discomfort and to compare them with that of placebo. Eighty participants will be randomly allocated to the HSF extract or placebo groups in a 1:1 ratio. The superiority of the HSF extract over placebo will be tested.

2. Methods and analysis

2.1. Study setting

This clinical trial will be conducted in two academic university hospitals in Korea, one in Seoul and the other in Daegu.

2.2. Eligibility criteria

This trial targets those individuals with subjective sleep complaints who are in their sub-health status, not the disease. Patients with severe insomnia will be excluded from the study.

2.2.1. Inclusion criteria

Participants aged between 19 and 65, with a Pittsburgh Sleep Quality Index (PSQI) global score of 5 or higher, Insomnia Severity Index (ISI) score between 8 and 21, and who agree to participate and sign the informed consent form will be included.

2.2.2. Exclusion criteria

The exclusion criteria are as follows: participants with severe diseases in cardiovascular system, immune system, respiratory system, gastrointestinal/hepatic and biliary system, kidney and urinary system, nervous system, musculoskeletal system, infectious disease, or malignant tumor; with diseases or symptoms that could affect sleep, such as nocturia; with mental diseases, including alcohol-use disorder, major depressive disorders, generalized anxiety disorders, post-traumatic stress disorders, and obsessive-compulsive disorder; with a past history of or currently suffering from schizophrenia or bipolar disorder; with cognitive decline; with sleep disorders including insomnia, narcolepsy, obstructive sleep apnea, and restless legs syndrome; with irregular sleep patterns due to night-shifts; current smokers, heavy caffeine drinkers, or excessive alcohol drinkers; those taking medications or dietary supplements that could affect sleep within 4 weeks. To exclude participants with clinical depression and anxiety, the Patient Health Questionnaire-9 (PHQ-9) (cut-off: 10 points) (26) and Generalized Anxiety Disorder-7 (GAD-7) (cut-off: 5 points) (27) will be used for the screening test. To exclude participants with a high risk of sleep apnea, STOP-Bang Sleep Apnea Questionnaire (cut-off: 5 points) (28) will be used for the screening test. The complete exclusion criteria with detailed information can be found in the clinical trial registration.¹

2.3. Intervention

Four capsules containing HSF extract or placebo will be orally administered 30–60 min before bedtime for 4 weeks. The investigational products are manufactured as brown-colored hard capsules. One HSF extract capsule (500 mg) includes 250 mg of HSF extract as an active ingredient. The participants in the HSF extract group will take 1,000 mg of HSF extract per day. Placebo capsules have an appearance identical to that of the HSF extract capsules and contain maltodextrin and no active ingredients.

Discontinuing or modifying the allocated intervention is not planned, except in case of the participant's refusal. To monitor adherence, the pharmacists will check for compliance at every visit after prescribing the HSF extract or placebo capsules, and all the remaining capsules will be returned to the clinical pharmacies. During the study period, concomitant care or interventions will be prohibited, except in exceptional cases. Only those medications, dietary

¹ <https://cris.nih.go.kr/cris/search/detailSearch.do/21497>

supplements, and other treatments initiated before participation in this study that will not affect the results of this study can be permitted. Furthermore, even during the course of the study, if the administration of a medicine is required for the transient treatment of other diseases and the medication is considered to not affect the result, it can be permitted.

2.4. Outcomes

2.4.1. Primary outcome

The primary outcome of this study is the change from the baseline of the PSQI (29, 30) global score after 4 weeks of administration. The PSQI is a representative self-rated questionnaire that assesses sleep quality and disturbances for over a month. A higher PSQI global score indicates poor sleep quality.

2.4.2. Secondary outcome

The secondary outcomes include the ISI (31, 32) and Epworth Sleepiness Scale (ESS) (33, 34) to assess the severity of insomnia and daytime sleepiness, respectively. The ISI and ESS will be measured at baseline, 2 weeks (during treatment), and 4 weeks (post-treatment). Polysomnography (PSG) will be performed at baseline and at 4 weeks (post-treatment) for one night, and the total sleep time (TST), sleep efficiency (SE), sleep onset latency (SOL), and wake-up after sleep onset (WASO) will be assessed. The participants will be instructed to keep a sleep diary during the study period. The TST, SE, SOL, and WASO for 7 days will be extracted from the sleep diary at baseline, 2 weeks, and 4 weeks. Blood biomarkers of cortisol, C-reactive protein, and adiponectin will be measured at baseline and at 4 weeks to assess the stress levels and inflammatory markers. The participant timeline is shown in Figure 1.

2.5. Sample size

The primary objective of this clinical trial is to evaluate the superiority of the PSQI global score improvement in the HSF extract group compared to that in the placebo group. To estimate the mean difference of the PSQI global score between both groups and the pooled standard deviation, the results of a previous randomized trial (35) will be used to assess the PSQI global score. In the earlier trial, the mean difference of change from baseline between the two groups was -3.95 (-3.96 in the treatment group and -0.01 in the placebo group). The standard deviation of the change from baseline was not presented, and the largest value of the standard deviation of the PSQI global score was 3.4. To calculate the sample size for this study, the mean difference and pooled standard deviation were estimated as -2.50 and 3.4, respectively. With a 5% level of significance, 80% power of the test, and 25% dropout rate, the required sample size for each group was calculated as 40.

2.6. Recruitment

Adults with sleep disturbance are being recruited based on the outpatients of two university hospitals in Korea. The clinical sites are located in two metropolitan cities in Korea: Seoul and Daegu. A poster

regarding this clinical trial is being posted on the bulletin board and internet homepage of both the hospitals. To enhance the recruitment rate, local advertisements can also be conducted at the bus stops near the hospitals.

2.7. Randomization and allocation concealment

An independent statistician generated the random allocation sequence using the randomization program of the SAS® system (version 9.4). The allocation ratio for the HSF extract and placebo was 1:1, and the block size was concealed from the other investigators. An investigator affiliated with Dongkook Pharmaceutical, who is in charge of the management of the random allocation sequence and packaging of investigational products, packed the HSF extract capsules and placebo capsules according to the allocated random number. The investigational products were packed identically, and each random number was labeled in the package. The investigators in charge of the enrollment of participants were blinded for the allocation sequence and sequentially assigned the random numbers to the enrolled participants.

2.8. Blinding

The participants of the trial, investigators, and outcome assessors will be blinded to the group assignment. Placebo and HSF extract capsules have been developed to have an identical appearance. Concealed envelopes containing information on the group assignment of each random number are being managed by the principal investigators at the two sites. These concealed envelopes will not be disclosed until the completion of this clinical trial unless unblinding is inevitable owing to serious adverse drug reactions or important clinical issues. In such cases, the investigators should immediately contact the sponsors and provide detailed information about the situation. The sponsors and investigator, only after thorough examination, will decide whether or not code breaking for the participant is necessary. The process and reason for the unblinding will be recorded, and the unblinded participants will be dropped from the trial.

2.9. Data collection methods

The validated Korean versions of the PSQI (30), ISI (32), and ESS (34) will be used. The PSQI is a self-rating questionnaire, and the investigators will check the answers of the participants every time to determine that they understand the question and respond properly and also to identify if a missing value or error exists. Sleep indicators extracted by PSG are also important outcomes of this trial. Qualified investigators will interpret the results of PSG. To minimize the difference among the assessors, the raw PSG data obtained at the two sites will be gathered at one site, which will take responsibility for interpreting the PSG results.

In the screening process, the PHQ-9 (26) and GAD-7 (27) will be measured to exclude participants with clinical depression or anxiety. In addition, the STOP-Bang (28) will be used to exclude participants



	STUDY PERIOD				
	Enrolment	Allocation	Post-allocation		Close-out
VISIT	1	2	3	4	
TIMEPOINT	~ -14d	0	14d±3d	28d±3d	+1d ¹
ENROLMENT:					
Informed consent	X				
Eligibility screen	X				
Demographics	X				
Life-styles	X			X	
Medical history	X				
Physical examination	X				
PHQ-9, GAD-7	X				
STOP-Bang	X				
Allocation		X			
INTERVENTIONS:					
<i>HSF extract</i>					
<i>Placebo</i>					
ASSESSMENTS:					
PSQI	X		X	X	
ISI	X		X	X	
ESS		X			
PSG		X			
Sleep diary	X	X	X	X	
Blood biomarkers	X				X
Adverse events			X	X	X
Self-assessment				X	
Compliance			X	X	

FIGURE 1

The schedule of enrolment, intervention, assessment, and visits for participants. ¹The day after the polysomnography. PHQ-9, Patient Health Questionnaire-9; GAD-7, Generalized Anxiety Disorder-7; PSQI, Pittsburgh Sleep Quality Index; ISI, Insomnia Severity Index; ESS, Epworth Sleepiness Scale; PSG, Polysomnography.

with a high risk of obstructive sleep apnea. Validated Korean versions of the PHQ-9 (36), GAD-7 (37), and STOP-Bang (38) will be used. The investigators will send messages to participants to inform them of the dates of visits and encourage them to complete follow-ups.

2.10. Data management

The data obtained from the source documents, such as questionnaires, worksheets, and medical records, will be entered into an electronic Case Report Form (eCRF). Using the validation data system of eCRF, data ranges are set for each value, and a query will

appear when outlier data are entered. Full Source Data Verification (SDV) for data entered into the eCRF will be conducted during routine monitoring visits. In addition, prior to trial initiation, a data management plan has already been prepared. The system query of the eCRF is planned to be checked bimonthly.

2.11. Statistical methods

2.11.1. Definition of the population to be analyzed

The main population to be analyzed for evaluating efficacy is the Per Protocol (PP) set, and Full Analysis (FA) set will be used

supplementary. The PP set will include participants who complete the trial without major deviations from the planned protocol. The FA set will include an additional population for evaluating the efficacy and will include participants who are randomized into groups and who complete more than one assessment after the administration of the investigational products. The main analysis population for evaluating safety will be the safety set, which includes participants administered the investigational products more than once. In the primary and secondary outcomes, there will be no missing data in the PP set, and missing data in the FA set will be imputed using the last observation carried forward method.

2.11.2. Statistical method for analyzing primary and secondary outcomes

The change from the baseline PSQI global score at 4 weeks between the two groups will be compared using a two-sample *t*-test or Wilcoxon rank sum test, according to the normality of data. Additionally, changes in the PSQI global score over time in each group will be compared using a paired *t*-test. A generalized linear model (GLM) with covariates of caffeine consumption, age, body mass index, smartphone usage time, and drinking habits can also be conducted. In case of significant differences in baseline characteristics between the two groups, these baseline characteristics can be considered as covariates in conducting the GLM.

The statistical method used for analyzing secondary outcomes is identical to that used to analyze the primary outcome.

2.12. Data monitoring and auditing

The estimated risk of the trial is low because the investigational product of this trial is a food. A data monitoring committee is not required and an interim analysis is not planned.

A contract research organization hired by sponsors will monitor the clinical trial to verify the process of informed consent acquisition, conduct the trial in compliance with the approved protocol, and obtain accurate and complete trial data. The initial monitoring visits for each site are scheduled within 7 days of the enrollment of the first participant. Routine monitoring will also be conducted 10–11 times at each site.

2.13. Harms

Adverse events will be carefully assessed through non-directive questioning during the trial period. The symptoms and signs of adverse events in participants will be collected at every visit, and their severity and causality will be assessed. Blood and urine tests will be conducted before and after the intervention, and clinically significant abnormal results will be assessed. Owing to the characteristics of the investigational product as a health functional food, product-related severe adverse events are not expected, and mild dyspepsia may occur.

3. Discussion

This clinical trial aims to test the potential of HSF extract as functional food for sleep improvement in humans. Approximately

one-third of the general population has low-quality sleep, whereas approximately 6–15% of the population is diagnosed with insomnia disorders (5). Some people who complain of insomnia may not require sleep medicine if their symptoms are not severe enough, and may instead benefit from functional food that can help improve their sleep quality. This protocol was developed to evaluate the functionality of HSF extract in improving sleep quality in that population. Patients with severe insomnia, depressive or anxiety disorders, and other sleep disorders are set to be excluded from this trial. Furthermore, a large effect size of health functional foods may not be obtained, and we have tried to exclude confounding factors as much as possible. Strict exclusion criteria will be applied, and participants with irregular sleep patterns due to night shifts, smoking, heavy caffeine or excessive alcohol consumption are set to be excluded. In addition, the eligibility criteria and outcomes in this trial have been planned according to the Korean MFDS functionality test guideline for health functional food that “may help to improve sleep quality” (39).

Regulations governing functional foods differ between countries. In the United States, there are three categories of health-related claims: nutrient content claims, structure/function claims, and health claims (40). However, sleep-related statements are not included in the health claims category. For instance, while valerian-containing products are promoted as sleep aids (12), they fall under the structure/function claims category and must carry a label indicating that they are not intended to diagnose, treat, cure, or prevent any disease (40, 41). In Japan, there are three types of functional foods: those with nutrient function claims, those with specified health uses, and those for special dietary uses. Since 2015, sleep-related health claims have been added to new functional products, making them one of the major health claims (42).

In Korea, functional ingredients are divided into two categories: those that have been notified by the Ministry of Food and Drug Safety (MFDS) and those that undergo individually recognized by the MFDS (43). The former includes 95 types of functional ingredients, such as vitamins, minerals, essential fatty acids, protein, dietary fiber, ginseng, and green tea extract (44). For an ingredient to obtain individual recognition as a functional ingredient, the applicant should submit data on the ingredient's safety and functionality. The MFDS then reviews the data consults with the Health Functional Food Deliberation Committee before making a decision on recognition (45). “May help to improve sleep quality” is one of the health claims included in the individual recognition as a functional ingredient category. This trial aims to test the potential of HSF extract to obtain individual recognition for improving sleep quality.

This study protocol has some limitations. First, this is the first human study on the effect of HSF extract on sleep improvement, and no previous study has calculated the effect size of HSF extracts. Therefore, we estimated the effect size of HSF extract on sleep improvement based on the results of a previous randomized trial with a similar design. Second, there are some limitations to measuring sleep using PSG in the hospital for a single night (46, 47). Although an actigraphy device would be a good option for monitoring sleep patterns in a home environment, we could not select it due to budget constraints. To complement this, a sleep diary will be maintained and various sleep characteristics extracted from both PSG and the sleep diary will be considered. We will collect a wide range of data regarding sleep using questionnaires, PSG, and blood biomarkers; this is one of

the strengths of this trial. Third, due to a delay in administrative procedures, this protocol was registered on the international clinical trials registry platform after the first participant enrolled. Nevertheless, the protocol was registered at the early stage of the trial, and the registered protocol version is the same as the version at the time of enrollment of the first participant.

4. Ethics and dissemination

4.1. Research ethics approval

This protocol was approved by the Institutional Review Boards (IRB) of Kyunghee University Hospital at Gangdong (IRB No. KHNMC 2021-11-024) and Keimyung University Dongsan Hospital (IRB No. DSMC 2021-11-07). In case protocol amendments are required, before applying the changes, approval from both the IRBs will be obtained for the revised version of the protocol. The current version of the protocol is 1.2 (date: 2022-01-10).

4.2. Consent or assent

Prior to the screening process, investigators delegated by the principal investigators will provide sufficient information on this clinical trial, and participants will have adequate time to decide whether or not to participate in this clinical trial. If a person decides to participate voluntarily, written informed consent will be obtained from them.

4.3. Confidentiality

To protect the confidentiality of participants, the initial and not the name of each participant will be entered into the eCRF, and each participant will be identified by the screening number of this trial. The two sponsoring institutes (Korea Institute of Oriental Medicine and Dongkook Pharmaceutical) will have access to the final trial dataset, and a blind review will be conducted to confirm the analysis set before the data is locked.

4.4. Dissemination policy

The research findings will be submitted to and published in peer-reviewed journals. In addition, the efficacy and safety results of this trial will be submitted to the Korean MFDS for individual recognition of the new functional ingredient as one that “may help to improve sleep quality.”

Ethics statement

The studies involving human participants were reviewed and approved by the Institutional Review Board of Kyunghee University Hospital at Gangdong and the Institutional Review Board of Keimyung University Dongsan Hospital. The patients/participants provided their written informed consent to participate in this study.

Author contributions

ML, YP, CY, DK, and KL have made contributions to the conception and design of the work. YC has drafted the manuscript. All authors substantively revised it, read, and approved the final manuscript.

Funding

This research was supported by a grant from the Korea Institute of Planning and Evaluation for Technology in Food, Agriculture and Forestry (IPET) through the Technology Commercialization Support Program, funded by the Ministry of Agriculture, Food and Rural Affairs (MAFRA) (821020-3).

Acknowledgments

We thank all the research staff at the Kyunghee University Hospital at Gangdong, Keimyung University Dongsan Hospital, and Neonutra Co., Ltd. for their contributions to the implementation of the trial.

Conflict of interest

ML was holding a patent for *Hibiscus syriacus* L. extract on improving sleep disturbance. YP, DK, and KL were employed by Dongkook Pharm. Co., Ltd.

The remaining authors declare that the research was conducted in the absence of any commercial or financial relationships that could be construed as a potential conflict of interest.

Publisher's note

All claims expressed in this article are solely those of the authors and do not necessarily represent those of their affiliated organizations, or those of the publisher, the editors and the reviewers. Any product that may be evaluated in this article, or claim that may be made by its manufacturer, is not guaranteed or endorsed by the publisher.

References

- Weinberg MK, Noble JM, Hammond TG. Sleep well feel well: An investigation into the protective value of sleep quality on subjective well-being. *Aust J Psychol.* (2016) 68:91–7. doi: 10.1111/ajpy.12098
- Gingerich SB, Seaverson ELD, Anderson DR. Association between sleep and productivity loss among 598 676 employees from multiple industries. *Am J Health Promot.* (2018) 32:1091–4. doi: 10.1177/0890117117722517
- Rosekind MR, Gregory KB, Mallis MM, Brandt SL, Seal B, Lerner D. The cost of poor sleep: Workplace productivity loss and associated costs. *J Occup Environ Med.* (2010) 52:91–8. doi: 10.1097/JOM.0b013e3181c78c30
- Ma Y, Liang L, Zheng F, Shi L, Zhong B, Xie W. Association between sleep duration and cognitive decline. *JAMA Netw Open.* (2020) 3:e2013573. doi: 10.1001/jamanetworkopen.2020.13573

5. Ohayon MM. Epidemiological overview of sleep disorders in the general population. *Sleep Med Res.* (2011) 2:1–9. doi: 10.17241/smr.2011.2.1.1
6. Ohayon MM. Epidemiology of insomnia: What we know and what we still need to learn. *Sleep Med Rev.* (2002) 6:97–111. doi: 10.1053/smr.2002.0186
7. Kim J, Lee SL, Kang I, Song YA, Ma J, Hong YS, et al. Natural products from single plants as sleep aids: A systematic review. *J Med Food.* (2018) 21:433–44. doi: 10.1089/jmf.2017.4064
8. Martirosyan DM, Singh J. A new definition of functional food by FFC: What makes a new definition unique? *Funct Foods Health Dis.* (2015) 5:209–23. doi: 10.31989/fthd.v5i6.183
9. Hu Z, Oh S, Ha TW, Hong JT, Oh KW. Sleep-aids derived from natural products. *Biomol Ther.* (2018) 26:343–9. doi: 10.4062/biomolther.2018.099
10. Chan V, Lo K. Efficacy of dietary supplements on improving sleep quality: A systematic review and meta-analysis. *Postgrad Med J.* (2022) 98:285–93. doi: 10.1136/postgradmedj-2020-139319
11. Bent S, Padula A, Moore D, Patterson M, Mehling W. Valerian for sleep: A systematic review and meta-analysis. *Am J Med.* (2006) 119:1005–12. doi: 10.1016/j.amjmed.2006.02.026
12. Office of Dietary Supplements, National Institutes of Health. Valerian, fact sheet for health professionals [Internet]. (2013). Available at: <https://ods.od.nih.gov/factsheets/Valerian-HealthProfessional/>
13. Leach MJ, Page AT. Herbal medicine for insomnia: A systematic review and meta-analysis. *Sleep Med Rev.* (2015) 24:1–12. doi: 10.1016/j.smr.2014.12.003
14. Hieu TH, Dibas M, Surya Dila KA, Sherif NA, Hashmi MU, Mahmoud M, et al. Therapeutic efficacy and safety of chamomile for state anxiety, generalized anxiety disorder, insomnia, and sleep quality: A systematic review and meta-analysis of randomized trials and quasi-randomized trials. *Phytother Res.* (2019) 33:1604–15. doi: 10.1002/ptr.6349
15. Ministry of Food and Drug Safety. Functional ingredients that may help to improve sleep quality [Internet]. Food Safety Korea. (2022). Available at: <https://www.foodsafetykorea.go.kr/portal/healthyfoodlife/functionalityView.do?viewNo=32>
16. Um MY, Kim JY, Han JK, Kim J, Yang H, Yoon M, et al. Phlorotannin supplement decreases wake after sleep onset in adults with self-reported sleep disturbance: A randomized, controlled, double-blind clinical and polysomnographic study. *Phytother Res.* (2018) 32:698–704. doi: 10.1002/ptr.6019
17. Yoon M, Kim JS, Jo J, Han D, Cho S. Sleep-promoting effect of *Ecklonia cava*: Ethanol extract promotes non-rapid eye movement sleep in C57BL/6N mice. *Fish Aquatic Sci.* (2014) 17:19–25. doi: 10.5657/FAS.2014.0019
18. Kim HJ, Kim J, Lee S, Kim B, Kwon E, Lee JE, et al. A double-blind, randomized, placebo-controlled crossover clinical study of the effects of alpha-s1 casein hydrolysate on sleep disturbance. *Nutrients.* (2019) 11:1466. doi: 10.3390/nu11071466
19. Um MY, Yang H, Han JK, Kim JY, Kang SW, Yoon M, et al. Rice bran extract supplement improves sleep efficiency and sleep onset in adults with sleep disturbance: A randomized, double-blind, placebo-controlled, polysomnographic study. *Sci Rep.* (2019) 9:12339. doi: 10.1038/s41598-019-48743-8
20. Jeong AH, Hwang J, Jo K, Kim S, Ahn Y, Suh HJ, et al. Fermented gamma aminobutyric acid improves sleep behaviors in fruit flies and rodent models. *Int J Mol Sci.* (2021) 22:3537. doi: 10.3390/ijms22073537
21. Deshpande A, Irani N, Balkrishnan R, Benny IR. A randomized, double blind, placebo controlled study to evaluate the effects of ashwagandha (*Withania somnifera*) extract on sleep quality in healthy adults. *Sleep Med.* (2020) 72:28–36. doi: 10.1016/j.sleep.2020.03.012
22. Ministry of Food and Drug Safety. Standards and specifications for food [Amended by Notification No. 2022-84, Dec. 1, 2020]. (2020).
23. Yoon SW, Lee KP, Kim DY, Hwang DI, Won KJ, Lee DW, et al. Effect of absolute from *Hibiscus syriacus* L. flower on wound healing in keratinocytes. *Pharmacogn Mag.* (2017) 13:85–9. doi: 10.4103/0973-1296.197644
24. Kim YH, Im AR, Park BK, Paek SH, Choi G, Kim YR, et al. Antidepressant-like and neuroprotective effects of ethanol extract from the root bark of *Hibiscus syriacus* L. *Biomed Res Int.* (2018) 2018:1–13. doi: 10.1155/2018/7383869
25. Kim YR, Lee SY, Lee SM, Shim I, Lee MY. Effect of *Hibiscus syriacus* Linnaeus extract and its active constituent, saponarin, in animal models of stress-induced sleep disturbances and pentobarbital-induced sleep. *Biomed Pharmacother.* (2022) 146:112301. doi: 10.1016/j.biopha.2021.112301
26. Kroenke K, Spitzer RL, Williams JBW. The PHQ-9: Validity of a brief depression severity measure. *J Gen Intern Med.* (2001) 16:606–13. doi: 10.1046/j.1525-1497.2001.016009606.x
27. Spitzer RL, Kroenke K, Williams JBW, Löwe B. A brief measure for assessing generalized anxiety disorder: The GAD-7. *Arch Intern Med.* (2006) 166:1092–7. doi: 10.1001/archinte.166.10.1092
28. Chung F, Subramanyam R, Liao P, Sasaki E, Shapiro C, Sun Y. High STOP-Bang score indicates a high probability of obstructive sleep apnoea. *Br J Anaesth.* (2012) 108:768–75. doi: 10.1093/bja/aes022
29. Buysse DJ, Reynolds CF, Monk TH, Berman SR, Kupfer DJ. The Pittsburgh sleep quality index: A new instrument for psychiatric practice and research. *Psychiatry Res.* (1989) 28:193–213. doi: 10.1016/0165-1781(89)90047-4
30. Sohn SI, Kim D, Lee M, Cho YW. The reliability and validity of the Korean version of the Pittsburgh sleep quality index. *Sleep Breath.* (2011) 16:803–12. doi: 10.1007/s11325-011-0579-9
31. Bastien CH, Vallières A, Morin CM. Validation of the insomnia severity index as an outcome measure for insomnia research. *Sleep Med.* (2001) 2:297–307. doi: 10.1016/S1389-9457(00)00065-4
32. Cho YW, Song ML, Morin CM. Validation of a Korean version of the insomnia severity index. *J Clin Neurol.* (2014) 10:210–5. doi: 10.3988/jcn.2014.10.3.210
33. Johns MW. A new method for measuring daytime sleepiness: The Epworth sleepiness scale. *Sleep.* (1991) 14:540–5. doi: 10.1093/sleep/14.6.540
34. Cho YW, Lee JH, Son HK, Lee SH, Shin C, Johns MW. The reliability and validity of the Korean version of the Epworth sleepiness scale. *Sleep Breath.* (2011) 15:377–84. doi: 10.1007/s11325-010-0343-6
35. Moosavi SM, Yazdani-Charati J, Amini F. Effects of Modafinil on sleep pattern during methamphetamine withdrawal: A double-blind randomized controlled trial. *Addict Health.* (2019) 11:165–72. doi: 10.22122/ahj.v11i3.219
36. Park SJ, Choi HR, Choi JH, Kim KW, Hong JP. Reliability and validity of the Korean version of the patient health Questionnaire-9 (PHQ-9). *Anxiety Mood.* (2010) 6:119–24.
37. Lee SH, Shin C, Kim H, Jeon SW, Yoon HK, Ko YH, et al. Validation of the Korean version of the generalized anxiety disorder 7 self-rating scale. *Asia Pac Psychiatry.* (2022) 14:e12421. doi: 10.1111/appy.12421
38. Jeon HJ, Bang YR, Yoon IY. A validation study on three screening questionnaires for obstructive sleep apnea in a Korean community sample. *Sleep Breath.* (2019) 23:969–77. doi: 10.1007/s11325-018-1748-x
39. Ministry of Food and Drug Safety. Health functional food functionality test guideline: May help to improve sleep quality. National Institute of Food and Drug Safety Evaluation. (2017).
40. Domínguez Díaz L, Fernández-Ruiz V, Cámara M. An international regulatory review of food health-related claims in functional food products labeling. *J Funct Foods.* (2020) 68:103896. doi: 10.1016/j.jff.2020.103896
41. Noonan W, Noonan C. Legal requirements for “functional food” claims. *Toxicol Lett.* (2004) 150:19–24. doi: 10.1016/j.toxlet.2003.05.002
42. Iwatani S, Yamamoto N. Functional food products in Japan: A review. *Food Sci Human Wellness.* (2019) 8:96–101. doi: 10.1016/j.fshw.2019.03.011
43. Ministry of Food and Drug Safety. Health Functional Foods Act [Act No.13330, 18. May, 2015, Partial Amendment] [Internet]. Act No.18359. (2015). Available at: <https://law.go.kr/LSW/lsInfoP.do?lsiSeq=171029&viewCls=engLsInfoR&urlMode=engLsInfoR#0000>
44. Ministry of Food and Drug Safety. Standards and specifications for health functional food [Amended by the Notification No. 2022-69, Sep. 15, 2022]. (2022)
45. Ministry of Food and Drug Safety. Regulation on approval of functional ingredient for health functional food [Amended by the Notification No. 2007-51, Jul. 11, 2007]. (2007).
46. Newell J, Mairesse O, Verbanck P, Neu D. Is a one-night stay in the lab really enough to conclude? First-night effect and night-to-night variability in polysomnographic recordings among different clinical population samples. *Psychiatry Res.* (2012) 200:795–801. doi: 10.1016/j.psychres.2012.07.045
47. Marino M, Li Y, Rueschman MN, Winkelman JW, Ellenbogen JM, Solet JM, et al. Measuring sleep: Accuracy, sensitivity, and specificity of wrist actigraphy compared to polysomnography. *Sleep.* (2013) 36:1747–55. doi: 10.5665/sleep.3142



OPEN ACCESS

EDITED BY

Yulia Smyatskaya,
Peter the Great St. Petersburg Polytechnic
University, Russia

REVIEWED BY

Kit Leong Cheong,
Guangdong Ocean University, China
Ivan Kojic,
University of Belgrade, Serbia

*CORRESPONDENCE

Meng-Liang Tian
✉ secondat@sicau.edu.cn

[†]These authors have contributed equally to this work

RECEIVED 09 March 2023

ACCEPTED 10 May 2023

PUBLISHED 24 May 2023

CITATION

Kang J, Zhao J, He L-F, Li L-X, Zhu Z-K and Tian M-L (2023) Extraction, characterization and anti-oxidant activity of polysaccharide from red *Panax ginseng* and *Ophiopogon japonicus* waste.

Front. Nutr. 10:1183096.

doi: 10.3389/fnut.2023.1183096

COPYRIGHT

© 2023 Kang, Zhao, He, Li, Zhu and Tian. This is an open-access article distributed under the terms of the [Creative Commons Attribution License \(CC BY\)](https://creativecommons.org/licenses/by/4.0/). The use, distribution or reproduction in other forums is permitted, provided the original author(s) and the copyright owner(s) are credited and that the original publication in this journal is cited, in accordance with accepted academic practice. No use, distribution or reproduction is permitted which does not comply with these terms.

Extraction, characterization and anti-oxidant activity of polysaccharide from red *Panax ginseng* and *Ophiopogon japonicus* waste

Jia Kang^{1†}, Jue Zhao^{1†}, Lan-Fang He^{1†}, Li-Xia Li², Zhong-Kai Zhu² and Meng-Liang Tian^{3*}

¹Hospital of Chengdu University of Traditional Chinese Medicine, Chengdu, China, ²Natural Medicine Research Center, College of Veterinary Medicine, Sichuan Agricultural University, Chengdu, China,

³College of Agronomy, Sichuan Agricultural University, Chengdu, China

Red ginseng and *Ophiopogon japonicus* are both traditional Chinese medicines. They have also been used as food in China for thousands of years. These two herbs were frequently used in many traditional Chinese patent medicines. However, the carbohydrate compositions of these two herbs were not normally used during the production of said medicine, such as Shenmai injection, resulting in a large amount of waste composed of carbohydrates. In this study, the extraction conditions were optimized by response surface methodology. The Shenmai injection waste polysaccharide was extracted by using distilled water that was boiled under the optimized conditions. The Shenmai injection waste polysaccharide (SMP) was thereby obtained. SMP was further purified by anion exchange chromatography and gel filtration. With this method, a neutral polysaccharide fraction (SMP-NP) and an acidic polysaccharide fraction (SMP-AP) were obtained. The results of structure elucidation indicated that SMP-NP was a type of levan, and SMP-AP was a typical acidic polysaccharide. SMP-NP exhibited potential stimulation activity on the proliferation of five different *Lactobacilli* strains. Therefore, SMP-AP could promote the antioxidant defense of IPEC-J2 cells. These findings suggest that Shenmai injection waste could be used as a resource for prebiotics and antioxidants.

KEYWORDS

red *Panax ginseng*, *Ophiopogon japonicus*, waste, polysaccharide, prebiotics, antioxidants

1. Introduction

Shenmai San, which consists of *Panax ginseng* and *Ophiopogon japonicus*, is an ancient Chinese patent medicine that first appeared in “Medical Origins.” It is used to treat diseases like heart attacks, congestive heart failure, and severe bronchitis induced by *Qi* and *Yin* deficiency (1). In modern China, Shenmai San has been developed into an injection preparation (Shenmai injection) that is a sterile aqueous solution prepared by the combination of Red ginseng ethanol extract and *O. japonicus* ethanol extract. Clinical pharmacy studies reveal that the Shenmai injection is more effective when used to treat cardiovascular diseases, such as coronary heart disease, viral myocarditis, and chronic pulmonary heart disease (1, 2). It is often combined with

chemotherapeutic drugs to increase their curative effects and improve the immune function of cancer patients (3). Saponin ingredients from *P. ginseng* and *O. japonicus* are the major components of the Shenmai injection (4). And yet, the carbohydrate composition of these two herbs is not used during the production of the Shenmai injection, resulting in a large amount of waste composed of carbohydrates. Due to the significant increase in the production of Shenmai injection in China, the development and utilization of waste based on its active carbohydrate ingredients would have economic and environmental benefits.

Panax ginseng is a traditional Chinese medicinal herb. For thousands of years, it has been used to increase vitality and boost the immune system. Multiple bioactive ingredients like ginsenosides, phytosterols, and polyacetylenes are isolated from *P. ginseng*, but polysaccharides are thought to be one of the most important ingredients due to their effective bioactivities (5, 6). Similar to *P. ginseng*, *O. japonicus* is important in traditional Chinese medicine. It has been used to nourish the Yin, promote body fluid production, and treat lung diseases. 71% of *O. japonicus* is made up of carbohydrates (7). So, it is not a surprise that the polysaccharides from it can be used for several bioactivities, such as anti-diabetes, antioxidants, and improved immunity (8, 9). While lots of studies reported the isolation and characterization of polysaccharides from *P. ginseng* and *O. japonicus* respectively, the polysaccharides from the combined extraction of these two medicinal herbs have not been well studied.

In this study, we aimed to perform single-factor extraction experiments and optimize them to isolate polysaccharides from Shenmai injection waste. We followed this with anion exchange chromatography and gel filtration to obtain the neutral and acidic polysaccharide fractions. Size exclusion chromatography, methanolysis, and NMR were performed to determine the molecular weight, monosaccharide composition, and glycosidic linkage of these polysaccharides. Finally, the prebiotic and antioxidant activities were analyzed by *in vitro* experiments.

2. Materials and methods

2.1. Materials and reagents

The dried red *Panax ginseng* and *Ophiopogon japonicus* residues from Shenmai injection production were obtained from Ya'an Sanjiu Pharmaceutical Co., Ltd. (Ya'an City, Sichuan Province, China). Both herbs were identified by Li-Xia Li of Sichuan Agriculture University. Specimens were deposited in the College of Veterinary Medicine, Sichuan Agricultural University.

DEAE-cellulose and Agarose gel 6FF were obtained from Beijing Ruidahenghui Science & Technology Development Co., Ltd. The MRS medium (HB0384-1), peptone (HB8276), and tryptone (HB8270) were purchased from Hopebio Biotechnology Co., Ltd. (Qingdao, China). The yeast extract powder (JM-500) was purchased from Biotopped Science and Technology Co., Ltd. (Beijing, China). The McIntosh Turbidimetric tube (G60346) was obtained from Wenzhou Kangtai Biotechnology Co., Ltd. (Zhejiang, China). The standard fructooligosaccharide (QHT-FOS-P95S) and inulin (Orafti®HP) were purchased from Quantum Hi-Tech Biological Co., Ltd. (Jiangmen, China) and Beneo-Orafti (Belgium), respectively.

The standard of fructose (Fru) and glucose (Glc) were purchased from Solarbio (Beijing, China). All other chemicals, such as phenol, sulfuric acid, acetone, boric acid, glycerin, etc., were of analytical grade and obtained from the Chengdu Kelong chemical factory (Chengdu, China).

2.2. Extraction and determination of polysaccharide from Shenmai injection waste

The powdered red *P. ginseng* and *O. japonicus* were mixed with a ratio of 1:1 (w/w) and isolated using distilled water and different extraction conditions. The aqueous extracts were collected and concentrated by Rotary Evaporator (Shanghai Yarong Biochemical Instrument Factory Co., Ltd). Four times the volume of ethanol was poured into the water extracts and placed at 4°C for 24 h. The mixture was centrifuged (3,500 rpm, 10 min), and the insoluble residue was separated. The polysaccharide was obtained after lyophilization. The content of the carbohydrate was determined by the phenol-sulfuric acid method (10). The extraction yield of the polysaccharide was calculated according to the content of the carbohydrate.

2.3. Design of extraction conditions

2.3.1. Single-factor experiment

The optimum extraction conditions of polysaccharides from Shenmai injection waste were measured by single-factor experiments and the response surface method (RSM). The single-factor experiment was executed in a designed extraction time (ranging from 0.5–3 h), a designed extraction temperature (ranging from 50°C–100°C), and with an extraction ratio of solvent to material (ranging from 10:1–50:1) with 1.0 g of red ginseng and *O. japonicus* powder mixture (after ethanol extraction) (11, 12). One factor was kept invariable for each study and each group in triplicate. After extraction, the aqueous extracts were centrifuged and freeze-dried. Then the powder was dissolved into 1 mg/mL, and the carbohydrate component was determined by the method described above.

2.3.2. Optimization of extraction conditions by BBD

Box–Behnken design (BBD) is a type of response surface design. It is an independent quadratic design in that it does not contain an embedded factorial or fractional factorial design. In this design the treatment combinations are at the midpoints of edges of the process space and at the center. These designs are rotatable (or near rotatable) and require 3 levels of each factor. It is more efficient and easier to arrange and interpret experiments in comparison with others (13). Based on the single-factor experiment described above, BBD experiment was adopted and revealed in Table 1 with three-level-three-factors. Those factors were mentioned above. The extraction temperature (X_1), the ratio of solvent to material (X_2), and the extraction time (X_3) were designed using SAS. JMP. 13.0 software (Statistical analysis system, United States).

The variables were coded according to the following formula:

TABLE 1 Central composite design and the extraction yield of polysaccharide.

Runs	Independent variables			Uncoded level			Extraction yield/%
	Coded level						
	X_1	X_2	X_3	X_1	X_2	X_3	
1	0	1	−1	90	1:40	20	51.3 ± 0.396
2	0	−1	−1	90	1:20	20	52.14 ± 3.43
3	−1	0	1	80	1:30	40	57.75 ± 0.1904
4	0	0	0	90	1:30	30	60.37 ± 3.274
5	−1	−1	0	80	1:20	30	51.93 ± 2.593
6	−1	0	−1	80	1:30	20	60.6 ± 1.5132
7	0	1	1	90	1:40	40	60.12 ± 1.35
8	0	0	0	90	1:30	30	62.67 ± 1.355
9	1	0	1	100	1:30	40	60.6 ± 1.355
10	0	−1	1	90	1:20	40	60.78 ± 1.047
11	1	−1	0	100	1:20	30	61.36 ± 2.079
12	1	0	−1	100	1:30	20	60.45 ± 0.997
13	1	1	0	100	1:40	30	60.75 ± 0.467
14	0	0	0	90	1:30	30	60.56 ± 1.817
15	−1	1	0	80	1:40	30	61.69 ± 0.9405

$$X_i = \frac{X_i - X_0}{\Delta x}$$

where X_i is the coded value of the variable X_i , X_0 is the value of X_i at the central point, and Δx is the amplitude of variation. The results were analyzed and fitted to a second-order polynomial model.

In the formula, Y is the response variable (the extraction yield of polysaccharide). A_0 , A_i , A_{ii} , and A_{ij} are the intercept linear, quadratic, and interaction coefficients of X_1 , X_2 , and X_3 , respectively. X_i and X_j are the coded independent variables, and the terms of X_i^2 represent the quadratic terms. Analyses of the variance were evaluated *via* the ANOVA procedure. The fitness of this predictive model was performed by the coefficient of determination R^2 and the adjusted- R^2 . Then the statistical significance and regression coefficients were checked using the F -test at a probability (p) of 0.01 or 0.05.

2.4. DEAE-cellulose ion exchange chromatography

300 mg of crude polysaccharide was dissolved with 20 mL of distilled water and filtered with a 0.45 μ m filter. Then the polysaccharide solution was injected into the DEAE-cellulose ion column (50 mm \times 40 cm, Beijing RuiDaHengHui Science & Technology Development Co., Ltd.), and distilled water was used as an elution buffer. The neutral fraction was eluted with a three-fold column volume of distilled water at the speed of 2 mL/min, combining the phenol-sulfuric acid method (14). We collected all the elution, concentrated it, and then preserved the solution *via* lyophilization, named SMP-NP. The column was further eluted using a gradient elution of NaCl (0–1.5 M), and the acidic fraction SMP-AP was obtained.

2.5. Molecular weight determination

Molecular weight was measured by size exclusion chromatography. Five types of dextrans were used as standard (10, 70, 200, 800, and 1,000 kDa). 2 mg of each of the standard dextrans were weighted, respectively. Then all standard dextrans were mixed and dissolved in a 10 mmol/L NaCl solution and filtrated *via* a 0.22 μ m filter. The mixture solution was then injected into the column and eluted with a 10 mmol/L NaCl solution at a speed of 0.2 mL/min. We kept 1 mL in volume per tube. After that, we collected all elution. The carbohydrate fraction was determined using the phenol-sulfuric acid method. We calculated the linear relationship between the molecular weight logarithm of the glucan and the elution volume and obtained the molecular weight of the carbohydrate fraction.

2.6. Chemical compositions and linkage determination

The SMP-AP was subjected to methanolysis with 3 M of hydrochloric acids in anhydrous methanol for 24 h at 80°C to obtain the methylglucosides. Then the monosaccharide composition was determined by gas chromatography (GC) after derivatization *via* the hexamethyl disilazane (HMDS) and the trimethylchlorosilane (TMS) reaction. The mannitol was added to the samples as the internal standard. Additionally, the presence of Fru was tested with the Urea-HCl colorimetric method (15).

The glycosidic linkages were determined by methylation. The carrier gas was Helium (pressure control: 80 kPa). The relative amount of each type of linkage was determined based on the area of each compound and related to the monosaccharide compositions of each fraction (16).

2.7. The NMR spectroscopy

After three deuterium exchanges using freeze-drying in D_2O (10 mg/mL) and performance on a Bruker AV600 instrument (Bruker, Rheinstetten, Germany) at 25°C, the 1H NMR and ^{13}C NMR spectra of SMP-NP and SMP-AP were recorded on the spectrometer (600 MHz). These peaks were labeled using MestReNova software (Version 6.0.2-5475, 2009, Mestrelab Research S.L., Spain).

2.8. Prebiotic effect

2.8.1. *Lactobacillus* bacterial strains

The *Lactobacillus buchneri* (BSS1, CCTCC No. AB2016284), *L. johnsonii* (BS15, CCTCC: M2013663), *L. plantarum* (BS10, CCTCC: M012487), *L. plantarum* (BSGP201683, CCTCC: M2016425) and *L. rhamnosus* GG (LGG, ATCC53103) were obtained from professor Xue-Qin Ni of Animal Microecology Institute, College of Veterinary Medicine, Sichuan Agricultural University, China. *L. johnsonii* (Hjg8, ATCC 33200) was provided by Dr. Bing-zhao Zhang of Shenzhen Institutes of Advanced Technology, Chinese Academy of Science, China. All these were stored at −80°C in MRS medium with 20% glycerin.

2.8.2. Bacterial growth

The basal medium (10 g peptone and tryptone, respectively, 5 g yeast extract, 1 mL of Tween 80, 0.5 g L-cysteine hydrochloride, 1 g/L carbohydrate source, and 1 L of distilled water with an adjusted pH at 6.5) and the MRS medium were used as culture mediums after being autoclaved at 121°C for 30 min. Two commercial prebiotic products were used as a positive control compared with SMP-NP. These products were P95s (96.1% fructo-oligosaccharides, DPn 2–9, with 2.7% glucose, fructose, and sucrose, the product of the partial enzymatic hydrolysis of chicory inulin) and Orafit®HP (99.8% inulin, DPav ≥23, with 0.2% glucose, fructose, and sucrose). Both were obtained from Quantum Hi-Tech (China) Biotechnology Co., Ltd., Shenzhen, China. These five strains of *Lactobacilli* were incubated in the 50 mL MRS medium at 37°C overnight in anaerobic chamber (Thermo Scientific 1,029, in 5% N₂, 10% H₂, 5% CO₂), then centrifuged 3,500 rpm, 10 min, and resuspended in saline and basal medium, successively, to remove the carbon source. Finally, they were resuspended with basal medium containing these three different carbon sources above (the CPPF and two commercially available prebiotic P95s, Orafit®HP), at a concentration of 10⁷–10⁸ CFU/mL, after adjusted by McIntosh Turbidimetric tube. 5 milliliter bacterial suspensions were divided in test tubes, and then incubated for 0 and 24 h. All test tubes were set in triplicate. Two hundred microliter of the basal medium was added to the 96-wells plates and the density of bacteria were measured at the wavelength of 600 nm (A600) using Multiscan Spectrum (Thermo Scientific, Varioskan Flash) after incubated for 0 h and 24 h. The bacterial growth was evidenced as the increment in A600 (ΔA_{600}) during 24 h of incubation in anaerobic chamber. After 24 h of incubation, the pH was measured by pH meter (A115200, Lichen Instrument technology Co. Ltd., Hunan, China) after removing bacteria by centrifuging at 4000 rpm for 20 min. Each tube was tested three times, triplicate each time, making sure high accuracy and precision (11).

2.9. Anti-oxidant activity determination

2.9.1. Cell culture

IPEC-J2 cell (Intestinal porcine epithelial cell lines) was obtained from and maintained in DMEM/F-12 medium (Beijing Solarbio Science & Technology Co., Ltd.). This was supplemented with 10% FBS (Thermo Fisher Scientific (China) Co., Ltd), 100 U/mL penicillin, and 100 U/mL streptomycin (Beijing Solarbio Science & Technology Co., Ltd.) in a humidified atmosphere of 5% CO₂ at 37°C.

2.9.2. Establishment of oxidative stress damages model

IPEC-J2 cells were seeded into 96-well plates at a density of 1.0×10^4 cells/well. After the cells were adhered in the 96-well plate, the culture medium was washed with a phosphate buffer saline (PBS, pH = 7.4, Beijing Solarbio Science & Technology Co., Ltd.) three times. 200 μ mol/mL of H₂O₂ (Sigma-Aldrich, United States) were added into the 96-well plate ($n = 12$) and cultured in a 37°C incubator. After 24 h incubation, 10 μ L of CCK8 (Wuhan Boster Biological Technology, LTD, Wuhan, China) was added to the 96-plate wells. After a 1 h incubation, the measurement was performed at 450 nm with a microwell reader (Bio-Rad).

2.9.3. Measurement of IPEC-J2 cells viability

IPEC-J2 cells were seeded into 96-well plates and cultured in a 37°C incubator for 24 h. 200 μ mol/mL of H₂O₂ was added to the plate and cultured for 24 h. Three concentrations of SMP-AP (20 μ g/mL, 10 μ g/mL, 5 μ g/mL) were added to the 96-well plate. After being cultured at 37°C for 24 h, the cell viability was determined by the CCK8 method.

2.9.4. Determination of antioxidant enzymes activity

IPEC-J2 cells were seeded into a 6-well plate, and an oxidative stress damages model was established using 200 μ mol/mL of H₂O₂. Different concentrations of SMP-AP (20 μ g/mL, 10 μ g/mL, 5 μ g/mL) were added to the six-well plate. After being cultured at 37°C for 24 h, plates were washed with PBS three times. Cells were collected by a cell culture dish and disrupted by a cell ultrasonic cell breaker (Shanghai Huxi Industry Co., Ltd). The cells were then centrifuged at 12,000 rpm for 3 min after cell disruption to obtain the supernatant for the determination of the antioxidant enzyme activity. The antioxidant enzyme activities were determined by a Biochemical Detection Kit (Nanjing Jiancheng Bioengineering Institute, Nanjing, China).

2.9.5. Quantitative real-time PCR

RNA extraction from the intestine cells and real-time PCR for antioxidant gene detection were performed as previously reported (17). In summary, IPEC-J2 cells were lysed with Trizol Regent (R1100, Beijing Solarbio Science & Technology Co., Ltd., China), and the total RNA was extracted from the cells according to the manufacturer's instructions. The RNA quality was determined by the agarose gel method, and the RNA concentration was determined by a spectrophotometer (NanoDrop 2000, Shanghai Institute of Thermal Sciences, China). The total RNA was reverse transcribed using reverse transcriptase which was done according to the manufacturer's instructions (Enzyme Tower, Waltham, Mass.). The Bio-Rad-CFX96 system was used for real-time quantitative PCR, and related gene expression was normalized with the internal control β -actin. The primer sequences of the SYBR green probe of the target gene are shown in Table 2.

2.10. Statistical analysis

The statistical values were represented as mean \pm SD. The statistical comparisons were applied with the one-way analysis of variance (ANOVA) by Duncan's test using SPSS version 20.0. Then the values of $p < 0.05$ and $p < 0.01$ were considered statistically significant and highly significant, respectively.

3. Results

3.1. Optimization of extraction process of Shenmai polysaccharide

3.1.1. Effects of temperature, solvent/material ratio, and extraction time on the yield of SMP

Optimized single-factor extraction experiments were performed to better isolate polysaccharides from the Shenmai injection waste

TABLE 2 qRT-PCR primers for antioxidant defense genes.

Gene	bp	Primer sequence
Nrf2	125	F: CACCACCTCAGGGTAATA
		R: GCGGCTGAATGTTGTGTC
NQO1	200	F: GATCATACTGGCCCACTCCG
		R: GAGCAGTCTCGGCAGGATAC
HO-1	130	F: AGCTGTTTCTGAGCCTCCAA
		R: CAAGACGGAAACACGAGACA
CAT	124	F: TGTGAACTGTCCCTTCCGTG
		R: CGTCTGTTCCGGAGCACTAA
SOD1	176	F: ACCTGGGCAATGTGACTG
		R: TCCAGCATTTCCCGTCT
GPXs	127	F: CGGACCACCTGTTGAAAGCTC
		R: TCCGCCAGTTCTTGTGTCCA
ZO-1	126	F: TTGATAGTGGCGTTGACA
		R: CCTCATCTTCATCATCTTCTAC
β -Actin	122	F: GATGAGATTGGCATGGCTTT
		R: CACCTTCACCGTTCCAGTTT

(named Shenmai polysaccharide, SMP). As shown in Figure 1A, the extraction yield of SMP increased as the extraction temperature increased ($p < 0.05$), showing a linear relationship. When the water extraction temperature reached 100°C, the extraction yield of polysaccharide reached its maximum amount (60.25%) (Figure 1A). Therefore, 90°C was chosen as the center level of extraction temperature in the response surface design. The other two temperature points were set at 80°C and 100°C. With the temperature at 100°C and an extraction time of 30 min, the extraction yield reached 58.80% when the solvent/material ratio was around 30 mL/g (Figure 1B). But when the solvent/material ratio was increased from 30 mL/g to 50 mL/g, the extraction yield was 60.75%, only increasing 1.95% (Figure 1B, $p > 0.05$). Thus, 30 mL/g was set as the central value in the response surface design. The other two values were set as 20 mL/g and 40 mL/g, respectively. With the temperature at 100°C and a solvent/material ratio of 30 mL/g, it was found that the polysaccharide extraction yield increased with increased extraction time, reaching a maximum value (56.79%) around 30 min (Figure 1C). Therefore, 30 min was set as the center point for extraction time. The other points for extraction time were set at 20 min and 40 min.

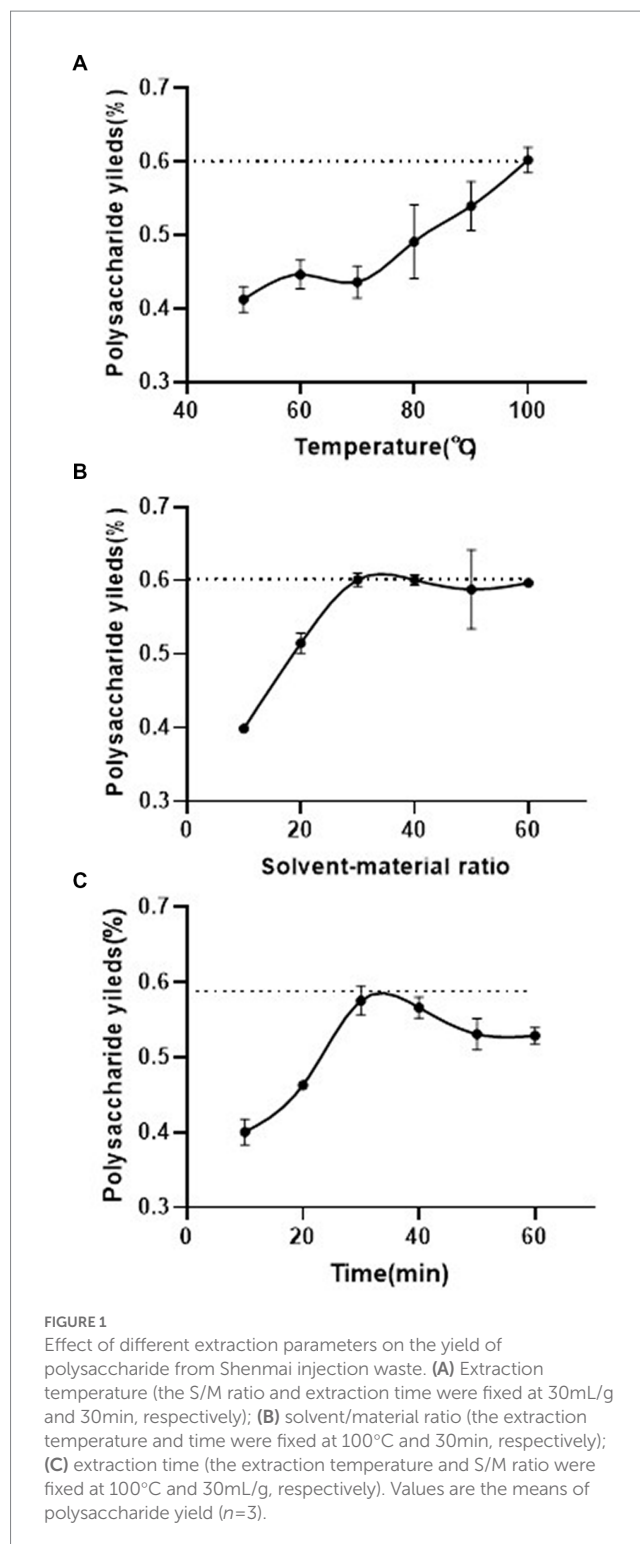
3.1.2. Optimization of extraction yield using RSM

3.1.2.1. Model fitting

SAS, JMP13.0 software was used to carry out a regression analysis of the data in Table 1. This provided the following predicted regression equation of the three factors corresponding to the yield of SMP:

$$Y = 4.4978X_1 + 3.1491X_2 + 3.0244X_3 - 0.0194X_1X_2 - 0.0145X_1X_3 - 0.0202X_2X_3 - 0.0178X_1^2 - 0.0091X_2^2 - 0.0155X_3^2 - 252.6963$$

X_1 , extraction temperature; X_2 , solvent/material ratio; X_3 , extraction time.



3.1.2.2. Analysis of response and contour surface plots

Variance analysis was conducted on the model (Table 3). It was found that the R^2 of this model was 0.97 ($p = 0.0023 < 0.01$), and the multiple regression relationship between dependent variables and all independent variables was significant (Table 3). The primary term X_1 (extraction temperature) of the model was extremely significant ($p < 0.001$), suggesting that extraction temperature had the greatest impact on the yield of SMP.

3.1.2.3. Optimization of extraction conditions

Obtained through the software's statistical analysis, the response surface figure is shown in Figure 2. It can be seen that the yield of SMP was greatly affected by the above three factors. This was consistent with the regression coefficient results in Table 1. When the extraction time was fixed at the 0 level, the yield of SMP increased with the increase of extraction temperature (X_1 , 80°C–97.70°C) and the solvent/material ratio (20–40 mL/g) (Figure 2A). However, when the temperature is higher than 97.70°C, the yield of SMP decreases again. When the solvent/material ratio is fixed at the 0 level, the yield of SMP increased as the extraction temperature (X_1 , 80°C–97.70°C) and extraction time (20–35.92 min) increased (Figure 2B). When the extraction temperature was fixed at the 0 level, the yield of SMP increased with the increase of the ratio of solvent/material (20–40 mL/g) and extraction time (20–35.92 min). When the extraction time exceeds 35.92 min, the yield of SMP decreased (Figure 2C). In addition, it can be seen from Figure 2 that the following pairs all have a linear relationship with the yield of

SMP: the extraction temperature (X_1) and the solvent/material ratio (X_2), the extraction temperature (X_1) and the extraction time (X_3), and the solvent/material ratio (X_2) and the extraction time (X_3). This is similar to the analysis results in Table 3. In summary, extraction temperature, solvent/material ratio, and extraction time all have a certain impact on the yield of SMP. The order of the three factors was extraction temperature, extraction time, and then solvent/material ratio.

3.1.2.4. Verification of the models

The fitting equation obtained in 3.1.2.1 was analyzed by JMP software. Based on the results, we concluded that when the extraction temperature was 93.10°C the solvent/material ratio was 40 mL/g, the extraction time was 27.94 min, and the yield of SMP reached its maximum value of 62.84%. To ensure convenient production, the optimal extraction process conditions were determined. They are as follows: an extraction temperature of 93°C, a solvent-material ratio of 40 mL/g, an extraction time of 30 min each time, extraction twice, and a predicted extraction rate of 62.78%.

To verify the accuracy of the above fitting model, the SMP was extracted twice for 30 min using the optimal extraction process. The final yield of SMP was 62.72%, which was close to the predicted value (62.78%), indicating a good fit with the above regression equation. This extraction process can accurately display the trend of SMP production. It meets the requirements of both experimental and actual production.

3.2. Chemical composition of crude Shenmai polysaccharide

The protein, polyphenols, and carbohydrate content in crude polysaccharides were determined. Crude SMP was 81.89% carbohydrates, 8.82% protein, and 2.31% polyphenols. Therefore, purification processes were performed to obtain purified Shenmai polysaccharides.

TABLE 3 Regression coefficients for three dependent variables.

Regression coefficients	p
X_1	0.00077 ^c
X_2	0.00119 ^b
X_3	0.00461 ^b
$X_1 * X_1$	0.03764 ^a
$X_1 * X_2$	0.01440 ^a
$X_1 * X_3$	0.04273 ^a
$X_2 * X_2$	0.16370
$X_2 * X_3$	0.01269 ^a
$X_3 * X_3$	0.03764 ^a

X_1 , extraction temperature; X_2 , S/M ratio; X_3 , extraction time.

^aSignificant at 0.05 level.

^bSignificant at 0.01 level.

^cSignificant at 0.001 level.

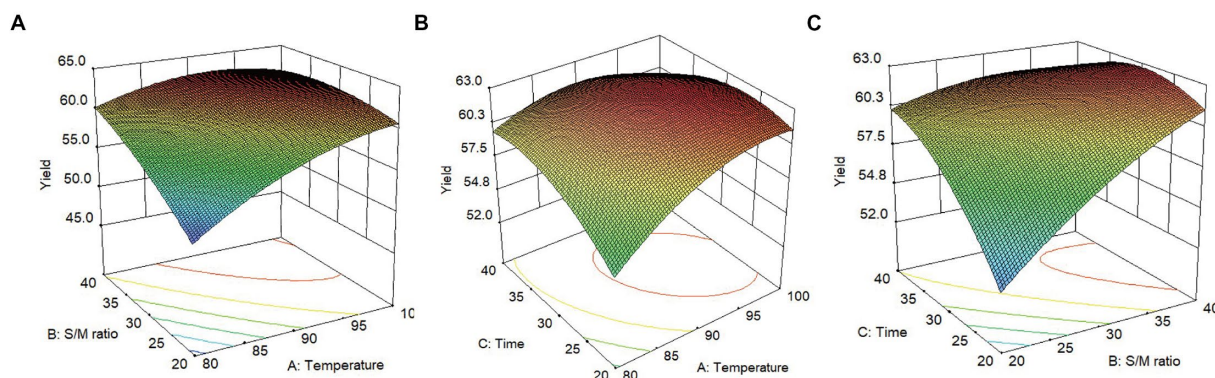
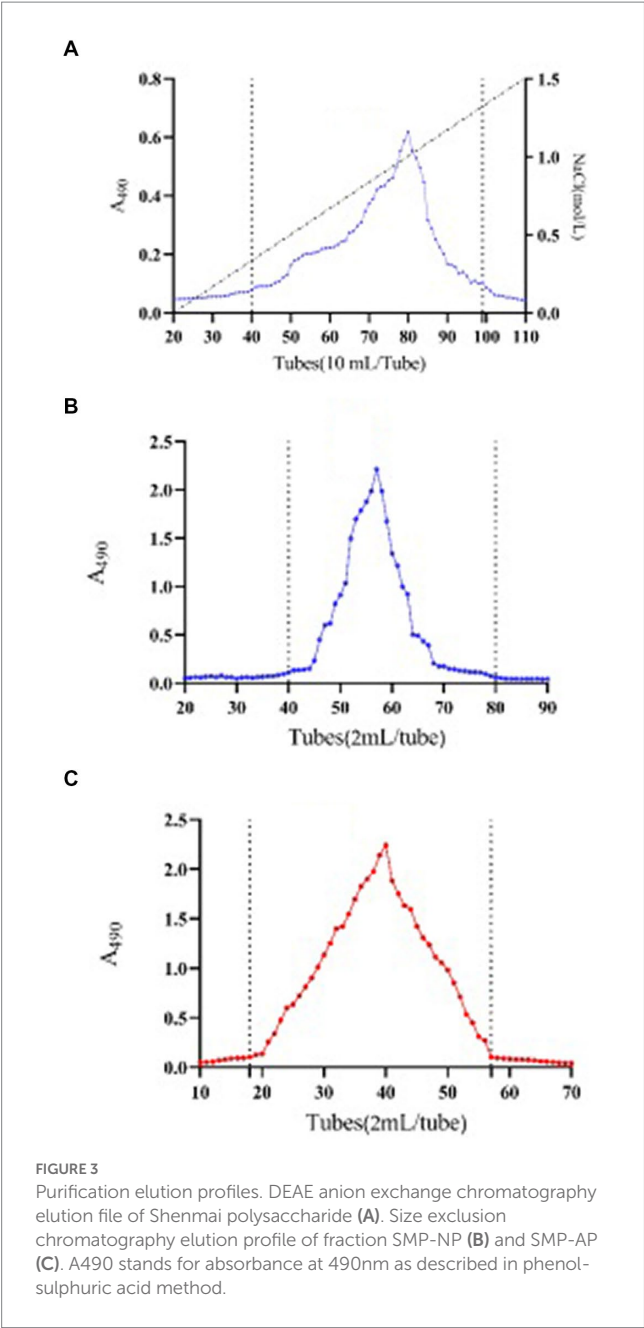


FIGURE 2

Effect of three factors interacting on the extraction yield of Shenmai polysaccharide (left, response surface plots; right, contour plots); (A) effect of extraction temperature (X_1) and solvent-material ratio (X_2) on the yield of Shenmai polysaccharide; (B) effect of extraction temperature (X_1) and extraction time (X_3) on the yield of Shenmai polysaccharides; (C) effect of solvent-material ratio (X_2) and extraction time (X_3) on the yield of Shenmai polysaccharides.



3.3. Purification of polysaccharide

The neutral polysaccharide of SMP was eluted by distilled water. 238.8 mg of neutral polysaccharide fraction was obtained from 310.7 mg of crude SMP, named SMP-NP. An acidic polysaccharide fraction with a mass of 15.63 mg was collected by DEAE anion exchange chromatography, named SMP-AP (Figure 3A). This data indicated that neutral polysaccharides (yield 76.86%) account for the majority of the SMP. To obtain the purified polysaccharide fraction, gel filtration was performed. One fraction was obtained with symmetrical and uniform curves for both SMP-NP (Figure 3B) and SMP-AP (Figure 3C), indicating that these two polysaccharides are homogeneous components.

TABLE 4 Monosaccharide composition determination results of SMP-NP and SMP-AP.

Sample	Monosaccharide composition	Mol %
SMP-NP	Glc	10.1
	Fru	89.9
SMP-AP	Glc	95.0
	Gal	2.0
	GalA	1.6
	Rha	0.8
	Ara	0.5

TABLE 5 Glycosidic linkage units of SMP-NP.

Monosaccharides	Glycosidic bond	Mol %
Fru	T-Fruf	8.5
	1,2-Fruf	53.0
	1,2,6-Fruf	27.4
Glc	T-Glcp	1.6
	1,4-Glcp	8.8
	1,6-Glcp	0.7

3.4. Molecular weight and monosaccharide composition determination

The molecular weight of the SMP-NP and SMP-AP were determined by size exclusion chromatography. The results showed that the molecular weight of SMP-NP and SMP-AP were 30.8 kDa and 256.7 kDa, respectively.

The results of the monosaccharide composition determination of these two polysaccharide components are shown in Table 4. There are two monosaccharide components in SMP-NP, glucose, and fructose. It has a glucose content of 10.1%, and the molar ratio of fructose to glucose is about 9:1. SMP-AP consists of five monosaccharide components: glucose, galactose, galacturonic acid, rhamnose, and arabinose. It has a molar ratio of 95:2.0:1.6:0.8:0.5.

3.5. Determination of glycosidic linkage

3.5.1. Glycosidic linkage units of SMP-NP

The results of the glycosidic linkage determination of SMP-NP are shown in Table 5. SMP-NP is mainly composed of Fru and Glc, which is consistent with the results of monosaccharide composition determination. The linkage units in Fru are mainly 1,2-Fruf and 1,2,6-Fruf, and these have a molar ratio of 53.0% and 27.4%, respectively. In addition, terminal Fruf is also presented in SMP-NP and has a molar ratio of 8.5%. The linkage units in Glc are 1,4-Glcp, 1,6-Glcp, and terminal Glcp. These contain a molar ratio of 8.8%, 0.6%, and 1.6%, respectively.

3.5.2. Glycosidic linkage units of SMP-AP

The glycosidic linkage unit determination results of SMP-AP are shown in Table 6. SMP-AP is composed of 1,4-GalAp and 1,4-Galp

TABLE 6 Glycosidic linkage units of SMP-AP.

Monosaccharides	Glycosidic units	Mol %
Rha	1,2-Rhap	1.9
	1,2,4-Rhap	7.4
Glc	T-Araf	6.1
	1,5-Araf	0.9
GalA	T-GalAp	1.5
	1,4-GalAp	51.1
Glc	1,3-Glcp	0.94
Gal	1,4-Galp	8.6

linked units, and these have a molar ratio accounting for 51.1% and 8.6%, respectively. Rha in SMP-AP contains the linkage units 1,2-Rhap and 1,2, 4-Rhap, which have a molar ratio of 1.9% and 7.4%, respectively. At the same time, Ara in SMP-AP also showed two kinds of glycosidic units. T-Araf was the main linkage unit and had a molar ratio of 6.1%. In addition to this, the Glc in SMP-AP is mainly connected by 1,3-Glcp.

3.6. NMR analysis

3.6.1. NMR analysis of SMP-NP

The ^1H spectrum of SMP-NP is shown in Figure 4A, and the ^{13}C NMR spectrum is shown in Figure 4B. ^{13}C -NMR results show that the carbon signal concentrated in δ 102–104 ppm assigned itself to the C-2 signal peak of the Fruf residue. Three of the most obvious signal peaks were δ 103.79, δ 103.65, and δ 103.17 ppm. According to previous reports, the heterocephalic carbon signals are δ 62.63 ppm, δ 60.50 ppm, and δ 60.40 ppm, respectively. The corresponding proton signals are δ 3.85, δ 3.84, and δ 3.66 ppm, respectively. This indicates that the three Fruf residues in SMP-NP are β -configuration (18–20). The heterocephalic carbon signals concentrated in δ 92–101 ppm should be attributed to Glc residues. The heterocephalic carbon signals of the three signal peaks were δ 92.13, 98.04, and 99.58 ppm, respectively. Combined with the results of ^1H spectrum, which has the H-1 signals at δ 5.27, 5.31, and 5.13 ppm, respectively, the three residues proved to be α -D-Glcp configuration (21–29). The specific chemical shifts of ^1H and ^{13}C of the above sugar residues are shown in Table 7. Based on the results of all the above SMP-NP structures, SMP-NP seemed to be a mixed fructan composed of Fru and Glc. 1,2- β -D-Fruf, 1,2,6- β -D-Fruf, and T- β -D-Fruf were its main backbone and are connected with the α -D-(1 \rightarrow 4)-Glcp, α -D-(1 \rightarrow 6)-Glcp and T-Glcp residues.

3.6.2. NMR analysis of SMP-AP

The ^1H spectrum of SMP-AP is shown in Figure 5A, and the ^{13}C spectrum is shown in Figure 5B. The signals of δ 17.69 ppm and δ 94.89 ppm in ^{13}C -NMR spectra were assigned to C-6 and C-2 of Rhap. The signals of δ 1.31 ppm and δ 5.30 ppm were assigned to H-6 and H-2 of Rhap. Taken together, those results indicated the presence of α -1,2-Rhap in SMP-AP (30, 31). The signals δ 170–173.55 ppm were assigned to C-6 of carboxyl signal peaks. This indicated that SMP-AP contains GalpA residues. The chemical shift of H-1 was δ 4.57 ppm, and the chemical shift of C-1 was δ 98.76 ppm. This suggested that the residue is α -D-GalAp. In addition, ^{13}C -NMR results showed that the H-1 proton signals of Ara were mainly concentrated around δ

5.0–5.25 ppm, while the C-1 carbon signals were mainly concentrated around δ 107–112 ppm (31–37). According to the literature, the signal at δ 5.14 ppm was assigned to H-1 of α -D-Galp, and the C-1 carbon signal of this residue was at δ 102.01 ppm (38).

Based on the above structural analysis of SMP-AP, the main backbone of SMP-AP was α -(1 \rightarrow 3)-Glcp, which is a typical glucan structure. At the same time, α -(1 \rightarrow 4)-GalA and α -L-(1 \rightarrow 4)-Rhap are on the main chain of SMP-AP, which is a typical RG-I pectin structure. In addition, there were Araf and Galp residues on the 2nd position of Rhap as branch chain connections. So, we speculated that there were a few arabinogalactan residues in SMP-AP. We concluded that SMP-AP is an acidic polysaccharide composed of glucan and RG-I pectin that has a small amount of arabinogalactan linked to it as branched chains (39).

3.7. Prebiotic activity

Five *Lactobacilli* strains were cultured in a medium with different carbon sources, and their density was evaluated after 48 h. As shown in Table 8, the bacterial density and the bacterial density increment of the SMP-NP group were significantly higher than those in the saline group ($p < 0.05$). This indicated that five different *Lactobacilli* strains can ferment and utilize SMP-NP as a carbon source to support their proliferation *in vitro*. We then compared this with Orafit®HP (DPn \geq 23). When p95s (DPn 2–9) was used as a carbon source, four *Lactobacilli* strains showed better growth and greater changes in bacterial density. This suggested that P95s were an easily used carbon source for these four different *Lactobacilli* strains. The effect of SMP-NP on the proliferation of the five different *Lactobacilli* strains was similar to that of P95s.

A vertical comparison of five different *Lactobacilli* strains showed that SMP-NP could promote the proliferation of five different *Lactobacilli* strains *in vitro*, but the extent to which the five *Lactobacilli* strains used SMP-NP was different. The greatest fermentation utilization rate of SMP-NP was by *L. johnsonii* BS15, and its bacterial density changed the most after 48 h of fermentation, reaching 30 times that of the saline group ($p < 0.05$). The utilization rate of SMP-NP by *L. plantarum* BS10 was also very good, and its bacterial density reached 16.5 times that of the saline group after 48 h of fermentation. *L. buchneri* BSS1 utilization rate was relatively poor, and the bacterial density after 48 h was about twice that of the saline group.

As shown in Table 9, five different strains of *Lactobacilli* were cultured in an anaerobic environment and they each displayed different pH values in the culture medium. The pH values of the five media supplemented with SMP-NP decreased in varying degrees. In addition, the pH values of the media supplemented with MRS were significantly decreased. However, in the medium supplemented with SMP-NP, there was no significant difference in the degree of pH reduction among the five *Lactobacilli* strains. The decrease in pH was due to the metabolites produced by *Lactobacilli*, such as lactic acid, acetic acid, and other types of short fatty acids. The increase in bacterial density and lower pH indicated the growth of probiotics and the effective use of SMP-NP.

3.8. Anti-oxidant activity

To evaluate the antioxidant effect of SMP-AP on intestinal epithelial cells, a porcine jejunal epithelial cell line (IPEC-J2) treated



Further biochemistry measurements showed that in the group supplement with SMP-AP, total antioxidant capacity (T-AOC), glutathione peroxidase activity (GSH-Px) and superoxide dismutase

TABLE 7 ^{13}C and ^1H chemical shifts (ppm) of polysaccharide fraction SMP-NP.

Residues	C-1/H-1	C-2/H-2	C-3/H-3	C-4/H-4	C-5/H-5	C-6/H-6
1 \rightarrow 2- β -D-Fruf	62.63/3.85	103.17	76.49/4.27	74.63/4.14	81.05/3.88	63.85/3.85
1,2,6- β -D-Fruf	60.50/3.84	103.65	76.72/4.14	75.02/4.09	80.97/3.61	62.34/3.74
T- β -D-Fruf	60.40/3.66	103.79	76.71/4.09	74.67/4.01	81.16/3.76	63.33/3.58
1 \rightarrow 4- α -D-Glcp	99.58/5.31	74.63/3.56	74.41/4.01	80.20/3.70	71.14/4.29	60.4/3.85
1 \rightarrow 6- α -D-Glcp	98.04/5.13	71.50/3.61	74.41/3.76	69.64/3.58	69.17/3.96	63.95/3.92
T- α -D-Glcp	92.13/5.27	71.14/3.45	73.21/3.76	74.34/3.89	74.63/3.74	60.72/3.66

activity (SOD) increased. However, lipid oxidation products—MDA decreased, indicating that the protective effect of SMP-AP on oxidative stress may be due to it mediating the cellular antioxidant defense of IPEC-J2 cells (Figures 6B–E). To analyze the regulatory mechanisms of SMA-AP in cellular antioxidant defense, we quantified the expressions of genes associated with these processes. First, we noted that in H_2O_2 -treated IPEC-J2 cells supplied with SMA-AP, expressions of some critical antioxidant genes were significantly increased (Figures 6C,F–I). These include antioxidant genes like catalase (CAT), glutathione peroxidase (GPX) and superoxidase dismutase (SOD), NQO-1. We concluded that this expression increase was responsible for increased cellular antioxidant defense activity. Secondly, we quantified the expression of the key transcriptional factor –Nrf2, a direct regulator of these antioxidant genes. In doing so, we found that SMA-AP could also enhance the expression of Nrf2 in H_2O_2 -treated IPEC-J2 cells (Figure 6J). In summary, our results indicated that SMA-AP could be used as an effective component to treat oxidative stress-related defects by regulating cellular antioxidant defense.

4. Discussion

4.1. Optimization of extraction process of polysaccharide from Shenmai injection waste by response surface methodology

Panax ginseng and *O. japonicus* are both traditional Chinese medicinal materials. Polysaccharide is one of the main active components of these two herbs and has been researched before. However, only a few studies focused on extracting SMP from the waste of the Shenmai injection. Through the optimal extraction conditions, 62.72% polysaccharide was obtained in this study. This proved that there were a large number of polysaccharide components in the production waste of the Shenmai injection, which needed further development and utilization.

Polysaccharide is a natural product and is supplied by several sources. Naturally, the technology used to extract it has always been the focus of research. Recently, there have been many reports on the extraction technology of polysaccharides from *P. ginseng* or *O. japonicus*. A study was conducted to investigate the effects of temperature, solid-material ratio, and extraction time on the yield of *P. ginseng* (40). The results showed that the optimal extraction process was as follows: the liquid–solid ratio was 12:1, the extraction time was 3.5 h, the extraction temperature was 100°C, and it was extracted twice, the yield of polysaccharides from *P. ginseng* reached 22% under these conditions. However, another study showed that the optimal

extraction process was when the ratio of material to liquid was 1:8, water bath extraction was used 3 times at 100°C and for 3 h each time (41). And yet, another study had optimum extraction conditions that put the extraction temperature at 100°C, extraction time at 4 h, and the liquid–solid ratio at 15:1 (42). In our study, the optimal extraction temperature of SMP was 93°C, the extraction time was 27.94 min, and the ratio of solvent to the material was 40 mL/g. These large differences in optimization may be due to different material treatment methods. Most of the Chinese medicinal materials in the other studies were extracted by direct shearing, while in our study, the two medicinal materials were ground into powder for extraction. Many studies have shown that the effective components in plant cells can be dissolved only after infiltration, swelling, more infiltration, and then diffusion. However, the pulverization of medicinal materials can significantly improve the wall-breaking rate of plant cells, thereby improving the dissolution of effective components (43, 44). This is likely the reason why we were able to have a high extraction rate of SMP in a short amount of time in this study. On a different note, other studies showed that the optimal water extraction process of *O. japonicus* polysaccharide was to extract twice at 100°C for 2 h each time and to keep a liquid to material ratio of 6:1. The order of factors affecting the water extraction of *O. japonicus* polysaccharide was said to be: extraction time > extraction temperature > ratio of liquid to material > extraction times (45). However, the results of this study showed that the most influential factors on the polysaccharide were extraction temperature, extraction time, and then the ratio of solvent to material. The above differences may have been caused by the variety of medicinal materials, harvest time, and polysaccharide content (46). Additionally, there are significant differences in the extraction rate and polysaccharide content of different herb medicines, so the combined extraction of red *P. ginseng* and *O. japonicus* may also be the reason for the differences in the extraction process between studies.

4.2. Isolation, purification, and structure elucidation of Shenmai polysaccharide

The structure of polysaccharides is closely related to biological activity. Polysaccharides with different structures have different pharmacological activities. The molecular weight is related to the advanced structures formed by the polysaccharides. Polysaccharide GRS1-I with a molecular weight of 4.611 kDa was obtained from *P. ginseng* by the method of amylase and alcohol precipitation (47). But another polysaccharide, this one with a molecular weight of 1.5 kDa, was obtained from *P. ginseng* by ethanol precipitation at different concentrations (41). The molecular weights of those two



polysaccharide fraction named, PGPW1, was isolated from *P. ginseng* with a Mw of 350kDa. This was higher than other reported *P. ginseng* polysaccharides (48). Regarding the

TABLE 8 Capacity to ferment SMP-NP or commercial prebiotics by *Lactobacilli* strains.

<i>Lactobacillus</i> strain	P95s	Orafti®HP	SMP-NP	Glc	Saline	MRS
<i>L. plantarum</i> X3	0.38 ± 0.03 ^{CB}	0.22 ± 0.06 ^{DC}	0.42 ± 0.07 ^{AB}	0.48 ± 0.02 ^{EB}	0.12 ± 0.00 ^{BD}	1.94 ± 0.03 ^{AA}
<i>L. johnsonii</i> BS15	0.59 ± 0.01 ^{BC}	0.63 ± 0.05 ^{BC}	0.6 ± 0.06 ^{CC}	0.83 ± 0.00 ^{BB}	0.02 ± 0.00 ^{DD}	1.44 ± 0.02 ^{DA}
<i>L. plantarum</i> BS10	0.59 ± 0.03 ^{BC}	0.35 ± 0.02 ^{CD}	0.66 ± 0.01 ^{BC}	1.1 ± 0.00 ^{AB}	0.04 ± 0.00 ^{DE}	1.86 ± 0.03 ^{BA}
<i>L. buchneri</i> BSS1	0.18 ± 0.00 ^{DC}	0.13 ± 0.00 ^{CC}	0.17 ± 0.00 ^{CC}	0.73 ± 0.01 ^{CB}	0.07 ± 0.01 ^{CD}	1.93 ± 0.03 ^{AA}
<i>L. rhamnosus</i> lgg	0.73 ± 0.12 ^{AB}	0.69 ± 0.03 ^{AB}	0.77 ± 0.04 ^{AB}	0.6 ± 0.05 ^{DC}	0.22 ± 0.07 ^{AD}	1.97 ± 0.00 ^{AA}

TABLE 9 The final pH of medium containing SMP-NP or commercially prebiotics by *Lactobacilli* strains.

<i>Lactobacillus</i> strain	P95s	Orafti®HP	SMP-NP	Glc	Saline	MRS
<i>L. plantarum</i> X3	5.4 ± 0.00 ^{BB}	5.93 ± 0.06 ^{AA}	5.3 ± 0.00 ^{BB}	5 ± 0.00 ^{BB}	6.2 ± 0.00 ^{BA}	4.5 ± 0.10 ^{CC}
<i>L. johnsonii</i> BS15	5.4 ± 0.00 ^{BB}	5.33 ± 0.06 ^{DB}	5.17 ± 0.06 ^{BB}	5 ± 0.10 ^{BB}	6.17 ± 0.06 ^{BA}	4.33 ± 0.15 ^{CC}
<i>L. plantarum</i> BS10	5.37 ± 0.06 ^{CB}	5.63 ± 0.06 ^{CB}	5.33 ± 0.12 ^{BB}	4.87 ± 0.06 ^C	6.27 ± 0.06 ^{ABA}	4.53 ± 0.06 ^{BC}
<i>L. buchneri</i> BSS1	5.62 ± 0.06 ^{AB}	5.67 ± 0.06 ^{CB}	5.67 ± 0.15 ^{AB}	5.43 ± 0.06 ^{AB}	6.33 ± 0.06 ^{AA}	5 ± 0.10 ^{CC}
<i>L. rhamnosus</i> lgg	5.2 ± 0.17 ^{DC}	5.77 ± 0.12 ^{BB}	5.7 ± 0.00 ^{AB}	5.33 ± 0.06 ^{AC}	6.3 ± 0.00 ^{AA}	4.87 ± 0.06 ^{AD}

polysaccharides from *O. japonicus*, there were several studies reported, such as MD-1, MD-2, OJP1, and OJP1 ~ 4 that had *Mw* ranging from 2.70 kDa to 324.65 kDa (28, 47). These polysaccharides were significantly different from the *Mw* of the two polysaccharide fractions obtained in the present study. This may be because the polysaccharides obtained in our study were isolated from a mixture of *P. ginseng* and *O. japonicus* rather than from a single plant.

Studies have shown that the polysaccharides in Chinese patent medicine may come from a single medicine and that new polysaccharides may be produced during the extraction process. Our results showed that the molar ratio of Fru and Glc was 35:1 and that the main connection between Fru was 2 → 1 or 2 → 6, which was very similar to the SMP-NP structure. Several studies were able to obtain a similar structure of polysaccharides from *O. japonicus*, but the molar ratio of Fru to Glc were 30:1 (49), 15:1 (50) and 12:1 (51). WGPA-N and WGP-N are neutral polysaccharides in *P. ginseng* that were eluted by distilled water (52). The study found that those two neutral polysaccharides were composed of Glc, Gal, and Ara. The study also found that the molar ratio of these three monosaccharides was 3.3:95.3:1.3 and 18.0:66.3:15.7, respectively. Glc was mainly connected as 1 → 4 or 1 → 6, which was similar to how Glc connected in SMP-NP. Two other researchers extracted two neutral polysaccharides from *P. ginseng*, using different methods (40), and found that those neutral polysaccharides not only contained Glc, Gal, and Ara but also held a small amount of mannose. The main linkage units of Glc were 1 → 4 linked Glc, with a small amount of 1 → 6 linked Glc, and the results were similar to SMP-NP. In summary, Fru in SMP-NP may come mainly from *O. japonicus*, while Glc may come mainly from *P. ginseng*. Some studies have shown that when the production process of polysaccharides is different, some polysaccharide components may change. These changes include things like losing a monosaccharide component or having inconsistent molar ratios of the monosaccharide (53). This may be the reason why SMP-NP develops different monosaccharide molar ratios with *P. ginseng* and/or *O. japonicus* between studies.

Acidic polysaccharides are polysaccharides with carboxyl groups. Most of the acidic polysaccharides that came from *P. ginseng* are pectic polysaccharides. Fewer studies reported acidic polysaccharides coming from *O. japonicus*. SMP-AP is an acidic polysaccharide composed of GalA, Gal, Ara, Glc, and Rha. This is very similar to the structure of the *P. ginseng* acidic polysaccharide that has been previously published (54–56). It shows that in the acidic polysaccharide S-A-I from *P. ginseng*, with a Gal residue connected by 1 → 6 Gal and further connected by 1 → 5 or 1 → 3, five Ara and GalA residues were presented as 1 → 4 linked GalA. This is very similar to how the monosaccharides in SMP-AP are connected. The difference is that these *P. ginseng* acidic polysaccharides do not contain Glc. The results of the structural elucidation of WRGP indicated that the main component of WRGP was RG-I pectin and that it contained more of the AG type side chain. However, unlike SMP-AP, WRGP also contained mannose. When isolated from *P. ginseng*, GPW-1, and GPW-2 have monosaccharide compositions similar to those of SMP-AP (54). Another study showed that all six acidic pectins from *P. ginseng* have glycosidic linkages. This is also similar to SMP-AP (57). Therefore, due to the similarity of glycosidic linkages and monosaccharide compositions, it is possible that the acidic polysaccharide of Shenmai injection waste mainly comes from *P. ginseng*. However, SMP-AP and the above-mentioned pectin showed different monosaccharide compositions and molar ratios. This may be due to the differences in materials, extraction, and purification methods, all of which can lead to changes in the monosaccharide composition.

4.3. Prebiotic activity

Prebiotics refer to organic substances that are not digested and absorbed by the host. Instead, they selectively promote the metabolism and proliferation of beneficial bacteria in the body, thereby improving the host's health (58). Polysaccharides are one of the most common prebiotics. In this study, the density of multiple

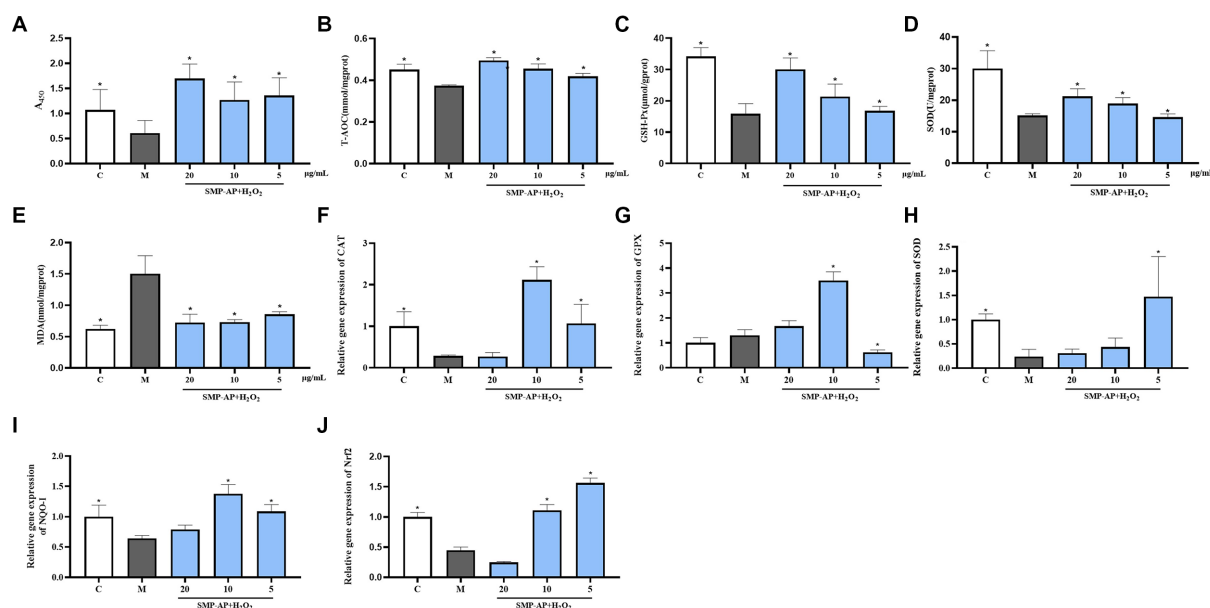


FIGURE 6

SMP-AP promote antioxidant defense of IPEC-J2 cells. (A) Quantification illustrates the cell viability of cells treated with 200 µmol/mL H₂O₂ for 24h and then with different concentrations of SMP-AP for 24h. (B) Quantification illustrates the level of T-AOC. (C–E) Quantification illustrates the activity of GSH-Px, SOD and the level of MDA. (F–J) qRT-PCR illustrates mRNA levels of CAT, GPX, SOD, NQO1 and Nrf2 in IPEC-J2 cells.

strains of *Lactobacilli* was measured after 48 h of incubation. The degree of proliferation over 48 h reflected the degree of carbon source utilization. The results showed that five different *Lactobacilli* strains could ferment and utilize SMP-NP as a carbon source. This increased bacterial density, indicating that SMP-NP could promote the proliferation of these five different *Lactobacilli* strains *in vitro*. At the same time, as the density of bacteria increased, their metabolites increased, such as lactic acid and acetic acid (59, 60). This resulted in a decrease in the pH of the culture medium. After measuring the pH values of different *Lactobacilli* strains cultured on different media, it was found that the medium supplement with SMP-NP could get a pH value much lower than the saline group. In summary, SMP-NP can promote the proliferation of five *Lactobacillus* strains and reduce the pH of the culture medium, meaning it has potential prebiotic activity.

4.4. Anti-oxidant activity

Oxidative stress and disruption of the intracellular redox balance have been identified as the key potential factors in the progression of animal diseases (61). With this in mind, SOD and CAT are important antioxidant enzymes. SOD plays a crucial role in balancing oxidative and antioxidant effects. It is a free radical scavenger that can scavenge superoxide anion radicals. Additionally, the high and low viability of SOD indirectly reflects the body's ability to scavenge free radicals (62). CAT is a ubiquitous enzyme that efficiently promotes the decomposition of H₂O₂ into H₂O and O₂ to prevent cellular oxidative damage (63, 64). MDA is the final product of these oxygen-free radicals' lipid peroxidation (65). The level of MDA content indirectly reflects the severity of the free radicals attacks on body cells.

In the past several decades, numerous natural polysaccharides and fructans have been shown to have significant antioxidant activity using different evaluation methods (60). Our results indicated that SMP-AP exhibited significant antioxidant activity. The SMP used in this study were extracted from a combination of red *P. ginseng* and *O. japonicus*. However, numerous studies have shown that *P. ginseng* polysaccharides can significantly increase the levels of the antioxidant enzymes SOD, CAT, and GPX-Px, as well as the non-enzymatic compound reduced glutathione (GSH). These studies also showed that *P. ginseng* polysaccharides can decrease malondialdehyde (MDA) levels against oxidative stress (66). The Shengmai injection was also investigated and had similar antioxidant activity, which was consistent with our study (67). However, the mechanism of the antioxidant activity of polysaccharides is still unknown, which need further study in future.

5. Conclusion

In this study, the optimal extraction conditions for crude polysaccharides from Shemmai injection waste were obtained by RSM. When the extraction temperature was at 93°C, the ratio of solvent to material was 40 mL/g, and the extraction time was 30 min, the maximum yield of SMP was 62.72%. After purification, a neutral fraction (SMP-NP) and an acidic fraction (SMP-AP) were obtained. The neutral fraction was a levan, and the acidic fraction was a pectic polysaccharide. SMP-NP could be fermented by five strains of *Lactobacillus*. It was able to reduce the pH of the culture medium, and it may be a potential prebiotic. The acidic polysaccharide SMP-AP exhibited potential antioxidant activity *in vitro*. All these results

suggested that, due to its polysaccharides, Shemmai injection waste could be used to develop potential prebiotics and anti-oxidants.

Data availability statement

The original contributions presented in the study are included in the article/supplementary material, further inquiries can be directed to the corresponding author.

Author contributions

JK and Z-KZ: conceptualization, methodology, validation, and investigation. JZ: software. Z-KZ: formal analysis and writing—original draft preparation. L-XL: resources. JK and JZ: data curation. JZ, L-FH, and M-LT: writing—review and editing. JK: visualization. L-XL and M-LT: supervision, project administration, and funding acquisition. All authors contributed to the article and approved the submitted version.

Funding

This study was funded by National Natural Science Foundation of China, grant number 82004041.

References

- Shi L, Xie Y, Liao X, Chai Y, Luo Y. Shenmai injection as an adjuvant treatment for chronic cor pulmonale heart failure: a systematic review and meta-analysis of randomized controlled trials. *BMC Complement Altern Med.* (2015) 15:418. doi: 10.1186/s12906-015-0939-2
- Xian S, Yang Z, Lee J, Jiang Z, Ye X, Luo L, et al. A randomized, double-blind, multicenter, placebo-controlled clinical study on the efficacy and safety of Shenmai injection in patients with chronic heart failure. *J Ethnopharmacol.* (2016) 186:136–42. doi: 10.1016/j.jep.2016.03.066
- Xiaohui F, Yi W, Yiyu C. LC/MS fingerprinting of Shenmai injection: a novel approach to quality control of herbal medicines. *J Pharm Biomed Anal.* (2006) 40:591–7. doi: 10.1016/j.jpba.2005.10.036
- Haijiang Z, Yongjiang W, Yiyu C. Analysis of 'SHENMAI' injection by HPLC/MS/MS. *J Pharm Biomed Anal.* (2003) 31:175–83. doi: 10.1016/s0731-7085(02)00565-4
- Guo M, Shao S, Wang D, Zhao D, Wang M. Recent progress in polysaccharides from *Panax ginseng* C. A. Meyer. *Food Funct.* (2021) 12:494–518. doi: 10.1039/d0fo01896a
- Kang S, Min H. Ginseng, the 'immunity boost': the effects of *Panax ginseng* on immune system. *J Ginseng Res.* (2012) 36:354–68. doi: 10.5142/jgr.2012.36.4.354
- Zheng Q, Feng Y, Xu DS, Lin X, Chen YZ. Influence of sulfation on anti-myocardial ischemic activity of *Ophiopogon japonicus* polysaccharide. *J Asian Nat Prod Res.* (2009) 11:306–21. doi: 10.1080/10286020902727363
- Chen MH, Chen XJ, Wang M, Lin LG, Wang YT. *Ophiopogon japonicus*—a phytochemical, ethnomedicinal and pharmacological review. *J Ethnopharmacol.* (2016) 181:193–213. doi: 10.1016/j.jep.2016.01.037
- Xu J, Wang Y, Xu DS, Ruan KF, Feng Y, Wang S. Hypoglycemic effects of MDG-1, a polysaccharide derived from *Ophiopogon japonicus*, in the Ob/Ob mouse model of type 2 diabetes mellitus. *Int J Biol Macromol.* (2011) 49:657–62. doi: 10.1016/j.ijbiomac.2011.06.026
- Xu J, Wei C. Optimization of extraction process of crude polysaccharides from wild edible bachu mushroom by response surface methodology. *Carbohydr Polym.* (2008) 72:67–74. doi: 10.1016/j.carbpol.2007.07.034
- Fu YP, Li LX, Zhang BZ, Paulsen BS, Yin ZQ, Huang C, et al. Characterization and prebiotic activity in vitro of inulin-type fructan from *Codonopsis pilosula* roots. *Carbohydr Polym.* (2018) 193:212–20. doi: 10.1016/j.carbpol.2018.03.065
- Kang C, Zhang L, Hao L, Ge H, Xu M, Cao J, et al. Response surface methodology optimization extraction of polysaccharides from maca (*Lepidium meyenii*) leaves and primary characterization In: H Liu, C Song and A Ram, editors. *Advances in applied biotechnology*. Singapore: Springer (2016)
- Zou Y, Chen X, Yang W, Liu S. Response surface methodology for optimization of the ultrasonic extraction of polysaccharides from *Codonopsis pilosula* Nannf. Var. *modesta* L.T.Shen. *Carbohydr Polym.* (2011) 84:503–8. doi: 10.1016/j.carbpol.2010.12.013
- Huang C, Cao X, Chen X, Fu Y, Zhu Y, Chen Z, et al. A pectic polysaccharide from *Ligusticum chuanxiong* promotes intestine antioxidant defense in aged mice. *Carbohydr Polym.* (2017) 174:915–22. doi: 10.1016/j.carbpol.2017.06.122
- Dedonder R. The glucides of the Jerusalem artichoke. I. Evidence of a series of glucofructosanes in the tubers; the isolation, analysis and structure of the least polymerized members of the series. *Bull Soc Chim Biol.* (1952) 34:144–56.
- Austarheim I, Mahamane H, Sanogo R, Togola A, Khaledabadi M, Vestreheim AC, et al. Anti-ulcer polysaccharides from *Cola cordifolia* bark and leaves. *J Ethnopharmacol.* (2012) 143:221–7. doi: 10.1016/j.jep.2012.06.027
- Huang C, Zhu Z, Cao X, Chen X, Fu Y, Chen Z, et al. A pectic polysaccharide from *Sijunzi* decoction promotes the antioxidant defenses of SW480 cells. *Molecules.* (2017) 22:1341. doi: 10.3390/molecules22081341
- Cérantola S, Kervarec N, Pichon R, Magné C, Bessieres MA, Deslandes E. NMR characterisation of inulin-type fructooligosaccharides as the major water-soluble carbohydrates from *Matricaria maritima* (L.). *Carbohydr Res.* (2004) 339:2445–9. doi: 10.1016/j.carres.2004.07.020
- Chen J, Cheong K, Song Z, Shi Y, Huang X. Structure and protective effect on UVB-induced keratinocyte damage of fructan from white garlic. *Carbohydr Polym.* (2013) 92:200–5. doi: 10.1016/j.carbpol.2012.09.068
- Xu DS, Feng Y, Zhou YH, Zhang XC, Deng HL. Active components of polysaccharide of *Ophiopogon japonicus* on acute myocardial ischemia. *Chin Tradit Pat Med.* (2004) 26:832–837. doi: 10.3969/j.issn.1001-1528.2004.10.018
- Chen Y, Li XH, Zhou LY, Li W, Lu YM. Structural elucidation of three antioxidative polysaccharides from *Tricholoma lobayense*. *Carbohydr Polym.* (2016) 157:484–92. doi: 10.1016/j.carbpol.2016.10.011
- Ganeshapillai J, Vinogradov E, Rousseau J, Weese JS, Monteiro MA. *Clostridium difficile* cell-surface polysaccharides composed of pentaglycosyl and hexaglycosyl phosphate repeating units. *Carbohydr Res.* (2008) 343:703–10. doi: 10.1016/j.carres.2008.01.002
- Isurd O, Zgheel F, Elghazoun M, Elmabruk M, Kermagi A, Kennedy JF, et al. A novel (1→4)- α -D-glucan isolated from the fruits of *Opuntia ficus indica* (L.) Miller. *Carbohydr Polym.* (2010) 82:848–53. doi: 10.1016/j.carbpol.2010.06.006
- Ma JS, Liu H, Han CR, Zeng SJ, He HJ. Extraction, characterization and antioxidant activity of polysaccharide from *Pouteria campechiana* seed. *Carbohydr Polym.* (2019) 229:115409. doi: 10.1016/j.carbpol.2019.115409

Acknowledgments

The authors are indebted to Suthajini Yogarajah, Department of Pharmaceutical Chemistry, University of Oslo, for the methanolysis and recording of the GC–MS experiments in the determination of glycosidic linkages. The authors also acknowledge the support from Featured Medicinal Plants Sharing and Service Platform of Sichuan Province.

Conflict of interest

The authors declare that the research was conducted in the absence of any commercial or financial relationships that could be construed as a potential conflict of interest.

Publisher's note

All claims expressed in this article are solely those of the authors and do not necessarily represent those of their affiliated organizations, or those of the publisher, the editors and the reviewers. Any product that may be evaluated in this article, or claim that may be made by its manufacturer, is not guaranteed or endorsed by the publisher.

25. Meng FY, Ning YL, Qi J, He Z, Jie J, Lin JJ, et al. Structure and antitumor and immunomodulatory activities of a water-soluble polysaccharide from *Dimocarpus longan* pulp. *Int J Mol Sci.* (2014) 15:5140–62. doi: 10.3390/ijms15035140
26. Peter S, Per-Erik J, Widmalm G. Synthesis, NMR spectroscopy and conformational studies of the four anomeric methyl glycosides of the trisaccharide D-Glcp-(1→3)-[D-Glcp-(1→4)]-α-D-Glcp. *J Chem Soc.* (1998) 2:639–48. doi: 10.1039/A707346A
27. Rout D, Mondal S, Chakraborty I, Pramanik M, Islam SS. Chemical analysis of a new (1→3)-, (1→6)-branched glucan from an edible mushroom, *Pleurotus florida*. *Carbohydr Res.* (2005) 340:2533–9. doi: 10.1016/j.carres.2005.08.006
28. Xu Y, Liu G, Yu Z, Song X, Li X, Yang Y, et al. Purification, characterization and antiglycation activity of a novel polysaccharide from black currant. *Food Chem.* (2016) 199:694–701. doi: 10.1016/j.foodchem.2015.12.078
29. Zhu Q, Jiang Y, Lin S, Wen L, Wu D, Zhao M, et al. Structural identification of (1→6)-α-D-glucan, a key responsible for the health benefits of longan, and evaluation of anticancer activity. *Biomacromolecules.* (2013) 14:1999–2003. doi: 10.1021/bm400349y
30. Agrawal PK. NMR-spectroscopy in the structural elucidation of oligosaccharides and glycosides. *Phytochemistry.* (1992) 31:3307–30. doi: 10.1016/0031-9422(92)83678-R
31. Qin Z, Liu HM, Lv TT, Wang XD. Structure, rheological, thermal and antioxidant properties of cell wall polysaccharides from Chinese quince fruits. *Int J Biol Macromol.* (2019) 147:1146–55. doi: 10.1016/j.jbiomac.2019.10.083
32. Chen Y, Mao W, Wang B, Zhou L, Gu Q, Chen Y, et al. Preparation and characterization of an extracellular polysaccharide produced by the deep-sea fungus *Penicillium griseofulvum*. *Bioresour Technol.* (2013) 132:178–81. doi: 10.1016/j.biortech.2012.12.075
33. Czaja J, Jachymek W, Niedziela T, Lugowski C, Kenne L. Structural studies of the O-specific polysaccharide from *Plesiomonas shigelloides* strain CNCTC 113/92. *Eur J Biochem.* (2000) 267:1672–9. doi: 10.1046/j.1432-1327.2000.01161.x
34. Ji X, Yan Y, Hou C, Shi M, Liu Y. Structural characterization of a galacturonic acid-rich polysaccharide from *Ziziphus Jujuba* cv. Muzao. *Int J Biol Macromol.* (2020) 147:844–52. doi: 10.1016/j.jbiomac.2019.09.244
35. Košťálová Z, Hromádková Z. Structural characterisation of polysaccharides from roasted hazelnut skins. *Food Chem.* (2019) 286:179–84. doi: 10.1016/j.foodchem.2019.01.203
36. Liu BZX. Structural features and anti-gastric cancer activity of polysaccharides from stem, root, leaf and flower of cultivated dendrobium huoshanense. *Int J Biol Macromol.* (2020) 143:651–64. doi: 10.1016/j.jbiomac.2019.12.041
37. Yan L, Lei X, Yunzhe C, Ge S, Han J, Wang G, et al. Structural characteristics and anticancer/antioxidant activities of a novel polysaccharide from *Trichoderma kangensis*. *Carbohydr Polym.* (2018) 205:63–71. doi: 10.1016/j.carbpol.2018.09.068
38. Pmac E, Kb D, Aaa C, Hhac E, Rna C, Haaa B, et al. Structural characterization and antioxidant activities of a water soluble polysaccharide isolated from *Glycyrrhiza glabra*. *Int J Biol Macromol.* (2020) 144:751–9. doi: 10.1016/j.jbiomac.2019.11.245
39. Lian Y, Zhu M, Yang B, Wang X, Zeng J, Yang Y, et al. Characterization of a novel polysaccharide from red ginseng and its ameliorative effect on oxidative stress injury in myocardial ischemia. *Chin Med.* (2022) 17:111. doi: 10.1186/s13020-022-00669-6
40. Zhang Y, Wang Q, Zhang S. Optimum technique research on the extraction of lentinan with ethanol subsiding method. *J Qingdao Agric Univ.* (2020) 37:43–46. doi: 10.3969/j.issn.1674-148X.2020.01.008
41. Zhang GR, Dong Y, Zhao Y, Jiang RP, Chen MN, Bing-Feng FU. Study on extraction technology of polysaccharide in red ginseng. *J Ginseng Res.* (2013) 4:6–8. doi: 10.19403/j.cnki.1671-1521.2013.04.002
42. Yan GE, Zheng F, Jing LI, Dai YL, Wang W, Yue H, et al. Study on the optimum extraction process of Ginseng polysaccharide. *J Ginseng Res.* (2016) 5:7–11. doi: 10.19403/j.cnki.1671-1521.2016.05.002
43. Yue DY, Wang Q, Zhang J, Qing WU, Wang YR. Comparative of chemical properties and pharmacodynamics between fine powder and ultra-fine powder of compound Beimu powder. *Chin J Exp Tradit Med Formulae.* (2012) 14, 39–43. doi: 10.13422/j.cnki.syfjx.2012.14.020
44. Zhang J, Chen G, Chu X. Effects of ultramicro pulverization on extracting flavones and polysaccharide from radix puerariae. *China Pharm.* (2008) 17, 45–46. doi: 10.3969/j.issn.1006-4931.2008.10.038
45. Jing LI, Wei-Wei SU, Wang YG, Peng W, Zhong WU, Pei-Bo LI. Extraction conditions optimization of ophiopogonis japonicus polysaccharide using orthogonal experimental design and its hypoglycemic effect. *Guiding J Tradit Chin Med Pharm.* (2017) 24, 52–54. doi: 10.13862/j.cnki.cn43-1446/r.2017.24.019
46. Bai X, Zhao Y, Liu H, Zhu L, Sun M. Content comparative study of total sugar, reducing sugar and soluble polysaccharide in ginseng from different regions. *Chin J Mod Appl Pharm.* (2012) 1, 39–42. doi: 10.13748/j.cnki.issn1007-7693.2012.01.009
47. Li C, Cai J, Geng Y, Wang Z, Li R. Purification, characterization and anticancer activity of a polysaccharide from *Panax ginseng*. *Int J Biol Macromol.* (2012) 51:968–73. doi: 10.1016/j.jbiomac.2012.06.031
48. Zhang X, Liu Z, Zhong C, Pu Y, Yang Z, Bao Y. Structure characteristics and immunomodulatory activities of a polysaccharide RGRP-1b from radix ginseng Rubra. *Int J Biol Macromol.* (2021) 189:980–92. doi: 10.1016/j.jbiomac.2021.08.176
49. Wu X, Dai H, Huang L, Gao X, Tsim K, Tu P. A fructan, from radix ophiopogonis, stimulates the proliferation of cultured lymphocytes: structural and functional analyses. *J Nat Prod.* (2006) 69:1257–60. doi: 10.1021/np060033d
50. Ping HU, Wan-Fang Q, Jun-Wen S, Chi Z, Hong-Yang Z, Min Z, et al. Study on the analysis method of monosaccharide composition in *ophiopogon japonicus* polysaccharides. *Chin J Pharm Anal.* (2013) 33, 50–56. doi: 10.16155/j.0254-1793.2013.01.004
51. Zhang X, Li Y, Bi H, Li X, Ni W, Han H, et al. Total fractionation and characterization of the water-soluble polysaccharides isolated from *Panax ginseng* C. A. Meyer. *Carbohydr Polym.* (2009) 77:544–52. doi: 10.1016/j.carbpol.2009.01.034
52. Zhang LZ, Shen R. Research advance of monosaccharide composition analysis. *Prog Microbiol Immunol.* (2013) 41, 77–81. doi: 10.13309/j.cnki.pmi.2013.01.020
53. Li RQ, Zhang YS. Purification and characterization of *Panax ginseng* C. A. Mey pectin. *Yao Xue Xue Bao.* (1984) 19:764. doi: 10.16438/j.0513-4870.1984.10.009
54. Jiao L, Zhang X, Wang M, Li B, Liu Z, Liu S. Chemical and antihyperglycemic activity changes of ginseng pectin induced by heat processing. *Carbohydr Polym.* (2014) 114:567–73. doi: 10.1016/j.carbpol.2014.08.018
55. Li RQ, Zhang YS. Structural studies of *Panax ginseng* C. A. Mey pectin. *Yao Xue Xue Bao.* (1986) 21:912. doi: 10.16438/j.0513-4870.1986.12.006
56. Liang Z.Y. (1988). An investigation on relation between polysaccharide and protein in *Panax ginseng* pectin. *J Integr Plant Biol.* 30, 396–402.
57. Zheng Y, Yang G, Zhao Z, Guo T, Shi H, Zhou Y, et al. Structural analysis of ginseng polysaccharides extracted by EDTA solution. *RSC Adv.* (2015) 6:2724–30. doi: 10.1039/C5RA22751H
58. Hu YC, Hu JL, Li J, Wang J, Zhang XY, Wu XY, et al. Physicochemical characteristics and biological activities of soluble dietary fibers isolated from the leaves of different quinoa cultivars. *Food Res Int.* (2023) 163:112166. doi: 10.1016/j.foodres.2022.112166
59. Dtw B, Yuan HB, Qin YC, Sw C, Ryga D, Ych A, et al. Effects of molecular weight and degree of branching on microbial fermentation characteristics of okra pectic-polysaccharide and its selective impact on gut microbial composition. *Food Hydrocoll.* (2022) 132:107897. doi: 10.1016/j.foodhyd.2022.107897
60. Wang M, Cheong KL. Preparation, structural characterisation, and bioactivities of fructans: a review. *Molecules.* (2023) 28:1613. doi: 10.3390/molecules28041613
61. Sies H, Berndt C, Jones DP. Oxidative stress. *Annu Rev Biochem.* (2017) 86:715–48. doi: 10.1146/annurev-biochem-061516-045037
62. Cao P, Sun J, Sullivan MA, Huang X, Wang H, Zhang Y, et al. *Angelica sinensis* polysaccharide protects against acetaminophen-induced acute liver injury and cell death by suppressing oxidative stress and hepatic apoptosis in vivo and in vitro. *Int J Biol Macromol.* (2018) 111:1133–9. doi: 10.1016/j.jbiomac.2018.01.139
63. Alfonso-Prieto M, Biarnés X, Vidossich P, Rovira C. The molecular mechanism of the catalase reaction. *J Am Chem Soc.* (2009) 131:11751–61. doi: 10.1021/ja9018572
64. Zhuang C, Wang Y, Zhang Y, Xu N. Oxidative stress in osteoarthritis and antioxidant effect of polysaccharide from *Angelica sinensis*. *Int J Biol Macromol.* (2018) 115:281–6. doi: 10.1016/j.jbiomac.2018.04.083
65. Kin H, Zhao ZQ, Sun HY, Wang NP, Corvera JS, Halkos ME, et al. Postconditioning attenuates myocardial ischemia-reperfusion injury by inhibiting events in the early minutes of reperfusion. *Cardiovasc Res.* (2004) 62:74–85. doi: 10.1016/j.cardiores.2004.01.006
66. Liu Z, Li C, Zhang Q, Tao M. Effect of renshen polysaccharides on oxidative injury in kidney IR rabbits. *Carbohydr Polym.* (2012) 90:773–7. doi: 10.1016/j.carbpol.2012.05.040
67. Zhu J, Ye Q, Xu S, Chang YX, Liu X, Ma Y, et al. Shengmai injection alleviates H₂O₂-induced oxidative stress through activation of AKT and inhibition of ERK pathways in neonatal rat cardiomyocytes. *J Ethnopharmacol.* (2019) 239:111677. doi: 10.1016/j.jep.2019.01.001



OPEN ACCESS

EDITED BY

Tomislav Tosti,
University of Belgrade, Serbia

REVIEWED BY

Sinisa Djurasevic,
University of Belgrade, Serbia
Fatjon Hoxha,
Agricultural University of Tirana, Albania

*CORRESPONDENCE

Huo Jinhai
✉ huojinhai@126.com
Wang Weiming
✉ 13561153193@126.com

[†]These authors have contributed equally to this work

RECEIVED 31 March 2023

ACCEPTED 10 May 2023

PUBLISHED 26 June 2023

CITATION

Yanan Z, Lu M, Lu Z, Jinhai H and Weiming W (2023) Effects and action mechanisms of lotus leaf (*Nelumbo nucifera*) ethanol extract on gut microbes and obesity in high-fat diet-fed rats. *Front. Nutr.* 10:1169843. doi: 10.3389/fnut.2023.1169843

COPYRIGHT

© 2023 Yanan, Lu, Lu, Jinhai and Weiming. This is an open-access article distributed under the terms of the [Creative Commons Attribution License \(CC BY\)](https://creativecommons.org/licenses/by/4.0/). The use, distribution or reproduction in other forums is permitted, provided the original author(s) and the copyright owner(s) are credited and that the original publication in this journal is cited, in accordance with accepted academic practice. No use, distribution or reproduction is permitted which does not comply with these terms.

Effects and action mechanisms of lotus leaf (*Nelumbo nucifera*) ethanol extract on gut microbes and obesity in high-fat diet-fed rats

Zhang Yanan^{1†}, Ma Lu^{1†}, Zhang Lu², Huo Jinhai^{1*} and Wang Weiming^{1*}

¹Heilongjiang Academy of Chinese Medicine Science, Institute of Chinese Materia Medica, Harbin, China, ²Institute of Chinese Materia Medica, Heilongjiang Nursing College, Harbin, China

Objective: The present study aimed to clarify the effect of the lotus leaf ethanol extract (LLEE) on the mechanism of antiobesity and the intestinal microbiota of obese rats.

Methods: A total of 40 specific pathogen-free (SPF) male Sprague–Dawley (SD) rats were split into the blank control group, the model control group, the Orlistat capsule control group, and the LLEE group. All the groups were intervened and fed specific diets for 5 months. During the experiment, we evaluated the rats' body weight, length, serum biochemical indicators, and inflammatory factor levels. After dissection, the liver; epididymal and perirenal white adipose tissue (WAT); and the contents of the cecum were collected for pathological evaluation and intestinal flora analysis.

Results: Lotus leaf alcohol extract can significantly reduce the serum total cholesterol, triglyceride, and low-density lipoprotein cholesterol levels. It also decreases the accumulation of fatty deposits in the liver of rats and the levels of serum inflammatory factors IL-6 and TNF- α and increases the level of IL-10. Lotus leaf alcohol extracts significantly increased the abundance of *Muribaculaceae* in the intestinal flora of rats, reduced the abundance of pro-inflammatory bacteria *Firmicutes*, and relieved fatty liver and other inflammation and diseases caused by a high-fat diet. Besides, the ethanol extract of the lotus leaf significantly regulated the abundance of *Ruminococcus*, suggesting that the ethanol extract of the lotus leaf may prevent hyperlipidemia.

Conclusion: We elucidated the effects and action mechanisms of LLEE on obesity in high-fat diet-fed rats to provide suggestions for regulating intestinal flora through dietary intervention and thus improving blood lipid metabolism.

KEYWORDS

lotus leaf ethanol extract, intestinal flora, inflammatory factor, obesity, lipid metabolism

Introduction

Obesity (1, 2) is caused by the excessive accumulation of body fat due to poor diet, lack of exercise, and other reasons, which are the basis of many diseases. With the improvement of people's living standards and the change in lifestyle, the incidence of obesity is getting higher and higher. Orlistat capsule (3, 4), as a well-known drug, is suitable for the long-term

treatment of obesity and overweight patients with moderate dietary control and exercise, including patients who have already presented with risk factors related to obesity. It serves as a medication control for the effect of lotus leaf ethanol extract (LLEE) in this study.

Lotus leaf, as a homologous substance of food and medicine, has potential advantages in regulating obesity (5). Its regulatory mechanism is characterized by multiple targets, stable efficacy, and high safety. Modern pharmacological studies have shown that lotus leaf extract can reduce the digestive capacity of the body, reduce the absorption of lipids and carbohydrates, and regulate energy consumption so as to effectively improve hyperlipidemia and obesity (6–8). The study of intestinal flora has become a hot topic in the field of medicine, and its composition is affected by genetics, diet, body weight, drugs, and host metabolic state (9, 10). Currently, few studies have shown whether there is a correlation between intestinal microbes and diseases (11, 12). The purpose of this study was to clarify the interaction between obesity caused by a high-fat diet and intestinal flora so as to provide an experimental basis for the development of new weight-loss products.

2. Materials and methods

2.1. Animals, materials, and reagents

Sprague–Dawley rats [Animal certificate: SCXK (H) 2019-001, HNU Animal Experiments Center]; Maintain Feed (production license No. 1016706714625204224, Beijing Keao–Xieli Feed Co., Ltd); High-fat feed (production license No. 1016712400381763584, Beijing Keao–Xieli Feed Co., Ltd); Orlistat capsules (Zhienyiyao Co., Ltd, Chongqing); Lotus Leaf (Beijing Tong Ren Tang Co., Ltd, Haerbin). Referring to the method discussed by Yan and Jun (13), raw lotus leaf products were crushed and sieved through a 20-mesh sieve to obtain lotus leaf powder. Then, we added 70% ethanol solution to the powder in a ratio of 40:1, and the mixture was soaked at room temperature for 30 min, ultrasonicated for 40 min (frequency 500 kW, 35°C), recovered by rotary evaporator ethanol, evaporated to dryness to obtain the extract, and stored in a refrigerator at 4°C for use.

A total cholesterol (TC) assay kit, triglyceride (TG) test kit, low-density lipoprotein cholesterol (LDL-C) test kit, rat interleukin-6 (IL-6) ELISA kit, rat interleukin-10 (IL-10) ELISA kit, and rat tumor necrosis factor- α (TNF- α) enzyme-linked immunoassay kit were obtained from Nanjing Jiancheng Bioengineering Institute, China and fecal total DNA extraction kit from Tiangen Bio, China.

2.2. Instruments and equipment

The following instruments were used: Phusion High-Fidelity PCR (Biolabs, New England), Master Mix with GC Buffer (Biolabs, New England), MiSeq Reagent Kit (Illumina, USA), Phusion High-Fidelity DNA polymerase (Biolabs, New England), Library Preparation Kit (Illumina, USA), Ultralow temperature refrigerator (SANYO Company, Japan), refrigerated high-speed centrifuge (Thermo Fisher Scientific, Inc., USA), Infinite M200 PRO microplate reader (Tecan, Switzerland), T100 Thermal Cycler (Bio-rad, USA), and Illumina NovaSeq 6000 Sequencing Platform (Illumina, USA).

2.3. Methods

2.3.1. Animal grouping and feeding

In this experiment, 40 SPF male SD rats were bred under an environment of a temperature of $22 \pm 2^\circ\text{C}$; relative humidity of $50 \pm 20\%$; and 12-h light–dark cycles. After a week of adaptive feeding, they were randomly and equally divided into four groups according to body weight (BW) and were given 5-month intervening feeding. The blank control group (BC) was fed with conventional feed, and the model control group (MC), Orlistat capsules control group (OC), and the lotus leaf extract group (LLEE) were fed with high-fat feed. The BC group and the MC group were given water daily. Rats in the OC group were fed an Orlistat capsule water solution at a dose of 0.035 mg/kg, and rats in the LLEE group were fed an LLEE water solution at a dose of 1,050 g/kg daily. According to the BW, each group was given a ratio of 1 ml/100 g intragastric administration once. The same animals (i.e., OC and LLEE groups), in addition to intragastric administration o.d. Orlistat or LLEE, were allowed to eat and drink freely. All animals were weighed and recorded each month.

2.3.2. Sample collection and processing

During the experiment, intraocular canthal blood (1.5 ml) was taken from rats at the first, second, third, fourth, and fifth months of the intervention. The supernatant was centrifuged and stored as serum samples in the refrigerator at -20°C . After the experiment, the rat cecal contents were collected aseptically and stored in a -80°C freezer. After the last administration, each group of rats fasted for 12 h, and ~ 2 ml of blood was collected from the abdominal aorta at 3,000 rpm/min at 4°C and centrifuged for 10 min to obtain serum in an ultralow temperature freezer at -80°C for use. After collecting blood, the liver was stripped and weighed, and the liver with a volume of 1 cm^3 was placed in 4% paraformaldehyde fixative solution and stored in a refrigerator at 4°C . WAT of epididymal and perirenal was separated and weighed.

2.4. Determination of relevant indexes in rats

2.4.1. General signs

The body weight and length of rats were recorded each month to calculate the Lee index [$= \sqrt[3]{\text{body weight (g)}/\text{naso-anal length (cm)}}$]. Epididymal and perirenal WATs were weighed to calculate the percentage of visceral fat coefficient [$= (\text{perirenal fat mass} + \text{epididymal fat mass})/\text{body weight}$].

2.4.2. Serum indexes of rats

Serum samples of rats were used to measure serum biochemical markers and inflammatory factors levels. Frozen serum samples were defrosted at room temperature for 30 min, and 100 μl of serum was drawn from a pipette. According to the instructions of the kit, the level of serum total cholesterol was measured by the CHOD-PAP method (Roche P-Modular), triglycerides were measured by the GPO-PAP method (Roche P-Modular), and low-density lipoprotein cholesterol was obtained by the Friedewald

TABLE 1 Body weight levels of 0–5 months of rats in each group (g).

Months	BC (N = 10)	MC (N = 10)	OC (N = 10)	LLEE (N = 10)
0	218.50 ± 17.41	218.50 ± 18.73	213.30 ± 16.57	212.30 ± 14.43
1	392.70 ± 14.97	427.70 ± 14.97	431.70 ± 14.97	429.70 ± 14.97
2	506.00 ± 26.13	572.00 ± 26.13	569.00 ± 26.13	571.00 ± 26.13
3	554.10 ± 28.14	573.90 ± 30.93	573.56 ± 25.71	582.75 ± 16.53
4	596.60 ± 21.33	610.50 ± 13.49	563.51 ± 23.54	549.93 ± 16.20
5	641.20 ± 79.36	678.40 ± 22.97	547.54 ± 18.66	511.44 ± 11.74

formula. The contents of IL-6, IL-10, and TNF- α were detected by enzyme-linked immunosorbent assay (ELISA).

2.4.3. Morphology of rat liver

The liver tissues of rats were cut into 1-cm³ pieces, fixed with 10% neutral formaldehyde, and dehydrated with gradient ethanol: 75% ethanol, 90 min; 95% ethanol, 90 min; 100% ethanol, 90 min, 3 times; and 100% xylene, 60 min, 2 times. Then, they were soaked with paraffin wax two times for 2 h. After embedding, sections were sliced into 6- μ m pieces and placed on slides for hematoxylin and eosin (HE) staining and optical microscope observation.

2.4.4. Sequencing of rat cecal contents

A certain amount of frozen stored fecal samples were thawed at room temperature for 30 min; DNA was extracted according to the instructions of the soil genomic DNA intense extraction kit and stored at -20°C. Amplification primers (338F5'-ACTCCTACGGGAGGCAGCA-3' and 806R5'GGACTACHVGGGTWTCTAAT-3') were used to amplify the V3–V4 regions of 16SrDNA. High-throughput sequencing of the V3–V4 region of 16SrDNA was performed using the Illumina Hiseq 2500 platform and QIIMEv1.8.0 software (Beijing Bimai Ke Biotechnology Co., Ltd, Beijing). The VSEARCH 2.8.1 software was used to merge the high-throughput sequencing data, remove primers, and eliminate redundancy. The usearch10 software was used to denoise the sequence exact sequence variant (ESVs). Referring to the Silva database, operational taxonomic units (OTUs) were obtained by clustering at a 97% similarity level. The NovoMagic analysis platform was used to construct and analyze the results of intestinal flora, and OTU clustering, species annotation, sample complexity analysis, and multisampling comparative analysis were performed.

2.5. Statistical analysis

All data were analyzed and processed using the SPSS Statistics 25.0 statistical software (IBM). The test data were expressed as mean \pm standard deviation. One-way analysis of variance (ANOVA) was used for the mean comparison among multiple groups, and the LSD method was used for further pair comparison. A *p*-value of <0.05 was considered a statistically significant difference.

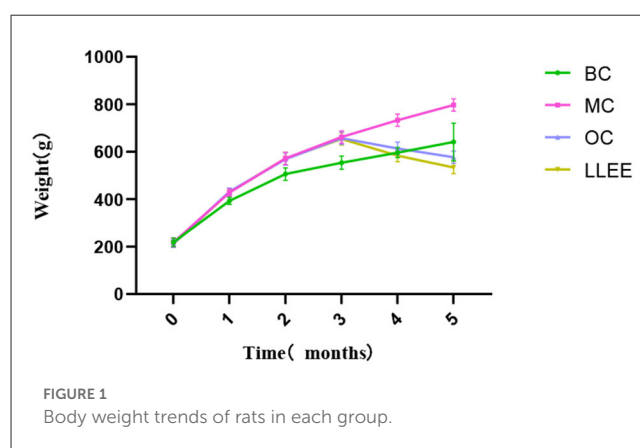


FIGURE 1
Body weight trends of rats in each group.

3. Results and analysis

3.1. General observation

During the experiment, all groups of rats were allowed to eat and drink freely. Except for bloating, diarrhea, and the dull fur color appearance of animals in the model group, animals in the other groups were generally in good condition with no abnormal signs.

3.2. Effects of LLEE on BW of rats

Presently, there is no unified standard for high-fat diet-induced obesity models in rats, and a large number of relevant studies take the body weight of the MC group as the evaluation standard, which is 20% higher than that of the BC group (14). There was no significant difference in initial body mass among all groups (*p* > 0.05). The body weight recorded during the experiment (Table 1) showed that the weight of the BC, OC, and LLEE groups was significantly lower than that of the MC group (*p* < 0.01), while there was no statistical difference between the OC and LLEE groups (*p* > 0.05) (Figure 1).

3.3. Effects of LLEE on the Lee index in rats

Presently, the Lee index is an effective index to evaluate the degree of obesity. In general, the higher the Lee index, the greater the degree of obesity. The Lee index of the OC, LLEE, and BC

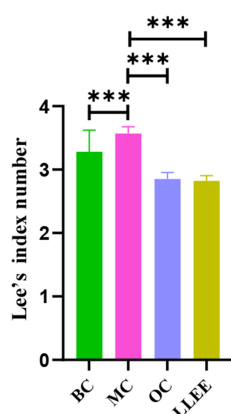


FIGURE 2
The Lee index of rats in each group. *** $P < 0.001$.

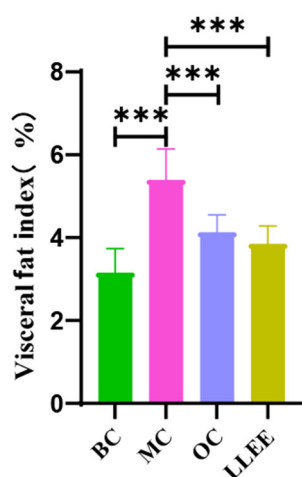


FIGURE 3
The percentage of visceral fat coefficient of rats in each group. *** $P < 0.001$.

groups was significantly different from that of the MC group ($p < 0.01$), while there was no significant difference between the Lee index of the OC and LLEE groups ($p > 0.05$) (Figure 2).

3.4. Effect of LLEE on visceral fat coefficient in rats

WAT is widely distributed around the subcutaneous tissue and viscera in the body. The main function of WAT is to store excess energy in the body in the form of neutral fat. In Figure 3, there was a significant difference ($p < 0.01$) in the visceral WAT ratio between the MC group and the BC group ($p < 0.01$), indicating that the high-fat diet successfully induced obesity in rats. Compared with the BC group, the LLEE group and the OC group showed significant intergroup differences ($p < 0.01$ and $p < 0.05$, respectively), which proved that LLEE had a more significant effect on reducing visceral WAT than the Orlistat capsule.

3.5. Effects of LLEE on liver tissue morphology

As shown in Figure 4, the liver tissue of rats in the BC group showed that the central lobule of the liver was the central vein, surrounded by hepatocytes and hepatic sinuses arranged in a roughly radial arrangement, and the hepatocytes were round and full. The liver plates were arranged regularly and neatly, and the hepatic sinuses were not significantly dilated or squeezed. There were no obvious abnormalities in the portal area between adjacent hepatic lobules. No significant abnormalities were observed. The liver tissue of rats in the MC group was widely observed with hepatocyte steatosis, tiny circular vacuoles (black arrows) in the cytoplasm, a large number of hepatocytes accompanied by balloon-like changes, swollen cells, vacuole-like cytoplasm (red arrows), and multiple small focal infiltrates of inflammatory cells (yellow arrows) in lobules and around veins. A small number of liver cells with mild steatosis were observed in the liver tissue of rats in the OC group, tiny circular vacuoles (black arrows) could be noted in the cytoplasm, and several small focal infiltrates of inflammatory cells (red arrows) could also be observed around the veins and in the lobules. Mild congestion of the hepatic sinuses in the LLEE group (black arrows) was noticed. Thus, compared with the Orlistat capsule, LLEE can significantly improve the morphology of liver cells and reduce the infiltration of inflammatory cells such as liver lobules.

3.6. Effects of LLEE on lipid levels in rats

The contents of TC, TG, and LDL-C in the serum of rats in each group were changed in the intervention stage, as shown in Figure 5. At the beginning of the experiment, there were no significant differences in the contents of TC, TG, and LDL-C in the serum of rats among all groups ($p > 0.01$). During the intervention, the serum biochemical indices of the BC group remained stable, while the serum TC and LDL-C contents of the MC, OC, and LLEE groups increased rapidly with the increase of feeding time. At the end of the intervention, the serum biochemical indices of the three groups were significantly different from those of the BC group, indicating that continuous feeding of a high-fat diet could lead to abnormal serum biochemical indices of the rats. Compared with the OC group, the serum biochemical indices in the LLEE group showed a similar increasing or decreasing trend, and the effect was more obvious ($p < 0.05$).

3.7. Effects of LLEE on serum inflammatory factors in rats

The serum expression of inflammatory factors of the rats in each group during the experiment is shown in Table 2. Enzyme-linked immunoassay kit was used to detect the expression of serum inflammatory factors. Compared with the BC group, the levels of a pro-inflammatory factor (IL-6, TNF- α) were significantly increased in the MC, OC, and LLEE groups, while the levels of an anti-inflammatory factor (IL-10) were significantly decreased, with a

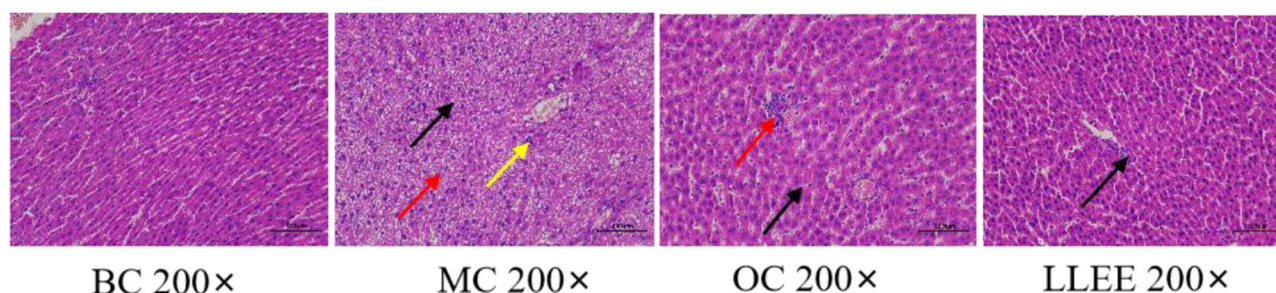


FIGURE 4
The liver tissue morphology of rats.

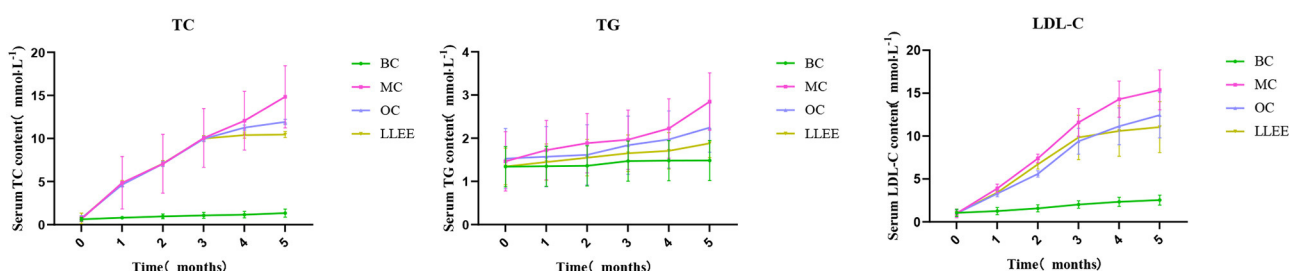


FIGURE 5
The trends of TC, TG, and LDL-C of rats in each group.

TABLE 2 The levels of serum inflammatory factors of rats in each group.

Group	TNF- α (N = 10) (ng/ml)	IL-6 (N = 10) (pg/ml)	IL-10 (N = 10) (pg/ml)
BC	70.60 \pm 22.70**	42.86 \pm 13.32**	48.53 \pm 20.15**
MC	142.72 \pm 97.61##	108.70 \pm 43.69##	12.32 \pm 6.87##
OC	91.14 \pm 23.72**	68.39 \pm 21.70***	28.02 \pm 11.42####
LLEE	60.07 \pm 26.02**	64.48 \pm 16.27**	29.68 \pm 10.07####

** $P < 0.01$, # $P < 0.05$, ## $P < 0.01$.

significant difference among groups ($p < 0.01$). Compared with the Orlistat capsule, LLEE significantly reduced the expression of the proinflammatory factor TNF- α ($p < 0.01$), while the expression of the anti-inflammatory factor IL-10 showed no significant difference (Figure 6). It was demonstrated that LLEE reduces the incidence of obesity by decreasing the expression of TNF- α .

3.8. Intestinal flora test results

To examine the species composition of each sample, OTU clustering was performed with a consistent 0.97 valid data for all samples, and the sequence of OTUs was specifically annotated. The data analysis discussed in the following subsections is based on the analysis of OTUs clustering results.

3.8.1. Species abundance clustering heat map

According to the species annotation and abundant information of all samples at the phylum and genus levels, the top 35 genera with the highest abundance were selected. According to their abundance values in each sample, clustering was carried out from the two levels of species and samples. The heat map was drawn as shown in Figure 7, which depicts the discovery of species with high aggregation or low content in the samples. The horizontal bands shown in the figure are sample information. The species annotation information is on the right, and the clustering tree on the left is a species clustering tree. The depth of color indicates the abundance of the species.

The abundance of different bacterial species in each group and the variation trend of bacterial abundance were analyzed. The t -test was used to test the species groups, and significant differences were found in each classification level ($p < 0.05$). Compared with the BC group, the content of *Bacteroidota* in the MC group was significantly decreased ($p < 0.05$). The ratio of *Firmicutes* and *Bacteroidota* in the LLEE group recovered to the level of the BC group after administration ($p < 0.05$). The abundance of *Proteobacteria* and *Verrucomicrobiota* showed an increasing trend. The content of *Actinobacteria* and *Desulfobacterota* is decreased ($p < 0.05$). *Euryarchaeota* expression could be significantly decreased in the OC group ($p < 0.05$). At the genus level, it was shown that the imbalance of intestinal flora caused by a high-fat diet was concentrated in *Firmicutes*. The abundance of *Limosilactobacillus* and *Candidatus Saccharimonos* may have decreased due to a high-fat diet.

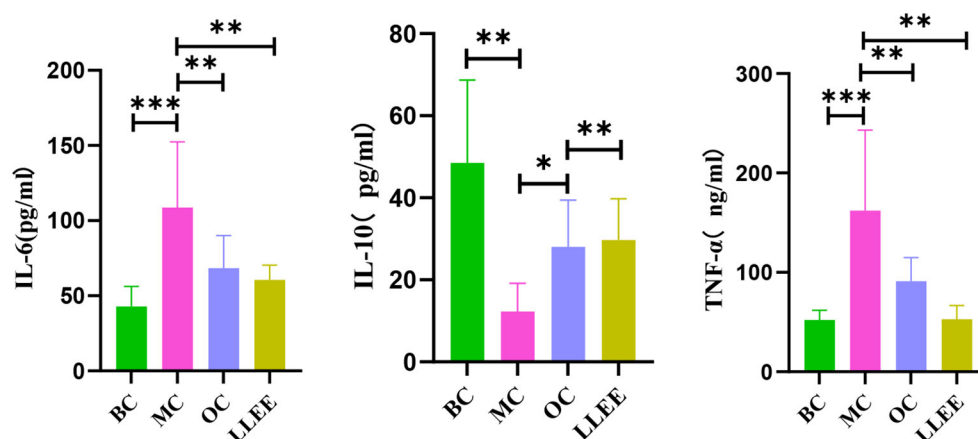


FIGURE 6

The levels of serum inflammatory factors of rats in each group. * $P < 0.05$, ** $P < 0.01$, *** $P < 0.001$.

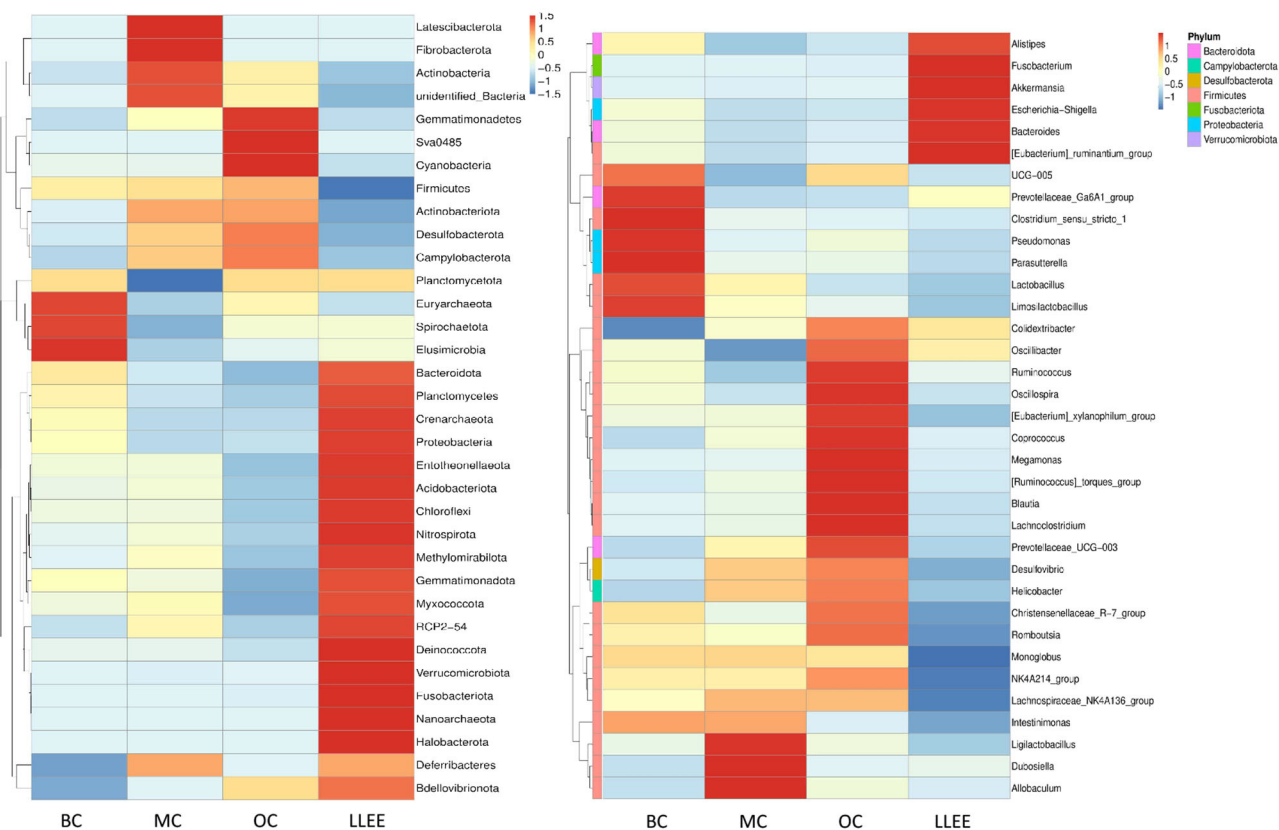


FIGURE 7

The level of species abundance clustering heat map at the phylum and genus levels.

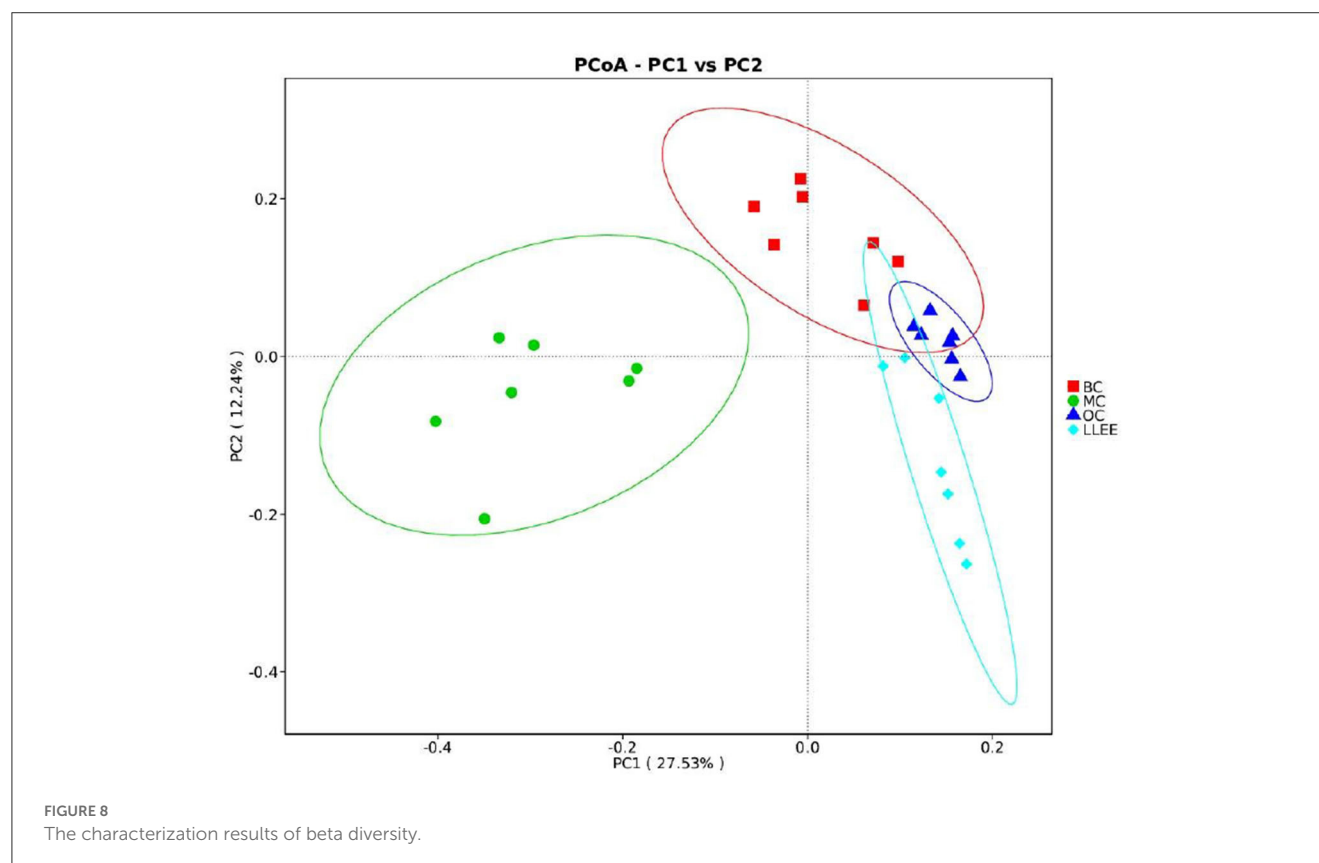
Colidextribacter, *Lachnoclostridium*, *Blautia*, *Faecalibaculum*, and *Holdemanella* showed an increasing trend in the MC group. For the OC group, a strong strain abundance fluctuation was caused. Although the same sample had a certain degree of microbial imbalance ability, its protective ability was obviously inferior to

that of the LLEE group. In terms of species-level differences, both LLEE and Orlistat capsules achieved species-level protection for beneficial bacteria. However, the Orlistat capsule caused some species abundance fluctuations, which might be related to drug side effects.

TABLE 3 Comparative analysis results of alpha diversity.

Group	Observed_species	Chao1	Ace	Shannon	Simpson	PD_whole_tree
BC	1,097.86 ± 128.35	1,199.62 ± 163.81	1,202.62 ± 144.07	7.70 ± 0.25	0.99 ± 0.00	54.14 ± 9.43
MC	1,057.86 ± 57.93	1,143.57 ± 75.35	1,157.42 ± 71.78	7.45 ± 0.38	0.98 ± 0.01	47.70 ± 2.97
OC	1,104.71 ± 110.97	1,182.97 ± 122.66*	1,206.93 ± 119.98	7.36 ± 0.28	0.98 ± 0.00*	51.66 ± 9.53*
LLEE	1,215.57 ± 64.51 ^{###}	1,328.29 ± 90.28 ^{###}	1,343.29 ± 61.41 ^{###}	6.75 ± 0.99 ^{###}	0.93 ± 0.07 ^{###}	65.40 ± 3.01 ^{###}

* $P < 0.05$, ** $P < 0.01$, [#] $P < 0.05$, ^{##} $P < 0.01$, * $P < 0.05$, ** $P < 0.01$.



3.8.2. Comparative analysis of alpha diversity

The analysis of alpha diversity was used to analyze the microbial community diversity within the sample. The diversity analysis of a single sample can reflect the richness and diversity of the microbial community within the sample. The alpha diversity indices (Chao1, Ace, Shannon, Simpson, PD_whole_tree) of samples in each group under the consistency threshold of 0.97 was statistically analyzed. The results are shown in Table 3.

3.8.3. Comparative analysis of beta diversity

Principal coordinates analysis (PCoA) analysis was used to extract the most important elements and structures from multidimensional data through a series of eigenvalues and eigenvector ordering. PCoA analysis was carried out based on Bray–Curtis distance and the principal coordinate combination

with the largest contribution rate was selected for graph display. It is generally believed that the closer the distance between samples, the more similar the species composition structure. As a result, samples with highly similar community structures tend to cluster together, while samples with very different communities are separated far apart. The characterization results are shown in Figure 8.

3.8.4. LEfSe analysis

LEfSe can directly analyze classification levels for statistical tests and difference analysis. Meanwhile, LEfSe placed more emphasis on finding stable biomarkers between groups. It is not limited to the analysis of community composition differences in different sample groups but can also go deep into different subgroups to select the signature microbial groups that show consistent performance in different subgroups. The analysis results showed that a high-fat diet had an effect on *Firmicutes*, *Christensenellaceae*, *Lachnospirales*,

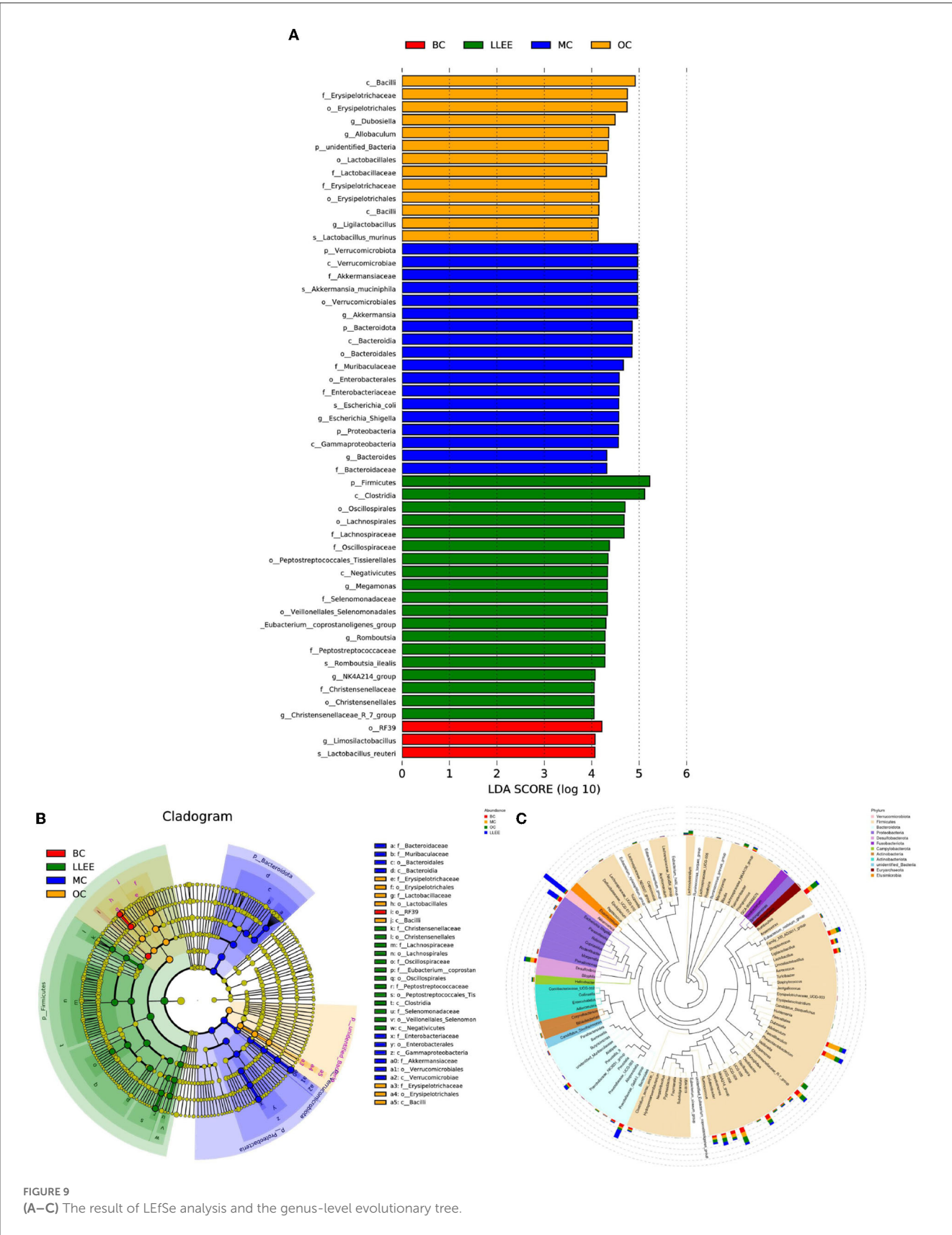


FIGURE 9 (A–C) The result of LefSe analysis and the genus-level evolutionary tree.

Oscillospiraceae, *Veillonellales-Selenomon*, *Eubacterium coprostan*, *Peptostreptococcaceae*, *Enterobacteriaceae*, *Akkermansiaceae*, *Bacteroidaceae*, *Muribaculaceae*, *Erysipelotrichaceae*. Moreover, LLEE mainly affects the abundance of *Bacilli*, *Erysipelotrichaceae*, *Lactobacillaceae*, *Limosilactobacillus*, *Lactobacillus reuteri*, *Clostridia*, and *Oscillospirales*. The amount of *Lachnospirales*, *Enterobacteriaceae*, *Gammaproteobacteria*, *Firmicutes*, and *Clostridia* was influenced with the Orlistat capsule (Figures 9A–C).

Although there were great individual differences in the composition of microbial flora, it was mainly composed of *Bacteroidetes* and *Firmicutes*. The dietary composition has an important effect on intestinal flora, and the relative proportion of these bacteria varies depending on diet. Diet cannot improve the body's condition without the mediation of intestinal flora (15–17). In this study, it was found that the abundance of *Bacteroidetes* increased, while the abundance of *Firmicutes* decreased in the cecum contents of rats on a high-fat diet. The LLEE intervention reversed the distribution of dominant flora abundance in the high-fat diet to some extent, indicating that the abundance ratio of *Bacteroidetes* and *Firmicutes* played an important role in the process of lipid-lowering (18, 19). LLEE protects against changes in the microbiota structure that are caused by fat intake. LLEE significantly reduced the abundance of *Brautella*, indicating that the liver weight and liver index of rats increased due to a high-fat diet. The damage to liver morphology and structure may be related to the increased abundance of *Brautella*. The LLEE intervention reduced the abundance of *Brautella* and improved liver damage. An experiment found that the abundance of *Brautzia* in patients with non-alcoholic steatohepatitis was significantly higher than that in healthy subjects, and the increase in abundance was in response to the intake of a high-fat diet (20). The results of this study also showed that LLEE significantly increased the abundance of *Parabacteroides* and decreased the abundance of *Previoidea*. It has been found that the abundance of *Parabacteroides* is higher in rats eating cellulose, and the abundance of *Parabacteroides* is negatively correlated with human body mass index (BMI) (21–23). The study showed that *Prevotella* mediates mucosal inflammation, inducing disease and inflammatory features by increasing the release of inflammatory mediators in immune cells and various stromal cells (24, 25). The results of this study showed that the abundance of *Parabacteroides* increased after LLEE intervention, while the abundance of *Prevotella* decreased. The study demonstrated that LLEE may play a preventive role in preventing obesity in rats fed a high-fat diet by upregulating the abundance of the beneficial bacterium *Parabacteroides* and downregulating the abundance of the proinflammatory bacterium *Prevosa*.

4. Discussion

The results of this study showed that LLEE could significantly reduce the body mass, Lee index, visceral WAT content, and serum biochemical indices TC, TG, and LDL-C levels of obese rats. At the same time, the serum levels of pro-inflammatory factor IL-6 and TNF- α were significantly decreased, and the serum levels of anti-inflammatory factor IL-10 were significantly increased. The HE staining results of liver tissue in each group showed that a high-fat diet could lead to fatty degeneration

of liver cells and small focal inflammatory cell infiltration, and LLEE could significantly improve the morphological changes of liver cells and inflammatory factor infiltration caused by a high-fat diet. Compared with the Orlistat capsule, LLEE was more effective in regulating the composition and abundance of beneficial microbial flora in intestinal microbes, providing experimental data for regulating intestinal flora through dietary intervention.

LLEE can promote liver metabolism to some extent. High-throughput sequencing analysis of intestinal flora demonstrated that LLEE can increase the diversity of intestinal flora in rats with high-fat diets and cause changes in the intestinal flora structure. High-fat diet increased the abundance of *Bacteroidetes*, which was positively correlated with fat content, and of *Brautella*, which was associated with hepatitis, resulting in increased liver index and liver structural damage (26, 27). After LLEE intervention, liver disease caused by high-fat diet intake was significantly alleviated, and *Prevotella* was downregulated to alleviate inflammation caused by a high-fat diet. LLEE may play a preventive role against obesity in rats with high-fat diets by upregulating the abundance of the beneficial bacterium *Parabacteroides* and downregulating the abundance of the proinflammatory bacterium *Prevotella*.

The results of this study indicate that LLEE can not only regulate blood lipids and relieve chronic inflammation but also prevent antiobesity. It also provides a theoretical basis for dietary intervention to regulate intestinal flora and improve body health.

Data availability statement

The original contributions presented in the study are included in the article/supplementary material, further inquiries can be directed to the corresponding author/s.

Ethics statement

The animal study was reviewed and approved by Heilongjiang Academy of Chinese Medicine Science (No. 2015-64).

Author contributions

ZY and ML: conceive ideas, complete experiments, data collection, arrangement, animal experiment implementation, and article revision. HJ: supportive work. WW: design and fund experiments. All authors contributed to the article and approved the submitted version.

Conflict of interest

The authors declare that the research was conducted in the absence of any commercial or financial relationships that could be construed as a potential conflict of interest.

Publisher's note

All claims expressed in this article are solely those of the authors and do not necessarily represent those of their affiliated

organizations, or those of the publisher, the editors and the reviewers. Any product that may be evaluated in this article, or

claim that may be made by its manufacturer, is not guaranteed or endorsed by the publisher.

References

- Zhu S-h. Bibliometric analysis of obesity research in the field of epidemiology from 2012 to 2021 based on web of science database. *J Med Inf.* (2022) 35:40–5.
- Younossi ZM, Koenig AB, Abdelatif D, Fazel Y, Henry L, Wymer M. Global epidemiology of nonalcoholic fatty liver disease-meta-analytic assessment of prevalence, incidence, and outcomes. *Hepatology.* (2016) 64:73–84. doi: 10.1002/hep.28431
- Mokrani M, Charradi K, Limam F, Aouani E, Urdaci MC. Effect of orlistat on gut microbiota of rats fed with high-fat diet. *J Hunan Agric Univ.* (2022) 444:69. doi: 10.13331/j.cnki.jhau.2022.05.012
- Cani PD. Microbiota and metabolites in metabolic diseases. *Nat Rev Endocrinol.* (2019) 15:69–70. doi: 10.1038/s41574-018-0143-9
- Wang PX, Deng XR, Zhang CH, Yuan HJ. Gut microbiota and metabolic syndrome. *Chin Med J (Engl).* (2020) 133:808–16. doi: 10.1097/CM9.0000000000000696
- Wang T, Han J, Dai H, Sun J, Ren J, Wang W, et al. Polysaccharides from *Lyophyllum decastes* reduce obesity by altering gut microbiota and increasing energy expenditure. *Carbohydr Polym.* (2022) 295:119862. doi: 10.1016/j.carbpol.2022.119862
- Su QJ, Lu ZZ, Deng QY, Wei BM. Alcoholic extract of lotus leaves improves lipid profile in rats with HIV protease inhibitor-induced dyslipidaemia. *West Indian Med J.* (2015) 64:195–200. doi: 10.7727/wimj.2014.373
- Wan Li. The effect of L-carnitine, green tea extract and lotus leaf extract on the body fat percentage in high energy diet-induced obese rats. *Obes Res.* (2020) 7:46–52. doi: 10.17140/OROJ-7-144
- Yang J-y, Jun MA, Tian-xiong W. Research progress on the relationship between intestinal flora imbalance and obesity. *Chin J Urban Rural Enterpr Hyg.* (2021) 36:26–8. doi: 10.16286/j.1003-5052.2021.03.011
- Atzeni A, Galié S, Muralidharan J, Babio N, Tinahones FJ, Vioque J, et al. Gut microbiota profile and changes in body weight in elderly subjects with overweight/obesity and metabolic syndrome. *Microorganisms.* (2021) 9:346. doi: 10.3390/microorganisms9020346
- Wan Y, Xia J, Xu JF, Chen L, Yang Y, Wu JJ, et al. 3Nuciferine, an active ingredient derived from lotus leaf, lights up the way for the potential treatment of obesity and obesity-related diseases. *Pharmacol Res.* (2021) 175:106002. doi: 10.1016/j.phrs.2021.106002
- Shizhe P. *Study on Effect of Alkaloid Salt from Lotus Leaf on Preventing of Diet-induced Obesity and Modulation of Gut microbiota in Mice.* Zhejiang University (2019). doi: 10.27461/d.cnki.gzjdx.2019.000550
- Yan Z, Jun L. Study on antioxidation of ethanol extraction of lotus leaf in mice with cerebral ischemia reperfusion. *Food and Drug.* (2012) 14:29–31.
- Chao W, Shun L, Xiangchun R, Meishi Z, Hai L. Effect of dietary intervention of hawthorn, lotus leaf and Pu'er tea on lipid metabolism in obese rats. *J Food Safe Qual.* (2022) 13:6306–11. doi: 10.19812/j.cnki.jfsq11-5956/ts.2022.19.046
- Agus A, Clément K, Sokol H. Gut microbiota-derived metabolites as central regulators in metabolic disorders. *Gut.* (2021) 70:1174–82. doi: 10.1136/gutjnl-2020-323071
- Cox LM, Yamanishi S, Sohn J, Alekseyenko AV, Leung JM, Cho I, et al. Altering the intestinal microbiota during a critical developmental window has lasting metabolic consequences. *Cell.* (2014) 158:705–21. doi: 10.1016/j.cell.2014.05.052
- Houtman TA, Eckermann HA, Smidt H, de Weerth C. Gut microbiota and BMI throughout childhood: the role of firmicutes, bacteroidetes, and short-chain fatty acid producers. *Sci Rep.* (2022) 12:3140. doi: 10.1038/s41598-022-07176-6
- Lee Y, Lee HY. Revisiting the bacterial phylum composition in metabolic diseases focused on host energy metabolism. *Diabetes Metab J.* (2020) 44:658–67. doi: 10.4093/dmj.2019.0220
- Stojanov S, Berlec A, Štrukelj B. The influence of probiotics on the firmicutes/bacteroidetes ratio in the treatment of obesity and inflammatory bowel disease. *Microorganisms.* (2020) 8:1715. doi: 10.3390/microorganisms8111715
- Shen F, Zheng R-D, Sun X-Q, Ding W-J, Wang X-Y, Fan J-G. Gut microbiota dysbiosis in patients with non-alcoholic fatty liver disease. *Hepatobil Pancreat Dis Int.* (2017) 16:375–81. doi: 10.1016/S1499-3872(17)60019-5
- Cui Y, Zhang L, Wang X, Yi Y, Shan Y, Liu B, et al. Roles of intestinal parabacteroides in human health and diseases. *FEMS Microbiol Lett.* (2022) 369:fnac072. doi: 10.1093/femsle/fnac072
- Wang K, Liao M, Zhou N, Bao L, Ma K, Zheng Z, et al. Parabacteroides distasonis alleviates obesity and metabolic dysfunctions via production of succinate and secondary bile acids. *Cell Rep.* (2019) 26:222–35.e5 doi: 10.1016/j.celrep.2018.12.028
- Wu T-R, Lin C-S, Chang C-J, Lin T-L, Martel J, Ko Y-F, et al. Gut commensal *Parabacteroides goldsteinii* plays a predominant role in the anti-obesity effects of polysaccharides isolated from *Hirsutella sinensis*. *Gut.* (2018) 68:248–62. doi: 10.1136/gutjnl-2017-315458
- Dong TS, Guan M, Mayer EA, Stains J, Liu C, Vora P, et al. Obesity is associated with a distinct brain-gut microbiome signature that connects Prevotella and Bacteroides to the brain's reward center. *Gut Microbes.* (2022) 14:2051999. doi: 10.1080/19490976.2022.2051999
- Si J, You HJ Yu J, Sung J, Ko G. Prevotella as a hub for vaginal microbiota under the influence of host genetics and their association with obesity. *Cell Host Microbe.* (2017) 21:97–105. doi: 10.1016/j.chom.2016.11.010
- Shen WD, Lin X, Liu HM Li BY, Qiu X, Lv WQ, et al. Gut microbiota accelerates obesity in peri-/post-menopausal women via Bacteroides fragilis and acetic acid. *Int J Obes.* (2022) 46:1918–24. doi: 10.1038/s41366-022-01137-9
- Kim Y, Son D, Kim BK, Kim KH, Seo KW, Jung K. Association between the blautia/bacteroides ratio and altered body mass index after bariatric surgery. *Endocrinol Metab.* (2022) 37:475–86. doi: 10.3803/EnM.2022.1481



OPEN ACCESS

EDITED BY

Tomislav Tosti,
University of Belgrade, Serbia

REVIEWED BY

Dimitrije Mara,
Institute of General and Physical Chemistry,
Serbia
Aleksandra Radulovic,
Institute of General and Physical Chemistry,
Serbia

*CORRESPONDENCE

Sisi Cui
✉ cuiss100@nenu.edu.cn

RECEIVED 06 May 2023

ACCEPTED 15 June 2023

PUBLISHED 29 June 2023

CITATION

Yan S, Liu X, Wang Y, Yang X, Bai L, Sun L,
Zhou Y and Cui S (2023) Structural
characterization and antioxidant activity of
pectic polysaccharides from *Veronica
peregrina* L.
Front. Nutr. 10:1217862.
doi: 10.3389/fnut.2023.1217862

COPYRIGHT

© 2023 Yan, Liu, Wang, Yang, Bai, Sun, Zhou
and Cui. This is an open-access article
distributed under the terms of the [Creative
Commons Attribution License \(CC BY\)](#). The
use, distribution or reproduction in other
forums is permitted, provided the original
author(s) and the copyright owner(s) are
credited and that the original publication in this
journal is cited, in accordance with accepted
academic practice. No use, distribution or
reproduction is permitted which does not
comply with these terms.

Structural characterization and antioxidant activity of pectic polysaccharides from *Veronica peregrina* L.

Su Yan, Xianbin Liu, Yuwen Wang, Xiaomin Yang, Lu Bai, Lin Sun,
Yifa Zhou and Sisi Cui*

Engineering Research Center of Glycoconjugates of Ministry of Education, Jilin Provincial Key Laboratory On Chemistry and Biology of Changbai Mountain Natural Drugs, School of Life Sciences, Northeast Normal University, Changchun, China

Background: Pectins are a class of acidic polysaccharides with complex structures. Different pectin molecules are composed of different domains, which have an important impact on their biological activity.

Objective: This study aimed to determine the structural features and the antioxidant activities of the pectic polysaccharides isolated from *Veronica peregrina* L.

Methods: The polysaccharide was isolated from *Veronica peregrina* L by water extraction and fractionated by ion exchange chromatography and gel permeation chromatography. The structure features of the pectic polysaccharides were determined by Fourier transform infrared spectroscopy (FT-IR) and Nuclear magnetic resonance (NMR). The antioxidant activities was evaluated by the DPPH, OH and ABTS radical scavenging ability.

Results: WVPP-A2b and WVPP-A3b, with molecular weights of 48.7×10^4 and 77.6×10^4 kDa, respectively, contained homogalacturonan (HG), rhamnogalacturonan I (RG-I), and rhamnogalacturonan II (RG-II) domains with a mass ratio of 2.08:2.64:1.00 and 3.87:4.65:1.00, respectively. The RG-I domain contained an arabinogalactan II backbone and arabinans consisting of t-Araf, (1→5)-α-Araf, and (1→3,5)-α-Araf. WVPP-A3b also contained short chains consisting of the [t-Araf-(1→5)-α-Araf-(1→)] structural unit. WVPP-A3b showed stronger ability to scavenge DPPH, hydroxyl, and ABTS radicals, which was potentially associated with its high content of galacturonic acid and presence of the HG domain.

Conclusion: The results provide information for enhancing knowledge of the structure-activity relationship of pectic polysaccharides from *V. peregrina* and their potential application in the healthcare food field.

KEYWORDS

Veronica peregrina, pectin, structural analysis, domain, antioxidant *Veronica peregrina*, antioxidant activity

1. Introduction

Pectins are a class of acidic polysaccharides with complex structures that are components of plant cell walls and have diverse biological effects. Pectins primarily contain three typical domains: homogalacturonan (HG), rhamnogalacturonan I (RG-I), and rhamnogalacturonan II (RG-II). The

HG domain, which accounts for ~65% of the total pectin, is a linear polysaccharide and composed of α -(1 \rightarrow 4)-GalAp, and some galacturonic acid (GalA) residues are methylated at O-3 and acetylated at the O-2 or O-3 position (1). The RG-I domain (20%–35% of the total pectin) is composed of [\rightarrow 2)- α -Rhap-(1 \rightarrow 4)- α -GalAp-(1 \rightarrow)] repeated units as the backbone with side chains attached at C4 of (1 \rightarrow 2)- α -Rhap. The side chains attached to RG-I are composed of arabinan, galactan, arabinogalactan-I (AG-I), and arabinogalactan-II (AG-II). The proportion of neutral sugar side chains varies from 25% to 80% depending on the source and extraction method of the pectin. The RG-II domain is a highly conserved sequence in plant cell walls and exhibits high similarity among plant species (2).

Pectins have a notable ability to scavenge free radicals because of the high GalA contents. Therefore, pectin is the focus of increasing attention as a potential antioxidant because of its unique physicochemical properties and low toxicity (3). As a biological macromolecule with a complex structure, the antioxidant activity of pectin largely depends on its structural characteristics, such as the monosaccharide composition, glycosidic bond type, sequence and configuration of sugar residues, branching degree, and substitution (4). Plant pectins have both common structural characteristics and individual characteristics peculiar to different plant sources (4). In addition, the composition and structural differences of the domains have an important impact on the biological activity of pectin. Although the main characteristics of the chemical structure of pectins have been clarified, subtle structural characteristics vary among plant species, such as the side-chain composition, esterification degree, molecular weight, branching degree, and chain conformation (5). Therefore, research on the fine structure of different plant pectins is crucial to evaluate the structure–activity relationship, and is important for the utilization of plant pectins in medicine and the food industry.

Veronica peregrina is an annual or biennial plant and a traditional Chinese medical herb, which belongs to the Scrophulariaceae family and is related to the widespread weed *V. polita*. *Veronica peregrina* is often used for treatment of oligomenorrhea, dysmenorrhea, and to lower blood pressure (6). To date, almost 20 compounds that exhibit antioxidant activity, such as protocatechuic acid, luteolin, veronicoside, and minicoside, have been isolated and identified from *V. peregrina* (7). However, few studies have examined the structure of pectic polysaccharides from *V. peregrina*, and especially lacking are studies of their structure–activity relationship. Therefore, in this study, pectins were extracted from *V. peregrina* and the structure was determined using a combination of chemical and instrumental methods. In addition, the antioxidative activity of *V. peregrina* pectin and its structure–activity relationship was investigated.

2. Materials and methods

2.1. Materials

Plant material of *Veronica peregrina* was purchased from Anhui province, China and stored in the herbarium of our laboratory. DEAE cellulose and Sepharose CL-6B were purchased from GE-Healthcare (United States). Monosaccharide standards were purchased from Sigma. All other chemicals were of analytical grade.

2.2. General methods

Total sugar content was measured using the phenol–sulfuric acid method, taking the mixture composed of the major monosaccharides as a standard (8). The uronic acid content was determined using the *m*-hydroxydiphenyl method taking GalA as the reference (9). Ultraviolet (UV) analysis was performed on a UV-2700 full wavelength UV scanner (Shimadzu, Japan). The absorbance ranging from 200 to 800 nm was recorded. The homogeneity and molecular weight (*M_w*) were determined using a Shimadzu high-performance liquid chromatography (HPLC) system equipped with a RID-20A UV detector and a TSKgel G3000PWXL column (7.8 cm \times 30.0 cm). Detection of 3-deoxy-D-manno-2-octulosonic acid (Kdo) was conducted using the thiobarbituric acid (TBA) method described by York et al. (10).

2.3. Preparation of pectin from *Veronica peregrina*

2.3.1. Extraction of pectin

The *V. peregrina* material was extracted with hot water in accordance with the protocol used in our library (5). Briefly, the dried material (1,000 g) was crushed, soaked in deionized water (16 L) and extracted at 100°C for 3 h. The process was repeated three times under the same conditions. The supernatant was collected and evaporated to 2 L at 80°C, then precipitated with 8 L of 95% ethanol, and incubated overnight at 4°C. The precipitates were washed with 95% ethanol and anhydrous ethanol in turn, and dried under vacuum at 60°C overnight to give the crude polysaccharide WVPP.

2.3.2. Fractionation of the pectin

WVPP (50 g) was fractionated using a DEAE-cellulose column (12 cm \times 43 cm, Cl[−]). The crude polysaccharide was eluted first with 4.5 L deionized water to obtain the neutral fraction (WVPP-N). The column was further eluted using 3 L of 0.5 M NaCl to give the crude pectin (WVPP-A).

WVPP-A (1 g) was fully dissolved in distilled water, centrifuged, and loaded onto a DEAE-cellulose column (12 cm \times 43 cm). The crude pectin was eluted with deionized water, then 0.2 M, 0.3 M, and 0.5 M NaCl solution in sequence. The flow rate was 25 mL/min. The total sugar content and uronic acid content in the eluate were detected, and the corresponding elution fractions were collected and designated WVPP-A2, WVPP-A3, and WVPP-A5. WVPP-A2 and WVPP-A3 were further fractionated using a Sepharose CL-6B column (3.0 cm \times 100 cm) and were eluted with 0.15 M NaCl at a flow rate of 0.5 mL/min. The two purified pectic polysaccharides WVPP-A2a and WVPP-A2b were obtained. The method of extraction and fractionation of the pectins from *V. peregrina* is summarized in Figure 1.

2.4. Chemical characterization analysis

A polysaccharide sample (2–4 mg) was hydrolyzed with 2 M anhydrous HCl–methanol solution and trifluoroacetic acid (TFA) in accordance with a previously reported method (11). The hydrolyzed polysaccharide was added to 1-phenyl-3-methyl-5-pyrazolone (PMP) and reacted at 70°C for 30 min. The PMP derivatives were purified by

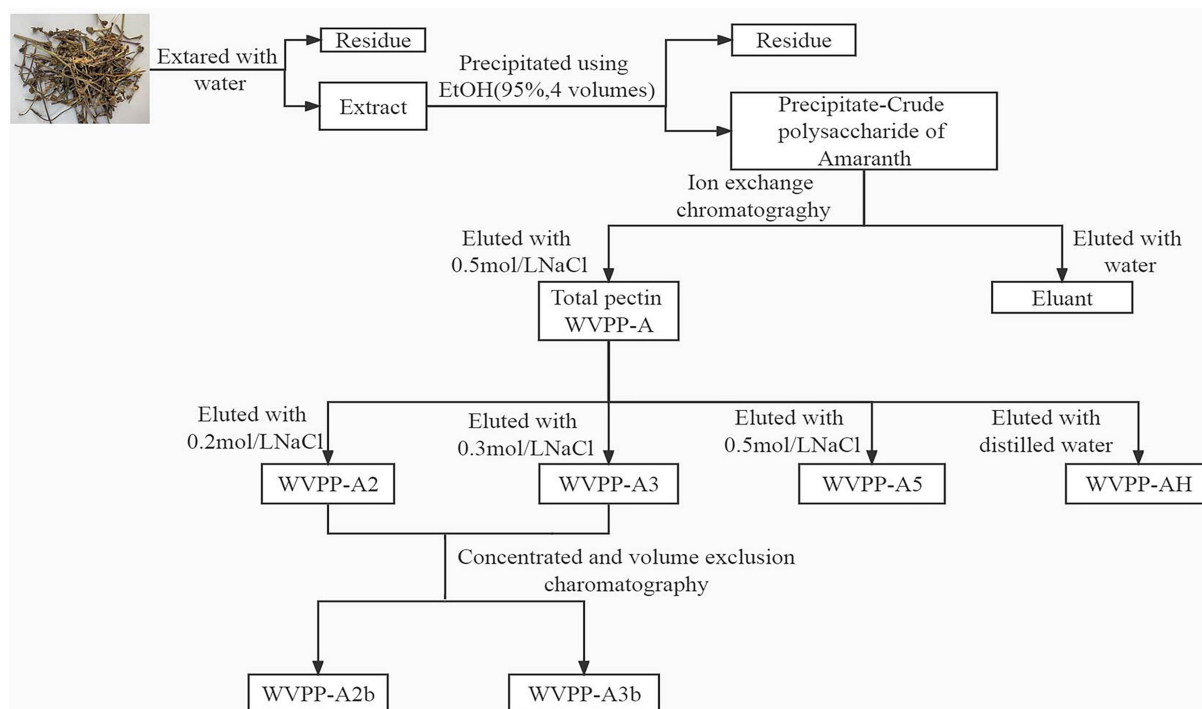


FIGURE 1

Isolation and purification of the pectic polysaccharides WVPP-A2b and WVPP-A3b from *Veronica peregrina*.

chloroform extraction, then analyzed using a HPLC system equipped with a SPD-20A UV–visible diode-array detector and a COSMOSIL 5C18-PAQ column. A volume (0.1 mol/L) of PBS (pH 6.9) solution containing 17% acetonitrile (v/v) was used as the mobile phase. The column temperature, detection wavelength, and flow rate were 35°C, 245 nm, and 1 mL/min, respectively.

2.5. Fourier transform–infrared spectroscopy

Fully dried samples (2 mg) were mixed thoroughly with potassium bromide (1:100, w/w) and determined using a Spectrum Two FT-IR spectrometer (PE, United States) in the range of 4,000–500 cm⁻¹.

2.6. Nuclear magnetic resonance analysis

Samples (20 mg) were dissolved in 0.5 mL D₂O (99.9%). The ¹H, ¹³C NMR, ¹H–¹H COSY, ¹H–¹³C HSQC, and HMBC spectra were recorded with a Bruker AV600 MHz NMR spectrometer (Germany) at 25°C.

2.7. De-esterification and enzymatic hydrolysis

WVPP-A2b and WVPP-A3b were saponified with precooled 0.1 M NaOH and incubated at 4°C for 4 h with mild stirring (5). The reaction solutions were neutralized with 10% glacial acetic acid to pH

7.0, desalted on a Sephadex G-10 column, and freeze-dried to obtain the de-esterified pectins (WVPP-A2b-D and WVPP-A3b-D).

WVPP-A2b-D and WVPP-A3b-D were dissolved in 50 mM HAc–NaAc solution (pH 4.5). Endo-polygalacturonase M2 (EC 3.2.1.15; 50 µL) was added to the solution and incubated at 40°C for 24 h, then the reaction solution was heated in a boiling water bath for 15 min to inactivate the pectinase. The enzymatic hydrolysates were separated with a Sephadex G-75 column (2.6 cm × 100 cm) and were eluted with 0.15 M NaCl at 0.4 mL/min. The corresponding eluent was collected, desalted using a Sephadex G-10 column, and freeze-dried. Three subfractions were obtained from each of WVPP-A2b (WVPP-A2b-E1–E3) and WVPP-A3b (WVPP-A3b-E1–E3).

2.8. Antioxidant activity analysis

2.8.1. DPPH radical-scavenging activity

The ability of the pectin fractions to scavenge the DPPH radical was determined in accordance with the method described by Chattopadhyay et al. (12). Briefly, 500 µL pectin solution at different concentrations (0.5, 1, 2, 5, and 10 mg/mL) was mixed with 2 mL of 0.5 mM DPPH solution. The resulting mixture was incubated in the dark for 30 min, then the absorbance was measured at 517 nm. Ascorbic acid (Vc) was used as a positive control, ultrapure water was used as a blank control, and an equal volume of anhydrous methanol instead of the DPPH solution served as an additional blank control. Each sample was repeated five times. The DPPH-scavenging activity of the fractions was calculated with the following formula:

$$\text{DPPH} - \text{scavenging activity (\%)} = \left[1 - \left(\frac{A_{\text{samples}} - A_{\text{control}}}{A_{\text{blank}}} \right) \right] \times 100\%$$

A_{samples} : The absorbance value of sample solution.

A_{control} : The absorbance value of background solution (anhydrous methanol instead of the DPPH solution).

A_{blank} : The absorbance value of the blank control.

2.8.2. Hydroxyl radical-scavenging activity

The ability of the pectin fractions to scavenge hydroxyl (OH) radicals was assessed in accordance with a previously described method (13). The 100 μL pectin solution at different concentrations (0.5, 1, 2, 5, and 10 mg/mL) was mixed with an equal volume of FeSO_4 solution (9.0 mmol/L) and absolute ethanol containing salicylic acid solution (9.0 mmol/L). The resulting mixture was reacted with 100 μL H_2O_2 solution (8.8 mmol/L) in a reaction tube at 25°C for 30 min. The absorbance at 532 nm was recorded. Ultrapure water was used as the blank control solution instead of the pectin sample, Vc was used as a positive control, and an equal volume of ultrapure water instead of the H_2O_2 solution served as an additional control. The hydroxyl radical-scavenging ability was calculated as follows:

$$\text{OH} - \text{scavenging activity (\%)} = \left[1 - \left(\frac{A_{\text{samples}} - A_{\text{control}}}{A_{\text{blank}}} \right) \right] \times 100\%$$

A_{samples} : The absorbance value of sample solution.

A_{control} : The absorbance value of background solution (ultrapure water instead of the H_2O_2 solution).

A_{blank} : The absorbance value of blank control.

2.8.3. ABTS radical-scavenging activity

The ability of the pectin fractions to scavenge ABTS radicals was evaluated in accordance with a previously reported method (14). The ABTS working solution was prepared fresh daily consistent with

a previously reported (14). To evaluate the ABTS radical-scavenging ability of the fractions, 400 μL of the sample solution at different concentrations (0.5, 1, 2, 5, and 10 mg/mL) was fully mixed with 400 μL ABTS working liquid in a reaction tube. The reaction was conducted in the dark for 30 min at 25°C. The absorbance at 732 nm was recorded. Equal volume of ultrapure water was used as the blank control solution instead of the samples. The ABTS radical-scavenging activity of the fractions was calculated with the following formula:

$$\text{ABTS} - \text{scavenging activity (\%)} = \left[1 - \left(\frac{A_{\text{samples}} - A_{\text{control}}}{A_{\text{blank}}} \right) \right] \times 100\%$$

A_{samples} : The absorbance value of sample solution.

A_{control} : The absorbance value of the background solution (PBS solution instead of ABTS working solution).

A_{blank} : The absorbance value of blank control.

2.9. Statistical analysis

The data for antioxidant effect are expressed as the mean \pm SD. All assays were performed as three parallel experiments. The experimental data were analyzed using IBM SPSS Statistics 23.0 software.

3. Results and discussion

3.1. Preparation of pectic polysaccharides from *Veronica peregrina*

The crude polysaccharides (WVPP) were extracted from *V. peregrina* by hot water extraction and ethanol precipitation with a yield of 6.9% relative to the dry mass. The proportions of total carbohydrates, total protein, and glucuronic acid in the WVPP were 41.2%, 27.0%, and 5.1%, respectively (Table 1). Monosaccharide

TABLE 1 Yield, molecular weight (Mw), and monosaccharide composition of pectic polysaccharides extracted from *Veronica peregrina*.

	WVPP	WVPP-N	WVPP-A	WVPP-A2b	WVPP-A3b
Yield (w%)	6.9 ^a	49.3 ^b	21.3 ^b	28.1 ^c	9.4 ^c
Mw (kDa)		ND	ND	48.7	77.6
Monosaccharide composition					
GalA	25.5	-	37.6	43.7	47.4
Rha	8.0	-	15.1	13.3	18.7
Gal	17.1	26.2	15.1	16.9	11.7
Ara	13.0	11.8	16.0	15.8	12.6
Glc	17.6	53	2.0	0.9	1.7
GlcA	7.5	-	4.4	1.7	2.5
Xyl	8.9	4.8	8.7	6.7	4.1
Man	2.3	4.2	0.7	0.9	1.2

^aYield relative to the dry weight of the plant material.

^bYield relative to WVPP.

^cYield relative to WVPP-A.

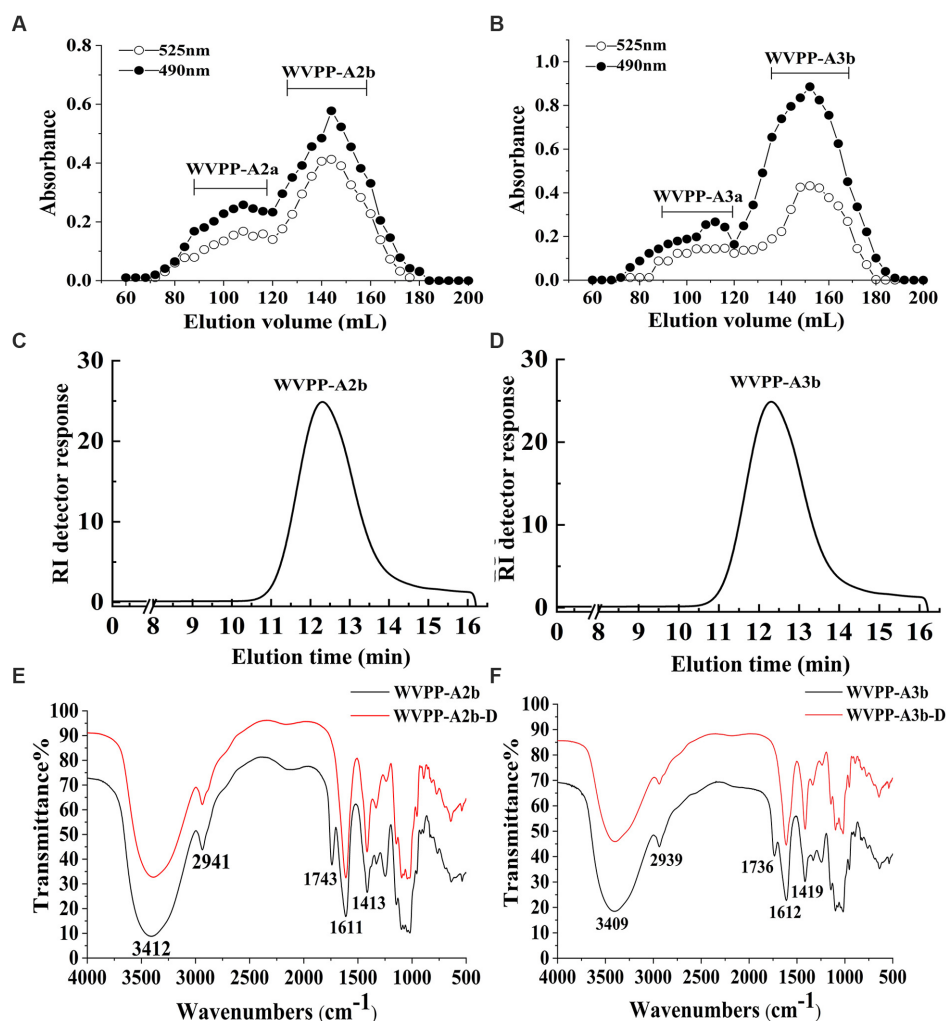


FIGURE 2
Characteristics of the WVPP-A2b and WVPP-A3b fractions. (A,B) Sepharose CL-6B elution curve; (C,D) HPGPC profiles; (E,F) FT-IR spectra.

analysis revealed that the WVPP contained GalA, Ara, Glc, Gal, Rha, GlcA, Man, and Xyl in molar ratios of 25.5:17.6:17.1:13.0:8.9:8.0:7.5:2.3.

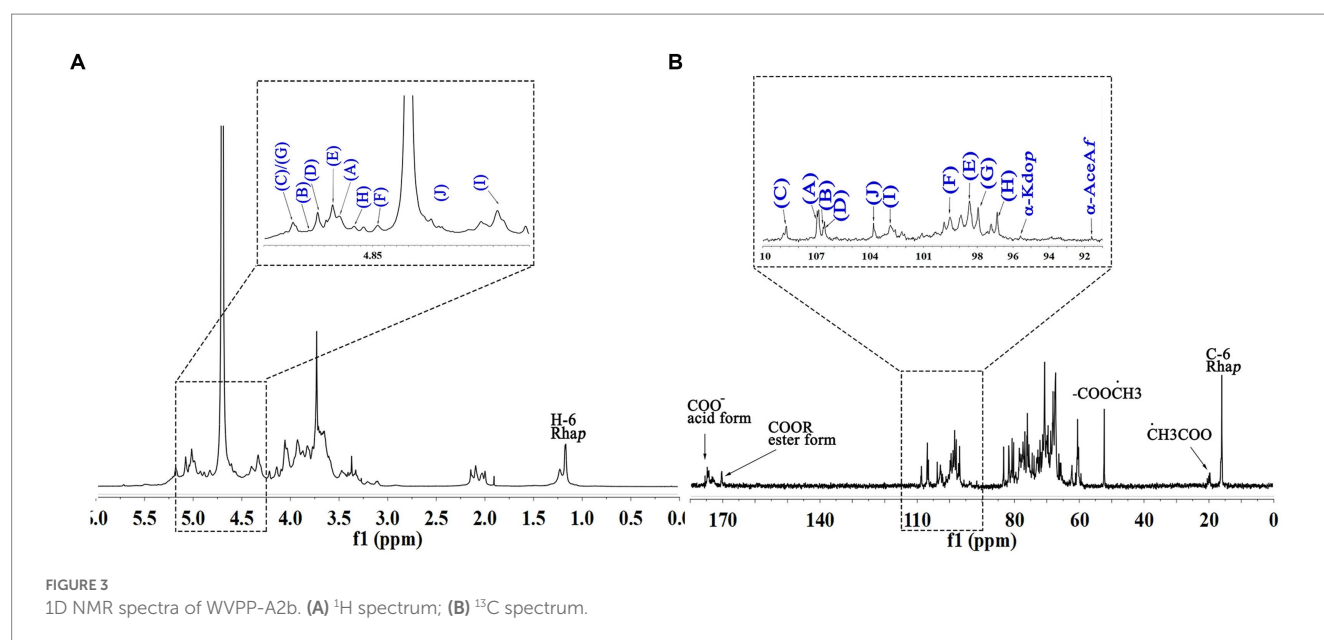
The WVPP was then fractionated by ion-exchange chromatography to obtain a neutral fraction (WVPP-N) with a yield of 49.3% (relative to the WVPP) and an acidic fraction (WVPP-A) with a yield of 21.3% (relative to the WVPP). WVPP-A was further fractionated with a DEAE-cellulose column, giving WVPP-AH (8.3%), WVPP-A2 (40.0%), WVPP-A3 (12.5%), and WVPP-A5 (4.1%). Subsequently, WVPP-A2 and WVPP-A3 were further purified using a Sepharose CL-6B column (Figures 2A,B), to yield the two major fractions WVPP-A2b (70.0%) and WVPP-A3b (75.0%). The monosaccharide compositions of WVPP-A2b and WVPP-A3b were similar; both fractions were predominantly composed of GalA, Rha, Ara, and Gal (collectively comprising approximately 90% of the total monosaccharides), and small amounts of Man, Xyl, Glc, and GlcA (Table 1). The presence of GalA, Rha, Gal, and Ara may reflect the presence of HG and RG-I domains in both WVPP-A2b and WVPP-A3b. In the TBA assay, WVPP-A2b and WVPP-A3b displayed positive results, indicating that both contained a RG-II-type pectin domain.

3.2. Purity, homogeneity, and molecular weight of WVPP-A2b and WVPP-A3b

WVPP-A2b and WVPP-A3b showed no absorbance at 260 and 280 nm, indicating the fractions were free of nucleic acids and proteins (Supplementary Figure S1). Therefore, the purification process yielded pectin of high purity. In this study, high-performance gel permeation chromatography (HPGPC) was first used to analyze the homogeneity of WVPP-A2b and WVPP-A3b. The HPGPC elution curves of the two pectin fractions showed narrow, single symmetrical peaks (Figures 2C,D), indicating that the fractions were homogeneous with M_w of 48.7×10^4 kDa (WVPP-A2b) and 77.6×10^4 kDa (WVPP-A3b).

3.3. FT-IR analysis of WVPP-A2b and WVPP-A3b

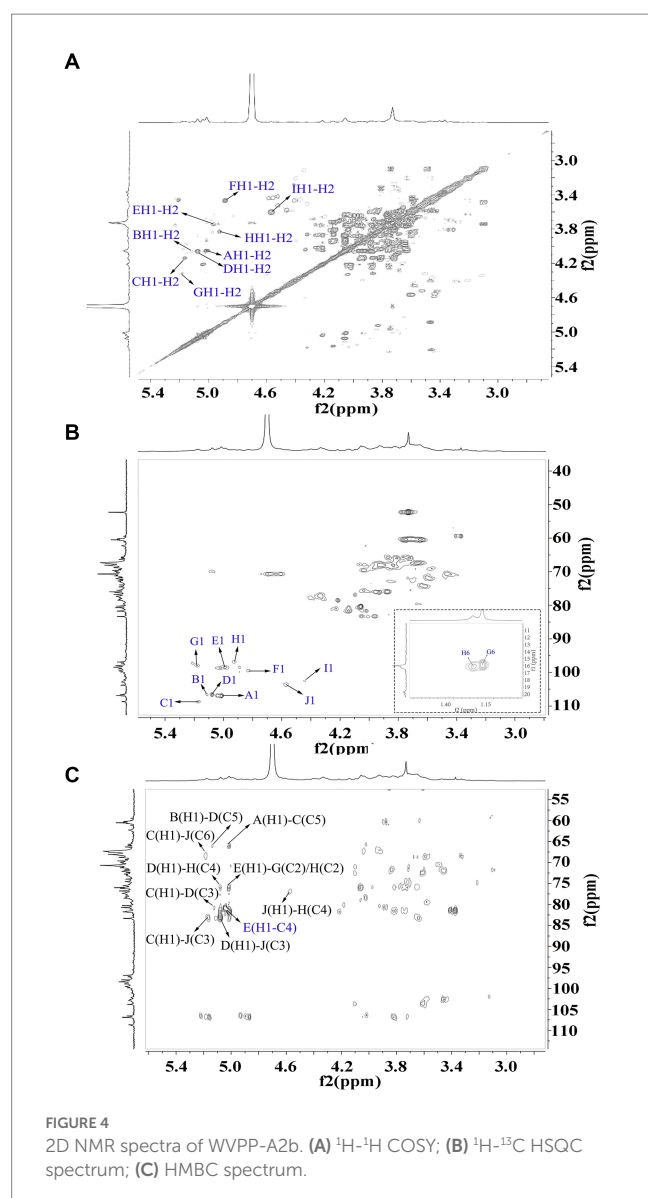
As a convenient and effective method for characterization of the primary structure of polysaccharides, FT-IR can be used to detect the glycosidic bond types, sugar residue substitution, and configuration of

TABLE 2 ^{13}C and ^1H NMR chemical shift assignments of the residues in WVPP-A2b.

Residues	Glycosidic linkage		1	2	3	4	5	6
A	$\alpha\text{-Araf-(1} \rightarrow \text{AII)}$	H	5.00	4.01	3.88	4.06	3.66	
		C	106.93	83.40	75.96	80.34	60.52	
B	$\alpha\text{-Araf-(1} \rightarrow \text{AIII)}$	H	5.11	3.96	3.88	4.06	3.74	
		C	106.62	83.27	75.96	80.34	60.44	
C	$\rightarrow 5)\text{-}\alpha\text{-Araf-(1} \rightarrow$	H	5.17	4.23	4.03	4.22	3.72	
		C	108.64	80.91	75.58	80.91	66.01	
D	$\rightarrow 3,5)\text{-}\alpha\text{-Araf-(1} \rightarrow$	H	5.08	4.31	4.06	3.96	3.72	
		C	106.57	78.16	80.39	83.27	66.01	
E	$\rightarrow 4)\text{-}\alpha\text{-GalAp-(1} \rightarrow$	H	5.01	3.67	4.04	4.02	4.69	
		C	98.46	67.41	69.58	81.63	70.69	174.86
F	$\rightarrow 4)\text{-}\alpha\text{-GalA6Mep-(1} \rightarrow$	H	4.83	3.67	4.04	4.05	4.60	
		C	99.46	67.41	69.58	80.51	70.73	170.14
G	$\rightarrow 2)\text{-}\alpha\text{-Rhap-(1} \rightarrow$	H	5.17	4.33	4.04	3.57	3.46	1.17
		C	97.91	76.14	69.37	71.90	70.60	15.89
H	$\rightarrow 2,4)\text{-}\alpha\text{-Rhap-(1} \rightarrow$	H	4.93	4.40	4.02	3.93	3.57	1.23
		C	96.88	76.14	73.44	77.77	69.10	16.12
I	$\rightarrow 3)\text{-}\beta\text{-Galp-(1} \rightarrow$	H	4.42	3.58	4.05	4.02	3.61	3.52
		C	102.55	71.79	83.26	68.18	74.43	70.84
J	$\rightarrow 3,6)\text{-}\beta\text{-Galp-(1} \rightarrow$	H	4.57	4.01	4.08	4.07	3.62	3.83
		C	103.64	73.68	83.08	67.83	74.26	66.09

sugar residues in polysaccharides (15). The WVPP-A2b and WVPP-A3b fractions exhibited similar FT-IR spectra (Figures 2E,F). The stronger absorption peaks at $3,412$ and $3,409\text{ cm}^{-1}$ were attributed to the O–H stretching vibration characteristic peak of the hydrogen bond of sugar residues. The weak absorption peaks near $2,941$ and $2,939\text{ cm}^{-1}$ were caused by the asymmetric C–H stretching vibration of the $-\text{CH}_2$ groups. The absorption peaks near $1,245$, $1,743$, and $1,611\text{ cm}^{-1}$ in the spectra

indicate the presence of uronic acid (16). Among these peaks, the vibration absorption peaks near $1,749\text{ cm}^{-1}$ and $1,611\text{ cm}^{-1}$ represent the characteristic peaks of C=O vibration in methyl-esterified and free carboxyl groups, respectively (17). The peak areas of these two characteristic peaks can be used to calculate the degree of methylation (DM) of acidic polysaccharides. The esterification degree of pectin can be calculated with the following formula: $\text{DE (\%)} = [A_{1740}/$

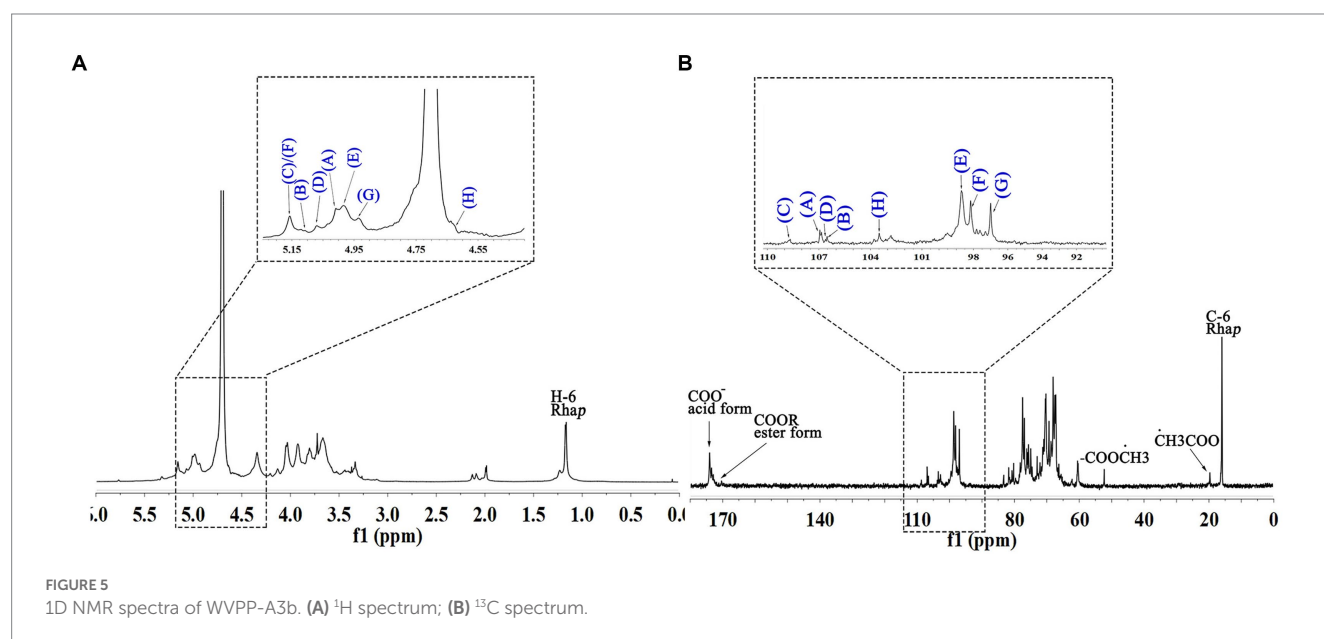


$(A_{1740} + A_{1611}) \times 100\%$, where A_{1740} is the characteristic peak area of esterified carboxyl groups (1740 cm^{-1}) and A_{1610} is the characteristic peak area of free carboxyl groups ($1,610\text{ cm}^{-1}$). Applying this formula, the DM of WVPP-A2b and WVPP-A3b was 18.7% and 19.6%, respectively.

3.4. NMR analysis of WVPP-A2b and WVPP-A3b

3.4.1. NMR analysis of WVPP-A2b

The signals at 4.57–5.17 ppm in the ^1H spectrum (Figure 3A; Table 2) were attributed to anomeric protons, indicating the presence of α - and β -glycoside residues in WVPP-A2b (18). The signals at 19.99 and 51.95 ppm in the ^{13}C spectrum were attributed to $-\text{OAc}$ and $-\text{OCH}_3$ groups (19). Small peaks observed at 95.65 and 91.97 ppm belonged to C2 of α -Kdp and α -AcefA (5), indicating the presence of a RG-II domain in WVPP-A2b (Figure 3B), which was consistent with the TBA detection results. Based on the ^1H , ^{13}C , ^1H - ^1H COSY (Figure 4A), and ^1H - ^{13}C HSQC (Figure 4B) spectra, as well as published data for pectins, the chemical shifts of all carbon and hydrogen atoms in the sugar residues of WVPP-A2b were assigned and are listed in Table 2. The anomeric proton and carbon signals at 5.00/106.93, 5.11/106.62, 5.17/108.64 ppm, and 5.08/106.57 ppm confirmed that the Ara α residues in WVPP-A2a were in the form of α -Ara α . The signals at 4.01/83.40, 3.88/75.96, 4.06/80.34 ppm, and 3.66/60.52 ppm were attributed to the H2/C2-H5/C5 of residue A, indicating that residue A was t- α -Ara α . Based on the ^1H - ^{13}C HSQC spectrum, the signal at 3.72/66.01 ppm was assigned to the H5/C5 of residues C and D. In comparison with the chemical shifts of residue A, the chemical shift of C5 of residue C shifted down-field, indicating the presence of a substitution at C5 of the residue. Therefore, residue A was assigned to α -(1 \rightarrow 5)-Ara α . Similarly, the down-field shift of C3 (83.15 ppm) and C5 (66.01 ppm) in residue D was observed, indicating that residue D was α -(1 \rightarrow 5)-Ara α and α -(1 \rightarrow 3,5)-Ara α (20). In the ^{13}C NMR spectrum, the signals at 170.14 and 174.86 ppm were assigned to esterified and non-esterified carboxyl groups of Gal α (21). The presence of signals at 5.01/98.46, 4.83/99.46, 4.02/81.63, and 4.05/80.51 ppm confirmed that residues E and F were α -(1 \rightarrow 4)-Gal α and



α -(1 \rightarrow 4)-GalA6Mep, respectively. The signals at 5.17 and 4.93 ppm indicated that residues G and H were α -Rhap (22). The cross peaks of H1/C1 for (1 \rightarrow 2)- α -D-Rhap and (1 \rightarrow 2,4)- α -D-Rhap were observed at 5.17/97.91 and 4.93/96.88 ppm, respectively (Figure 4B), and H6/C6 was observed at 1.17/15.89 and 1.23/16.12 ppm, respectively. The signal at 5.47/103.64 ppm was assigned to H1/C1 of residue I, indicating that it was in the β -configuration. The chemical shifts of C3 (83.15 ppm) and C6 (68.24 ppm) in residue G were down-field relative to the chemical shift of β -Gal, indicating that residue G was (1 \rightarrow 3, 6)- β -D-Galp (23).

As observed in the HMBC spectrum (Figure 4C), the cross peak at 5.01/81.67 ppm was attributed to EH1-EC4, indicating the presence of a HG domain. The EH1-GC2, EH1-HC2, GH1-EC4, and HH1-EC4 indicated the presence of the [\rightarrow 4]-GalpA-(1 \rightarrow 2)-Rhap-(1 \rightarrow 4)-GalpA-(1 \rightarrow 2,4)-Rhap-(1 \rightarrow 4)-GalpA-(1 \rightarrow] structural units, which formed the backbone of the RG-I domain. The presence of AH1-CC5, CH1-DC3, and BH1-DC5 in the HMBC spectrum indicated that WVPP-A2a contained an arabinan as the side chain. In addition, the cross peaks of DH1-IC3 and CHI-IC6 indicated the presence of an arabinogalactan (AG-II) side chain in WVPP-A2a. The presence of DH1-GC4 and IH1-GC4 confirmed that the side chains in WVPP-A2a were linked to the backbone of RG-I via (1 \rightarrow 3,5)-Araf(D) and (1 \rightarrow 3,6)-Galp(I).

3.4.2. NMR analysis of WVPP-A3b

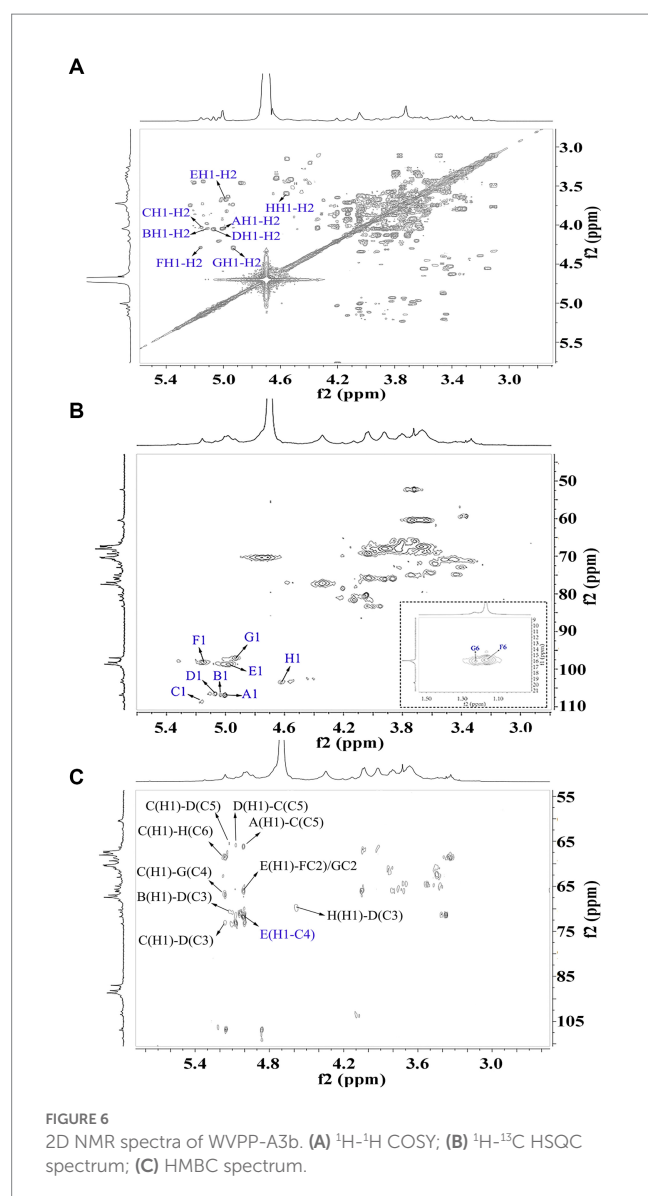
The anomeric proton and carbon regions were distributed at 95–110 ppm (Figures 5A,B; Table 3), indicating the presence of both α - and β -configurations for glycosidic linkages in WVPP-A3b. Based on the ^1H , ^{13}C , ^1H - ^{13}C COSY (Figure 6A), and ^1H - ^{13}C HSQC spectra (Figure 6B), WVPP-A3b contained the same sugar residues as WVPP-A2b. The signals observed at 5.01/106.94 ppm (5.10/106.52 ppm), 5.16/108.59, 5.07/106.55, 4.98/98.69, 5.16/98.17, 4.93/97.00, and 4.9358/103.48 ppm were attributed to

H1-C1 of α -t-Araf(A and B), (1 \rightarrow 5)- α -L-Araf(C), (1 \rightarrow 3,5)- α -L-Araf(D), (1 \rightarrow 4)- α -D-Galp(E), (1 \rightarrow 2)- α -D-Rhap(F), (1 \rightarrow 2,4)- α -D-Rhap(G), and (1 \rightarrow 3,6)- β -D-Galp(H), respectively. Other chemical shifts of all residues in WVPP-A3b are listed in Table 2. Similar to WVPP-A2b, a distinct signal at 52.56 ppm was observed, indicating the presence of methylated GalA in WVPP-A3b.

The sequence of sugar residues in WVPP-A3b was analyzed based on the HMBC spectrum (Figure 6C). The cross peak at 4.98/81.63 ppm, assigned to EH1-EC4, confirmed the presence of [\rightarrow 4]- α -D-Galp-(1 \rightarrow 4)- α -D-Galp-(1 \rightarrow) repeating units. The EH1-GC2, EH1-HC2, FH1-EC4, and EH1-EC4 indicated that (1 \rightarrow 4)- α -D-Galp, (1 \rightarrow 2)- α -D-Rhap, and (1 \rightarrow 2,4)- α -D-Rhap were linked alternately to form the backbone of the RG-I domain in WVPP-A3b. The cross peaks at 5.16/76.02 ppm (CH1-EC4) and 5.01/66.14 ppm (AH1-CC5) indicated the presence of [α -L-Araf-(1 \rightarrow 5)- α -L-Araf-(1 \rightarrow)] units connected to the main chain of RG-I via C4 of (1 \rightarrow 2,4)- α -D-Rhap. These results showed that both pectins contained short side chains composed of α -L-Ara, which exhibited differences in the number and type of sugar residues and in the connection with the RG-I backbone. The signals at HH1-DC3 and DH1-HC3 suggested that WVPP-A2b also had AG-II side chains that contained repeating units formed by alternating connection of (1 \rightarrow 3,6)- β -D-Galp and (1 \rightarrow 3,5)- α -L-Araf, respectively, through (1 \rightarrow 3)-glycosidic linkages. This result indicated that the AG-II side chains of WVPP-A3b might exhibit a higher degree of branching than those of WVPP-A2b. The signal at DH1-CC5 suggested that the AG-II side chains were connected to the backbone through (1 \rightarrow 5)- α -L-Araf. According to the 1D and 2D NMR results, both WVPP-A2b and WVPP-A3b contained typical HG domains, which consisted of a linear skeleton composed of [\rightarrow 4]-GalAp-(1 \rightarrow 4)-GalAp (1 \rightarrow) structural units, with methylation and acetylation of GalpA in the HG domain to different degrees. In addition, the pectins contained a similar

TABLE 3 ^{13}C and ^1H NMR chemical shift assignments of the residues in WVPP-A3b.

Residue	Glycosidic linkage		1	2	3	4	5	6
A	α -Araf-(1 \rightarrow AII)	H	5.01	4.00	3.87	4.05	3.64	
		C	106.94	83.40	76.00	80.41	60.43	
B	α -Araf-(1 \rightarrow AIII)	H	5.10	4.04	3.92	4.05	3.74	
		C	106.52	83.16	76.11	80.41	60.48	
C	\rightarrow 5)- α -Araf-(1 \rightarrow	H	5.16	4.22	4.03	4.22	3.72	
		C	108.59	81.10	75.70	81.59	66.14	
D	\rightarrow 3,5)- α -Araf-(1 \rightarrow	H	5.07	4.21	4.06	3.95	3.72	
		C	106.55	78.51	80.60	83.28	65.53	
E	\rightarrow 4)- α -GalAp-(1 \rightarrow	H	4.98	3.67	4.04	4.05	4.74	
		C	98.69	67.44	69.32	81.63	70.37	174.01
F	\rightarrow 2)- α -Rhap-(1 \rightarrow	H	5.16	4.34	4.04	3.57	3.45	1.16
		C	98.17	76.02	69.32	72.04	70.91	15.84
G	\rightarrow 2,4)- α -Rhap-(1 \rightarrow	H	4.93	4.34	4.04	3.92	3.57	1.22
		C	97.00	76.02	69.32	76.85	72.04	16.05
H	\rightarrow 3,6)- β -Galp-(1 \rightarrow	H	4.58	4.01	4.04	4.06	3.61	3.80
		C	103.48	75.70	83.16	67.95	74.47	68.37



backbone to the RG-I domain, which was composed of $[\rightarrow 4)\text{-}\alpha\text{-GalAp-(1}\rightarrow 2)\text{-}\alpha\text{-Rhap-(1}\rightarrow]$ and $[\rightarrow 4)\text{-}\alpha\text{-GalAp-(1}\rightarrow 2,4)\text{-}\alpha\text{-Rhap-(1}\rightarrow]$ repeating units with the branches located at C4 of $\alpha\text{-Rhap}$. However, the branching points of RG-I differ in pectins from different plant sources. Naran et al. isolated a RG-I pectin from flax seed mucilage in which the branching point was located at C-3 of $(1\rightarrow 2)\text{-}\alpha\text{-Rhap}$ (24). Although WVPP-A2b and WVPP-A3b both contained typical HG and RG-I domains, the neutral side chains differed and the AG-II structure in WVPP-A3b was more complex.

3.5. Enzymatic analysis of WVPP-A2b and WVPP-A3b

Based on the monosaccharide composition and NMR results, WVPP-A2b and WVPP-A3b both contained HG, RG-I, and RG-II domains. For further analysis of the pectin structure and function, WVPP-A2b and WVPP-A3b were hydrolyzed using endo-PG hydrolysis and the different domains were separated by HPGPC.

3.5.1. Preparation of de-esterified pectin

Endo-polygalactonase M2 (EC 3.2.1.15) specifically recognizes and hydrolyzes the unesterified GalA in a HG-type domain. The presence of methyl and acetyl groups in HG often affects the enzymatic hydrolysis of pectinase, thereby affecting the purity of the HG domain (25). Therefore, in this study, the de-esterification of the pectin was conducted at a lower temperature in a weakly alkaline environment. FT-IR, HPGPC, and monosaccharide composition analysis were used to evaluate the de-esterification effect and the structural integrity of WVPP-A2b and WVPP-A3b. Based on the HPGPC elution profiles (Figures 7A,B), no significant change in the M_w distribution of WVPP-A2b and WVPP-A3b was observed after saponification treatment, suggesting that the long chain of the pectin was not broken during the saponification reaction. In

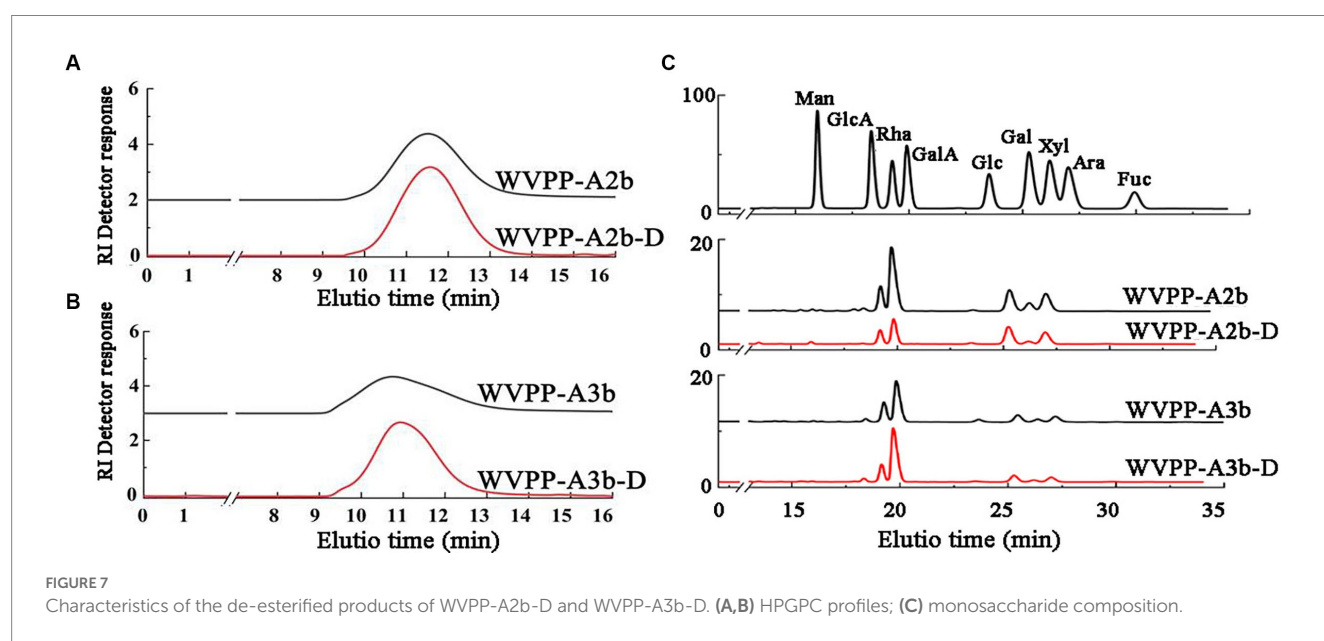


TABLE 4 Yield, molecular weight (*M_w*), and monosaccharide composition of enzymatic hydrolysates (E1–E3 fractions) of the pectins WVPP-A2b and WVPP-A3b.

Fractions	Yield ^a (w%)	TBA test	<i>M_w</i> (kDa)	Monosaccharide composition (mol%)							
				GalA	Rha	Gal	Ara	Glc	GlcA	Man	Xyl
WVPP-A2b-E1	46.2	–	59.7	15.8	15.6	29.0	29.3	1.5	1.0	7.8	–
WVPP-A2b-E2	17.5	+	9.7 and 5.4	39.1	19.8	11.9	16.7	1.9	4.0	0.8	5.8
WVPP-A2b-E3	36.4	–	<2.0	91.3	–	1.2	0.6	1.3	0.7	4.2	0.7
WVPP-A3b-E1	50.2	–	73.6	31.0	30.6	19.3	14.3	1.9	1.8	1.1	0.9
WVPP-A3b-E2	10.8	+	10.4 and 6.4	27.4	16.0	20.5	23.6	3.4	6.3	1	1.8
WVPP-A3b-E3	41.8	–	<2.0	95.9	–	0.5	0.5	1.0	0.3	1.4	0.4

^aYield relative to WVPP-A2b or WVPP-A3b.

addition, the monosaccharide compositions of WVPP-A2b-D and WVPP-A3b-D were not significantly changed from that of the original pectin fraction (Figure 7C). In the FT-IR spectra of WVPP-A2b-D and WVPP-A3b-D (Figures 2E,F), the signal near 1749 cm⁻¹ attributed to C=O of the methylated –COO⁻ disappeared, whereas the signal near 1,610 cm⁻¹ increased significantly, indicating that the methyl groups of WVPP-A2b and WVPP-A3b were removed completely.

3.5.2. Analysis of enzymatic hydrolysates

Endo-PG specifically degrades unesterified GalA, degrading the HG domain to oligogalacturonide structural units, while releasing the RG-I and RG-II-type domains from the pectin. In this study, endo-PG was used to degrade the two pectins and resulted in two enzymatic hydrolysates, namely, WVPP-A2b-DE and WVPP-A3b-DE. Based on the HPGPC results (Supplementary Figure S2), the *M_w* of WVPP-A2b and WVPP-A3b changed significantly, and multiple chromatographic peaks were observed in the HPGPC profiles. WVPP-A2b-DE and WVPP-A3b-DE were further fractionated using a Sephadex G-75 column and three types of hydrolysates (E1–E3) were prepared for both WVPP-A2b and WVPP-A3b (Supplementary Figure S3).

The *M_w* of WVPP-A2b-DE1 and WVPP-A3b-DE1 was 59.7 and 73.6 kDa, respectively (Table 4). The de-esterified hydrolysates were mainly composed of GalA, Rha, Gal, and Ara, and the molar ratio of Rha/GalA was close to 1, indicating that the hydrolysates were RG-I-type pectins. WVPP-A2b-DE1 contained higher proportions of Gal (29.0%) and Ara (29.3%) than WVPP-A3b-DE1. The ratio of (Ara + Gal)/Rha reflects the average length and relative monosaccharide proportions of the neutral side chains in the RG-I domain (25). The molar ratio of (Gal + Ara)/Rha in WVPP-A2b-DE1 was 3.7, which was approximately 3.4 times higher than that of WVPP-A3b-DE1. This result indicated that the neutral sugar side chains in WVPP-A2b-DE1 were longer or more highly branched than in WVPP-A3b-DE1. Both WVPP-A2b-DE2 and WVPP-A3b-DE2 showed positive results in TBA reactions, suggesting that both are RG-II-type pectins. Double peaks were observed in the HPGPC spectra, with *M_w* distributions of 5.4–10.4 kDa. The *M_w* of WVPP-A2b-DE3 and WVPP-A3b-DE3 was less than 2.0 kDa and both hydrolysates were mainly composed of GalA (82.9%–95.9%), indicating that they were oligogalacturonides produced by endo-PG hydrolysis of the HG-type domains.

3.6. Antioxidant activity analysis

The *in vitro* antioxidant activities of WVPP-A2b and WVPP-A3b were measured as the ability to scavenge DPPH, hydroxyl, and ABTS radicals. Within the tested range (0.5–10 mg/mL), WVPP-A2b and WVPP-A3b showed significant abilities to scavenge DPPH, hydroxyl, and ABTS radicals in a dose-dependent manner (Figures 8A–F). The 50% inhibition concentrations (IC₅₀) of WVPP-A2b toward the three radicals were 10.23, 11.21, and 11.33 mg/mL, respectively, whereas the corresponding IC₅₀ values of WVPP-A3b were 6.22, 8.76, and 5.12 mg/mL. These results indicated that the radical-scavenging ability of WVPP-A3b was superior to that of WVPP-A2b in the present test system, but was lower than that of Vc.

To further investigate the relationship between the antioxidant activity and structure of WVPP-A2b and WVPP-A3b, the radical-scavenging abilities of the de-esterified pectins (WVPP-A2b-D and WVPP-A3b-D) and their different domains, comprising WVPP-A2b-E1 (RG-I), WVPP-A2b-E2 (RG-II), and WVPP-A2b-E3 (oligogalacturonides), were measured. The degree of methyl-esterification is an important factor affecting the antioxidant activity of pectin. Generally, the degree of methylation of the pectin plays an important role in the antioxidant activity. Wikiera et al. observed that the antioxidant activity of apple pectins was negatively correlated with the degree of methylation (26). In this study, WVPP-A2b and WVPP-A3b showed similar degrees of methyl-esterification, but WVPP-A3b showed a stronger ability to scavenge DPPH, hydroxyl, and ABTS radicals. Interestingly, after de-esterification, the antioxidant effect of WVPP-A3b was significantly enhanced; however, the effect of de-esterification on the antioxidant ability of WVPP-A2b was extremely weak. These results indicated that the relationship between the structure of the pectin and its antioxidant activity is quite complex and may be a result of the interaction of many factors. Molecular weight is an important factor affecting the antioxidant activity of polysaccharides. It is generally believed that high-molecular-weight pectin facilitates the formation of a large number of intermolecular or intramolecular hydrogen bonds, leading to a decrease in the activity of hydroxyl groups. However, pectin with a lower molecular weight may have a relatively loose conformation that facilitates the exposure of free hydroxyl groups and the reaction of radicals to remove them (27). In contrast, the monosaccharide composition of the polysaccharides plays an important role in their antioxidant

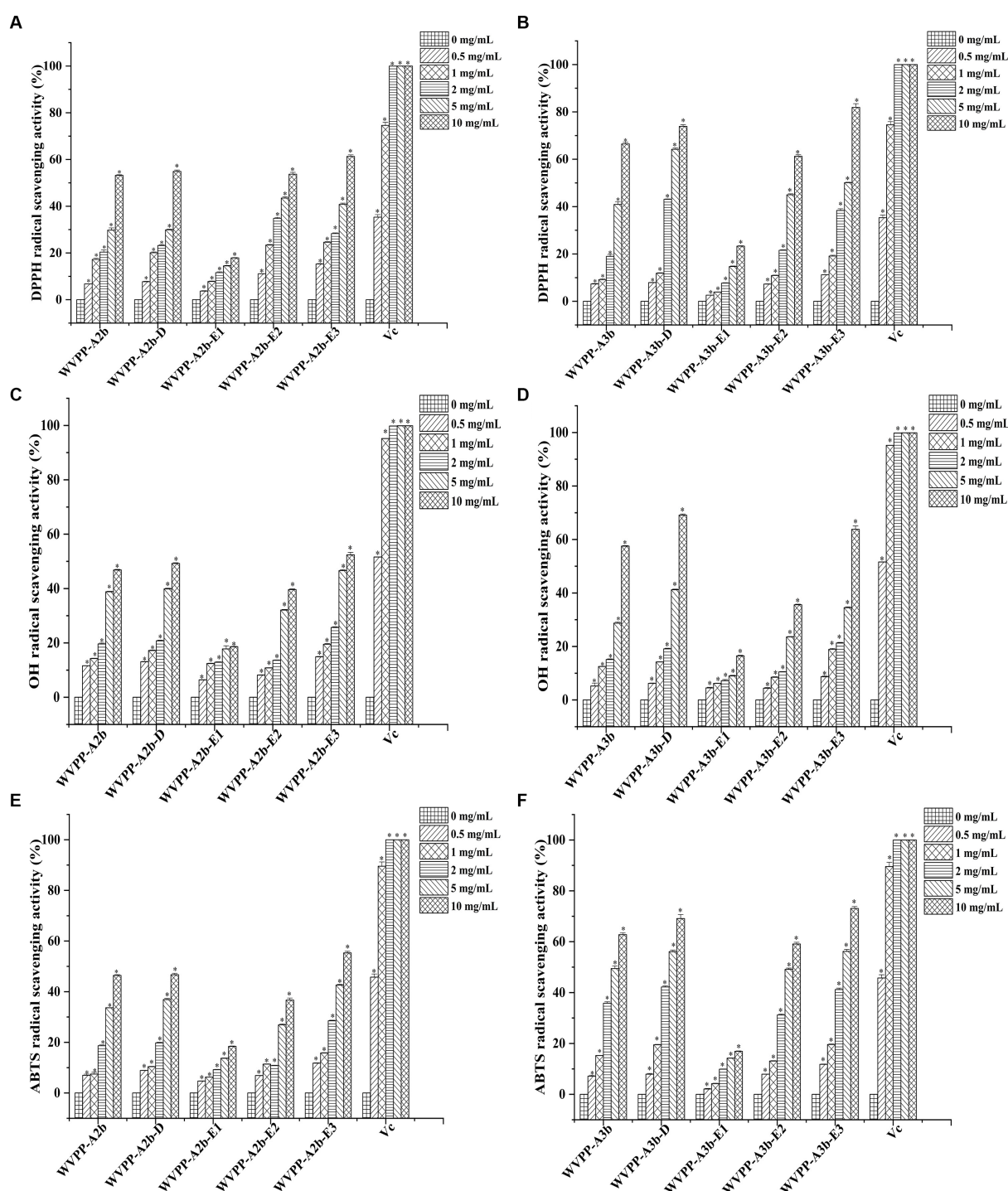


FIGURE 8

Ability of *Veronica peregrina* pectin fractions to scavenge (A,B) DPPH radicals, (C,D) hydroxyl radicals, and (E,F) ABTS radicals. Ascorbic acid (Vc) was used as a positive control. Each value represents the mean \pm SD ($n=3$; * $p<0.05$). All experiments were performed in triplicate.

activity. Li et al. found that GlcA and GalA had significant effect on the scavenging ability of *Cissus pteroclada* Hayata (CPHP) on DPPH, superoxide radical, hydroxyl radical, and ABTS radical (3). Some neutral monosaccharide, such as Gal, Ara, and Glc had significantly effects on the DPPH radical scavenging ability of polysaccharides (28, 29). The research of Qu et al. shown that 3-O-methylated- α -D-galactopyranosyl (3-O-Me-Galp) in

Pleurotus Ostreatus polysaccharide functions as an antioxidant (30). Pectins that contain a certain amount of GalA are potent antioxidants; the content of uronic acid and its degree of polymerization may impart the antioxidant activity to the pectin (31). The ability of the three domains obtained by enzymatic hydrolysis of WVPP-A2b and WVPP-A3b to scavenge free radicals is summarized in Figure 8. Within the dose range of

0.5–10 mg/mL, the radical-scavenging ability of the three domains varied greatly. The relative radical-scavenging ability was as follows: that of oligogalacturonides (which had the highest amount of GalA and the lowest *M_w*) was higher than that of the RG-II domain (E2), and the RG-I domain (E1; which had a lower content of GalA and higher number of branches) showed the lowest radical-scavenging ability. Furthermore, the radical-scavenging ability of oligogalacturonides was dose-dependent and was superior to that of the pectins (WVPP-A2b and WVPP-A3b) at the same concentration. The results were in accordance with the results of previous study, which confirmed that pectin containing higher content of GalA and HG type domains has stronger radical scavenging capacity (5, 32).

Based on these results, WVPP-A3b had stronger antioxidant activity than did WVPP-A2b, which may be due to the higher GalA content and lower molecular weight of WVPP-A3b. However, the presence of methyl groups weakened its ability to scavenge free radicals. The *in vitro* antioxidant ability of WVPP-A2b and WVPP-A3b was the result of the synergistic effects of different pectin domains, of which the HG domain contributed the most, followed by the RG-II domain; the RG-I domain, which had a higher number of branches and higher *M_w*, contributed the least to the antioxidant activity of the pectin.

4. Conclusion

In this study, two pectins, designated WVPP-A2b and WVPP-A3b, were prepared from *V. peregrina*, and their structural properties and antioxidant activity were investigated. The *M_w* distributions of WVPP-A2b and WVPP-A3b are 48.7×10^4 and 77.6×10^4 kDa, respectively. The principal monosaccharides in both pectins are GalA, Rha, Gal, and Ara, with the total proportion exceeding 80%. Both pectins contain HG, RG-I, and RG-II domains with mass ratios of 2.08:2.64:1.00 and 3.87:4.65:1.00, respectively. The branches of both polysaccharides are located at C4 of α -Rhap. The RG-I domains of both WVPP-A2b and WVPP-A3b contain arabinan and AG-II structures. In addition, WVPP-A2b also contains a disaccharide short side chain formed by the [t- α -Araf-(1 \rightarrow 5)- α -Araf-(1 \rightarrow)] structural unit. The two pectins exhibit similar methyl esterification but differ in their radical-scavenging ability. WVPP-A3b, which has a higher content of GalA and HG domain, exhibits stronger radical-scavenging activity and is a potential natural antioxidant agent for use in medicine or functional foods.

References

- Yapo BM. Pectic substances: From simple pectic polysaccharides to complex pectins—a new hypothetical model. *Carbohydr Polym.* (2011) 86:373–85. doi: 10.1016/j.carbpol.2011.05.065
- Goellner EM, Utermohlen J, Kramer R, Classen B. Structure of Arabinanogalactan from *Larix laricina* and its reactivity with antibodies directed against type-II-Arabinanogalactans. *Carbohydr Polym.* (2011) 86:1739–44. doi: 10.1016/j.carbpol.2011.07.006
- Wang JQ, Hu SZ, Nie SP, Yu Q, Xie MY. Reviews on Mechanisms of In Vitro Antioxidant Activity of Polysaccharides. *Oxidative Med Cell Longev.* (2016) 2016:5692852. doi: 10.1155/2016/5692852
- Cui JF, Zhao CY, Feng LP, Han YH, Du HJ, Xiao H, et al. Pectins from fruits: Relationships between extraction methods, structural characteristics, and functional properties. *Trends Food Sci Technol.* (2021) 110:39–54. doi: 10.1016/j.tifs.2021.01.077
- Ning X, Liu Y, Jia MD, Wang QD, Sun ZY, Ji L, et al. Pectic polysaccharides from *Radix Sophorae Tonkinensis* exhibit significant antioxidant effects. *Carbohydr Polym.* (2021) 262:117925. doi: 10.1016/j.carbpol.2021.117925
- Kwak JH, Kim HJ, Lee KH, Kang SC, Zee OP. Antioxidative Iridoid Glycosides and Phenolic Compounds from *Veronica peregrina*. *Arch Pharm Res.* (2009) 32:207–13. doi: 10.1007/s12272-009-1137-x
- Linhart YB. Intra-population differentiation in annual plants I. *Veronica peregrina* L. raised under non-competitive conditions. *Evolution.* (1974) 28:232–43. doi: 10.1111/j.1558-5646.1974.tb00742.x
- Dubois M, Gilles KA, Hamilton JK, Rebers PA, Smith F. Colorimetric method for determination of sugars and related substances. *Anal Chem.* (1956) 28:350–6. doi: 10.1021/ac60111a017

Data availability statement

The original contributions presented in the study are included in the article/[Supplementary material](#), further inquiries can be directed to the corresponding author.

Author contributions

SY and XL: investigation and writing—original draft. YW and LB: investigation. YZ: formal analysis. LS and SC: writing—review and editing. All authors contributed to the article and approved the submitted version.

Funding

This work was supported by the National Natural Science Foundation of China (no: 32271339 and 32000907) and the Scientific and Technologic Foundation of Jilin Province (no: 20210401060YY).

Conflict of interest

The authors declare that the research was conducted in the absence of any commercial or financial relationships that could be construed as a potential conflict of interest.

Publisher's note

All claims expressed in this article are solely those of the authors and do not necessarily represent those of their affiliated organizations, or those of the publisher, the editors and the reviewers. Any product that may be evaluated in this article, or claim that may be made by its manufacturer, is not guaranteed or endorsed by the publisher.

Supplementary material

The Supplementary material for this article can be found online at: <https://www.frontiersin.org/articles/10.3389/fnut.2023.1217862/full#supplementary-material>

9. Blumenkrantz N, Asboe-Hansen G. New method for quantitative determination of uronic acids. *Anal Biochem.* (1973) 54:484–9. doi: 10.1016/0003-2697(73)90377-1
10. York WS, Darvill AG, McNeil M, Albersheim P. 3-deoxy-d-manno-2-octulosonic acid (KDO) is a component of rhamnogalacturonan II, a pectic polysaccharide in the primary cell walls of plants. *Carbohydr Res.* (1985) 138:109–26. doi: 10.1016/0008-6215(85)85228-9
11. Zhang X, Yu L, Bi H, Li X, Ni W, Han H, et al. Total fractionation and characterization of the water-soluble polysaccharides isolated from *Panax ginseng* C. A Meyer. *Carbohydr Polym.* (2009) 77:544–52. doi: 10.1016/j.carbpol.2009.01.034
12. Chattopadhyay N, Ghosh T, Sinha S, Chattopadhyay K, Karmakar P, Ray B. Polysaccharides from *Turbinaria conoides*: Structural features and antioxidant capacity. *Food Chem.* (2010) 118:823–9. doi: 10.1016/j.foodchem.2009.05.069
13. Yang X, Wang RF, Zhang S, Zhu W, Tang J, Liu J, et al. Polysaccharides from *Panax japonicus* C.A. Meyer and their antioxidant activities. *Carbohydr Polym.* (2014) 101:386–91. doi: 10.1016/j.carbpol.2013.09.038
14. Zhang S, Li XZ, Wu ZP, Kuang CT. Antioxidant Activity of Polysaccharide from Camellia Cake against ABTS and DPPH Free Radicals. *Adv Mater Res.* (2012) 550-553:1545–9. doi: 10.4028/www.scientific.net/AMR.550-553.1545
15. Boulet JC, Williams P, Doco T. A Fourier transform infrared spectroscopy study of wine polysaccharides. *Carbohydr Polym.* (2007) 69:79–85. doi: 10.1016/j.carbpol.2006.09.003
16. Singthong J, Cui SWS, Ningsanond H, Goff D. Structural characterization, degree of esterification and some gelling properties of Krueo Ma Noy (*Cissampelos pareira*) pectin. *Carbohydr Polym.* (2004) 58:391–400. doi: 10.1016/j.carbpol.2004.07.018
17. Chen X, Qi Y, Zhu C, Wang Q. Effect of ultrasound on the properties and antioxidant activity of hawthorn pectin. *Int J Biol Macromol.* (2019) 131:273–81. doi: 10.1016/j.ijbiomac.2019.03.077
18. Guo R, Tian S, Li X, Wu X, Wu Y. Pectic polysaccharides from purple passion fruit peel: A comprehensive study in macromolecular and conformational characterizations. *Carbohydr Polym.* (2020) 229:115406. doi: 10.1016/j.carbpol.2019.115406
19. Li N, Liu X, He XX, Wang SY, Cao SJ, Zheng X, et al. Structure and anticoagulant property of a sulfated polysaccharide isolated from the green seaweed *Monostroma angicava*. *Carbohydr Polym.* (2017) 159:195–206. doi: 10.1016/j.carbpol.2016.12.013
20. He TB, Huang YP, Huang YW, Wang XJ, Hu JM, Sheng J. Structural elucidation and antioxidant activity of an Arabinogalactan from the leaves of *Moringa oleifera*. *Int J Biol Macromol.* (2018) 112:126–33. doi: 10.1016/j.ijbiomac.2018.01.110
21. Yang BK, Prasadb N, Jiang YM. Structure identification of a polysaccharide purified from litchi (*Litchichinensis* Sonn.) pulp. *Carbohydr Polym.* (2016) 137:570–5. doi: 10.1016/j.carbpol.2015.10.088
22. Halliwell B, Gutteridge JMC. Oxygen toxicity, oxygen radicals, transition metals and disease. *Biochem J.* (1984) 219:1–4. doi: 10.1042/bj2190001
23. Ojha AK, Maiti D, Chandra K, Mondal S, Roy DDSK, Ghosh K, et al. Structural assignment of a heteropolysaccharide isolated from the gum of *Cochlospermum religiosum* (Katira gum). *Carbohydr Res.* (2008) 343:1222–31. doi: 10.1016/j.carres.2008.03.010
24. Naran R, Chen GB, Carpita NC. Novel Rhamnogalacturonan I and Arabinanoxylan Polysaccharides of Flax Seed Mucilage. *Plant Physiol.* (2008) 148:132–41. doi: 10.1104/pp.108.123513
25. Lin YP, An FP, He H, Geng F, Song H, Huang Q. Structural and rheological characterization of pectin from passion fruit (*Passiflora edulis* f. *flavicarpa*) peel extracted by high-speed shearing. *Food Hydrocoll.* (2021) 114:106555. doi: 10.1016/j.foodhyd.2020.106555
26. Wikiera A, Koziol A, Mika M, Bozena S. Structure and bioactivity of apple pectin isolated with Arabinanase and mannanase. *Food Chem.* (2022) 388:133020. doi: 10.1016/j.foodchem.2022.133020
27. Teng H, He Z, Li X, Shen W, Wang J, Zhao D, et al. Chemical structure, antioxidant and anti-inflammatory activities of two novel pectin polysaccharides from purple passion fruit (*Passiflora edulia* Sims) peel. *J Mol Struct.* (2022) 1264:133309. doi: 10.1016/j.molstruc.2022.133309
28. Li Y, Lin D, Jiao B, Xu C, Qin J, Ye G, et al. Purification, antioxidant and hepatoprotective activities of polysaccharide from *Cissus pteroclada* Hayata. *Int J Biol Macromol.* (2015) 77:307–13. doi: 10.1016/j.ijbiomac.2015.03.039
29. Zhu ZY, Song XY, Jiang YZ, Yao JR, Jiang Y, Li Z, et al. Chemical structure and antioxidant activity of a neutral polysaccharide from *Asteris Radix* et *Rhizoma*. *Carbohydr Polym.* (2022) 286:119309. doi: 10.1016/j.carbpol.2022.119309
30. Qu YH, Yan JM, Zhang X, Song CC, Zhang MS, Mayo KH, et al. Structure and antioxidant activity of six mushroom-derived heterogalactans. *Int J Biol Macromol.* (2022) 209:1439–49. doi: 10.1016/j.ijbiomac.2022.04.135
31. Teng C, Qin P, Shi Z, Zhang W, Yang X, Yao Y, et al. Structural characterization and antioxidant activity of alkali-extracted polysaccharides from quinoa. *Food Hydrocoll.* (2021) 113:106392. doi: 10.1016/j.foodhyd.2020.106392
32. Liu Y, Zhang B, Ibrahim SA, Gao SS, Yang H, Huang W. Purification, characterization and antioxidant activity of polysaccharides from *Flammulina velutipes* residue. *Carbohydr Polym.* (2016) 145:71–77. doi: 10.1016/j.carbpol.2016.03.020



OPEN ACCESS

EDITED BY

Tomislav Tosti,
University of Belgrade, Serbia

REVIEWED BY

Ivan Kojic,
University of Belgrade, Serbia
Snežana Filip,
University of Novi Sad, Serbia

*CORRESPONDENCE

A. F. M. Shahid Ud Daula,
✉ shahid@nstu.edu.bd
Abdullah Al Mamun,
✉ pharmaalmamun@yahoo.com

†These authors have contributed equally to this work and share first authorship

RECEIVED 29 November 2023

ACCEPTED 19 January 2024

PUBLISHED 14 February 2024

CITATION

Ahmed S, Ahmed KS, Rahman MN, Hossain H, Han A, Geng P, Daula AFMSU and Mamun AA (2024), Polyphenols and extracts from *Zingiber roseum* (Roxb.) Roscoe leaf mitigate pain, inflammation and pyrexia by inhibiting cyclooxygenase-2: an *in vivo* and *in silico* studies.
Front. Pharmacol. 15:1344123.
doi: 10.3389/fphar.2024.1344123

COPYRIGHT

© 2024 Ahmed, Ahmed, Rahman, Hossain, Han, Geng, Daula and Mamun. This is an open-access article distributed under the terms of the Creative Commons Attribution License (CC BY). The use, distribution or reproduction in other forums is permitted, provided the original author(s) and the copyright owner(s) are credited and that the original publication in this journal is cited, in accordance with accepted academic practice. No use, distribution or reproduction is permitted which does not comply with these terms.

Polyphenols and extracts from *Zingiber roseum* (Roxb.) Roscoe leaf mitigate pain, inflammation and pyrexia by inhibiting cyclooxygenase-2: an *in vivo* and *in silico* studies

Shakhawat Ahmed^{1†}, Khondoker Shahin Ahmed^{2†},
Md. Naiemur Rahman¹, Hemayet Hossain², Aixia Han³,
Peiwu Geng³, A. F. M. Shahid Ud Daula ^{1*} and
Abdullah Al Mamun ^{3*}

¹Department of Pharmacy, Noakhali Science and Technology University, Sonapur, Bangladesh, ²Chemical Research Division, Bangladesh Council of Scientific and Industrial Research (BCSIR), Dhaka, Bangladesh, ³Central Laboratory of The Sixth Affiliated Hospital of Wenzhou Medical University, Lishui People's Hospital, Lishui, Zhejiang, China

Zingiber roseum (Roxb.) Roscoe, a perennial herb from the Zingiberaceae family, has a long history of traditional use in the treatment of several ailments including pain, inflammation, fever, cough, arthritis, skin diseases, and liver infections. This study sought to confirm the efficacy of *Zingiber roseum* (Roxb.) Roscoe leaves methanol extract (ZrLME) as reported in traditional usage by evaluating its analgesic, anti-inflammatory, and antipyretic capabilities. In addition, *in silico* molecular docking of the metabolites identified in ZrLME was studied to verify the experimental outcomes. ZrLME demonstrated strong dose-dependent analgesic efficacy against all analgesic tests. ZrLME (400 mg/kg) showed higher anti-inflammatory activity than the standard in the carrageenan-induced paw edema test model. A significant reduction of rectal temperature (3.97°F↓) was also recorded at the same dose of ZrLME after 24 h of treatment. Seven polyphenolic metabolites were identified and quantified by HPLC-DAD analysis, including 3, 4- dihydroxy benzoic acid, (-) epicatechin, rutin hydrate, p-coumaric acid, trans-ferulic acid, rosmarinic acid, and myricetin. Strong binding affinities (ranges from -5.8 to -8.5 Kcal/mol) between the aforesaid polyphenols and cyclooxygenase-2 were discovered. Moreover, molecular dynamics simulations (MDS) demonstrated that these polyphenols exhibit significant COX-2 inhibitory activity due to their high stability in the COX-2 active site. In computational prediction, the polyphenols were also found to be nontoxic, and a variety of biological activities, such as antioxidant, analgesic,

Abbreviations: ZrLME, *Zingiber roseum* (Roxb.) Roscoe leaves methanol extract; ANOVA, Analysis of variance; 5HT, 5-hydroxytryptamine; COX-2, Cyclooxygenase-2; PGE2, Prostaglandin E2; PASS, Prediction of activity spectra for substance; SEM, Standard error of mean; Da, Dalton; nm, nanometer; TNF-α, Tumor necrosis factor alpha; BW, Body weight; kg, kilogram; mg, milligram; IL-1, Interleukin-1; μg, microgram.

anti-inflammatory, antipyretic, and hepatoprotective, were observed. The results of this study revealed that ZrlME possesses notable analgesic, anti-inflammatory, and antipyretic properties.

KEYWORDS

Zingiber roseum, polyphenols, analgesic activity, anti-inflammatory activity, antipyretic activity

1 Introduction

The social and healthcare systems are heavily burdened by pain, fever, and inflammatory consequences, which have been known to harm people for generations. The frequency and incidence of pain-related diseases are increasing day by day, with 30% of adults worldwide experiencing pain and inflammatory diseases and 20% receiving a chronic illness diagnosis each year (Javed et al., 2020). They commonly manifest in a diverse array of pathological circumstances, encompassing wounds, infections, tissue injury, inflammation, and many diseased states. Pain is an unpleasant feeling brought on by sensory and tissue damage, and it profoundly impacts many aspects of human functioning (Puebla Díaz, 2005). In addition to sleeplessness, anxiety, weariness, decreased appetite, and even limb dysfunctions, pain can occur in any part of the body, including the head, stomach, limbs, muscles, and joints (Chou et al., 2016). Inflammation is a complex process that is brought on by a variety of factors, including mechanical injury, tissue ischemia, pathogenic agents, and toxic substances. It is characterized by tissue alterations that allow for the rapid migration of immune cells to the sites of inflammation (Chen et al., 2018; Gupta et al., 2018). Fever, or pyrexia, is a complicated immunophysiological illness that is brought on by a series of biochemical responses to inflammatory or infectious stimuli in the body (Muhammad et al., 2019). Inflammatory and pathogenic diseases, such as IL-6, CRF, IL-1, chemokines, and especially PGE₂, cause the production of many endogenous pyrogens (Roth et al., 2006). Prostaglandin E₂ (PGE₂) is a key eicosanoid component of the central nervous system during fever in animals (Gaetano et al., 2010). Conventional non-steroidal anti-inflammatory medicines (NSAIDs) suppress the synthesis of prostaglandins, which are the most significant inflammatory mediators, by non-specifically blocking the activity of both COX-1 and COX-2 enzymes (Botting, 2010). For fever, pain, and inflammation, commonly recommended NSAIDs and narcotic analgesics are those with efficacy data. However, NSAIDs are frequently used to treat a variety of inflammatory disorders, but their prolonged use is associated with a number of negative side effects, including liver and kidney damage, gastrointestinal ulcers and bleeding, and gastrointestinal hemorrhage (Kwiecień et al., 2015). In this context, natural medications made from numerous medicinal plants can be compelling substitutes.

Medicinal plants are alluring sources of biologically active substances that can protect people from a range of serious ailments. An essential category of secondary metabolites consists of polyphenols, which are significant for the countless potential health benefits they may provide. They are classified into several subgroups, including tannins, quinones, curcuminoids, flavonoids, phenolic acids, lignans, coumarins, and stilbenes. Various biological

effects can be attributed to these phenolic chemicals, including anti-thrombotic, antibacterial, immunomodulatory, vasodilatory, hepatoprotective, anti-inflammatory, analgesic, antipyretic, and anti-arthritis effects (Benavente-García et al., 1997; Middleton et al., 2000; Manach et al., 2005a). However, due to their negligible side effects, plant-derived metabolites have caught the attention of researchers as a possible substitute therapy for arthritis, inflammation, fever and other neuropathic pain.

Zingiber roseum (Roxb.) Roscoe, often known as “Jangli Adrak,” is an upright, perennial herb in the Zingiberaceae family. Despite its rarity, this plant can be found all over the Himalayas (Babu, 1977). It features long leaves, a tuberous rhizome, an upright stem, red blooms, and white seeds. *Z. roseum* features a ligule that is 1.2–1.5 cm long, dull red spikes with white colour bottom, a long peduncle, red petals with white bases, a bump in the rhizomes, a complete labellum with a light yellow edge (Rahman and Yusuf, 2013). The plant is indigenous to Bangladesh and can be found in South China, Thailand, and Myanmar. *Z. roseum* is utilized by the Munchingputtu Mandal tribes of India, Visakhapatnam District, to heal wounds, ulcers, night blindness, piles, coughs, swelling throats, stomachaches, and cardiac infections. It has also been used for centuries to cure dyspepsia, skin problems, coughs, liver infections, and fevers (Mahawer et al., 2023; Rahman et al., 2023). The rhizomes of *Z. roseum* are used by traditional healers in Bangladesh to cure rheumatic diseases, asthma, and wounds (Al-Amin et al., 2019). The acute toxicity assessment of this plant’s rhizomes indicates that they are safe for human consumption (Amanat et al., 2023). Despite the extensive historical usage of *Z. roseum* in traditional medicine, there remains a significant lack of understanding regarding the majority of its pharmacological effects. The present investigation aimed to evaluate the *in vivo* analgesic, anti-inflammatory, and antipyretic properties of ZrlME, with the objective of substantiating its traditional medicinal application. The current study’s objective was also to identify and analyze phenolic metabolites in ZrlME using HPLC-DAD analysis.

The docking technique is now widely used as a common computational tool for discovering new active metabolites and their affinity to specific receptors (Parenti and Rastelli, 2012). Using molecular docking studies, we also tried to identify the potential mechanism behind the analgesic, anti-inflammatory, and antipyretic activities of identified polyphenols. For molecular docking investigations, the target enzyme cyclo-oxygenase-2 (COX-2) was selected. In order to inhibit the production of prostaglandins, which are linked to pain, fever, and inflammation, we must inhibit the activity of the COX-2 enzyme, which is produced during an inflammatory response and results in pain, swelling, and stiffness (Hawkey, 1999). Therefore, we tried to figure out how well the identified chemicals bound to the cyclo-oxygenase-2 (COX-2) enzyme. In addition, to validate the results of the experiments,

absorption, distribution, metabolism, excretion, and toxicity (ADMET) profile of the discovered polyphenols of ZrlME were also investigated.

2 Materials and methods

2.1 Plant materials

After collection from the Sitakunda hill region in Chattagram, Bangladesh, the plant specimen was identified and verified by Professor Shaikh Bokhtear Uddin, a faculty member in the Department of Botany at Chittagong University. The herbarium at Chittagong University has a voucher specimen of this plant species (Accession number, SBU11064).

2.2 Extract preparation

The leaves of the plant were clipped, cleaned, and pulverized into a fine powder after being shade-dried at room temperature. A clean glass container with a flat bottom filled with 400 g of the powder of the dried leaves of the plant and 1,500 mL of methanol was added. The mixture was allowed to sit at room temperature for 15 days while being sometimes shaken and stirred. After filtering with Whatman filter paper No. 1, the solution was concentrated using a rotary evaporator. The resultant extracts were then vacuum dried and stored in sealed glass vials in a refrigerator.

2.3 HPLC-DAD analysis

Shimadzu LC-20A system (Tokyo, Japan) was used to analyze the extract's phenolic content. The instrument setup and solvent system were followed according to Talukder et al., 2022; Talukder et al., 2022). The following settings were used: injection volume of 20 L, 0.5 mL/min flow rate, 5%–25% solution A for the first 0.01–20 min, 25–40 min, 40–60 min, 60 to 35 min, 30%–5% minutes, and 5% minutes for the next 40–50 min. Based on the peak area, the concentrations of each metabolite were determined, and the values were represented in mg per 100 g dry extract.

2.4 Experimental animals

The Swiss-albino mice, weighing between 20 and 25 g, were obtained from the animal house located at Jahangirnagar University in Dhaka, Bangladesh. The mice were housed in plastic cages with ambient illumination that alternated between 12 h of darkness and 12 h of light. During the duration of the study, mice were given unrestricted access to food and drinks. In each of the conducted studies, there were four distinct groups, with each group including six individual mice. The utilization of animals in the investigations was authorized by the Animal Ethics Committee of Noakhali Science and Technology University, under reference No. 61/2021.

2.5 Analgesic activity assay

2.5.1 Writhing test

For the acetic acid-induced writhing test, the previously described procedure was applied with certain modifications (Siegmund et al., 1957). A total of twenty mice were divided into four groups of five mice each. Normal saline was administered orally to the control group at a dosage of 10 mL/kg body weight (BW). Aspirin (100 mg/kg BW) was administered to the standard group. The two remaining groups were administered ZrlME at dosages of 200 and 400 mg/kg, respectively. After one-hour therapy, all the experimental animals received an intraperitoneal injection of acetic acid (0.2 mL, 3%) to produce painful writhing. In order to calculate the writhing movements, they were granted entry to an observation chamber, whereby the act of observation transpired during a duration ranging from 5 to 15 min. We defined writhing as trunk twisting, abdominal contractions, body lengthening, and/or the pelvis terminating with the stretching of the limbs. The data was processed using the mean percent inhibition of writhing (PIW):

$$\text{PIW} = \frac{\text{Count of writhes (control)} - \text{Count of writhes (treated)}}{\text{Count of writhes (control)}} \times 100$$

2.5.2 Formalin-induced nociception model

The formalin-induced licking test was conducted with slight adjustments to the procedure previously outlined in the literature (Hunskar and Hole, 1987). The control group received a dosage of 10 mL/kg body weight of normal saline, whereas the experimental group was administered a dosage of 100 mg/kg body weight of aspirin. The ZrlME was provided to two groups at doses of 200 and 400 mg/kg. Following an hour of individual treatments, all test animals received a subcutaneous injection of 20 µL of a 1% formalin solution with the intention of inducing discomfort. Subsequently, the mice were confined within a designated space for the purpose of conducting observations, wherein any instances of bites or licks directed towards the injected paw were duly noted and considered indicative of distress. The neurogenic or initial response time was observed to range from 0 to 5 min, but the late or inflammatory pain response was documented to occur between 20 and 30 min following the injection. The data were subjected to analysis utilizing the subsequent equation, which represented the mean percentage inhibition of the licking reaction (PIL):

$$\text{PIL} = \frac{\text{Licking reaction time (control)} - \text{Licking reaction time (treated)}}{\text{Licking reaction time (control)}} \times 100$$

2.5.3 Hot plate test

The hot plate test was conducted using an analgesimeter, following the methodology outlined by Yi et al. (2010) (Yi et al., 2010). During the course of the experiment, the temperature of the plate was maintained at a constant value of $131 \pm 1.6.9^{\circ}\text{F}$. The mice that exhibited a response time of less than or equal to 10 s to the heat stimulus on the plate were selected for the future phase of the experiment. The control group received a dosage of normal saline at a rate of 10 mL per kilogram of body weight, while the standard group received a dose of Ketorolac at a rate of 10 mg per kilogram of

body weight. The remaining two experimental groups were administered doses of 200 mg/kg and 400 mg/kg of extract. The latency duration was thereafter assessed at designated time intervals, and the termination of the latency phase was defined as the point at which the mouse initiated jumping or paw licking. In order to mitigate the risk of tissue damage, a predetermined time limit of 20 s was established. The data was subjected to analysis mean percent maximal effect (%MPE) utilizing the subsequent equation:

$\%MPE = [(La-Lb)/(C-Lb)] \times 100$; Where, La represents the latency observed after administering a drug, Lb represents the latency observed before administering the drug, and C indicates the cut-off time.

2.6 Anti-inflammatory activity

Using a paw edema test with carrageenan, anti-inflammatory activity was assessed. Animals were initially divided into four groups of five animals each. A Vernier scale was used to measure each rat's right hind paw size. Then, we administered oral doses of 10 mL/kg BW of normal saline for the control group and 10 mg/kg BW of indomethacin for the standard group, respectively. The remaining two test groups received 200 mg/kg and 400 mg/kg doses of ZrlME. After the above agents were administered for 30 min, 0.1 mL of 1% carrageenan was injected into the plantar tissue of the right hind paw of each rat to cause edema (Vázquez et al., 1996). Paw thickness was assessed at "0 h," right before the carrageenan injection, and then at "1, 2, 3, and 4 h" (hours) later. The increase in paw thickness was calculated as the difference between paw thickness at "0 h" and paw thickness at the relevant hours.

2.7 Antipyretic activity

A well-established methodology was employed to assess the antipyretic (Reza et al., 2021). To induce fever, mice were subcutaneously injected with a 30% yeast solution. Following a period of 18 h of fasting, the presence of elevated body temperature in mice, indicative of pyrexia, was ascertained through a measured rise of 1.5°F in rectal temperature. The participants in the placebo group ingested a volume of 10 mL per kilogram of body weight of normal saline. The control group was given a dosage of 150 mg/kg body weight of paracetamol, while the other two groups received dosages of 200 and 400 mg/kg body weight of leaf extract, respectively. The temperature was recorded at intervals of 30 min, 1 h, 2 h, 3 h, and 24 h.

2.8 Bioactivity prediction

The bioactivity profile of identified polyphenols, namely 3, 4-dihydroxy benzoic acid, rosmarinic acid, p-coumaric acid, (-) epicatechin, rutin hydrate, trans-ferulic acid, and myricetin, were investigated using PASS program. Pa values (probability "to be active") and Pi values (probability "to be inactive") are used to represent predicted data for each molecule for each activity. In the present study, a Pa value beyond 0.7 ($pa > 0.7$) signifies a likely activity level surpassing 70%. Experimental techniques have a higher

probability of uncovering a specific pharmacological action when the value of Pa exceeds Pi ($Pa > Pi$), particularly when the Pa value surpasses 0.7 (Marwaha et al., 2007).

2.9 In silico studies

2.9.1 Molecular docking

The molecular docking experiments were conducted on the seven discovered ligands in order to assess their potential as *in vivo* inhibitors of cyclooxygenase-2. The 3D crystal structures of proteins were obtained by utilizing the PDB files from the Protein Data Bank (Rose et al., 2016). The selected protein is identified by the accession code 3LN1, also known as COX-2. Prior to utilization, the Discovery Studio 2020 client removed water molecules, other cofactors, and associated ligands (Emon et al., 2020). The 3-dimensional (3D) structures of seven polyphenols and celecoxib, a widely used cyclooxygenase-2 inhibitor, were obtained in SDF format from the PubChem chemical molecule database (Kim et al., 2016). Subsequently, with the Open Babel graphical user interface (GUI), namely version 3.1.1, the ligands and proteins were translated into the PDBQT format (O'Boyle et al., 2011). The protein docking simulation was conducted using AutoDock Tools version 1.5.6 (Huey et al., 2012). Finally, the binding modes were viewed using the Discovery studio 2020 client (Neugebauer et al., 2002).

2.9.2 Molecular dynamics simulation (MDS)

Molecular dynamics simulation (10 ns) was performed for both apo-COX-2 and ligand-bound COX-2. The dynamics simulation was performed using the GROMACS 2021.3 simulation software. The topology for the protein and ligand were generated using the CHARMM36 force field (Omar, 2020). Subsequently, both topologies were merged to create the complex. The protein-ligand system was immersed in water using the TIP3P water model. To nullify the arrangement, counterions were introduced into the system. The entire system underwent energy minimization through 5000 iterations of steepest descent minimization. A position restraint topology was created to impose restraints on the ligands. The ligands were combined with the protein to facilitate temperature coupling. Subsequently, the system was stabilized using NVT and NPT equilibration, and then subjected to MDS. Following the completion of the molecular dynamics simulation, several parameters were assessed root-mean-square deviation (RMSD), radius of gyration, root-mean-square fluctuation (RMSF), and hydrogen bonds number between the protein and ligand.

2.10 ADMET prediction

The rate of success in drug discovery and development has significantly increased because to the use of computational screening tools for the examination of prospective metabolites' absorption, distribution, metabolism, excretion, and toxicity (ADMET) properties. These analyses of pharmacokinetics provide a descriptive concept of the action of the target metabolites in the body of human and forecast their potential

as therapeutic candidates. Human intestine absorption, plasma protein binding (PPB), Caco-2 cell permeability, blood-brain barrier penetration, skin permeability, Madin-Darby Canine Kidney (MDCK) cell permeability, and toxicity features like a mutagenic or irritating effect are examples of pharmacokinetic properties. The blood-brain barrier (BBB) penetration is a crucial aspect of drug distribution for therapeutic prospects in the central nervous system (CNS). CNS active refers to drug candidates that have the best BBB penetration potential. It must be greater than 0.40 (>0.40) for their BBB penetration rate. Greater than 90% plasma protein binding indicates a drug candidate that is strongly bound, whereas a percentage of less than 90% indicates a candidate that is weakly bound. Additionally, *in vitro* models for Caco-2 and MDCK cells' permeability have been successfully applied to predict oral drug candidates' intestine absorption. Metabolites are classified as poorly, moderately, or highly permeable based on their permeability through Caco-2 cells. A metabolite is highly permeable via Caco-2 cells if its value is greater than 70, moderately permeable through Caco-2 cells if its value is between 4 and 70, and weakly permeable through Caco-2 cells if its value is less than 4. Likewise, a score for MDCK cell permeability >500 indicates that the metabolite is highly permeable, a value between 25 and 500 indicates that it is moderately permeable, and values less than 25 indicate that it is weakly permeable. Drug candidates appropriate for oral delivery can also be found through studies on human intestinal absorption (HIA) and skin permeability. Considering their increasing negative value, substances in an *in silico* investigation exhibit features like skin permeability. The percentage of human intestinal absorption (%HIA) is used to calculate the bioavailability of drugs administered via the hepatic portal vein; a number between 70 and 100 indicates good absorbance. A therapeutic candidate with promising pharmacological characteristics may be eliminated due to toxicity concerns throughout the drug design process. A chemical is supported as a safe medication candidate when the *in silico* toxicity results are negative.

2.11 Risk assessment for bioactivity and toxicity

Using molinspiration and Osiris property explorer, seven chosen ligands were assessed for a number of bioactivities and toxicity risks. Nuclear receptor-ligand (NRL), G protein-coupled receptor ligand (GPCRL), kinase inhibitor (KI), ion channel modulator (ICM), enzyme inhibitor (EI), and protease inhibitor (PI) interaction were among the qualities expected for the bioactivity evaluation. Factors including drug score and drug likeness were used to estimate toxicity risks. The predicted analysis indicated that the chosen ligands were nontoxic substances.

2.12 Statistical analysis

The statistical studies were performed using GraphPad Prism software, specifically version 8.0.2. The data was subjected to statistical analysis using a one-way analysis of variance (ANOVA) followed by

the Bonferroni *post hoc* test. A significance level of $p < 0.05$ (*) was used to determine statistical significance.

3 Results

3.1 Phenolic composition

The phenolic profiles of ZrlME are presented in Table 1 and Figure 1. The extract included seven polyphenolic metabolites that were identified by comparing their retention times of standard. (-) Epicatechin (108.98 mg/100 g) was found to be the most prevalent in leaf extracts. The leaves extract also included significant amounts of rosmarinic acid (35.26 mg/100 g), rutin hydrate (17.37 mg/100 g), and 3,4 dihydroxy benzoic acid (12.06 mg/100 g), whereas the least amounts of myricetin (7.89 mg/100 g), trans-ferulic acid (6.24 mg/100 g), and p-Coumaric acid (2.10 mg/100 g) were identified.

3.2 Analgesic activity

3.2.1 Writhing test

Control mice writhed 31.6 times on average after being treated with acetic acid. A dose-dependent inhibition of writhes was observed in mice treated with leaf extract (Table 2). Both dosages of ZrlME prevented writhing by 22.78% and 58.28%, respectively, in comparison to the control group. On the other hand, the aspirin treated group decreased writhing by 68.35% as compared to the control group.

TABLE 1 Compounds identified in *Zingiber roseum* leaves extract.

Name of standard	Content (mg/100 g DE)
Gallic acid	Nd.
Rutin hydrate	17.37 ± 0.43
Catechin hydrate	Nd.
Catechol	Nd.
(-) Epicatechin	108.98 ± 1.47
Syringic acid	Nd.
3,4 dihydroxy benzoic acid	12.06 ± 0.28
p-Coumaric acid	2.10 ± 0.55
Caffeic acid	Nd.
Trans-Ferulic acid	6.24 ± 0.33
Vanillic acid	Nd.
Rosmarinic acid	35.26 ± 0.20
Myricetin	7.89 ± 0.24
Quercetin	Nd.
Trans-Cinnamic acid	Nd.
Kaempferol	Nd.

DE, Dry extract and Nd., Not detected

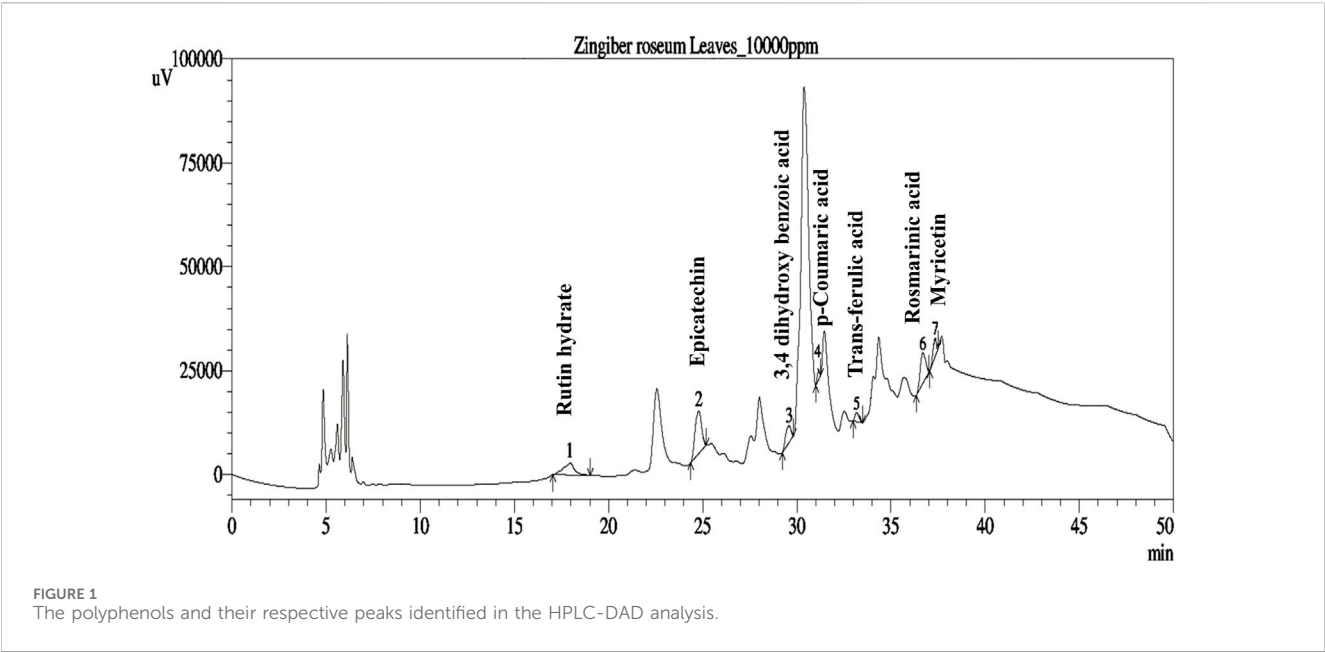


TABLE 2 The impact of *Z. roseum* (leaf) extract on the suppression of acetic acid-induced writhing.

Group	Counting writhing	% of inhibition
Control	31.50 ± 4.31	-
Aspirin	10.00 ± 1.14**	68.35
ZrIME 200 mg/kg	24.40 ± 2.11	22.78
ZrIME 400 mg/kg	13.20 ± 1.83**	58.28

The Mean ± SEM (n = 5) is used to represent all values; ZrIME represents methanol extract of *Z. roseum*. In comparison to control, *p < 0.05 and **p < 0.01, are deemed significant.

3.2.2 Formalin induced paw-licking test

In the early and late phases of the formalin test, the control group’s average licking time was 30.20 and 21 s, respectively. ZrIME dose-dependently suppressed the licking response during both stages (Figure 2). ZrIME 200 mg/kg and ZrIME 400 mg/kg decreased paw licking by 29.13% and 46.35%, respectively, in the initial phase, which was comparable to standard (49%) (Table 3). However, in the late phase, aspirin’s maximum inhibition was noted (59.04%), and ZrIME 200 mg/kg demonstrated 58.09% inhibition.

3.2.3 Hot plate test

The plant extract demonstrated a dose-dependent increase in latency against thermal stimuli (Figure 3). At 1 hour, antinociceptive activity from ZrIME at 400 mg/kg dosage (53.92%) was found higher than that from standard ketorolac (37.99%). A similar trend was also observed after 2 h, where ZrIME (400 mg/kg) produced a higher mean percent maximal effect (67.46%) than conventional ketorolac (46.03%) (Figure 4).

3.3 Anti-inflammatory activity

The results of the anti-inflammatory test are summarized in Table 4. After 1 h of the injection of carrageenan, notably, a

significant reduction (p < 0.001) of edema was detected at both doses of extracts (200 and 400 mg/kg) from ZrIME. At 4 h post-injection of carrageenan, ZrIME (200 and 400 mg/kg) demonstrated higher inhibition (68.20% and 72.73%,

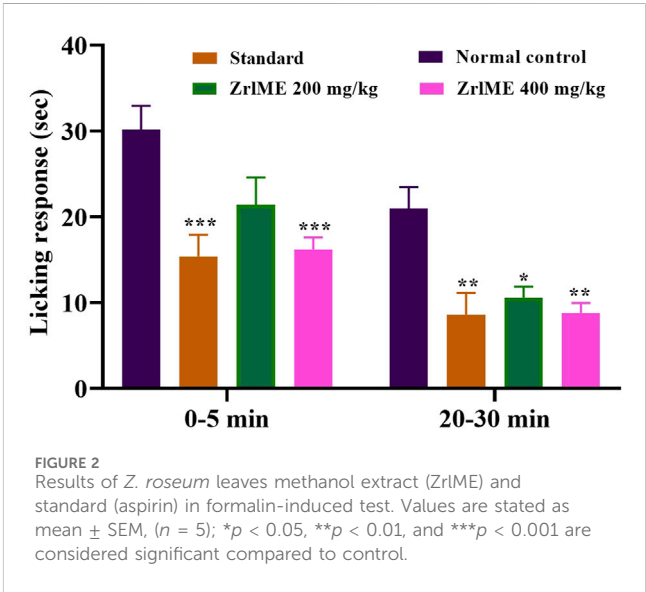


TABLE 3 Results of *Z. roseum* leaves methanol extract (ZrIME) and standard (aspirin) on % inhibition of the licking reaction.

Group	% of inhibition of licking	
	Early phase (0–5 min)	Late phase (20–30 min)
Aspirin	49.00	59.04
ZrIME 200 mg/kg	29.13	49.52
ZrIME 400 mg/kg	46.35	58.09

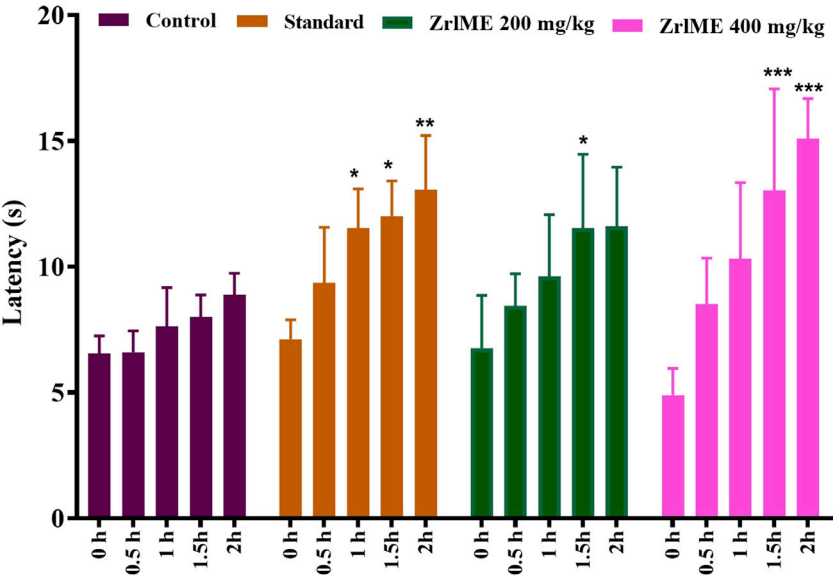


FIGURE 3 Effect of methanol extract of *Z. roseum* leaves (ZrIME) and standard (ketorolac) on the hot plate test. Values are stated as mean \pm SEM, ($n = 5$); Following an ANOVA and Bonferroni test, all data were evaluated. * $p < 0.05$, ** $p < 0.01$, and *** $p < 0.001$ are considered significant compared to control.

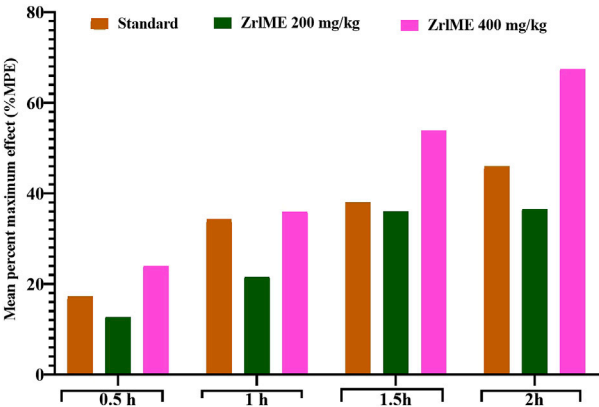


FIGURE 4 Effect of ZrIME and standard (ketorolac) on the hot plate test. This panel presented the mean percent maximum effect (%MPE) of standard and various dosages of plant extract.

respectively) than indomethacin (68.18%). The results as a whole suggested that the extract is effective and has noticeable outcomes.

3.4 Antipyretic activity

Rectal temperatures in all animals boosted after 18 h of yeast injection, as demonstrated in (Table 5). Following treatment with the ZrIME, the elevated rectal temperature was decreased in a dose-dependent manner. The antipyretic effect began immediately following the extract treatment. After 0.5, 1, 2, 3, and 24 h of therapy, the temperature was considerably lowered by 1.08°F, 1.43°F, 1.83°F, 2.23°F, and 3.17°F for ZrIME at a dose of 200 mg/kg, and by 1.44°F, 2.14°F, 3.00°F, 3.15°F, and 3.97°F for ZrIME at a dose of 400 mg/kg. Standard paracetamol at 150 mg/kg resulted in a maximum temperature drop of 4.62°F after 24 h, while ZrIME 200 mg/kg and ZrIME 400 mg/kg resulted in maximum temperature reductions of 3.17°F and 3.97°F, respectively.

3.5 Predicting biological activity

On the basis of the Pa value ($Pa > 0.07$), the bioactivity of each polyphenol was selected. The predicted biological characteristics and potential MOA for these substances are shown in Supplementary Table S1.

TABLE 4 Anti-inflammatory activity of *Z. roseum* leaves methanol extract (ZrIME) against paw edema test.

Treatment	0 h	1 h	2 h	3 h	4 h
Control	2.36 ± 0.21	3.00 ± 0.10	2.88 ± 0.05	2.84 ± 0.09	2.80 ± 0.12
Std 10 mg/kg	2.38 ± 0.13	2.76 ± 0.06** (40.63%)	2.64 ± 0.04** (50.00%)	2.60 ± 0.12** (54.16%)	2.52 ± 0.08*** (68.18%)
ZrIME 200 mg/kg	2.28 ± 0.08	2.68 ± 0.08*** (37.5%)	2.56 ± 0.09*** (46.15%)	2.48 ± 0.13*** (58.33%)	2.42 ± 0.16*** (68.20%)
ZrIME 400 mg/kg	2.28 ± 0.08	2.59 ± 0.11*** (51.56%)	2.48 ± 0.11*** (61.54%)	2.44 ± 0.08*** (66.67%)	2.40 ± 0.07*** (72.73%)

Values are stated as mean ± SEM, (n = 5); ZrIME represents methanol extract of *Z. roseum*; Std represents the reference standard, indomethacin. In comparison to control, *p < 0.05, **p < 0.01, and ***p < 0.001 are deemed significant.

TABLE 5 Antipyretic effect of *Z. roseum* leaves methanol extract (ZrIME) on Baker's yeast test.

Group	Rectal temperature (°F) ^a	Rectal temperature measured following the appropriate treatment (°F)				
		0.5 h	1 h	0.5 h	3 h	0.5 h
Control	101.72 ± 0.26	101.56 ± 0.34	101.72 ± 0.26	101.56 ± 0.34	101.72 ± 0.26	101.56 ± 0.34
Paracetamol	101.4 ± 0.60	99.3 ± 1.36	101.3 ± 0.70	99.3 ± 1.27	101.3 ± 0.70	99.3 ± 1.27
ZrIME 200 mg/kg	99.64 ± 0.52	98.56 ± 0.28*	99.64 ± 0.52	98.56 ± 0.28*	99.64 ± 0.52	98.56 ± 0.28*
ZrIME 400 mg/kg	99.80 ± 0.46	98.36 ± 0.47*	99.80 ± 0.46	98.36 ± 0.47*	99.80 ± 0.46	98.36 ± 0.47*

^aRectal temperature after 18 h of yeast injection Values are stated as mean ± SEM, (n = 5); ZrIME represents methanol extract of *Z. roseum*. In comparison to control, *p < 0.05, **p < 0.01, and ***p < 0.001 are deemed significant.

3.6 In-silico study

3.6.1 Molecular docking

The molecular docking was conducted to examine the interaction between the phytochemicals identified in ZrIME and COX-2. The findings of this analysis are presented in [Supplementary Table S2](#). The 2D and 3D interactions between polyphenols and the cyclooxygenase-2 enzyme are depicted in [Figures 5, 6](#), respectively. Seven polyphenols that target particular receptors had their free binding energies compared to celecoxib, a powerful COX-2 inhibitor, and non-steroidal anti-inflammatory medication. Rutin hydrate had a free binding energy with COX-2 of −8.5 Kcal/mol, which was nearly identical to standard celecoxib's free binding energy of −8.7 Kcal/mol. Also, the significant free binding energy of myricetin was −7.7 Kcal/mol and that of epicatechin was −7.0 Kcal/mol.

3.6.2 Molecular dynamics simulation (MDS)

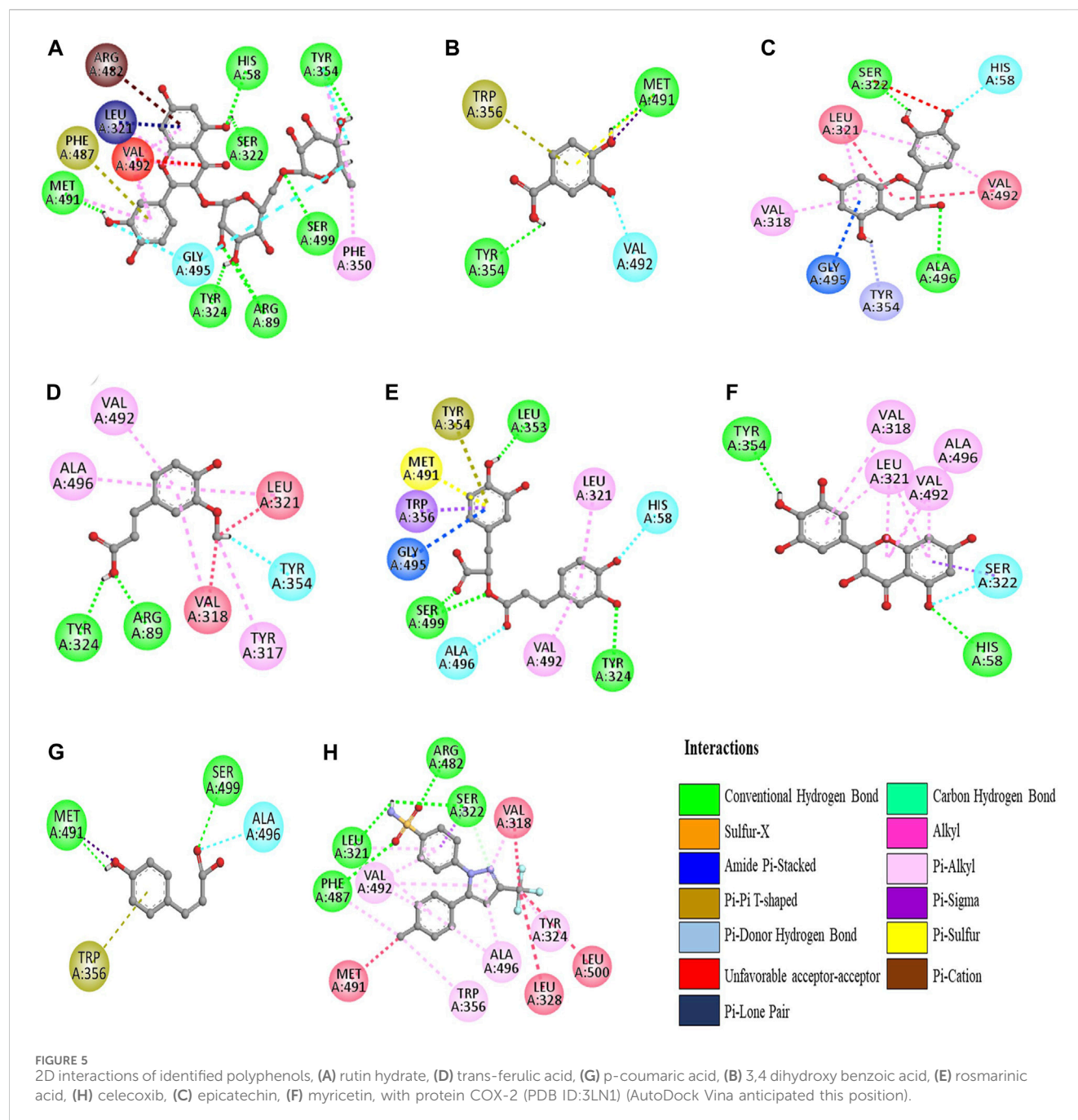
A 10 ns duration simulation was conducted to study the dynamics of the conventional medicine celecoxib and polyphenols with COX-2 enzyme, as shown in [Figure 7](#). MDS has been performed for the apo form of COX-2. The root mean square deviation (RMSD) of the alpha-carbon of apo COX-2 remained between 0.1 nm and 0.25 nm throughout the simulation, suggesting a higher level of stability. When celecoxib is coupled to COX-2, the RMSDs for the alpha carbon range from 0.1 to 0.15 nm, suggesting a high level of structural stability. Rutin hydrate, 3,4 dihydroxy benzoic acid and myricetin exhibited comparable RMSD values to celecoxib ([Figure 7A](#)). Based on the data presented in [Figure 7B](#), the RMSF values for both the apo and ligand-bound forms of COX-2 are nearly identical. Upon examining the hydrogen bonding area of COX-2 and ligands, it becomes apparent that the residues involved in hydrogen

bonding with the ligands demonstrated less variability compared to apo COX-2.

The protein's structural compactness is measured by the radius of gyration (Rg). The more compact the protein, the smaller the variations in the Rg. The consistent uniformity of the Rg ([Figure 7C](#)) throughout the simulation indicates improved system rigidity. Ligand and protein stability are highly dependent on hydrogen bond interactions [36]. The observed intermolecular hydrogen bonds formed by ligands and COX-2 during the 10 ns MDS are displayed in [Figure 8](#). Throughout the 10 ns duration, COX-2 and the control drug celecoxib consistently formed 1-3 hydrogen bonds ([Figure 8A](#)). At the beginning of the dynamics, rutin hydrate and COX-2 form 4–7 hydrogen bonds; however, by the end, this number decreases to 2–5 ([Figure 8B](#)). 3,4 Dihydroxy benzoic acid produced 2-4 hydrogen bonds throughout the simulation ([Figure 8C](#)). It's noteworthy that both of these polyphenols exhibited a higher frequency of hydrogen bond formation compared to celecoxib when interacting with COX-2. As shown in [Figure 8D](#), myricetin consistently formed 1 to 3 hydrogen bonds during the MDS, mirroring the behavior of celecoxib.

3.7 ADMET properties

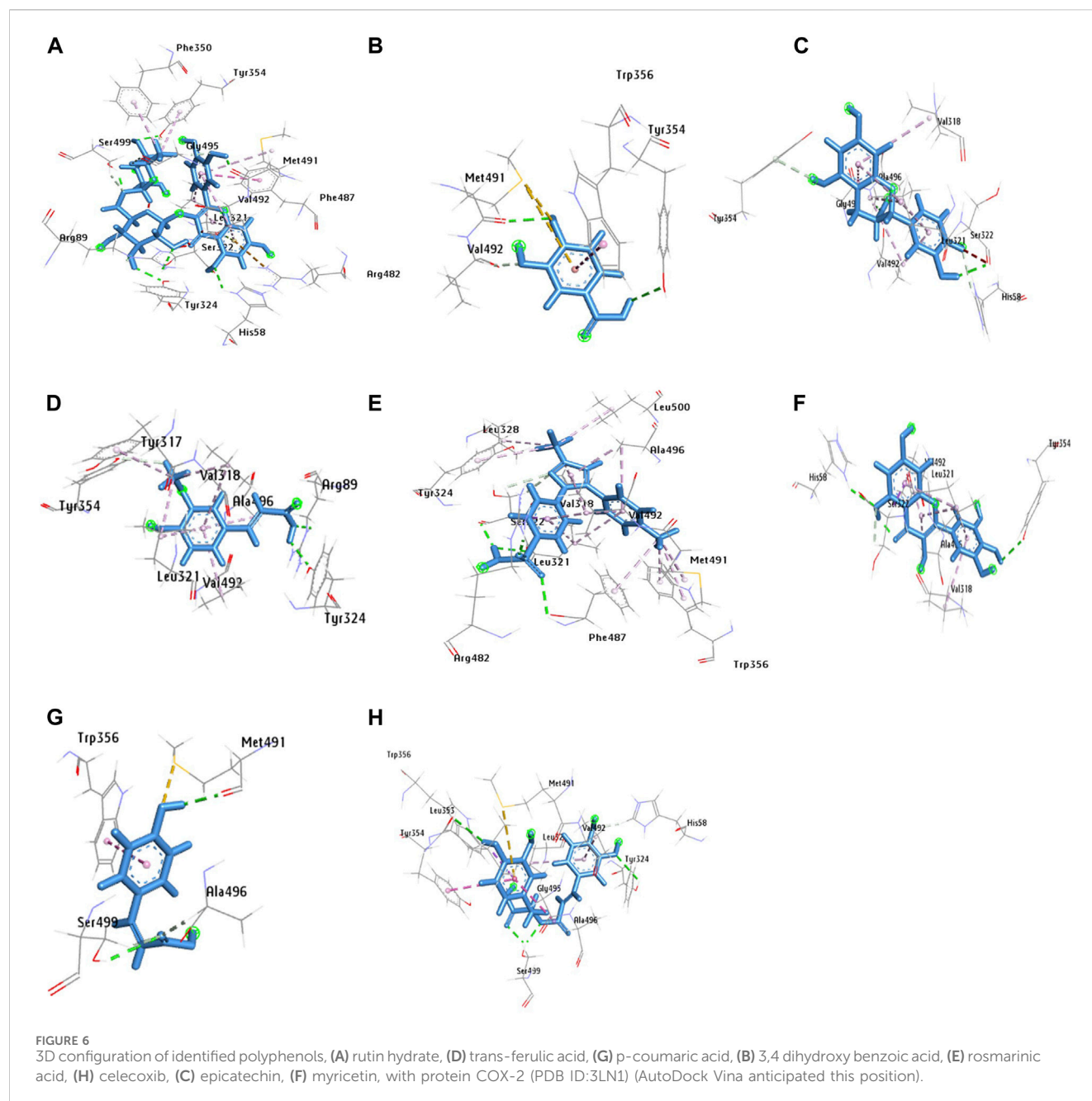
The investigation of ADMET characteristics ([Supplementary Table S3](#)) predicted that all of the chosen ligands have BBB penetration rates in the range of 0.028625–0.758419, which suggests that they are more effective at reaching the central nervous system. Except for rutin hydrate (0.028252), all of the selected ligands had a greater BBB penetration rate compared to the celecoxib (0.027635) standard. Seven ligands were found, with values for *in vitro* Caco-2 cell permeability ranging from 0.656962 to 21.1177 nm/sec, compared to a value of 0.499443 for the reference



drug celecoxib. Caco-2 cells had a moderate permeability to 3,4-dihydroxy benzoic acid, trans-ferulic acid, rutin hydrate, rosmarinic acid, and p-coumaric acid but not to other ligands. Epicatechin (100%) and myricetin (96.78%) had significantly higher affinity to plasma protein than celecoxib (91.077216). The percentage of HIA was determined to be between 0.941542 and 92.095876. 3,4 Dihydroxy benzoic acid (74.749630), Trans-ferulic acid (90.603297), and p-Coumaric acid (92.095876) have shown a good absorbance. All the ligands tested negative for skin permeability (−4.5272 to −1.70767). The result of toxicity was also negative, recommending that all selected ligands are safe and non-toxic.

3.8 Bioactivity & toxicity risk studies

Supplementary Table S4 provides a summary of seven ligands' bioactivity and toxicity risk profiles. The results showed that all of the ligands were approximately comparable to the bioactivity properties of the standard celecoxib value. Moreover, the drug-likeness of all the ligands were within range of −2.07–3.31, which was higher than the standard celecoxib value of −8.11. Furthermore, the drug scores of these ligands were estimated to be in the 0.19–0.89 range, which is comparable to the drug scores of celecoxib (0.37). Finally, the study of bioactivity and toxicity reveals that all ligands are safe as potential medicinal agents.



4 Discussion

Isolating new therapeutic metabolites from medicinal plants has become increasingly important in recent years. Unfortunately, most of the plants are yet unexplored in terms of their pharmacological and toxicological characteristics, as well as the identification of valuable bioactive metabolites. *Zingiber roseum* (Roxb.) Roscoe is a medicinal plant with undisclosed medicinal and pharmacological effects. Seven polyphenols (3, 4- dihydroxy benzoic acid, (-) epicatechin, rutin hydrate, p-coumaric acid, trans-ferulic acid, rosmarinic acid and myricetin) were identified by HPLC analysis in ZrLME. These plant metabolites have been reported to possess diverse pharmacological actions such as hepatoprotective, anti-arthritis, immunomodulatory, analgesic, anti-arthritis, antipyretic,

antibacterial, and anti-inflammatory properties (Benavente-García et al., 1997; Middleton et al., 2000; Puupponen-Pimiä et al., 2001; Manach et al., 2005b).

Acetic acid is the causative agent for the augmentation of capillary permeability. Pain is caused by the stimulation of nerve endings, which is activated by the production of different substances that promote pain, such as prostaglandin, peritoneal mast cells and others (Bueno and Fioramonti, 2002). Conventional nonsteroidal anti-inflammatory drugs (NSAIDs) alleviate pain and inflammation by blocking the function of COX in peripheral tissues and primary afferent nociceptors' signal transduction (Burian et al., 2005). ZrLME 400 mg/kg dose substantially ($p < 0.001$) reduced the writhing responses in our investigation, which could be attributed to the disruption of pain and inflammatory pathways. However, due to the

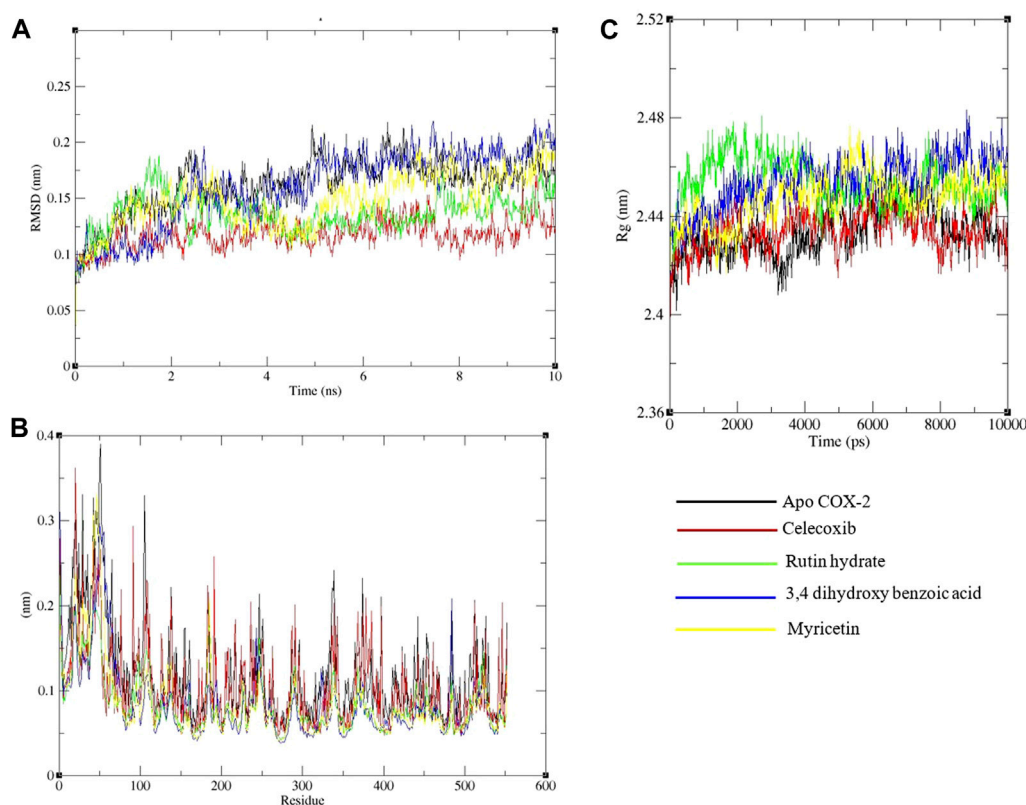


FIGURE 7
Analysis of a 10 ns molecular dynamics simulation of Cox-2 with ligands. (A) Root mean square deviation (RMSD), (B) Root mean square fluctuations on a residue-wise basis, and (C) Radius of gyration.

lack of specificity in this investigation, it is imperative to employ a different experimental approach to confirm the results obtained from the writhing test. Therefore, we utilized a biphasic paw licking experiment as a more accurate approach to evaluate the effectiveness of biphasic pain relief. The biphasic nociceptive response is triggered by injecting formalin into the skin, and the response during the first phase (0–5 min) is believed to be caused by the activation of peripheral nociceptors by formalin, leading to the sudden hindrance of activity. Conversely, during the second phase (lasting from 10 to 45 min), the inflammatory response is believed to occur as a result of inflammatory cytokines, such as prostaglandins, serotonin, bradykinin, etc., into the peripheral nociceptors of the spinal cord (Pethő and Reeh, 2012). Since ZrlME 400 mg/kg significantly ($p < 0.001$) inhibited the paw-licking responses in both stages, it is reasonable to infer that there is a potential for suppressing cytokines generated by inflammation in the peripheral or spinal cord.

The hot plate approach demonstrates that various dosages of ZrlME result in a dose-dependent escalation in reaction time, with the most significant inhibition occurring after 2 h of the trial. The opioid μ receptor plays a key role in regulating thermal pain in response to thermal stimuli, and activating this receptor leads to the production of analgesic activity in the spinal cord (Sun et al., 2019). The rise in response time may be centrally regulated as a result of its impact on the opioid receptor. Polyphenols have been found to produce an analgesic effect through the activation of opioid

receptors (De Feo et al., 2020). Fields, H. L. (1984) reported that centrally-acting analgesic medications stimulate the release of endogenous peptides through the periaqueductal grey matter, resulting in the suppression of pain signal transmission in the dorsal horn (Fields, 1984). ZrlME also showed the ability to suppress nociceptive response as evaluated using the hot plate test, indicating its promise as a centrally mediated pain reliever.

Carrageenan is commonly employed as a proinflammatory substance in scientific studies to investigate the anti-inflammatory properties of natural substances (Morris, 2003). Injecting carrageenan subcutaneously causes paw swelling or edema. It is well accepted that the induction of edema with carrageenan injection follows a two-phase pattern. The initial phase of the inflammatory reaction, occurring approximately 1–2 h after the injection of carrageenan, often entails the release of bradykinins, histamine, and serotonin from the mast cells in the injured tissue (Myers et al., 2019). In contrast, during the second phase (often occurring 3–6 h after carrageenan injection), the inflammatory response is triggered by the activation of several inflammatory mediators, such as IL-6, IL-10, IL-1 β , TNF- α , and different arachidonate metabolites like leukotrienes and prostaglandins (Loram et al., 2007). The ZrlME dose of 400 mg/kg had the most pronounced effect during the fourth hour in our experiment. Therefore, it may be inferred that this dosage of extract exhibited anti-inflammatory effects via impeding the release of inflammatory mediators.

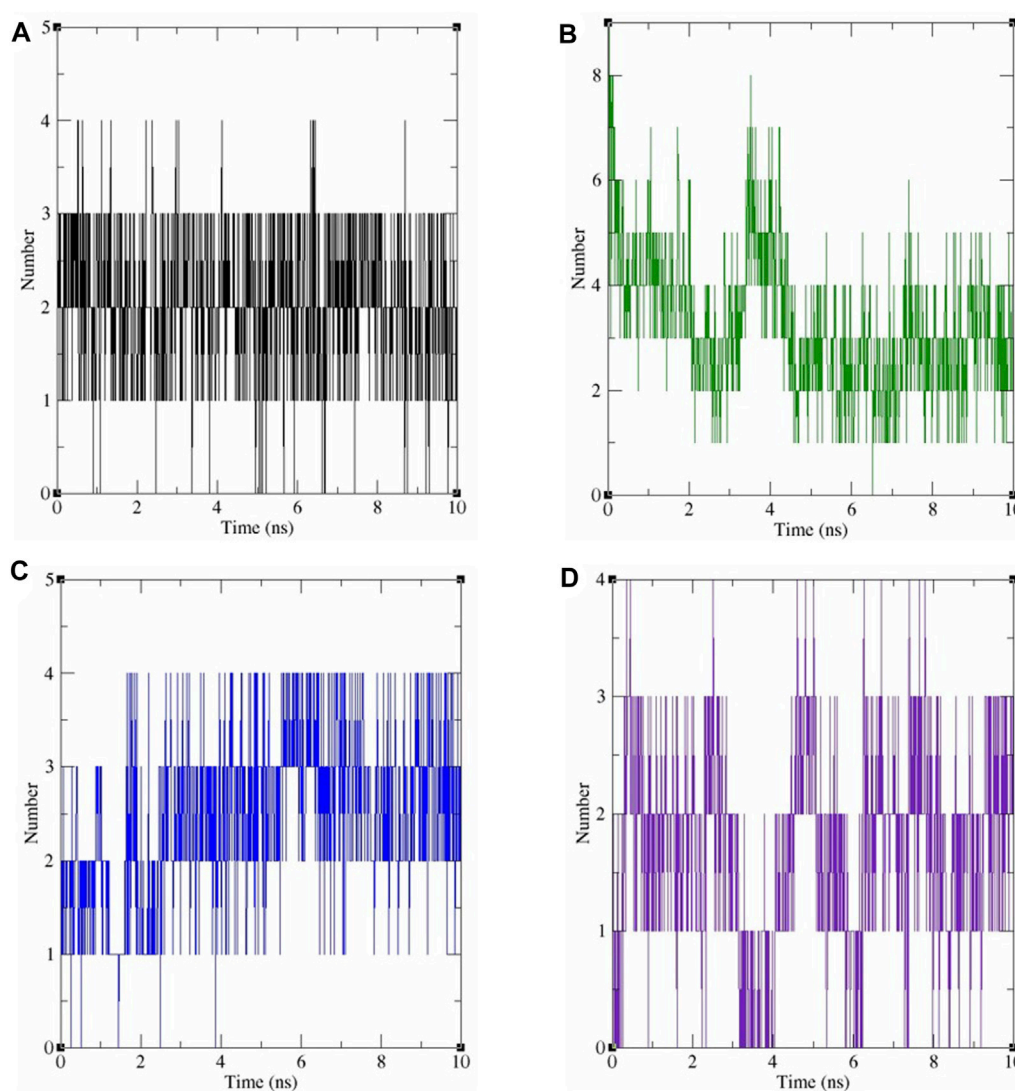


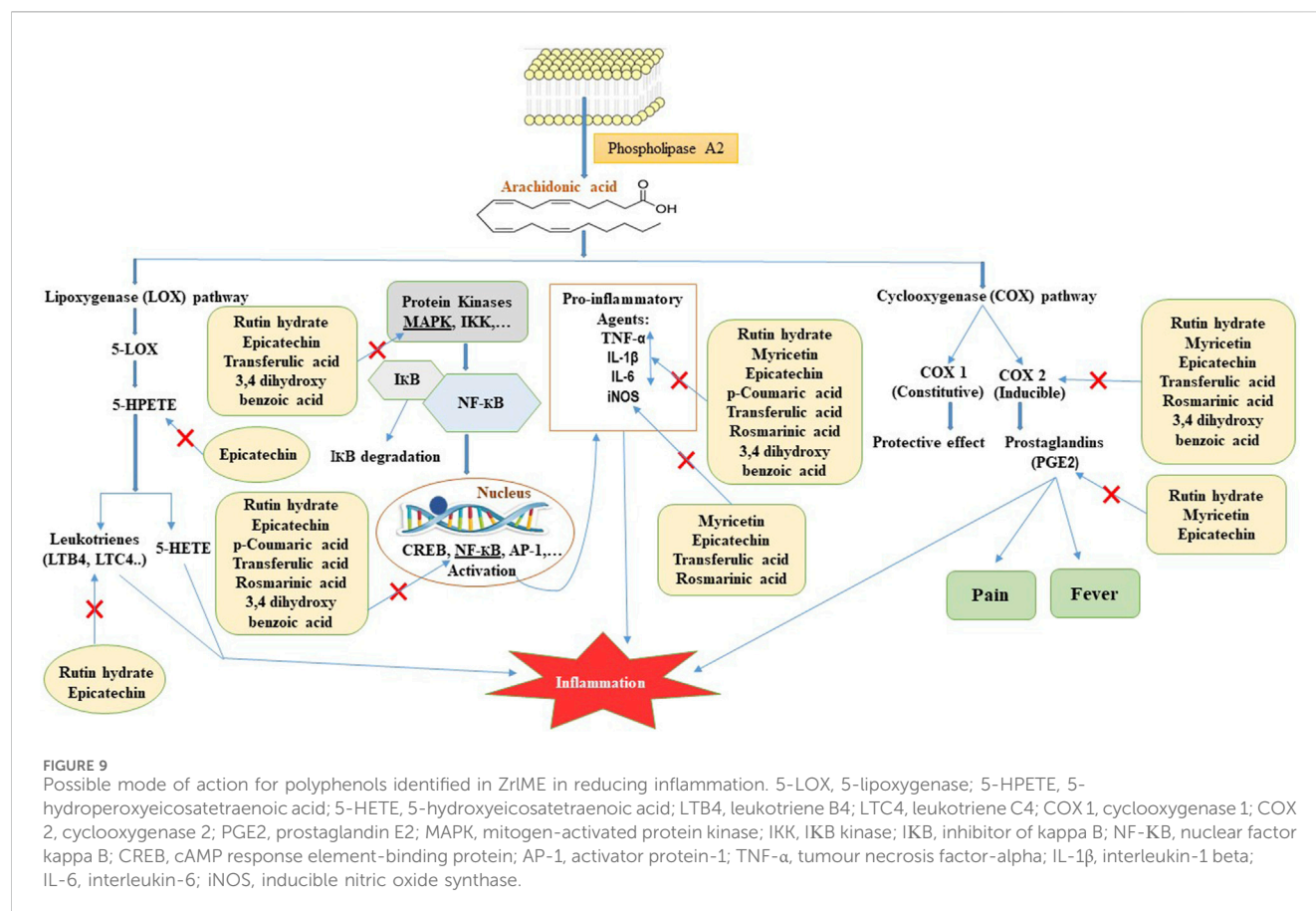
FIGURE 8

The number of hydrogen bonds produced during 10 ns dynamics simulation between COX-2 and the following ligands: (A) celecoxib, (B) rutin hydrate, (C) 3,4 dihydroxy benzoic acid, and (D) myricetin.

According to previous reports, the injection of carrageenan caused the release of arachidonic acid (AA) and lactate dehydrogenase from pleural cells in rats (Lucetti et al., 2010). AA produces three main categories of eicosanoids: prostaglandins, thromboxanes, and leukotrienes, which play a significant role in causing inflammation. Prior research demonstrated that polyphenols has the ability to impede the COX-2 and LOX-5 enzyme, which plays a crucial role in the synthesis of prostaglandins and leukotrienes from AA (Stoner and Wang, 2013). Hence, the suppression of the eicosanoids signaling pathway could potentially explain the anti-inflammatory impact of ZrlME (Figure 9).

Reactive oxygen species (ROS) induce alterations in inhibitor of nuclear factor kappa B (I κ B) proteins, which serve as inhibitors of NF- κ B kinase (IKK) (Gloire et al., 2006). This alteration results in the deterioration of I κ B, causing the liberation of NF- κ B to migrate to the nucleus and stimulate the production of several

genes that produce inflammatory proteins, either independently or in conjunction with other transcription factors (Gloire et al., 2006). Hence, suppressing ROS-mediated signaling pathways would be an optimal therapeutic approach for controlling inflammatory diseases. According to earlier reports, rosmarinic acid exhibits anti-inflammatory effects by blocking the NF- κ B signaling pathway (Lv et al., 2019). Myricetin is a promising polyphenol that exerts anti-inflammatory effects through many pathways. It has the ability to inhibit the synthesis of multiple pro-inflammatory substances, such as nitric oxide (NO), inducible nitric oxide synthase (iNOS), tumour necrosis factor- α (TNF- α), interleukin-6 (IL-6), prostaglandin E2 (PGE2), and interleukin-12 (IL-12) (Figure 9) (Song et al., 2021). Earlier studies also reported that epicatechin has anti-inflammatory properties by decreasing the synthesis of inflammatory substances such as TNF- α , NO, PGE2, IL-1 β , IL-6 MAPKs, NF- κ B, and JAK2/STAT3 signaling



pathways (Figure 9) (Morrison et al., 2014; Amanat et al., 2021). Evidence also showed that rutin can effectively alleviate inflammation by decreasing the levels of pro-inflammatory markers such as TNF-α, IL-6, COX-2, IL-1β (Figure 9) (Hasan et al., 2022; Muvhulawa et al., 2022). The aforementioned polyphenols have been found in significant quantities in ZrIME. Therefore, the remarkable anti-inflammatory activity of ZrIME might be attributed via one of the mentioned pathways.

Fever is an immune system-related acute phase reaction. Fever develops when the hypothalamus's set point is disrupted (Javed et al., 2020). Fever is caused by simple injury of tissue, which causes inflammation, or by the activity of lipopolysaccharides termed pyrogens, which cause leukocytes to produce cytokines, according to prior study. Prostaglandin E2 (PGE2) is the primary mediator of fever, and it is produced by COX-2 in response to the stimulation of cytokines in the hypothalamus. Microvascular endothelial cells, which abundantly produce COX-2 in response to stress, are the primary cell type in the CNS that create PGE2. The pyretic response is also influenced by activated macrophages, leukocytes, and endothelial cells in inflammatory regions (Taiwe et al., 2011). Subcutaneous administration of the exogenous pyrogen, baker's yeast, augments the production and secretion of several cytokines such as interleukins (IL-1, IL-6), prostaglandins, TNF, and others (Roy et al., 2019). Most antipyretics work by blocking PGE2 in the hypothalamus to reduce fever, but peripheral active leukocytes and endothelial

cells may also be potential therapeutic targets (Javed et al., 2020). At both doses, ZrIME demonstrated a strong antipyretic activity. Both doses, as well as standard paracetamol, resulted in a fast decrease in high rectal temperature, which steadily decreased over time. Paracetamol suppresses prostaglandin synthesis by inhibiting COX pathway; the phytochemical(s) in ZrIME may inhibit COX activity, bringing the body temperature back to normal.

Molecular docking is a popular and widely used method in the realm of drug development. Better understanding of binding mechanisms and the potential for binding of various proteins can be attained using this method (Khan et al., 2019). The seven identified ligands were assessed as possible cyclooxygenase-2 inhibitors utilizing molecular docking and MDS. The phenolic metabolites had high binding affinities (range from 8.5 to 5.8 Kcal/mol) to the COX-2 protein and formed a notable number of hydrogen bonds, surpassing those of celecoxib. The number of hydrogen bonds formed by rutin hydrate, 3,4 dihydroxy benzoic acid and myricetin with COX-2 during the dynamics simulation was comparable to that of celecoxib. The most abundant polyphenols, (-) epicatechin, was reported to have a very stable interaction with COX-2 (Mazumder et al., 2022). Talukder et al. (2022) also revealed the enduring association of rosmarinic acid (second most abundant polyphenols in ZrIME) with the active region of COX-2, signifying noteworthy inhibitory effect of ZrIME against COX-2 (Talukder et al., 2022).

5 Conclusion

The current study demonstrated promising analgesic, anti-inflammatory, and antipyretic efficacy of the ZrlME. The molecular docking and MDS analysis also indicated that the phenolic metabolites present in ZrlME exhibited potential inhibition of COX-2 activity. The observed pharmacological effects of ZrlME could be attributed to the presence of these bioactive polyphenols. In-depth clinical research on experimental substances is still needed to confirm their efficacy and safety profile. In conclusion, the ZrlME was proved to be a natural, safe remedy for the treatment of analgesia, inflammation, and pyrexia.

Data availability statement

The original contributions presented in the study are included in the article/[Supplementary Material](#), further inquiries can be directed to the corresponding authors.

Ethics statement

The animal studies were approved by Animal Ethics Committee of Noakhali Science and Technology University. The studies were conducted in accordance with the local legislation and institutional requirements. Written informed consent was obtained from the owners for the participation of their animals in this study.

Author contributions

SA: Investigation, Writing—original draft. KA: Data curation, Formal Analysis, Writing—original draft. NR: Formal Analysis, Investigation, Writing—original draft. HH: Methodology, Writing—review and editing. AH: Formal Analysis, Project administration, Writing—original draft. PG: Software,

Visualization, Writing—review and editing. AD: Writing—review and editing, Conceptualization, Supervision. AM: Supervision, Writing—review and editing, Funding acquisition.

Funding

The author(s) declare financial support was received for the research, authorship, and/or publication of this article. This study was partially supported by the funds of Municipal Public Welfare Self-Financing Technology Application Research Project of Lishui (2022SJZC074&2022SJZC079) and Post-Doctoral Research Start-Up Fund of Lishui People's Hospital (2023bsh001).

Conflict of interest

The authors declare that the research was conducted in the absence of any commercial or financial relationships that could be construed as a potential conflict of interest.

Publisher's note

All claims expressed in this article are solely those of the authors and do not necessarily represent those of their affiliated organizations, or those of the publisher, the editors and the reviewers. Any product that may be evaluated in this article, or claim that may be made by its manufacturer, is not guaranteed or endorsed by the publisher.

Supplementary material

The Supplementary Material for this article can be found online at: <https://www.frontiersin.org/articles/10.3389/fphar.2024.1344123/full#supplementary-material>

References

- Al-Amin, M., Siddiqui, M. A., Ruma, S. A., Eltayeb, N. M., Sultana, G., Salhimi, S. M., et al. (2019). Antimicrobial activity of the crude extract, fractions and isolation of zerumbone from the rhizomes of Zingiber roseum. *Marmara Pharm. J.* 23 (3), 559–566. doi:10.12991/jrp.2019.163
- Amanat, M., Daula, A. S. U., and Singh, R. J. P. R. (2023). Acute toxicity assessment of methanolic extract of Zingiber roseum (Roscoe.) rhizome in swiss albino mice. *Pharmacol. Res. - Mod. Chin. Med.* 7, 100244. doi:10.1016/j.prmcm.2023.100244
- Amanat, M., Reza, M. S., Shuvo, M. S. R., Ahmed, K. S., Hossain, H., Tawhid, M., et al. (2021). Zingiber roseum Rosc. rhizome: a rich source of hepatoprotective polyphenols. *Biomed. Pharmacother.* 139, 111673. doi:10.1016/j.biopha.2021.111673
- Babu, C. R. (1977). *Herbaceous flora of dehra dun*. New Delhi: Council of Scientific and Industrial Research.
- Benavente-García, O., Castillo, J., Marin, F. R., Ortuño, A., Del Río, J. A. J. J., and chemistry, F. (1997). Uses and properties of citrus flavonoids. *J. Agric. Food Chem.* 45 (12), 4505–4515. doi:10.1021/jf970373s
- Botting, R. M. J. P. R. (2010). Vane's discovery of the mechanism of action of aspirin changed our understanding of its clinical pharmacology. *Pharmacol. Rep.* 62 (3), 518–525. doi:10.1016/s1734-1140(10)70308-x
- Bueno, L., and Fioramonti, J. J. G. (2002). Visceral perception: inflammatory and non-inflammatory mediators. *Gut* 51 (Suppl. 1), i19–i23. doi:10.1136/gut.51.suppl_1.i19
- Burian, M., Geisslinger, G. J. P., and therapeutics, (2005). COX-dependent mechanisms involved in the antinociceptive action of NSAIDs at central and peripheral sites. *Pharmacol. Ther.* 107 (2), 139–154. doi:10.1016/j.pharmthera.2005.02.004
- Chen, L., Deng, H., Cui, H., Fang, J., Zuo, Z., Deng, J., et al. (2018). Inflammatory responses and inflammation-associated diseases in organs. *Oncotarget* 9 (6), 7204–7218. doi:10.18632/oncotarget.23208
- Chou, R., Gordon, D. B., de Leon-Casasola, O. A., Rosenberg, J. M., Bickler, S., Brennan, T., et al. (2016). Management of postoperative pain: a clinical practice guideline from the American pain society, the American society of regional anesthesia and pain medicine, and the American society of anesthesiologists' committee on regional anesthesia, executive committee, and administrative council. *Am. Soc. Regional Anesth. Pain Med. Am. Soc. Anesthesiologists' Comm. regional Anesth. Exec. Comm. Adm. Counc.* 17 (2), 131–157. doi:10.1016/j.jpain.2015.12.008
- De Feo, M., Paladini, A., Ferri, C., Carducci, A., Del Pinto, R., Varrassi, G., et al. (2020). Anti-inflammatory and anti-nociceptive effects of cocoa: a review on future perspectives in treatment of pain. *Pain Ther.* 9, 231–240. doi:10.1007/s40122-020-00165-5
- Emon, N. U., Alam, S., Rudra, S., Chowdhury, S., Rajbangshi, J. C., and Ganguly, A. (2020). Evaluation of pharmacological potentials of the aerial part of *Achyranthes aspera* L.: *in vivo*, *in vitro* and *in silico* approaches. *Adv. Traditional Med.* 22, 141–154. doi:10.1007/s13596-020-00528-5
- Fields, H. L. (1984). Neurophysiology of pain and pain modulation. *Neurophysiology pain pain Modul.* 77 (3), 2–8. doi:10.1016/s0002-9343(84)80097-2

- Gaetano, L., Watanabe, K., Barogi, S., and Cocceani, F. J. A. p. (2010). Cyclooxygenase-2/microsomal prostaglandin E synthase-1 complex in the preoptic-anterior hypothalamus of the mouse: involvement through fever to intravenous lipopolysaccharide. *Acta Physiol.* 200 (4), 315–324. doi:10.1111/j.1748-1716.2010.02157.x
- Gloire, G., Legrand-Poels, S., and Piette, J. J. B. (2006). NF-kappaB activation by reactive oxygen species: fifteen years later. *fifteen years later* 72 (11), 1493–1505. doi:10.1016/j.bcp.2006.04.011
- Gupta, S. C., Kunnumakkara, A. B., Aggarwal, S., and Aggarwal, B. B. (2018). Inflammation, a double-edge sword for cancer and other age-related diseases. *Front. Immunol.* 9, 2160. doi:10.3389/fimmu.2018.02160
- Hasan, T., Jahan, E., Ahmed, K. S., Hossain, H., Siam, S. M. M., Nahid, N., et al. (2022). Rutin hydrate and extract from *Castanopsis tribuloides* reduces pyrexia via inhibiting microsomal prostaglandin E synthase-1. *Biomed. Pharmacother.* 148, 112774. doi:10.1016/j.biopha.2022.112774
- Hawkey, C. J. (1999). COX-2 inhibitors. *Lancet* 353 (9149), 307–314. doi:10.1016/S0140-6736(98)12154-2
- Huey, R., Morris, G. M., and Forli, S. J. (2012). Using AutoDock 4 and AutoDock vina with AutoDockTools: a tutorial. *Scripps Res. Inst. Mol. Graph. Laboratory* 10550, 92037.
- Hunnskaar, S., and Hole, K. J. P. (1987). The formalin test in mice: dissociation between inflammatory and non-inflammatory pain. *Pain* 30 (1), 103–114. doi:10.1016/0304-3959(87)90088-1
- Javed, F., Jabene, Q., Aslam, N., and Awan, A. M. (2020). Pharmacological evaluation of analgesic, anti-inflammatory and antipyretic activities of ethanolic extract of *Indigofera argentea* Burm. f. *Burm. F.* 259, 112966. doi:10.1016/j.jep.2020.112966
- Khan, S., Nazir, M., Raiz, N., Saleem, M., Zengin, G., Fazal, G., et al. (2019). Phytochemical profiling, *in vitro* biological properties and *in silico* studies on *Caragana ambigua* stocks (Fabaceae): a comprehensive approach. *Ind. Crops Prod.* 131, 117–124. doi:10.1016/j.indcrop.2019.01.044
- Kim, S., Thiessen, P. A., Bolton, E. E., Chen, J., Fu, G., Gindulyte, A., et al. (2016). PubChem substance and compound databases. *PubChem Subst. Compd. databases* 44 (D1), D1202–D1213. doi:10.1093/nar/gkv951
- Kwieceń, S., Magierowska, K., Śliwowski, Z., Wójcik, D., Magierowski, M., and Brzozowski, T. J. (2015). New insight into the mechanisms of gastroduodenal injury induced by nonsteroidal anti-inflammatory drugs: practical implications. *Pol. Arch. Med. Wewn.* 125 (3), 191–198. doi:10.20452/pamw.2715
- Loram, L., Fuller, A., Fick, L., Cartmell, T., Poole, S., and Mitchell, D. J. (2007). Cytokine profiles during carrageenan-induced inflammatory hyperalgesia in rat muscle and hind paw. *J. Pain* 8 (2), 127–136. doi:10.1016/j.jpain.2006.06.010
- Lucetti, D. L., Lucetti, E. C., Bandeira, M. A. M., Veras, H. N., Silva, A. H., Leal, L. K. A., et al. (2010). Anti-inflammatory effects and possible mechanism of action of lupal acetate isolated from *Himatanthus drasticus* (Mart.) Plumel. *Plumel.* 7 (1), 1–11. doi:10.1186/1476-9255-7-60
- Lv, R., Du, L., Liu, X., Zhou, F., Zhang, Z., and Zhang, L. J. L. s. (2019). Rosmarinic acid attenuates inflammatory responses through inhibiting HMGB1/TLR4/NF-κB signaling pathway in a mouse model of Parkinson's disease. *Life Sci.* 223, 158–165. doi:10.1016/j.lfs.2019.03.030
- Mahawer, S. K., Kumar, R., Prakash, O., Arya, S., Singh, S., de Oliveira, M. S., et al. (2023). A comprehensive review on phytochemistry, Ethnopharmacology, and pharmacological properties of zingiber roseum (roxb.) Roscoe. *Curr. Top. Med. Chem.* 23, 931–942. doi:10.2174/1568026623666230126143635
- Manach, C., Mazur, A., and Scalbert, A. J. C. o.i.l. (2005a). Polyphenols and prevention of cardiovascular diseases. *Curr. Opin. Lipidol.* 16 (1), 77–84. doi:10.1097/00041433-200502000-00013
- Manach, C., Williamson, G., Morand, C., Scalbert, A., and Révész, C. J. T. (2005b). Bioavailability and bioefficacy of polyphenols in humans. I. Review of 97 bioavailability studies. *Rev. 97 Bioavailab. Stud.* 81 (1), 230S–242S. doi:10.1093/ajcn/81.1.230S
- Marwaha, A., Goel, R., Mahajan, M. P. J. B., and letters, M. C. (2007). PASS-predicted design, synthesis and biological evaluation of cyclic nitrones as neurotrophins. *Bioorg. Med. Chem. Lett.* 17 (18), 5251–5255. doi:10.1016/j.bmcl.2007.06.071
- Mazumder, T., Hasan, T., Ahmed, K. S., Hossain, H., Debnath, T., Jahan, E., et al. (2022). Phenolic compounds and extracts from *Crotalaria calycina* Schrank potentially alleviate pain and inflammation through inhibition of cyclooxygenase-2: an *in vivo* and molecular dynamics studies. *An vivo Mol. Dyn. Stud.* 8 (12), e12368. doi:10.1016/j.heliyon.2022.e12368
- Middleton, E., Kandaswami, C., and Theoharides, T. C. J. P. r. (2000). The effects of plant flavonoids on mammalian cells: implications for inflammation, heart disease, and cancer. *heart Dis. cancer* 52 (4), 673–751.
- Morris, C. J. (2003). Carrageenan-induced paw edema in the rat and mouse. *Methods Mol. Biol.* 7, 115–121. doi:10.1385/1-59259-374-7:115
- Morrison, M., van der Heijden, R., Heeringa, P., Kaijzel, E., Verschuren, L., Blomhoff, R., et al. (2014). Epicatechin attenuates atherosclerosis and exerts anti-inflammatory effects on diet-induced human-CRP and NFκB *in vivo*. *Atherosclerosis* 233 (1), 149–156. doi:10.1016/j.atherosclerosis.2013.12.027
- Muhammad, A., Khan, B., Iqbal, Z., Khan, A. Z., Khan, I., Khan, K., et al. (2019). Viscosine as a potent and safe antipyretic agent evaluated by yeast-induced pyrexia model and molecular docking studies. *ACS Omega* 4 (10), 14188–14192. doi:10.1021/acsomega.9b01041
- Muvhulawa, N., Dlodla, P. V., Ziqubu, K., Mthembu, S. X., Mthiyane, F., Nkambule, B. B., et al. (2022). Rutin ameliorates inflammation and improves metabolic function: a comprehensive analysis of scientific literature. *Pharmacol. Res.* 178, 106163. doi:10.1016/j.phrs.2022.106163
- Myers, M. J., Deaver, C. M., and Lewandowski, A. J. J. M. i. (2019). Molecular mechanism of action responsible for carrageenan-induced inflammatory response. *Mol. Immunol.* 109, 38–42. doi:10.1016/j.molimm.2019.02.020
- Neugebauer, J., Reiher, M., Kind, C., and Hess, B. A. (2002). Quantum chemical calculation of vibrational spectra of large molecules—Raman and IR spectra for buckminsterfullerene. *J. Comput. Chem.* 23 (9), 895–910. doi:10.1002/jcc.10089
- O'Boyle, N. M., Banck, M., James, C. A., Morley, C., Vandermeersch, T., and Hutchison, G. R. (2011). *Open Babel An open Chem. toolbox* 3 (1), 1–14. doi:10.1186/1758-2946-3-33
- Omar, M. T. (2020). Data analysis of molecular dynamics simulation trajectories of β-sitosterol, sonidegib and cholesterol in smoothened protein with the CHARMM36 force field. *Data Brief.* 33, 106350. doi:10.1016/j.dib.2020.106350
- Parenti, M. D., and Rastelli, G. J. (2012). Advances and applications of binding affinity prediction methods in drug discovery. *Adv. Appl. Bind. affinity Predict. methods drug Discov.* 30 (1), 244–250. doi:10.1016/j.biotechadv.2011.08.003
- Pethő, G., and Reeh, P. W. (2012). Sensory and signaling mechanisms of bradykinin, eicosanoids, platelet-activating factor, and nitric oxide in peripheral nociceptors. *Physiol. Rev.* 92 (4), 1699–1775. doi:10.1152/physrev.00048.2010
- Puebla Diaz, F. J. O. (2005). Tipos de dolor y escala terapéutica de la O.M.S.: dolor iatrogénico. *Dolor iatrogénico* 28 (3), 33–37. doi:10.4321/s0378-48352005000300006
- Puupponen-Pimiä, R., Nohynek, L., Meier, C., Kähkönen, M., Heinonen, M., Hopia, A., et al. (2001). Antimicrobial properties of phenolic compounds from berries. *J. Appl. Microbiol.* 90 (4), 494–507. doi:10.1046/j.1365-2672.2001.01271.x
- Rahman, M. A., and Yusuf, M. J. (2013). Zingiber salarkhanii (Zingiberaceae), A new species from Bangladesh. *Zingiber salarkhanii (Zingiberaceae), a new species Bangladesh* 20 (2), 239–242. doi:10.3329/bjpt.v20i2.17398
- Rahman, M. N., Ahmed, K. S., Ahmed, S., Hossain, H., and Daula, A. S. (2023). Integrating *in vivo* and *in silico* approaches to investigate the potential of Zingiber roseum rhizome extract against pyrexia. *Inflamm. pain* 30 (4), 103624. doi:10.1016/j.sjbs.2023.103624
- Reza, M. S., Jashimuddin, M., Ahmed, J., Abeer, M., Naznin, N. E., Jafrin, S., et al. (2021). Pharmacological investigation of analgesic and antipyretic activities of methanol extract of the whole part of *Aeginetia indica*. *J. Ethnopharmacol.* 271, 113915. doi:10.1016/j.jep.2021.113915
- Rose, P. W., Prlić, A., Altunkaya, A., Bi, C., Bradley, A. R., Christie, C. H., et al. (2016). The RCSB protein data bank: integrative view of protein, gene and 3D structural information. *gkw1000*.
- Roth, J., Rummel, C., Barth, S. W., Gerstberger, R., and Hübschle, T. J. N. (2006). Molecular aspects of fever and hyperthermia. *Mol. aspects fever Hyperth.* 24 (3), 421–439. doi:10.1016/j.ncl.2006.03.004
- Roy, R., Daula, A. S. U., Akter, A., Sultana, S., Barek, M. A., Liya, I. J., et al. (2019). Antipyretic and anti-nociceptive effects of methanol extract of leaves of *Fimbristylis miliacea* in mice model. *J. Ethnopharmacol.* 243, 112080. doi:10.1016/j.jep.2019.112080
- Siegmund, E., Cadmus, R., and Lu, G. J. P. (1957). A method for evaluating both non-narcotic and narcotic analgesics. *Proc. Soc. Exp. Biol. Med.* 95 (4), 729–731. doi:10.3181/00379727-95-23345
- Song, X., Tan, L., Wang, M., Ren, C., Guo, C., Yang, B., et al. (2021). Myricetin: a review of the most recent research. *Biomed. Pharmacother.* 134, 111017. doi:10.1016/j.biopha.2020.111017
- Stoner, G., and Wang, L.-S. (2013). "Natural products as anti-inflammatory agents." in *Obesity, inflammation and cancer* (Berlin, Germany: Springer), 341–361.
- Sun, J., Chen, S. R., Chen, H., and Pan, H. L. (2019). μ-Opioid receptors in primary sensory neurons are essential for opioid analgesic effect on acute and inflammatory pain and opioid-induced hyperalgesia. *J. Physiol.* 597 (6), 1661–1675. doi:10.1113/JP277428
- Taiwe, G. S., Bum, E. N., Talla, E., Dimo, T., Weiss, N., Sidiki, N., et al. (2011). Antipyretic and antinociceptive effects of *Nauclea latifolia* root decoction and possible mechanisms of action. *Pharm. Biol.* 49 (1), 15–25. doi:10.3109/13880209.2010.492479
- Talukder, S., Ahmed, K. S., Hossain, H., Hasan, T., Liya, I. J., Amanat, M., et al. (2022). *Fimbristylis aestivalis* Vahl: a potential source of cyclooxygenase-2 (COX-2) inhibitors. *Inflammopharmacology* 30, 2301–2315. doi:10.1007/s10787-022-01057-0
- Vázquez, B., Avila, G., Segura, D., and Escalante, B. J. J. (1996). Antiinflammatory activity of extracts from *Aloe vera* gel. *Aloe vera gel* 55 (1), 69–75. doi:10.1016/s0378-8741(96)01476-6
- Yi, X., Liang, Y., Huerta-Sanchez, E., Jin, X., Cuo, Z. X. P., Pool, J. E., et al. (2010). Sequencing of 50 human exomes reveals adaptation to high altitude. *Science* 329 (5987), 75–78. doi:10.1126/science.1190371



OPEN ACCESS

EDITED BY

Saša Đurović,
Institute of General and Physical Chemistry,
Serbia

REVIEWED BY

Gu Haofeng,
Ankang University, China
Snežana Filip,
University of Novi Sad, Serbia
Guangping Lyu,
Nanjing Normal University, China

*CORRESPONDENCE

Lijun Guan
✉ qqaipph@sina.com
Shuwen Lu
✉ shuwenlu@sina.com

RECEIVED 22 December 2023

ACCEPTED 13 February 2024

PUBLISHED 22 February 2024

CITATION

Zhu L, Guan L, Wang K, Ren C, Gao Y,
Li J, Yan S, Zhang X, Yao X, Zhou Y, Li B and
Lu S (2024) Recent trends in extraction,
purification, structural characterization, and
biological activities evaluation of *Perilla
frutescens* (L.) Britton polysaccharide.
Front. Nutr. 11:1359813.
doi: 10.3389/fnut.2024.1359813

COPYRIGHT

© 2024 Zhu, Guan, Wang, Ren, Gao, Li, Yan,
Zhang, Yao, Zhou, Li and Lu. This is an open-
access article distributed under the terms of
the [Creative Commons Attribution License
\(CC BY\)](https://creativecommons.org/licenses/by/4.0/). The use, distribution or reproduction
in other forums is permitted, provided the
original author(s) and the copyright owner(s)
are credited and that the original publication
in this journal is cited, in accordance with
accepted academic practice. No use,
distribution or reproduction is permitted
which does not comply with these terms.

Recent trends in extraction, purification, structural characterization, and biological activities evaluation of *Perilla frutescens* (L.) Britton polysaccharide

Ling Zhu^{1,2}, Lijun Guan^{1,2*}, Kunlun Wang^{1,2}, Chuanying Ren^{1,2},
Yang Gao^{1,2}, Jialei Li^{1,2}, Song Yan^{1,2}, Xindi Zhang^{1,2},
Xinmiao Yao^{1,2}, Ye Zhou^{1,2}, Bo Li^{1,2} and Shuwen Lu^{2*}

¹Institute of Food Processing, Heilongjiang Province Academy of Agricultural Sciences, Harbin, China,

²Heilongjiang Province Key Laboratory of Food Processing, Harbin, China

Perilla frutescens (L.) Britton is an annual herb plant of the *Perilla* genus in the Labiatae family, which is commonly utilized as an edible and medicinal resource. Polysaccharides are among the major components and essential bioactive compounds of *P. frutescens*, which exhibit a multitude of biological activities, including antioxidant, antitumor, anti-fatigue, immunoregulation, hepatoprotective, anti-inflammatory, and lipid-lowering effects. As a natural carbohydrate, *P. frutescens* polysaccharide has the potential to be utilized in the development of drugs and functional materials. In this paper, we provide an overview of progress made on the extraction, purification, structural characterization, and bioactivity of polysaccharides from different parts of *P. frutescens*. The challenges and opportunities for research are discussed, along with the potential development prospects and future areas of focus in the study of *P. frutescens* polysaccharides.

KEYWORDS

Perilla frutescens, polysaccharides, extraction, structural characterization, bioactivities

1 Introduction

Perilla frutescens (L.) Britton, also known as zisu in China, is an annual herb plant of the Labiatae family (1, 2). Although *P. frutescens* is widespread in Asian countries (Figure 1A) (3, 4), China is proposed to be the main genetic center of this species, where it has been cultivated for more than 2,000 years (5, 6). According to the variation of plant leaf color, *P. frutescens* can be divided into two main varieties circulating in China: *P. frutescens* var. *arguta* (the lower part of the leaf is red or purple) and *P. frutescens* var. *frutescens* (the upper and lower leaf surfaces are green) (7, 8). *P. frutescens* is considered a medicine and food homologous plant, as the dried stems, leaves (Figure 1B), and seeds (Figure 1C) can be used as a natural herbal medicine for pain relief, hemostasis, relief of cough, purgative, detoxification, relief of stomach upset, dissipating colds, and anti-inflammation (8–10). As part of the daily diet, *P. frutescens* leaves can be used in



barbecue, sashimi, sushi, and as a culinary condiment given their aromatic flavor (9, 11). Additionally, the oil of *P. frutescens* seeds can be used in baking pastries as an alternative to hydrogenated oils or cream (9). *P. frutescens* is becoming a more popular item in home cooking as it is increasingly recognized as a health-promoting food source.

In recent years, the chemical composition of *P. frutescens* has been extensively investigated (12). *P. frutescens* contains multiple active ingredients, including polysaccharides, anthocyanins, flavonoids, terpenoids, phenols, volatile oils, fatty acids, and proteins (13, 14). Among these compounds, polysaccharide is an essential component, which has been increasingly researched for various applications owing to its advantages of natural origin, safety, and low toxicity (15). The polysaccharides obtained from *P. frutescens* have proven to exhibit antioxidant, hepatoprotective, antitumor, and immunomodulatory activities (16–19), highlighting their broad application prospects in the food and biomedicine industries. To date, studies in this field have

mainly focused on the small-molecule compounds of *P. frutescens* and their pharmacological effects; however, a comprehensive review of the macromolecular polysaccharides of *P. frutescens* is lacking. Hence, in the present paper, the extraction, purification, structural characteristics, and biological activities of *P. frutescens* polysaccharides are systematically summarized with a view to further expand their application areas.

2 Extraction and purification of polysaccharides from *Perilla frutescens*

2.1 Extraction of polysaccharides from *Perilla frutescens*

The extraction of polysaccharides from raw materials is the first and key step in their effective utilization. Therefore, identifying

optimal extraction methods has been a primary research focus. *P. frutescens* polysaccharides are mainly extracted from the leaf and seed meal (a by-product of the seed after oil extraction) of the plant. Typically, a suitable solvent (such as petroleum ether, butane, or *n*-hexane) is selected to degrease the *P. frutescens* raw material in a Soxhlet extractor prior to polysaccharide extraction (15, 18, 20). Polysaccharides are a class of highly polar, highly water-soluble, and ethanol-insoluble substances that can be obtained by hot water extraction (HWE) in combination with ethanol precipitation (21). For instance, Zhou and Sheng (22) prepared polysaccharides from *P. frutescens* seeds using HWE at 80 °C followed by 70% ethanol alcohol precipitation. To increase the polysaccharide yield, response surface methodology (RSM) can be used to optimize the extraction conditions. For example, Ding (23) determined the following optimized HWE conditions for the extraction of *P. frutescens* leaf polysaccharide using RSM: material-to-liquid ratio of 1:30, extraction time of 4 h, extraction three times, and ethanol concentration for precipitation of 60% (v/v). Under the above conditions, the extraction yield of crude *P. frutescens* leaf polysaccharide reached up to $5.22 \pm 0.17\%$. HWE has advantages of being a relatively simple, low-cost, and non-polluting process (24); however, this method suffers from the drawbacks of a long operating time, low yield, and the need for repetitive operations (25). Thus, HWE should be combined with other innovative technologies such as ultrasonic-assisted extraction (UAE), microwave-assisted extraction (MAE), and ultrasonic-assisted enzyme extraction (UAEE).

UAE can promote the release and dissolution of intracellular and cell wall polysaccharides through the high shear pressure generated via cavitation, which has the benefits of a high extraction rate, simple operation, and low solvent dosage (26). Zhang et al. (18) optimized the experimental scheme for the extraction of polysaccharides from *P. frutescens* seed meal (PSMP) by UAE through RSM, obtaining an average extraction yield of $6.137 \pm 0.062\%$ using a liquid-to-solid ratio of 26.00 mL/g, extraction temperature of 43.00°C, ultrasonic time of 52.00 min, and ultrasonic power of 229.00 W. Compared with the time required using HWE, the extraction time for obtaining *P. frutescens* polysaccharides could be shortened by two-thirds and the extraction temperature was reduced by 33.70–57.40% with UAE (20).

MAE has the advantages of high permeability, selectivity, and extraction efficiency (27), demonstrating its suitability for the extraction of *P. frutescens* polysaccharide. Microwave is an electromagnetic wave with a frequency in the range of 300 MHz to 300 GHz (24). Microwave heating is produced by the ionic conduction of dissolved ions and molecular friction due to the dipolar rotation of polar solvents (28). The optimized conditions for the MAE of *P. frutescens* seed polysaccharides were determined to be a liquid-to-feed ratio of 25 mL/g, microwave power of 480 W, and microwave processing time of 3 min, which resulted in a yield of 9.06% with subsequent HWE (90°C, 3 h) (29). In another study, using the MAE method to extract polysaccharides from *P. frutescens* leaf powder with a short microwave treatment (800 W) of only 30 s after hot water immersion (80°C) for 2 h resulted in improvement of the yield to 3.99% compared to a yield of only 2.21% obtained with the HWE method, which required a total extraction time of 6 h at 80°C (30). Therefore, the extraction of *P. frutescens* polysaccharides by MAE can save substantial time while improving the efficiency compared with the HWE method.

Enzyme-assisted extraction of polysaccharides involves the use of enzymes capable of breaking down the cell wall, which offers benefits of environmental friendliness, low-energy consumption, and high extraction efficiency (31, 32). Under the optimal conditions of 1771.85 U/g cellulase, enzyme activation temperature of 53.7°C, and enzyme digestion time of 36.2 min, the extraction rate of *P. frutescens* leaf polysaccharides reached 17.91 mg/g (33). Ultrasonic extraction can further enhance the affinity of the enzyme for the substrate and thereby increase the speed of the enzymatic reaction (24). Therefore, enzyme-assisted extraction can be combined with UAE (i.e., UAEE) to effectively increase the extraction rate. Recently, Li et al. (34) optimized the UAEE process to extract polysaccharides from *P. frutescens* leaves according to a single-factor test and Box-Behnken design (BBD), obtaining a yield of 3.84% when the liquid-to-solid ratio was 41:1, enzymatic time was 40 min, enzymatic temperature was 49 °C, and ultrasonic power was 204 W. Subsequently, Zhang et al. (35) applied RSM analysis with a BBD to identify the optimal conditions for the UAEE of *P. frutescens* seed meal polysaccharides (PSMP). With the optimized conditions of a compound enzyme dose of 6.6%, liquid-to-solid ratio of 25 mL/g, extraction time of 61 min, and extraction temperature of 62°C, the PSMP yield was $7.711 \pm 0.201\%$.

In addition to the methods described above, various novel approaches for extracting polysaccharides have also been proposed, including pressurized-liquid extraction, supercritical-fluid extraction, ionic-liquid extraction, and pulsed electric field-assisted extraction (27, 32). However, these novel approaches have not yet been employed for extracting polysaccharides from *P. frutescens*, requiring further investigation in the future.

2.2 Purification of polysaccharides from *Perilla frutescens*

The crude polysaccharide obtained after ethanol precipitation normally contains impurities such as proteins, pigments, and small molecules, necessitating subsequent separation and purification processes to obtain the pure polysaccharide (36). The Sevag method is commonly used to remove proteins from crude polysaccharide solutions, which is based on the principle of protein denaturation in chloroform and other organic solvents (17). In brief, the crude polysaccharide solution is blended with Sevag's reagent (1-butanol/chloroform, 1/4 v/v) at a certain proportion, the mixture is shaken well, and the supernatant is collected after centrifugation to remove some of the proteins (37, 38). The Sevag method offers advantages of mild conditions, without causing the denaturation of polysaccharides (39), and can achieve a good effect of removing proteins from the crude *P. frutescens* polysaccharide solution after multiple repeated operations (20, 23, 34). Zhang (30) discovered that under the conditions of a 4:1 ratio of chloroform to *n*-butanol, 1:1 ratio of polysaccharide solution to Sevag reagent, 35 min of deproteinization time, and two deproteinization steps, the deproteinization rate of *P. frutescens* leaf polysaccharide reached 73.6%. However, the deproteinized *P. frutescens* polysaccharide solution needs to be further dialyzed to remove residual Sevag reagent and other small-molecule impurities (15, 35).

To obtain homogeneous polysaccharides, further isolation and purification of the crude polysaccharides is required. Column

chromatography is the most extensively applied approach for the purification of polysaccharides owing to its good purification effect and simple operation procedures (40–42). Column chromatography mainly includes ion-exchange column chromatography and gel-column chromatography (43). Ion-exchange chromatography involves the use of either cation- or anion-exchange resins (44), with anionic columns most frequently used in the purification of *P. frutescens* polysaccharides. Anion-exchange chromatography enables strong binding to acidic polysaccharides without interacting with neutral polysaccharides, thus, the neutral polysaccharides are eluted first (45) and those obtained from different fractions can be separated by a stepwise elution process using solutions with different ionic strengths (46). For example, Li et al. (34) eluted four types of *P. frutescens* leaf polysaccharides on a DAE-Cellulose 52 column (2.6 × 30 cm) at a flow rate of 0.6 mL/min using different concentrations of sodium chloride solution (0, 0.1, 0.2, 0.3, and 0.5 mol/L).

Gel-column chromatography (Sephadex-G series and Sephacryl-S series) is an effective method to separate polysaccharides with different molecular weights (47). High-molecular-weight polysaccharides will be eluted first with the mobile phase, while the low-molecular-weight polysaccharides will diffuse into the pores of the gel and elute later (48). Ding et al. (15) used a Sephadex G-200 gel column (1.6 cm × 30 cm) to purify and obtain a *P. frutescens* leaf polysaccharide (PFP) with purity reaching up to 89.73%. Different columns can be used synergistically in the separation and purification of polysaccharides to achieve a better effect. Kim et al. (16) first used a DEAE-Toyopearl 650 M column (4.0 × 30 cm) to isolate one polysaccharide, designated PFB-1-0. This polysaccharide was then eluted using a Sephadex G-100 gel column (2.5 × 94 cm) with 0.2 mol/L NaCl at a flow rate of 0.2 mL/min to obtain fractions PFB-1-0i and PFB-1-0ii with 43.2 ± 2.5% and 82.8 ± 4.8% purity, respectively. In the majority of studies, DEAE-52 cellulose, DEAE-Toyopearl 650 M, Sephadex G-100 gel, and Sephadex G-200 gel chromatography columns are employed for the separation of *P. frutescens* polysaccharides, the eluate is collected, concentrated, and freeze-dried to finally obtain purified *P. frutescens* polysaccharides. The flow chart of the extraction and purification procedure of *P. frutescens* polysaccharides is displayed in Table 1 and Figure 2.

3 Structure of *Perilla frutescens* polysaccharides

Structural characterization of polysaccharides is important since the structure is closely related to biological activity (54). The key structural features of polysaccharides include their monosaccharide composition, molecular weight (M_w), chemical components, and bonding information (55). Different plant parts (i.e., the roots, leaves, stems, or seeds), extraction methods, and isolation and purification steps can lead to variations in polysaccharide structure (56). The structural characteristics of polysaccharides derived from different parts of *P. frutescens* are summarized in Table 2.

3.1 Monosaccharide composition

Monosaccharide composition is an essential foundation for the structural analysis of polysaccharides. The acid hydrolysis method is

used to completely break the glycosidic bonds of polysaccharides; after hydrolysis, the polysaccharide sample is neutralized, filtered, and derivatized for analysis of monosaccharide composition (57). High-performance liquid chromatography (HPLC), gas chromatography-mass spectrometry (GC-MS), gas chromatography (GC), gas-liquid chromatography, and ion chromatography (IC) are common methods employed to measure the monosaccharide composition and molar ratio of polysaccharides (15, 16, 47, 48). Using GC-MS analysis, the monosaccharide composition of a PSMP was determined to comprise rhamnose (Rha), arabinose (Ara), xylose (Xyl), mannose (Man), glucose (Glu), and galactose (Gal) at a mass ratio of 3.196%: 43.901%: 21.956%: 4.244%: 4.706%: 21.997% (18). Using IC analysis, the PFP extracted from the leaves was reported to comprise six major monosaccharides, including Rha, Ara, Gal, Glu, Xyl, and galacturonic acid (GalA), with the Glu and Gal monosaccharides being the most abundant (15). Furthermore, analysis of *P. Frutescens* polysaccharides extracted from the leaves and purified with DEAE-Toyopearl 650 M and Sephadex G-100 column chromatography showed that the proportions of Ara, Xyl, and Gal were gradually reduced during the progression of purification, whereas the proportion of Man and Glu significantly increased, which ultimately accounted for the major portion of the obtained *P. frutescens* leaf polysaccharides (16). Subsequent GC analysis showed that the PFB-1-0 fraction consisted of Ara (8.9%), Xyl (0.9%), Man (25.9%), Glu (16.8%), and Gal (24.9%) after DEAE-Toyopearl 650 M column chromatography purification, and the PFB-1-0-ii fraction consisted of Ara (9.6%), Xyl (0.2%), Man (39.8%), Glu (45.6%), and Gal (14.5%) after Sephadex G-100 column chromatography purification.

3.2 Molecular weight

The M_w not only affects the physical properties of polysaccharides, such as viscosity and solubility, but also affects their biological activities, forming the basis for characterizing the properties of polysaccharides (58). To date, the M_w of *P. Frutescens* polysaccharide has mainly been analyzed using HPLC and high-performance gel-permeation chromatography (HPGPC) detection techniques (16, 23, 51). Based on the available literature, the M_w of *P. frutescens* polysaccharide ranges from approximately 1.6 × 10³ Da to 1.18 × 10⁶ Da. For example, PFB-1-0-ii obtained from extraction of *P. frutescens* leaves using HWE and ethanol precipitation, followed by further separation and purification on a DEAE-Toyopearl 650 M column and a Sephadex G-100 chromatographic column, had an M_w of 10 kDa determined by HPGPC (16). By contrast, Niu et al. (52) obtained three main polysaccharide fractions from *P. frutescens* leaves by HWE, ethanol precipitation, and further purification on a DEAE-52 column with an M_w of 2.2 kDa and 1589.8 Da for PFP-2 and PFP-4, respectively, whereas PFP-3 was mainly composed of two segments with an M_w of 5.2 and 40.0 kDa, respectively, as determined by HPGPC. The difference in M_w among these *P. frutescens* polysaccharides is mainly attributed to variations in factors such as source, treatment method, and separation equipment. Similar variations in M_w have also been observed in studies on polysaccharides from *Bupleuri Radix*, and *Nelumbo nucifera* Gaertn. (lotus), and *Radix Hedysari* (26, 59, 60).

TABLE 1 Extraction and purification of polysaccharides from the different parts of *P. frutescens*.

Polysaccharide name	Source	Extraction method	Crude polysaccharide yield	Separation and purification progress	References
PFP	Leaf	Petroleum ether, degreasing, HWE, solid to liquid ratio of 1:30, 100°C, 3 replicate extractions, EtOH precipitation	5.22 ± 0.17%	Water dialysis for 2 days, Sephadex G-200 gel column chromatography	(15)
PFB-1-0-ii	Leaf	HWE, 20 mL/g liquid-solid ratio, 100°C, methanol reflux, 80% EtOH precipitation	9.8%	DEAE-Toyopearl 650 M, Sephadex G-100 column chromatography	(16)
PEPF	Leaf	HWE, 10 mL/g liquid-solid ratio, 90°C, 2h, 70% EtOH precipitation	ND	Dialysis	(14)
PLP1, PLP2, PLP3, PLP4	Leaf	UAE, liquid-to-solid ratio of 41:1, 49°C, 40 min, ultrasonic power of 204 W, dehydrated ethanol precipitation	3.84%	Sevag method deproteinization, DEAE-52, Sephadex G-100 column chromatography	(34)
PFB-1-0	Leaf	HWE, 20 mL/g liquid-solid ratio, 100°C, methanol reflux, 80% EtOH precipitation	98 g/kg	DEAE-Toyopearl 650 M chromatography, tap water dialysis	(49)
<i>P. leaf</i> polysaccharide	Leaf	UAEE, enzymolysis time 40 min, enzymolysis temperature 20.4°C, cellulases quantity 2000 U/g, ultrasonic time 60 min, 80% EtOH precipitation	4.54%	ND	(50)
PFPS	Leaf	HWE, 20 mL/g liquid-solid ratio, 80°C, 3h, 2 replicate extractions, 95% EtOH precipitation, Sevag method deproteinization, dialysis	3.57%	ND	(51)
<i>P. frutescens</i> leaf polysaccharide	Leaf	EAE, 40 mL/g liquid-solid ratio, 1771.85 U/g cellulase, enzyme action temperature 53.7°C, enzyme treatment time 36.2 min, EtOH precipitation	17.91 mg/g	ND	(33)
PFP-1, PFP-2, PFP-3, PFP-4	Leaf	Ethanol degreasing, HWE, 20 mL/g liquid-solid ratio, 95% EtOH precipitation	ND	DEAE-52 cellulose column chromatography, dialysis	(52)
PLP-0.1-I, PLP-0.2-I, PLP-0.3-I	Leaf	UAE, 35.3 mL/g liquid-solid ratio, 210 W, 66.7°C, 51.5 min	6.853 ± 0.321%	Macroporous adsorbent resin D101, DEAE 52, Sephadex G-200, column chromatography, Sevag method deproteinization	(20)
PLP	Leaf	UEAE, compound enzyme dosage of 5.54%, 15 mL/g liquid-solid ratio, 48 min, 40°C	7.326 ± 0.291%	ND	(20)
<i>P. frutescens</i> leaf polysaccharide	Leaf	HWE, 30 mL/g liquid-solid ratio, 80°C, 6h; Firstly, soak in hot water at 70°C for 3h, then, using MAE to extract, loading volume of 10 mL, microwave time of 30 s, microwave power of 800 W	2.21%; 3.99%	Activated carbon decolorization, Sevag method deproteinization, DEAE-cellulose column chromatography	(30)

(Continued)

TABLE 1 (Continued)

Polysaccharide name	Source	Extraction method	Crude polysaccharide yield	Separation and purification progress	References
PFSP-2-1	Seed	Petroleum ether degreasing, HWE, 20 mL/g liquid-solid ratio, 85°C, 2.5 h, 3 replicate extractions, 75% EtOH precipitation	3.42 ± 1.97%	Sevag method deproteinization, polyamide chromatography column method decolorization, DEAE 52, Sephacryl S-500 HR column chromatography	(53)
<i>P. frutescens</i> seed polysaccharide	Seed	WAE, 25 (mL/g) liquid-to-feed ratio, 480 W microwave power, 3 min microwave processing time, hot water extraction at 90°C for 3 h, Sevag method deproteinization, EtOH precipitation	9.06%	ND	(29)
<i>P. frutescens</i> polysaccharide	Seed	Petroleum ether de-oiling, HWE, 80°C, 4 h, 70% EtOH precipitation	ND	ND	(22)
PSMP-0.1-I; PSMP-0.2-I; PSMP-0.3-I	Seed meal	UAE, 26.1 mL/g liquid-solid ratio, 229 W, 42°C, 51.8 min	6.137 ± 0.062%	Macroporous adsorbent resin D101, DEAE 52, Sephadex G-200, column chromatography, Sevag method deproteinization	(20)
PSMP	Seed meal	UEAE, compound enzyme dosage of 6.60%, 24.7 mL/g liquid-solid ratio, 60.5 min, 62°C	7.611 ± 0.20%	ND	(20)
PSMP-1	Seed meal	UAEE, 6.6% compound enzyme, 25 mL/g liquid-solid ratio, 62°C, 61 min, 80% ethanol (EtOH) precipitation	7.711 ± 0.201%	D101 resin adsorption, Sevag method deproteinization, DEAE-52 column chromatography	(35)
PSMP	Seed meal	N-hexane degreasing, UAE, liquid–solid ratio of 26.00 mL/g, 43°C, 52.00 min, 229.00 W ultrasonic power	6.137 ± 0.062%	ND	(18)
PFSP-1; PFSP-2; PFSP-3	Seed meal	Petroleum ether, degreasing 6 h, HWE, 20 mL/g liquid-solid ratio, 85°C, 2 h, 3 times, EtOH precipitation, Sevag method deproteinization	8.38%	DEAE-52 Cellulose, Sephadex G-100 column chromatography	(17)

ND stands for not detected.

3.3 Chemical structures

The biological significance of polysaccharides is intimately associated with their complex structural properties and unique backbone features (47). Therefore, determining the chemical structure of polysaccharides is an important element in the investigation of their pharmacological effects and improvement of their applications (61). Chromatographic techniques, spectroscopic analysis, and other chemical analyses are effective methods for studying the structural characteristics of *P. frutescens* polysaccharides, including the types and linkages of sugar residues. According to the results of Fourier-transfer infrared spectroscopy (FT-IR), *P. frutescens* seed meal polysaccharide had five absorption peaks at 3,356 cm^{−1} (O–H), 2931 cm^{−1} (C–H),

1658 cm^{−1} (–C=O and –CHO), 1415 cm^{−1} (C–O), and 1,317 and 1,245 cm^{−1} (–COOH). The strong peaks noted at 1,072 and 1,047 cm^{−1} suggested the presence of galactopyranose and arabinofuranose in the backbone and branches of the sugar chain. GC-MS and one-dimensional nuclear magnetic resonance (NMR) spectrum (1H, 13C) analyses showed that *P. frutescens* seed meal polysaccharide was composed of β-D-Xyl, α-L-Ara, β-D-Gal, and β-L-Ara sugar residues, and was free of glucuronic acid (18). Moreover, Li et al. (53) obtained a homogenous polysaccharide faction of PFSP-2-1 from *P. frutescens* seed. Based on FT-IR, IC, methylation, and one- and two-dimensional NMR analysis, the structure of PFSP-2-1 showed a backbone of →1)-Araf-(5→1)-Galp-(6→1)-Galp-(6→1)-Araf-(5→1)-Araf-(5→1)-Galp-(6→1)-Araf-(5→1)-Araf-(5→1)-Araf-(3→1)-Xylp-(4→; and three

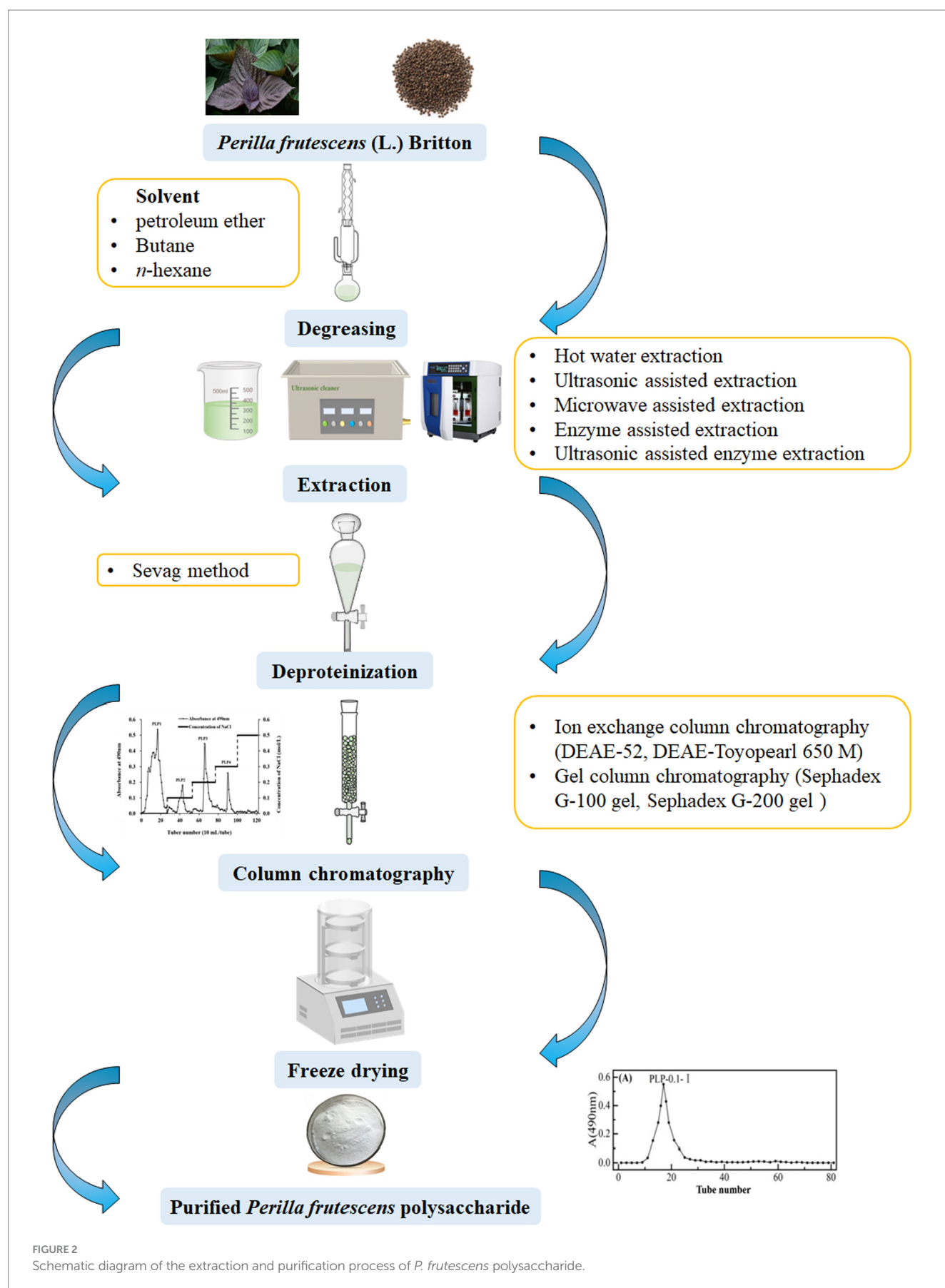


FIGURE 2
Schematic diagram of the extraction and purification process of *P. frutescens* polysaccharide.

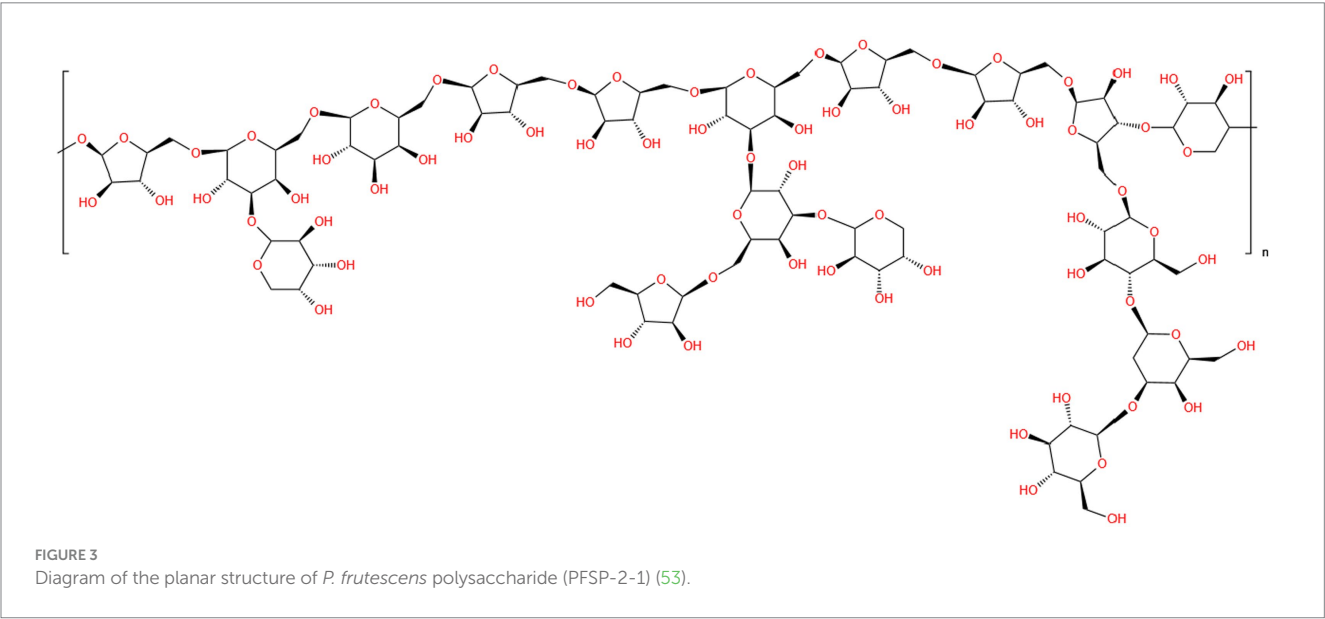
TABLE 2 Structural characterization of polysaccharides from the different parts of *P. frutescens*.

Polysaccharide name	Source	Molecular weight	Monosaccharide composition	Structural characterization	Analysis technique	References
PFP	Leaf	1.18 × 106 Da	Rha, Ara, Gal, Glc, Xyl, and GalA in a molar ratio of 0.13: 0.55: 1.40: 1.00: 0.13: 0.22	α-L-Araf-(1→, →6)-β-D-Galp-(1→, →4)-α-D-Glcp-(1→, →1,4)-β-D-Xylp(1→, →4)-α-GalpA-(1→, →2,4)-α-L-Rhap-(1→	HPGPC, FT-IR, IC, NMR	(15)
PFB-1-0-ii	Leaf	10 kDa	Ara (9.6%), Xyl (0.2%), Man (39.8%), Gal (14.5%) and Glu (45.6%)	ND	HPLC, GLC	(16)
PEPF	Leaf	ND	ND	ND	ND	(14)
PLP1, PLP2, PLP3, PLP4	Leaf	ND	ND	ND	ND	(34)
PFB-1-0	Leaf	ND	ND	ND	ND	(49)
<i>P. leaf</i> polysaccharide	Leaf	ND	ND	ND	ND	(50)
PFPS	Leaf	ND	ND	N-H(-CONH-), C-O-C glycosidic bonds	FT-IR	(51)
<i>P. frutescens</i> leaf polysaccharide	Leaf	ND	ND	ND	ND	(33)
PFP-1, PFP-2, PFP-3, PFP-4	Leaf	ND; 2.2 kDa; 5.2 kDa; 1.6 kDa	Man, Glu, Gal, Ara in a ratio of 51.3:32.1; Man, Rha, GluA, GalA, Glu, Gal, Ara, fructose (Fuc) in a ratio of 1.7: 7.2:1.2:65.9:0.8:11.3:10.7:1.1; Man, Rha, GluA, GalA, Glu, Gal, Ara, Fuc in a ratio of 5.8:15.7:2.9:33.1:2.3:24.7:14.5:0.9; Man, Rha, GluA, GalA, Glu, Gal, Ara, Fuc in a ratio of 4.8:5.7:5.6:8.3:14.4 :34.9:23.8:2.5	ND	HPGPC, HPLC	(52)
PLP-0.1-I, PLP-0.2-I, PLP-0.3-I	Leaf	ND	Rha, Fuc, Ara, Xyl, Man, Glu, Gal in a molar ratio of 22.88, 2.20:14.41:1.00:3.88:4.47: 24.55; Rha, ribose (Rib), Fuc, Ara, Man, Glu, Gal in a molar ratio of 20.44:1.00:1.98:6.55:4.5 8:15.45:21.52; Rha, Rib, Fuc, Ara, Xyl, GluA, Man, Glu, Gal in a molar ratio of 27.55:2.91:5.07:16.04:4.03:1.00:18.66:39. 62:64.26	β-D-Glucopyranose	GC-MS, FT-IR	(20)
PLP	Leaf	ND	ND	ND	ND	(20)
<i>P. frutescens</i> leaf polysaccharide	Leaf	ND	ND	ND	ND	(30)
PFSP-2-1	Seed	8.81 × 106 Da	Ara, Gal, Glu, Xyl, GluA in a molar ratio of 20.207:11.223:1.228:18.232:0.33 1	The main chain is →1)-Araf-(5→1)-Galp-(6→1)-Galp-(6→1)-Araf-(5→1)-Araf-(5→1)-Galp-(6→1)-Araf-(5→1)-Araf-(5→1)-Araf-(3→1)-Xylp-(4→ with side chains of →1,6)-Galp-(3→1)-Arap, →1,6)-Galp-(3→1,3)-Galp-(6→1)-Araf, →1,6)-Galp-(3→1)-Arap, and →1,3)-Araf-(5→1)-Glc-(4→1)-Galp-(3→1)-Glc	HPGPC, IC, FT-IR, methylation analysis, NMR	(53)

(Continued)

TABLE 2 (Continued)

Polysaccharide name	Source	Molecular weight	Monosaccharide composition	Structural characterization	Analysis technique	References
<i>P. frutescens</i> seed polysaccharide	Seed	ND	ND	ND	ND	(29)
<i>P. frutescens</i> polysaccharide	Seed	ND	ND	ND	ND	(22)
PSMP-0.1-I; PSMP-0.2-I; PSMP-0.3-I	Seed meal	ND	Rha, Ara, Xyl, GalA, Man, Glu, Gal in a molar ratio of 1.31:22.98:5.60:2.72:3.21:1.00:12.44; Rha, Fuc, Ara, Xyl, GalA, Man, Glu, Gal in a molar ratio of 8.58:2.08:20.36:6.39:3.63:1.00:6.10:18.49; Rha, Rib, Fuc, Ara, Xyl, GalA, Man, Glu, Gal in a molar ratio of 12.91:1.00:2.21:9.55:8.03:6.71:1.42:29.58:22.24	β -D-Glucopyranose	GC-MS, FT-IR	(20)
PSMP	Seed meal	ND	ND	ND	ND	(20)
PSMP-1	Seed meal	ND	Rha, Ara, Xyl, Man, Glu, and Gal in a molar ratio of 0.69:11.13:5.55:0.90:1.00:4.71	β -D-glucopyranose	FT-IR, GC-MS	(35)
PSMP	Seed meal	ND	Rha, Ara, Xyl, Man, Glu, and Gal in the mass ratio of 3.196%:43.901%:21.956%:4.244%:4.706%:21.997%	β -D-Xyl, α -L-Ara, β -D-Gal, β -L-Ara, (1 \rightarrow 6) glycosidic, and (1 \rightarrow 3/4) glycosidic	GC-MS, FT-IR, NMR	(18)
PFSP-1; PFSP-2; PFSP-3	Seed meal	1.06 \times 10 ⁵ ; 5.96 \times 10 ⁴ ; 3.72 \times 10 ⁴	Man, Gal, Xyl, Ara in a molar ratio of 0.01:0.06:0.11:0.81; Man, Xyl, Ara in a molar ratio of 0.28:0.28:0.41; Rha, glucuronic acid (GluA), Glu, Gal, Xly, Ara with a molar ratio of 0.013:0.024:0.040:0.080:0.120:0.700	Pyranose ring, C-O glycosidic bond	HPLC, FT-IR	(17)



branches consisting of \rightarrow 1,6)-Galp-(3 \rightarrow 1)-Arap, \rightarrow 1,6)-Galp-(3 \rightarrow 1,3)-Galp-(6 \rightarrow 1)-Araf, \rightarrow 1,6)-Galp-(3 \rightarrow 1)-Arap, and \rightarrow 1,3)-Araf-(5 \rightarrow 1)-Glc-(4 \rightarrow 1)-Galp-(3 \rightarrow 1)-Glc. The link sites were at position C-3 of \rightarrow 3,6)-Galp-(1 \rightarrow , C-3 of \rightarrow 3,6)-Galp-(1 \rightarrow , and C-5 of \rightarrow 3,5)-Araf-(1 \rightarrow , respectively (Figure 3). Using FT-IR, IC, and NMR spectroscopy, PFP was confirmed to be an acidic polysaccharide with a backbone comprising six sugar residues: α -L-Araf-(1 \rightarrow , \rightarrow 6)- β -D-Galp-(1 \rightarrow , \rightarrow 4)- α -D-Glcp-(1 \rightarrow ,

$\rightarrow 1,4$)- β -D-Xylp-(1 \rightarrow , $\rightarrow 4$)- α -GalpA-(1 \rightarrow , and $\rightarrow 2,4$)- α -L-Rhap-(1 \rightarrow (15). However, the detailed chemical structures of polysaccharides from *P. frutescens* leaf, such as the linkage of sugar residues, have been not reported to date. Therefore, the detailed structures of *P. frutescens* polysaccharides from different sources and parts of the plant need to be analyzed more deeply and comprehensively to further understand the physicochemical and biological properties of *P. frutescens* polysaccharides.

3.4 Conformational features

Conformation refers to the three-dimensional structure created by the penetrating bonds formed by the molecular structure of the polymer and the physical force penetrating the space (62). Polysaccharides possess complicated substituents and

diversified chemical structures, and their spatial conformation largely determines the various biological functions (63). Scanning electron microscopy (SEM) observations showed that the apparent morphology of polysaccharides obtained from *P. frutescens* leaves represents a combination of reticulated, lamellar, and chained forms, while the surface of the polysaccharides extracted from the *P. frutescens* seed meal is dominated by meshes and sheets (20) (Figure 4). Ding (23) carried out a comprehensive characterization of the morphological features of *P. frutescens* leaf polysaccharides via Congo red staining, circular dichroism, and SEM observations. The results revealed an overall orderly spatial structure of the *P. frutescens* polysaccharide, without a triple-helix structure, and the surface was smooth and flaky. Zhao et al. (51) similarly found a smooth lamellar structure on the surface of a *P. Frutescens* polysaccharide extracted from the leaves based on SEM observations.

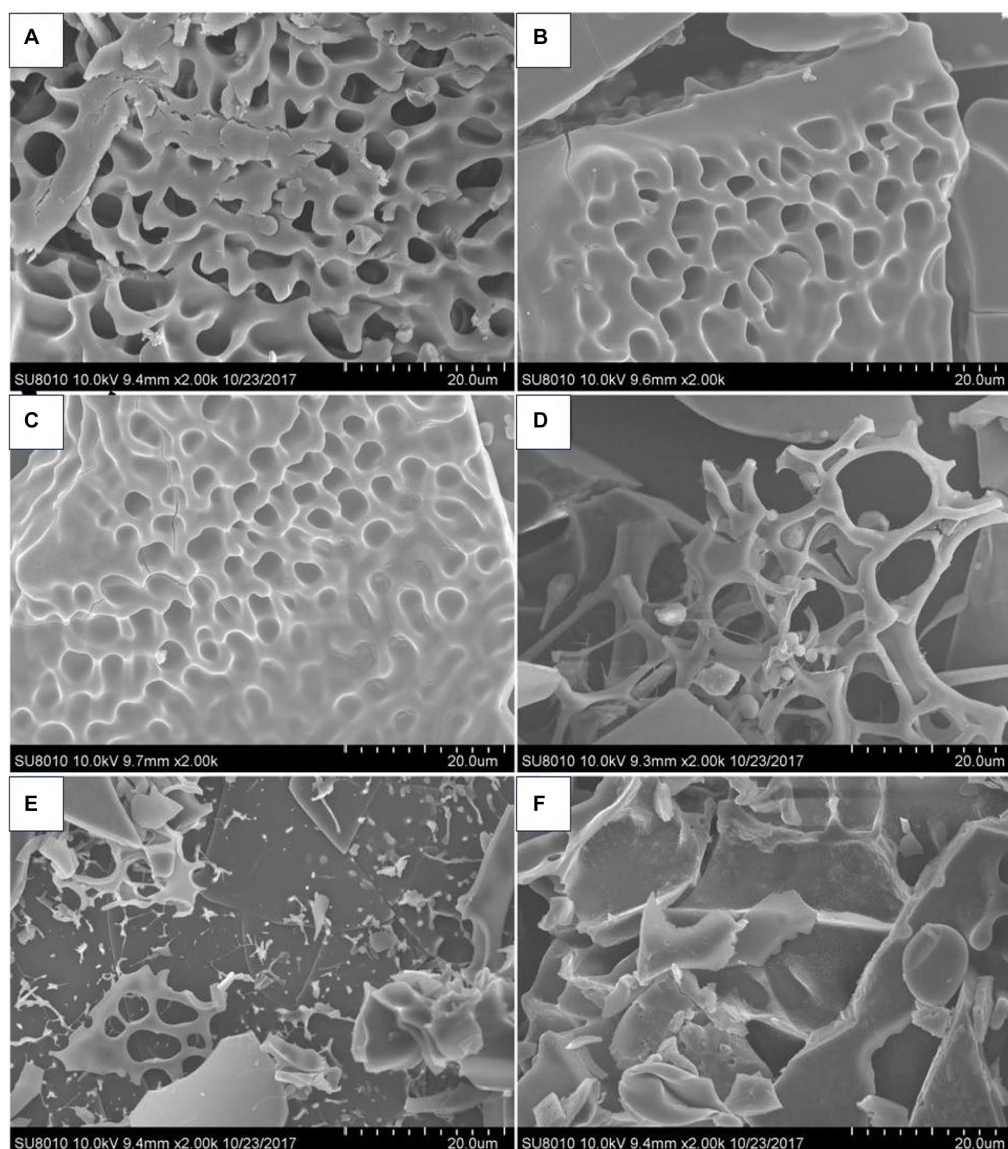


FIGURE 4

SEM micrographs of *P. frutescens* leaf polysaccharides (A: PLP-0.1-I; C: PLP-0.2-I; E: PLP-0.3-I) and *P. frutescens* seed meal polysaccharides (B: PSMP-0.1-I; D: PSMP-0.2-I; F: PSMP-0.3-I) (20).

4 Biological activities

P. frutescens exhibits numerous edible and medicinal benefits, and its polysaccharide is an essential component conferring these characteristics. Indeed, *P. frutescens* polysaccharide possess a variety of biological activities, including antioxidant, antitumor, anti-fatigue, immunoregulation, hepatoprotective, anti-inflammatory, and lipid-lowering effects, which are summarized in Figure 5.

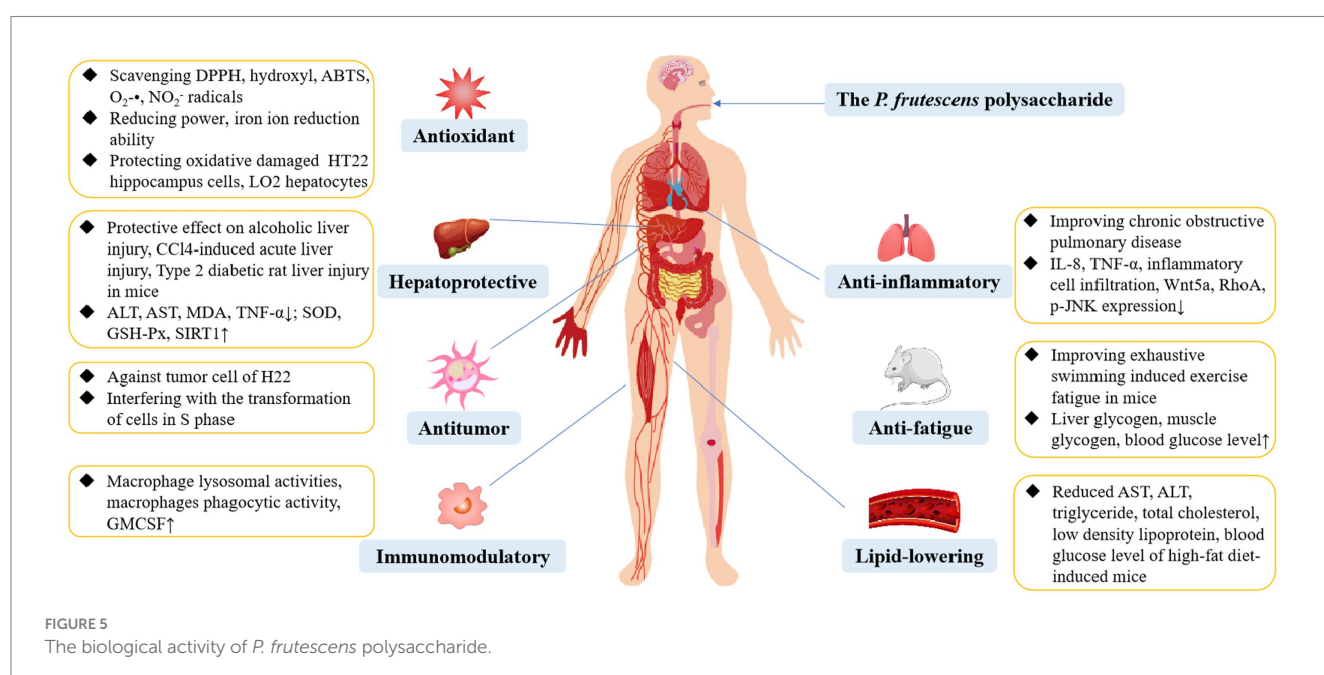
4.1 Antioxidant activity

Reactive oxygen species (ROS) are oxygen radicals in biological bodies, consisting of oxygen and oxygenated highly active molecules (e.g., superoxide anion, tissue peroxidation products, and free radicals). Typically, appropriate levels of ROS can facilitate immunity, repair, survival, and growth (64, 65). However, the excessive production of ROS will disrupt the dynamic redox balance, causing the human body to suffer damage, leading to multiple diseases (66). Hence, supplementation of antioxidants exogenously is essential for the body to fight or mitigate oxidative stress damage. *P. frutescens* polysaccharides demonstrate potential as effective antioxidants. The antioxidant activities of *P. frutescens* polysaccharides have been evaluated *in vitro* by examining the potential for scavenging 2,2-diphenyl-1-picrylhydrazyl (DPPH), 2,2'-azino-bis (3-ethylbenzothiazoline-6-sulfonic acid) diammonium salt (ABTS), hydroxyl (\bullet OH), superoxide anion ($O_2^{\bullet-}$), and nitrite ion (NO_2^-) radicals, along with iron-reduction capacity assays (14, 20, 37). For example, 1,000 μ g/mL of a *P. frutescens* seed meal polysaccharide (PMP) showed scavenging rates on \bullet OH, $O_2^{\bullet-}$, NO_2^- , and DPPH radicals of $49.70 \pm 2.10\%$, $21.76 \pm 1.09\%$, $60.75 \pm 2.19\%$, and $72.95 \pm 4.19\%$, respectively (67). The scavenging ability of PMP for $O_2^{\bullet-}$ showed a certain dose-dependent effect at a polysaccharide mass concentration range of 62.5–1,000 μ g/mL. However, Zhu et al. (68) showed that the

scavenging rate of *P. frutescens* seed meal polysaccharide on $O_2^{\bullet-}$ radicals exhibited a trend of initial increase followed by a decrease; when the concentration of the polysaccharide reached 1,000 μ g/mL, the formation of free radicals was promoted rather than suppressed. The reason for these discrepant effects could be attributed to the different structures and compositions of polysaccharides. Moreover, a PSMP exhibited a 73.83% scavenging rate of \bullet OH radicals at 5,000 μ g/mL and a 91.10% scavenging rate of ABTS radicals at 600 μ g/mL (18). In general, the high antioxidant activity of polysaccharides is related to the enrichment of uronic acid groups (39). However, no uronic acid was detected in the PSMP, and the antioxidant properties were instead attributed to the presence of Man and Glu (18). Overproduction of ROS induced by oxidative stress also plays a key role in neuronal damage. In H_2O_2 -induced neurotoxic cellular assays, *P. frutescens* polysaccharide reduced ROS production, lowered malondialdehyde (MDA) levels, increased intracellular superoxide dismutase (SOD) activity, and counteracted H_2O_2 -induced neuronal cell death by activating the PI3K/AKT pathway and negatively regulating the mitogen-activated protein kinase (MAPK) and nuclear factor-kappa B (NF- κ B) pathways in HT22 hippocampus cells (14).

4.2 Antitumor activity

Cancer remains a major global public health challenge. In the last few years, polysaccharides have attracted considerable attention in cancer research owing to their reported antitumor activity and low side effects (69). The antitumor effects of *P. Frutescens* polysaccharides could be attributed to their strong immunomodulatory abilities (15, 17). Treatment of H22 tumor-bearing mice with a *P. frutescens* leaf polysaccharide (PFP) at doses of 100 mg/kg and 300 mg/kg for three weeks significantly decreased tumor volume and weight and reduced thymic atrophy and splenomegaly in mice in a dose-dependent manner (15). *In vitro* investigations further showed that the PFP also



inhibited tumor proliferation by blocking the S-phase of the cell cycle and decreasing mitochondrial membrane potential. The antitumor effect of PFP may be related to the Gal component. Treatment of tumor-bearing mice with *P. frutescens* seed polysaccharide (0.1, 0.3, and 0.5 mg for 10 days) significantly reduced the levels of lactate dehydrogenase, aldolase, and interleukin (IL)-10; increased the levels of IL-2 and tumor necrosis factor- α (TNF- α) in the serum of mice; and down-regulated the expression of the anti-apoptotic protein Bcl-2 and up-regulated the expression of the pro-apoptotic protein Bax (17). Collectively, these results indicated that *P. frutescens* seed polysaccharide can inhibit the growth of tumor cells *in vivo* by enhancing the autoimmunity of mice. Li et al. (53) found that a *P. frutescens* seed polysaccharide (PFSP-2-1) could significantly inhibit the growth of three types of hepatocellular carcinoma cells (HepG2, Hep3b, and SK-Hep-1), and the inhibitory effect gradually increased with the increase of PFSP-2-1 concentration. It has been hypothesized that Ara and Xyl in PFSP-2-1 are some of the factors inhibiting the growth of liver cancer cells. Moreover, the triple-helix high-level structure of PFSP-2-1 is also an important factor in its anti-tumor activity. In summary, *P. frutescens* polysaccharides exhibit excellent antitumor properties; however, the therapeutic effects will need to be further investigated on more cancer models along with determination of the conformational relationships.

4.3 Hepatoprotective effect

The liver is a crucial organ with essential functions in regulating metabolism, biotransformation, and detoxification (70). Factors such as autoimmune aggression of liver cells, medication misuse, alcohol consumption, infections with viruses, and cardiovascular disease predispose the liver to injury (71, 72). Several studies have demonstrated that *P. frutescens* polysaccharides have a hepatoprotective effect, which may be associated with their antioxidant and anti-inflammatory activities (19, 73). Li et al. (29) reported that *P. frutescens* seed meal polysaccharide administered at doses of 100, 300, and 500 mg/kg for 7 days alleviated CCl₄-induced acute liver injury in an animal model. Specifically, the *P. frutescens* seed meal polysaccharide decreased serum aspartate aminotransferase (AST) and alanine aminotransferase (ALT) activities, as well as liver and spleen coefficients. In a type 2 diabetic rat liver injury model induced by high-fat and high-sugar feeding combined with intraperitoneal injection of streptozotocin, gavage of *P. frutescens* leaf polysaccharide at 0.15, 0.30, 0.60 g/kg for 28 days significantly reduced the levels of MDA, C-reactive protein, IL-6, TNF- α , and acetylated forkhead transcription factor protein in liver tissues, while the activities of glutathione peroxidase (GSH-Px), catalase (CAT), and SOD as well as the expression of sirtuin 1 (SIRT1) and FoxO1 proteins in liver tissues were significantly elevated (73). Thus, the *P. frutescens* leaf polysaccharide could improve type 2 diabetes-induced rat liver injury by inhibiting oxidative stress and inflammation, while regulating activation of the SIRT1/FoxO1 signaling pathway. Additionally, Tao et al. (19) found that *P. frutescens* leaf polysaccharide significantly improved hepatocyte inflammatory cell infiltration, bleeding, and liver steatosis in a mouse model of alcoholic liver injury disease (ALD) induced by chronic ethanol gavage. After gavage of the *P. frutescens* polysaccharides, the contents of IL-1 β , IL-6, TNF- α , and MDA in the liver tissues of ALD mice were significantly decreased; the SOD and GSH-Px activities were significantly increased; and the

relative expression levels of p-AMPK α /AMPK α and SIRT1 were significantly increased. These findings suggested that *P. frutescens* polysaccharide from the leaves might ameliorate liver injury in ALD model mice by modulating the activity of the SIRT1-AMPK signaling pathway in the liver tissues.

4.4 Immunomodulatory effect

Immunomodulation involves recognition of the body's own and external substances, along with maintenance of the body's physiological balance via the immune response to external antigens, which plays an essential role in the resistance to infections, tumors, and other diseases (31, 74). Natural polysaccharides play a vital role in immune regulation by stimulating immune cells such as T lymphocytes, B cells, macrophages, and cytotoxic T cells (75). To date, the immunomodulatory activity of *P. frutescens* polysaccharides has been demonstrated in a variety of *in vitro* and *in vivo* models. Kwon et al. (49) obtained a fraction from the crude polysaccharides extracted from *P. frutescens* leaves (PFB-1) by DEAE-Toyopearl 650 M chromatographic column elution named PFB-1-0, which significantly increased lysosomal enzyme activity as well as nitric oxide and TNF- α levels in mouse peritoneal macrophages. Moreover, PFB-1 could stimulate the production of IL-6 and granulocyte-macrophage colony-stimulating factors in mice. In a corroborative study, Kim et al. (16) showed that the active polysaccharide fractions (PFB-1, PFB-1-0, PFB-1-0-ii) from *P. frutescens* leaves at a concentration range of 1–100 μ g/mL promoted macrophage lysosomal enzyme activity in a concentration-dependent manner. The immunomodulatory activity of these four *P. frutescens* leaf polysaccharides was attributed to the Man, Gal, and Glu components. Moreover, the high-molecular-weight *P. Frutescens* polysaccharide exhibited more effective macrophage-stimulating activity than the low-molecular-weight *P. Frutescens* polysaccharide. PFB-1-0-ii showed the best effect among all polysaccharide fractions, with 100 μ g/mL PFB-1-0-ii increasing macrophage lysosomal enzyme activity by 245% in comparison to that of the untreated control. Together, these studies indicate that *P. Frutescens* polysaccharides have the potential to be developed into drugs and functional foods with novel immunostimulatory activities; however, the interaction mechanism between polysaccharides and the immune system remains unclear, warranting further research.

4.5 Other activities

In addition to the above biological activities, *P. Frutescens* polysaccharides also contribute to other health dimensions, including anti-fatigue, anti-inflammatory, and lipid-lowering effects. In a mouse model of fatigue induced by exhaustive swimming, gavage of *P. Frutescens* polysaccharides extracted from the leaves (5, 10, and 20 mg/kg for 4 weeks) significantly increased the forceful swimming time of mice, as well as the blood glucose level, liver glycogen content, and muscle glycogen content after exercise (76). These findings demonstrated a protective effect of the *P. Frutescens* polysaccharide in accelerating the removal of certain fatigue-causing metabolic substances, maintaining the normal physiological function of cells, and delaying fatigue. Wang et al. (77) tested the effectiveness of *P. Frutescens* leaf polysaccharide as an

TABLE 3 Summary of biological activities of polysaccharides from *P. frutescens* ("↓," decrease; "↑," increase).

Biological activities	Polysaccharide name	Types	Testing subjects	Doses/duration	Effects	Mechanisms	References
Antioxidant	PSMP	<i>In vitro</i>	DPPH, hydroxyl, ABTS radicals	2,000 µg/mL for DPPH radical, 5,000 µg/mL for hydroxyl radical, 600 µg/mL for ABTS radical	DPPH, hydroxyl, and ABTS scavenging rate was 75.00%, 73.83%, and 91.10%, respectively	ND	(18)
	PEPF	<i>In vitro</i>	DPPH, ABTS radicals, reducing power, ferric antioxidant power, H ₂ O ₂ -induced HT22 hippocampus cells	0.25–2 mg/mL in DPPH, and ABTS scavenging test, 0.25–2 mg/mL in reducing power and ferric antioxidant power assay, 500 µg/mL for oxidatively damaged HT22 hippocampus cells	Radical-scavenging activities, reducing power, and ferric antioxidant power↑; MDA, Bax, sub-G1 cells phase population↓; SOD, PARP, Bcl-2↑	Activating PI3K/AKT, negatively regulating the MAPK and NF-κB pathways	(14)
	PSMP-1	<i>In vitro</i>	DPPH, ABTS radicals	0.10–5.00 mg/mL in DPPH scavenging assay, 0.0625–2.00 mg/mL in ABTS scavenging assay	Scavenging DPPH and ABTS radicals, the IC ₅₀ was 2.078 ± 0.092 and 0.266 ± 0.009 mg/mL, respectively	ND	(35)
	PLP1, PLP2, PLP3, PLP4	<i>In vitro</i>	Reducing power, DPPH, hydroxyl, ABTS radicals	0.1–5.0 mg/mL for reducing power test, 0.1–5.0 mg/mL for DPPH, ABTS, hydroxyl radicals	DPPH, ABTS, hydroxyl radical-scavenging capacity and reducing power↑; antioxidant power of the four fractions was in the order of PLP3 > PLP2 > PLP1 > PLP4	ND	(34)
	PFP-1, PFP-2, PFP-3, PFP-4	<i>In vitro</i>	DPPH, ABTS radicals, iron ion reduction ability	0.03–5.0 mg/mL for DPPH radical, 0.25–7.0 mg/mL for ABTS radical, 0.5–7.0 mg/mL in iron ion reduction ability assay	DPPH and ABTS scavenging capacity and iron reduction ability↑	ND	(52)
	<i>P. frutescens</i> leaf polysaccharide	<i>In vitro</i>	DPPH, hydroxyl radicals	0.1 mg/mL in DPPH scavenging test; 1.0 mg/mL in hydroxyl scavenging test	DPPH scavenging rate (94.17%) and hydroxyl scavenging rate (90.06%)	ND	(50)

(Continued)

TABLE 3 (Continued)

Biological activities	Polysaccharide name	Types	Testing subjects	Doses/duration	Effects	Mechanisms	References
	PMP	<i>In vitro</i>	Hydroxyl, O ₂ •-, NO ₂ •-, DPPH radicals, H ₂ O ₂ -induced oxidative damaged LO2 hepatocytes	62.5–1,000 µg/mL for hydroxyl, O ₂ •-, NO ₂ •-, and DPPH radicals; 200, 400, 800, 1,000 µg/mL for LO2 cell	Scavenging hydroxyl, O ₂ •-, NO ₂ •-, and DPPH radicals, the EC ₅₀ was 964.59, 6376.84, 275.24, and 333.55 µg/mL, respectively; LO2 cell survival rate, lactic dehydrogenase, mitochondrial membrane potential, GSH, SOD, CAT, Bcl-2 expression↑; ROS, MDA, Bax expression, PARP expression↓	Regulation of the mitochondria-mediated apoptosis signaling pathway	(67)
	PLP-0.1-I, PLP-0.2-I, PLP-0.3-I, PSMP-0.1-I, PSMP-0.2-I, PSMP-0.3-I	<i>In vitro</i>	DPPH, hydroxyl, ABTS radicals	1–5,000 µg/mL for DPPH, hydroxyl, ABTS radicals, 1–500 µg/mL for reducing power assay	DPPH, hydroxyl, and ABTS radical-scavenging activities, and reducing power↑; ABTS scavenging ability was in the order of PLP-0.1-I > PLP-0.2-I > PLP-0.3-I > PSMP-0.1-I > PSMP-0.2-I > PSMP-0.3-I	ND	(20)
Antitumor	PFSP-2-1, PFSP-2-2	<i>In vitro</i>	HepG2, Hep3b, SK-Hep-1 cells	100, 200, 400, 800, and 1,600 µg/mL	Ability to inhibit the activity of HepG2, Hep3b, and SK-Hep-1 cells↑; HepG2, Hep3b, and SK-Hep-1 cells survival rates were 53.34%, 70.33%, 71.06% and 61.07%, 75.58%, 64.02% treating with 1600 µg/mL of PFSP-2-1 and PFSP-2-2, respectively	ND	(53)
	PFP	<i>In vivo</i>	H22 hormonal mice	100 and 300 mg/kg for 3 weeks	Thymus index, tumor weight and volume, mitochondrial membrane potential↓; spleen index and tumor cell apoptosis↑	Interference with the transformation of cells in S phase	(15)

(Continued)

TABLE 3 (Continued)

Biological activities	Polysaccharide name	Types	Testing subjects	Doses/duration	Effects	Mechanisms	References
	PFSP-2	<i>In vivo</i>	H22 hormonal mice	0.1, 0.3, 0.5 mL (1 mg/mL), 10 days	LDH, aldolase, IL-10, Bcl-2 protein expression↓; IL-2, TNF- α , and proapoptotic protein Bax expression↑	Activates the ability of immune cells to produce cytokines	(79)
Hepatoprotective	<i>P. frutescens</i> leaf polysaccharide	<i>In vivo</i>	ALD mice	0.3, 0.6 g/kg for 60 days	Hepatic fat cell degeneration score, ALT, AST, TG, TC, LDL, IL-1 β , IL-6, TNF- α , MDA, and SREBP1c relative expression↓; HDL, SOD, GSH-Px, p-AMPK α /AMPK α , and SIRT1 relative expression↑	Activation of the SIRT1-AMPK signaling pathway, reduction in oxidative stress and inflammation in the body	(19)
	<i>P. frutescens</i> leaf polysaccharide	<i>In vivo</i>	Type 2 diabetic rat liver injury model	0.15, 0.30, 0.60 g/kg for 28 days	Fasting blood-glucose, liver index, TG, TC, AST, ALT, MDA, CRP, IL-6, TNF- α , Ac-FoxO1 expression↓; body mass, GSH-Px, CAT, SOD, SIRT1, FoxO1 expression↑	Inhibition of oxidative stress, anti-inflammation, modulation of SIRT1/ FoxO1 signaling pathway activation	(73)
	<i>P. frutescens</i> seed polysaccharide	<i>In vivo</i>	CCl4-induced acute liver injury in mice	100, 300, 500 mg/kg for 7 days	ALT, AST, liver coefficient, spleen coefficient, and spotted necrotic lesions on the surface of the liver↓	ND	(29)
Immunomodulatory	PFB-0, PFB-1, PFB-1-0, PFB-1-0-ii	<i>In vitro</i>	Male ICR mice macrophages	1, 10, 100 μ g/mL	Macrophage lysosomal relative activities↑; stimulatory effect of four components on macrophage lysosomal enzyme activity in the order PFB-1-0-ii > PFB-1-0 > PFB-1 > PFB-0	ND	(16)
	PFB-1-0, PFB-1	<i>In vitro</i> , <i>in vivo</i>	Murine peritoneal macrophages	100 μ g/mL for <i>in vitro</i> test; 0.5, 0.75, 1.0 and 1.25 g/kg for specific pathogen free ICR mice for 8 days	Murine peritoneal macrophages lysosomal enzyme activity, mouse peritoneal macrophages phagocytic activity, nitric oxide, tumor necrosis factor, IL-6, and GM-CSF↑	ND	(49)

(Continued)

TABLE 3 (Continued)

Biological activities	Polysaccharide name	Types	Testing subjects	Doses/ duration	Effects	Mechanisms	References
Anti-fatigue	<i>P. frutescens</i> leaf polysaccharide	<i>In vivo</i>	5, 10, 20 mg/kg for 4 weeks	Exhaustive swimming induced exercise fatigue in mice	Liver glycogen, muscle glycogen, and exhaustion swimming time, blood glucose level↑	ND	(76)
Anti-inflammatory	<i>P. frutescens</i> leaf polysaccharide	<i>In vivo</i>	20 mg/kg for 4 weeks	Chronic obstructive pulmonary disease rat	Forced vital capacity, forced expiratory volume in one second, peak expiratory flow, and average alveolar number↑; IL-8, TNF-α, alveolar expansion, inflammatory cell infiltration, mean interalveolar lining, Wnt5a, RhoA, and p-JNK protein relative expression↓	Inhibition of the Wnt/PCP pathway	(77)
Lipid-lowering	PFSP	<i>In vivo</i>	50, 100, 200 mg/kg for 8 weeks	High-fat diet-induced mice	Liver index, AST, ALT, triglyceride, total cholesterol, low-density lipoprotein, blood glucose level, MDA, and <i>CPT-1</i> and <i>ATGL</i> mRNA expression↓; high-density lipoprotein, SOD, peroxidase, glutathione peroxidase enzyme, and FAS mRNA expression↑	ND	(78)

ND stands for not detected.

anti-inflammatory agent in a rat model of smoking combined with lipopolysaccharide-induced chronic obstructive pulmonary disease (COPD); treatment with 20 mg/kg *P. Frutescens* polysaccharide for 4 weeks *in vivo* resulted in improvement of lung function in COPD model rats. *P. Frutescens* polysaccharide treatment significantly decreased the expression levels of IL-8, TNF-α, Ras homologous protein A, Wnt5a, and p-JNK; reduced the thickness of bronchial wall and smooth muscle; and improved lung histopathologic changes. The inhibitory effect of *P. Frutescens* leaf polysaccharide on inflammation in COPD rats was mainly achieved by inhibiting the Wnt/PCP signaling pathway. In addition, Liu et al. (78) demonstrated the ameliorative effects of a *P. frutescens* seed polysaccharides (PFSP) on abnormal lipid metabolism and oxidative stress induced by a high-fat diet in mice. Supplementation of the PFSP (50, 100, and 200 mg/kg) in the feed for 8 weeks significantly decreased the levels of AST, ALT, triglyceride, total cholesterol, low-density lipoprotein, blood glucose, MDA, and the mRNA and protein expression levels of fatty acid synthesis-related genes. By contrast, PFSP

supplementation increased the levels of high-density lipoprotein, fatty acid catabolism-related genes (*CPT-1*, *ATGL*) mRNA and protein expression, and the activities of SOD, GSH-Px, and CAT. Collectively, PFSP ameliorated high-fat diet-induced oxidative stress and fatty liver in mice. Based on the above research, the detailed biological effects or mechanisms of *P. Frutescens* polysaccharides are summarized in Table 2.

5 Conclusion and future prospects

Perilla frutescens is a highly promising edible and medicinal homologous resource; as the main components of *P. frutescens*, the polysaccharides of this herb have received increasing research attention in recent years. In this review, the extraction, purification, structural characterization, and associated biological activities of *P. Frutescens* polysaccharides have been summarized. Despite the remarkable advances achieved in *P. Frutescens*

polysaccharide research, there are still several opportunities and challenges that remain to be resolved (Table 3).

First, studies have been carried out to extract *P. Frutescens* polysaccharides by HWE, MAE, UAE, enzyme-assisted extraction, and UAEE. There is still a great deal of scope for the development of other extraction methods. In particular, efforts should be focused on developing new environmentally friendly and high-yield extraction technologies. Second, the isolation and purification methods of *P. Frutescens* polysaccharides are currently limited to the laboratory level; thus, these methods should be further optimized to obtain reproducible and stable products that are suitable for industrial-scale production. Third, investigations on the structure of *P. Frutescens* polysaccharides have primarily focused on the monosaccharide composition and molecular weight. However, research is lacking on the more detailed structures of the sequence of monosaccharides, types, and positions of glycosidic bonds, and structural fragments. Various classical approaches, including FT-IR, NMR, X-ray diffraction, atomic force microscopy, and methylation analysis, can be applied to characterize the chemical structure of *P. Frutescens* polysaccharides. Fourth, to date, researchers have mostly focused on the antioxidant activity of *P. Frutescens* polysaccharides, with fewer studies on other bioactivities and their relationship with *P. Frutescens* polysaccharides structure. Therefore, it is imperative to establish more appropriate pharmacological models to investigate the additional biological activities of *P. Frutescens* polysaccharides and further study the structure-activity relationships of the polysaccharide, as well as the exact molecular mechanisms underlying the observed activities. Finally, research on *P. Frutescens* polysaccharides is still limited to theoretical studies in animal and *in vitro* experiments, with a notable lack of relevant clinical, toxicity, and pharmacokinetic studies. Developing and applying *P. Frutescens* polysaccharides as nutraceuticals or natural medicines is a huge challenge. Hence, a large number of clinical trials should be carried out to ensure the efficacy and safety of *P. Frutescens* polysaccharides toward creating novel products with *P. Frutescens* polysaccharides as the active ingredient.

In summary, *P. Frutescens* polysaccharides possess diverse biological functions, which offer extensive prospects in the fields of food and medicine; however, there is still a long way to go to achieve the transformation of *P. Frutescens* polysaccharides into practical functional foods, nutraceuticals, or natural medicines. We hope that more researchers will pay attention to PFP in the future and further investigate its precise structure, active mechanism, and clinical

utilization, to offer a scientific foundation for its further development and utilization as functional foods and therapeutic drugs.

Author contributions

LZ: Validation, Writing – original draft, Writing – review & editing. LG: Writing – review & editing. KW: Conceptualization, Writing – review & editing. CR: Data curation, Writing – review & editing. YG: Methodology, Writing – review & editing. JL: Investigation, Software, Writing – review & editing. SY: Project administration, Writing – review & editing. XZ: Formal analysis, Writing – review & editing. XY: Resources, Writing – review & editing. YZ: Methodology, Writing – review & editing. BL: Writing – review & editing. SL: Writing – review & editing.

Funding

The author(s) declare financial support was received for the research, authorship, and/or publication of this article. This work was supported by the National Key Research and Development Program of China (2021YFD2100902) and the Agricultural Science and Technology Innovation Project of Heilongjiang Academy of Agricultural Sciences (CX23GG16-04).

Conflict of interest

The authors declare that the research was conducted in the absence of any commercial or financial relationships that could be construed as a potential conflict of interest.

Publisher's note

All claims expressed in this article are solely those of the authors and do not necessarily represent those of their affiliated organizations, or those of the publisher, the editors and the reviewers. Any product that may be evaluated in this article, or claim that may be made by its manufacturer, is not guaranteed or endorsed by the publisher.

References

- Adam G, Robu S, Flutur MM, Cioanca O, Vasilache IA, Adam AM, et al. Applications of *Perilla frutescens* extracts in clinical practice. *Antioxidants*. (2023) 12:727. doi: 10.3390/antiox12030727
- Sa KJ, Jang SJ, Lee S, Park H, Cho J, Sung J, et al. Characterization of volatile compounds of *Perilla* crop (*Perilla frutescens* L.) in South Korea. *Appl Biol Chem*. (2023) 66:1–13. doi: 10.1186/s13765-023-00801-6
- Tavan M, Hanachi P, Mirjalili MH, Dashtbani-Roozbehani A. Comparative assessment of the biological activity of the green synthesized silver nanoparticles and aqueous leaf extract of *Perilla frutescens* (L.). *Sci Rep*. (2023) 13:6391. doi: 10.1038/s41598-023-33625-x
- Wang P, Jin B, Lian C, Guo K, Ma C. Comparative analysis of polycyclic aromatic hydrocarbons and halogenated polycyclic aromatic hydrocarbons in different parts of *Perilla frutescens* (L.). *Britt. Molecules*. (2022) 14:738–54. doi: 10.3390/molecules14020738
- Zhou XJ, Yan LL, Yin PP, Shi LL, Zhang JH, Liu YJ, et al. Structural characterisation and antioxidant activity evaluation of phenolic compounds from cold-pressed *Perilla frutescens* Var *Arguta* seed flour. *Food Chem*. (2014) 164:150–7. doi: 10.1016/j.foodchem.2014.05.062
- Wang R, Zhang Q, Feng C, Zhang J, Qin Y, Meng L, et al. Advances in the pharmacological activities and effects of *Perilla* ketone and *Isoegomaketone*. *Evid Based Complement Alternat Med*. (2022) 2022:1–10. doi: 10.1155/2022/8809792
- Chen J, Zhang D, Wang Q, Yang A, Zheng Y, Wang L. Comprehensive comparison of two color varieties of *Perillae folium* by Gc-MS-based Metabolomic approach. *Molecules*. (2022) 27:6792. doi: 10.3390/molecules27206792
- Ethnomedicinal AH. Phytochemical and pharmacological investigations of *Perilla frutescens* (L.) Britt. *Molecules*. (2018) 24:102. doi: 10.3390/molecules24010102
- Wu X, Dong S, Chen H, Guo M, Sun Z, Luo H. *Perilla frutescens*: a traditional medicine and food homologous plant. *Chin Herb Med*. (2023) 15:369–75. doi: 10.1016/j.chmed.2023.03.002
- Fujiwara Y, Kono M, Ito A, Ito M. Anthocyanins in *Perilla* plants and dried leaves. *Phytochemistry*. (2018) 147:158–66. doi: 10.1016/j.phytochem.2018.01.003

11. Ahmed HM, Al-Zubaidy MA, Othman-Qadir G. Biological investigations on macro-morphological characteristics, polyphenolic acids, antioxidant activity of *Perilla frutescens* (L) Britt. Grown under open field. *Saudi J Biol Sci.* (2022) 29:3213–22. doi: 10.1016/j.sjbs.2022.01.059
12. Hou T, Netala VR, Zhang H, Xing Y, Li H, Zhang Z. *Perilla frutescens*: a rich source of pharmacological active compounds. *Molecules.* (2022) 27:3578. doi: 10.3390/molecules27113578
13. Huang S, Nan Y, Chen G, Ning N, Du Y, Lu D, et al. The role and mechanism of *Perilla frutescens* in Cancer treatment. *Molecules.* (2023) 28:5883. doi: 10.3390/molecules28155883
14. Byun EB, Cho EJ, Kim YE, Kim WS, Byun EH. Neuroprotective effect of polysaccharide separated from *Perilla frutescens* Britton Var. *Acuta kudo* against H₂O₂-induced oxidative stress in HT22 Hippocampus cells. *Biosci Biotechnol Biochem.* (2018) 82:1344–58. doi: 10.1080/09168451.2018.1460572
15. Ding SY, Yan ZQ, Liu HP, Chen P, Shi SY, Chang ML. Structural characterization and antitumor activity of a polysaccharide extracted from *Perilla frutescens* Var. *frutescens*. *Ind Crop Prod.* (2022) 187:115334. doi: 10.1016/j.indcrop.2022.115334
16. Kim YJ, Hwang JS, Kwon KH. Extraction, purification and macrophage stimulatory activity of polysaccharide isolated from leaves of *Perilla frutescens* Britton Var. *Crispa*. *Prog Nutr.* (2019) 21:399–405. doi: 10.23751/pn.v21i1-S.5525
17. Liu Z, Yin H, Yang A, An Q, Li C, Jin T. Separation, purification and anti-tumor activity of polysaccharides from *Perilla frutescens* seeds. *Food Sci.* (2022) 43:158–65. doi: 10.7506/spkx1002-6630-20210708-087
18. Zhang H, Li H, Zhang Z, Hou T. Optimization of ultrasound-assisted extraction of polysaccharides from *Perilla* seed meal by response surface methodology: characterization and *in vitro* antioxidant activities. *J Food Sci.* (2021) 86:306–18. doi: 10.1111/1750-3841.15597
19. Tao YD, Tian HJ, Li Y, Luo XY. Protective effect of *Perilla frutescens* polysaccharides on alcoholic liver injury in mice. *Northwest J Pharm.* (2022) 37:51–6. doi: 10.3969/j.issn.1004-2407.2022.02.010
20. Zhang HJ. Isolation, purification, structural characterization and application of *Perilla* polysaccharides. *North Univ China.* (2022). doi: 10.27470/d.cnki.gbhgc.2022.000026
21. Li X, Chen C, Leng A, Qu J. Advances in the extraction, purification, structural characteristics and biological activities of *Eleutherococcus senticosus* polysaccharides: a promising medicinal and edible resource with development value. *Front Pharmacol.* (2021) 12:753007. doi: 10.3389/fphar.2021.753007
22. Zhou QC, Sheng GH. Pyrolytic and kinetic characteristics of the thermal decomposition of *Perilla frutescens* polysaccharide. *PLoS One.* (2012) 7:e52597. doi: 10.1371/journal.pone.0052597
23. Ding SY. Study on extraction, structure characterization and anti-tumor activity of polysaccharide from *Perilla frutescens* var. *frutescens*. *Tianjin Univ Sci Technol.* (2022). doi: 10.27359/d.cnki.gtqgu.2022.000729
24. Ke L, Duan X, Cui J, Song X, Ma W, Zhang W, et al. Research Progress on the extraction technology and activity study of *Epimedium* polysaccharides. *Carbohydr Polym.* (2023) 306:120602. doi: 10.1016/j.carbpol.2023.120602
25. Jing Y, Yan M, Liu D, Tao C, Hu B, Sun S, et al. Research Progress on the structural characterization, biological activity and product application of polysaccharides from *Crataegus pinnatifida*. *Int J Biol Macromol.* (2023) 244:125408. doi: 10.1016/j.ijbiomac.2023.125408
26. Yu X, Miao Z, Zhang L, Zhu L, Sheng H. Extraction, purification, structure characteristics, biological activities and pharmaceutical application of Bupleuri Radix polysaccharide: a review. *Int J Biol Macromol.* (2023) 237:124146. doi: 10.1016/j.ijbiomac.2023.124146
27. Ahmad MM, Chatha SAS, Iqbal Y, Hussain AL, Khan I, Xie F. Recent trends in extraction, purification, and antioxidant activity evaluation of plant leaf-extract polysaccharides. *Biofuels Bioprod Biorefin.* (2022) 16:1820–48. doi: 10.1002/bbb.2405
28. Yang Y, Lei Z, Zhao M, Wu C, Wang L, Xu Y. Microwave-assisted extraction of an acidic polysaccharide from *Ribes nigrum* L.: structural characteristics and biological activities. *Ind Crop Prod.* (2020) 147:112249. doi: 10.1016/j.indcrop.2020.112249
29. Li C, Song Y, Sun Q. Extraction of polysaccharide from *Perilla frutescens* seed with microwave and its Hepatoprotective activity. *Chin Agri Sci Bulltin.* (2014) 30:285–90. Available at: <https://webofscience.clarivate.cn/wos/alldb/full-record/CSCD:5104335>.
30. Zhang LH. Study on the extraction and antioxidant activity of *Perilla* leaf polysaccharide. Fujian Agriculture and Forestry University (2013). Available at: https://kns.cnki.net/kcms2/article/abstract?v=WVdZDAe5jxaZxl7s-UrUg1EFJDINVIOZad9BlVOQ_KdRsAsAgovyqBv7N0iYVTVMRnmI0sAlr-tKmZM2bPA4RbM21-yk-TmxSioaG9hRYYoWde0BGzqXbLzWZmQQOQp0Cy-Z8IBKsljiLw1CLJA==&uniplatform=NZKPT&language=CHS.
31. Luo L, Xue J, Shao Z, Zhou Z, Tang W, Liu J, et al. Recent developments in *Salvia miltiorrhiza* polysaccharides: isolation, purification, structural characteristics and biological activities. *Front Pharmacol.* (2023) 14:1139201. doi: 10.3389/fphar.2023.1139201
32. Kumar M, Hasan M, Sharma A, Suhag R, Maheshwari C, Radha, et al. *Tinospora cordifolia* (Willd.) Hook.F. & Thomson polysaccharides: a review on extraction, characterization, and bioactivities. *Int J Biol Macromol.* (2023) 229:463–75. doi: 10.1016/j.ijbiomac.2022.12.181
33. Lv CX, Li MM, Xu XM, Li JR, Zhu SM, Liu RR. Optimization of Cellulase extraction process of *Perilla frutescens* polysaccharides by response surface analysis. *Food Chem.* 34:6–10.
34. Li H, Zhang H, Zhang Z, Cui L. Optimization of ultrasound-assisted enzymatic extraction and *in vitro* antioxidant activities of polysaccharides extracted from the leaves of *Perilla frutescens*. *Food Sci Technol.* (2020) 40:36–45. doi: 10.1590/fst.29518
35. Zhang H, Li H, Netala VR, Hou T, Zhang Z. Optimization of complex enzyme-ultrasonic synergistic extraction of water-soluble polysaccharides from *Perilla frutescens* seed meal: purification, characterization and *in vitro* antioxidant activity. *J Food Process Preserv.* (2022) 46:e16201. doi: 10.1111/jfpp.16201
36. Gong H, Gan X, Li Y, Chen J, Xu Y, Shi S, et al. Review on the genus *Polygonatum* polysaccharides: extraction, purification, structural characteristics and bioactivities. *Int J Biol Macromol.* (2023) 229:909–30. doi: 10.1016/j.ijbiomac.2022.12.320
37. Keltoum AK, Lilia B, Selma N, Khaoula QD, Nora G, Dalila B. Anti-inflammatory and antioxidant activity of the hot water-soluble polysaccharides from *Anacyclus pyrethrum* (L.) lag. Roots. *J Ethnopharmacol.* (2021) 281:114491. doi: 10.1016/j.jep.2021.114491
38. Chen F, Huang S, Huang G. Preparation, activity, and antioxidant mechanism of Rice bran polysaccharide. *Food Funct.* (2021) 12:834–9. doi: 10.1039/d0fo02498h
39. Qin D, Han S, Liu M, Guo T, Hu Z, Zhou Y, et al. Polysaccharides from *Phellinus linteus*: a systematic review of their extractions, purifications, structures and functions. *Int J Biol Macromol.* (2023) 230:123163. doi: 10.1016/j.ijbiomac.2023.123163
40. Li B, Huang G. Preparation, structure-function relationship and application of *Grifola umbellata* polysaccharides. *Ind Crop Prod.* (2022) 186:115282. doi: 10.1016/j.indcrop.2022.115282
41. Li J, Huang G. Extraction, purification, separation, structure, derivatization and activities of polysaccharide from Chinese date. *Process Biochem.* (2021) 110:231–42. doi: 10.1016/j.procbio.2021.08.018
42. Tang W, Liu D, Yin J, Nie S. Consecutive and progressive purification of food-derived natural polysaccharide: based on material, extraction process and crude polysaccharide. *Trends Food Sci Technol.* (2020) 99:76–87. doi: 10.1016/j.tifs.2020.02.015
43. Ai X, Yu P, Li X, Lai X, Yang M, Liu F, et al. Polysaccharides from *Spirulina platensis*: extraction methods, structural features and bioactivities diversity. *Int J Biol Macromol.* (2023) 231:123211. doi: 10.1016/j.ijbiomac.2023.123211
44. Ji X, Peng Q, Yuan Y, Shen J, Xie X, Wang M. Isolation, structures and bioactivities of the polysaccharides from jujube fruit (*Ziziphus Jujuba* mill.): a review. *Food Chem.* (2017) 227:349–57. doi: 10.1016/j.foodchem.2017.01.074
45. Ren Y, Bai Y, Zhang Z, Cai W, Flores DRA. The preparation and structure analysis methods of natural polysaccharides of plants and Fungi: a review of recent development. *Molecules.* (2019) 24:3122. doi: 10.3390/molecules24173122
46. Ji X, Hou C, Shi M, Yan Y, Liu Y. An insight into the research concerning *Panax ginseng* C. A. Meyer polysaccharides: a review. *Food Rev Intl.* (2020) 38:1149–65. doi: 10.1080/87559129.2020.1771363
47. Liu H, Wei S, Shi L, Tan H. Preparation, structural characterization, and bioactivities of polysaccharides from *Psidium guajava*: a review. *Food Chem.* (2023) 411:135423. doi: 10.1016/j.foodchem.2023.135423
48. Borjigin G, Wei F, Jiang S, Li Q, Yang C. Extraction, purification, structural characterization and biological activity of polysaccharides from *Fritillaria*: a review. *Int J Biol Macromol.* (2023) 242:124817. doi: 10.1016/j.ijbiomac.2023.124817
49. Kwon KH, Kim KI, Jun WJ, Shin DH, Cho EJ, Hong BS. *In vitro* and *in vivo* effects of macrophage-stimulatory polysaccharide from leaves of *Perilla frutescens* Var. *crispa*. *Biol Pharm Bull.* (2002) 25:367–71. doi: 10.1081/SCC-120023425
50. Liang LX, Huang XC, Huang XT. An Experimenton using ultrasonic cleaning machine and Cellulase to extract polysaccharides from *Perilla* leaves and their antioxidant activity. *Farm Prod Process.* (2022) 14:27–32. doi: 10.16693/j.cnki.1671-9646(X).2022.07.036
51. Zhao YN, Guo JT, Zhou TT, Li MH, Li HZ. Modification of *Perilla frutescens* polysaccharides with selenic acid and analysis of their physicochemical structural characteristics. *Food Chem.* (2023) 44:1–9. doi: 10.7506/spkx1002-6630-20230206-048
52. Niu XR, Zhu TT, Gao ZJ, Han CY, Liu EW, Han LF, et al. Separation and purification of *Perilla frutescens* polysaccharides and their antioxidant activities *in vitro*. *Food Res Dev.* (2023) 44:30–5. doi: 10.12161/j.issn.1005-6521.2023.09.005
53. Li H, Liu M, Liu Z, Cheng L, Li M, Li C. Purification, structural characterization, and antitumor activity of a polysaccharide from *Perilla* seeds. *Int J Mol Sci.* (2023) 24:15904. doi: 10.3390/ijms242115904
54. Hu YC, Hu JL, Li J, Wang J, Zhang X, Wu X, et al. Physicochemical characteristics and biological activities of soluble dietary fibers isolated from the leaves of different quinoa cultivars. *Food Res Int.* (2023) 163:112166. doi: 10.1016/j.foodres.2022.112166
55. Luan F, Ji Y, Peng L, Liu Q, Cao H, Yang Y, et al. Extraction, purification, structural characteristics and biological properties of the polysaccharides from *Codonopsis pilosula*: a review. *Carbohydr Polym.* (2021) 261:117863. doi: 10.1016/j.carbpol.2021.117863
56. Xue T, Ruan K, Tang Z, Duan J, Xu H. Isolation, structural properties, and bioactivities of polysaccharides from *Althaea officinalis* Linn.: a review. *Int J Biol Macromol.* (2023) 242:125098. doi: 10.1016/j.ijbiomac.2023.125098

57. Zhou W, Zhou X, Wang Y, Ling Y, Li P, Zhang F. Research Progress on pretreatment and analysis methods for polysaccharides in traditional Chinese medicine. *J Instrum Anal.* (2020) 39:1168–75. doi: 10.3969/j.issn.1004-4957.2020.09.017
58. Li Y, Liang J, Gao JN, Shen Y, Kuang HX, Xia YG. A novel Lc-MS/MS method for complete composition analysis of polysaccharides by Aldononitrile acetate and multiple reaction monitoring. *Carbohydr Polym.* (2021) 272:118478. doi: 10.1016/j.carbpol.2021.118478
59. Wang M, Hu W, Wang Q, Yang B, Kuang HX. Extraction, purification, structural characteristics, biological activities, and application of the polysaccharides from *Nelumbo nucifera* Gaertn. (Lotus): a review. *Int J Biol Macromol.* (2023) 226:562–79. doi: 10.1016/j.ijbiomac.2022.12.072
60. Mo X, Guo D, Jiang Y, Chen P, Huang L. Isolation, structures and bioactivities of the polysaccharides from *Radix Hedysari*: a review. *Int J Biol Macromol.* (2022) 199:212–22. doi: 10.1016/j.ijbiomac.2021.12.095
61. Zeng J, Luan F, Hu J, Liu Y, Zhang X, Qin T, et al. Recent research advances in polysaccharides from *Undaria pinnatifida*: isolation, structures, bioactivities, and applications. *Int J Biol Macromol.* (2022) 206:325–54. doi: 10.1016/j.ijbiomac.2022.02.138
62. Ain NU, Wu S, Li X, Li D, Zhang Z. Isolation, characterization, pharmacology and biopolymer applications of licorice polysaccharides: review. *Materials.* (2022) 15:3654. doi: 10.3390/ma15103654
63. Kirschner KN, Woods RJ. Solvent interactions determine carbohydrate conformation. *Proc Natl Acad Sci USA.* (2001) 98:10541–5. doi: 10.1073/pnas.191362798
64. McCord JM. The evolution of free radicals and oxidative stress. *Am J Med.* (2000) 108:652–9. doi: 10.1016/S0002-9343(00) 00412-5
65. Reczek CR, Chandel NS. ROS-dependent signal transduction. *Curr Opin Cell Biol.* (2015) 33:8–13. doi: 10.1016/j.ceb.2014.09.010
66. Yu Y, Shen M, Song Q, Xie J. Biological activities and pharmaceutical applications of polysaccharide from natural resources: a review. *Carbohydr Polym.* (2018) 183:91–101. doi: 10.1016/j.carbpol.2017.12.009
67. Wang SB, Kong LX, Liu JJ. *In vitro* antioxidant activity of *Perilla frutescens* meal polysaccharides and their protective effect on oxidative damage of liver cells. *China Oils Fats.* (2023):1–10. doi: 10.19902/j.cnki.zgyz.1003-7969.230284
68. Zhu JF, Deng YX, Ran YL, Tang CH, Yu HB. Study on the antioxidant activity of *Perilla frutescens* meal polysaccharide Pwps. *J Chongqing Technol Business Univ.* (2012) 29:83–6. Available at: https://kns.cnki.net/kcms2/article/abstract?v=-0THPtffOh0_SnYDmMVQ8kiE_ofjsTLPVJ0q11Ga95LY0Q5H8s3kCArkCfAZLm8UZOujvFasoqEQuQrgFoIsk_Hz4ePbls3el25FlveZi5CeWlqLk0zA0SrCFvtQ_i2sMsD9IciG664=&uniplatform=NZKPT&language=CHS.
69. Li N, Wang C, Georgiev MI, Bajpai VK, Tundis R, Simal-Gandara J, et al. Advances in dietary polysaccharides as anticancer agents: structure-activity relationship. *Trends Food Sci Technol.* (2021) 111:360–77. doi: 10.1016/j.tifs.2021.03.008
70. Chen S, Guan X, Yong T, Gao X, Xiao C, Xie Y, et al. Structural characterization and Hepatoprotective activity of an acidic polysaccharide from *Ganoderma lucidum*. *Food Chem X.* (2022) 13:100204. doi: 10.1016/j.fochx.2022.100204
71. Zhang Y, Yao L, Liu Y, Chen B, Wang C, Gong K, et al. Acidic polysaccharide from corn silk: structural & conformational properties and hepatoprotective activity. *Int J Biol Macromol.* (2023) 236:123851. doi: 10.1016/j.ijbiomac.2023.123851
72. Qu J, Huang P, Zhang L, Qiu Y, Qi H, Leng A, et al. Hepatoprotective effect of plant polysaccharides from natural resources: a review of the mechanisms and structure-activity relationship. *Int J Biol Macromol.* (2020) 161:24–34. doi: 10.1016/j.ijbiomac.2020.05.196
73. Sun GP, Yuan L, Fang XL, Yang HB. Study on the role and mechanism of *Perilla frutescens* polysaccharide in ameliorating liver injury in type 2 diabetic rats. *J Chin Med Mater.* (2020) 43:037. doi: 10.13863/j.issn1001-4454.2020.11.037
74. Cai W, Wong K, Huang Q. Isolation, structural features, rheological properties and bioactivities of polysaccharides from *Lignosus rhinocerotis*: a review. *Int J Biol Macromol.* (2023) 242:124818. doi: 10.1016/j.ijbiomac.2023.124818
75. Wen Y, Peng D, Li C, Hu X, Bi S, Song L, et al. A new polysaccharide isolated from morchella importuna fruiting bodies and its immunoregulatory mechanism. *Int J Biol Macromol.* (2019) 137:8–19. doi: 10.1016/j.ijbiomac.2019.06.171
76. Liu SH. Protective effect of *Perilla frutescens* leaf polysaccharides on exercise induced fatigue in mice induced by exhaustive swimming. *Heilongjiang Sci Technol Inform.* (2015) 35:115–6. Available at: https://kns.cnki.net/kcms2/article/abstract?v=-0THPtffOh0M530Ke8zt7uKdmrdDcgcln3WKuV8TmojW6hGLDFTFKO-gYXc2x3WO9-qgX7IATfRXhVi4ky-doS0ZQMnzs8JhBAIVt9e4rdCIMW8VOglDS29LKBpdKOtS3NmBnym0CS_a_iTurFvJlNw==&uniplatform=NZKPT&language=CHS.
77. Wang WJ, Liu XM, Zhang GQ. Effect of *Perilla* leaf polysaccharide on airway inflammation and airway remodeling in COPD rats through Wnt/PCP pathway. *Chin Med Guide.* (2021) 27:37–41. doi: 10.13862/j.cnki.cn43-1446/r.2021.10.007
78. Liu M, Zhang L, Wang D, Wang CW. Effects of *Perilla frutescens* seeds polysaccharide on lipid metabolism and antioxidants in mice fed high-fat diet. *Food Res Dev.* (2022) 43:70–7. doi: 10.12161/j.issn.1005-6521.2022.18.010
79. Liu ZK, Yin H, Yang AH, An QY, Li CW, Jin T. Isolation and purification of polysaccharides from *Perilla frutescens* seeds and their antitumor activity. *Food Sci.* (2022) 43:158–65.



OPEN ACCESS

EDITED BY

Saša Đurović,
Institute of General and Physical Chemistry,
Serbia

REVIEWED BY

Ana Tomić,
University of Novi Sad, Serbia
Olja Šovljanski,
University of Novi Sad, Serbia

*CORRESPONDENCE

Abdullah Al Mamun,
✉ pharmaalmamun@yahoo.com

RECEIVED 22 December 2023

ACCEPTED 31 January 2024

PUBLISHED 29 February 2024

CITATION

Shompa SA, Hasnat H, Riti SJ, Islam MM, Nur F, Alam S, Shao C, Wang S, Geng P and Mamun AA (2024), Phyto-pharmacological evaluation and characterization of the methanolic extract of the *Baccaurea motleyana* Müll. Arg. seed: promising insights into its therapeutic uses. *Front. Pharmacol.* 15:1359815. doi: 10.3389/fphar.2024.1359815

COPYRIGHT

© 2024 Shompa, Hasnat, Riti, Islam, Nur, Alam, Shao, Wang, Geng and Mamun. This is an open-access article distributed under the terms of the [Creative Commons Attribution License \(CC BY\)](https://creativecommons.org/licenses/by/4.0/). The use, distribution or reproduction in other forums is permitted, provided the original author(s) and the copyright owner(s) are credited and that the original publication in this journal is cited, in accordance with accepted academic practice. No use, distribution or reproduction is permitted which does not comply with these terms.

Phyto-pharmacological evaluation and characterization of the methanolic extract of the *Baccaurea motleyana* Müll. Arg. seed: promising insights into its therapeutic uses

Suriya Akter Shompa ¹, Hasin Hasnat ¹, Saima Jahan Riti¹, Md. Mirazul Islam¹, Farjahan Nur¹, Safaet Alam ², Chuxiao Shao³, Shuanghu Wang ³, Peiwu Geng ³ and Abdullah Al Mamun ^{3*}

¹Department of Pharmacy, School of Pharmaceutical Sciences, State University of Bangladesh, Dhaka, Bangladesh, ²Drugs and Toxins Research Division, BCSIR Laboratories Rajshahi, Bangladesh Council of Scientific and Industrial Research, Rajshahi, Bangladesh, ³Central Laboratory of The Sixth Affiliated Hospital of Wenzhou Medical University, Lishui People's Hospital, Lishui, Zhejiang, China

Introduction: Plants and their extracts have been integral to the development of medicinal treatments throughout history, offering a vast array of compounds for innovative therapies. *Baccaurea motleyana* Müll. Arg., commonly known as Rambai, is an evergreen tree with economic importance in the Old-World Tropics.

Method: The study investigates its phytochemical composition through Gas Chromatography-Mass Spectrometry (GC-MS) and evaluates its pharmacological properties, including antidiabetic, antidiarrheal, antimicrobial, and antidepressant effects.

Result and Discussion: The GC-MS analysis revealed 15 bioactive compounds in the methanol extract, with Phenol, 3,5-bis(1,1-dimethylethyl)-, Methyl stearate, and Hexadecanoic acid, methyl ester being the predominant ones. The cytotoxicity assay demonstrated significant activity in the ethyl acetate fraction. Antimicrobial assays indicated mild to moderate antibacterial activity. *In vivo* studies on mice revealed significant hypoglycemic, antidiarrheal, and antidepressant properties. Molecular docking studies against EGFR, DHFR, GLUT-3, KOR, and MOA identified promising compounds with potential therapeutic effects. The identified compounds exhibited favorable ADME/T properties, emphasizing their potential for drug development. The study underscores the promising therapeutic potential of *Baccaurea motleyana*, showcasing its diverse bioactive compounds with significant medicinal properties.

Conclusion: These findings lay the groundwork for future research, emphasizing the exploration of *B. motleyana* as a source of natural remedies for addressing prevalent health conditions.

KEYWORDS

Baccaurea motleyana, GC–MS, phytochemical, cytotoxic, antimicrobial, hypoglycemic, antidiarrheal, antidepressant

Introduction

Plants, having played a pivotal role in the historical development of remarkable medicines, stand poised to contribute significantly to a diverse array of innovative treatments (Alam et al., 2021a; Zaman et al., 2023). According to the World Health Organization (WHO), 80% of the global population relies on traditional healthcare for primary health services (Islam et al., 2022). The exploration of naturally occurring compounds for novel medication development has been a comprehensive endeavor (Alam et al., 2021a). For over 5,000 years, plants have been harnessed for their therapeutic properties, serving as sources for antibiotics, antineoplastic agents, analgesics, cardioprotective compounds, and various other medicinal applications (Taher et al., 2023). Interestingly, plant-derived medicines are predicted to comprise 25% of drugs in developed countries and 80% in rapidly advancing nations like India and China. Despite 400,000 global secondary plant metabolites, only 10,000 have been identified, emphasizing the untapped potential of phytochemicals as vital sources for novel medications (Hasnat et al., 2023).

Baccaurea motleyana Müll. Arg., commonly known as rambai, belongs to a lesser-known group of plants with economic importance in the Old World tropics, specifically in regions spanning from India to the Pacific. This evergreen tree, widely distributed in Southeast Asia, including Malaysia, Indonesia, and Thailand, is renowned for its brownish-yellow, globose fruits with an edible aril (Nurmayani et al., 2021; Debnath et al., 2022). The fruit is known as rambi in the Philippines, mafaifarang (general), ramai, or lam-khae (pattani), and raa-maa tee-ku (narathiwat) in Thailand. In Assam, India, it is referred to as leteku, while in Bangladesh, it goes by the names latkan or “bubi” (Debnath et al., 2022). Rambai is rich in vitamins, minerals, and bioactive compounds like phenolic acids and flavonoids, and they are utilized in various forms, such as raw consumption, cooking, stewing, and processing into jams and wines (Lim and Lim, 2012). Cultivated in various Southeast Asian nations, rambai has an oval-shaped fruit that undergoes a color transformation upon ripening, offering versatility in culinary applications (Lim and Lim, 2012; Nurmayani et al., 2021). Additionally, rambai’s bark has a historical application as an eye medicine and a postpartum medication for mothers (Prodhan and Mridu, 2021).

Since ancient times, the plant component of *B. motleyana* has been utilized in traditional medicine to address various health conditions. This plant serves as a medicinal plant, with applications in treating eye and skin inflammation. Additionally, rambai’s ecological significance extends to being a food source for various animals, including birds, rodents, deer, monkeys, and orangutans (Ramayani, 2020). Evidence showed that *B. motleyana* exhibits diverse medicinal uses across various cultures. The inner bark is traditionally employed for treating eye inflammation, exhibiting

antibacterial activity against *Staphylococcus aureus*, *Bacillus cereus*, *Bacillus subtilis*, *Proteus vulgaris*, and *Escherichia coli* (Mohamed et al., 1994; Lim and Lim, 2012). The bark is also utilized in postpartum care, included in concoctions for mothers after childbirth, and applied in skincare products for its soothing effects (Mohamed et al., 1994; Lim and Lim, 2012). Furthermore, it plays a role in women’s healthcare, addressing issues such as leucorrhea and menstrual decay (Sisillia, 2009). Other traditional uses include its application as a remedy for diarrhea, strep throat, malaria, and sleep disorders and as an antibacterial agent (Prodhan and Mridu, 2021).

Plant secondary metabolites, including alkaloids, flavonoids, and steroids, play a vital role in plant defense and are utilized in the pharmaceutical industry for therapeutic purposes (Jain et al., 2019). The isolation of morphine in 1806 marked a transformative era, highlighting the medicinal importance of these compounds with a history spanning over 4,000 years (Elshafie and Camele, 2023). Constituting over 30% of medicinal products, alkaloids, and flavonoids among them, they exhibit diverse structural and therapeutic properties, making them valuable candidates for drug development (Twaij and Hasan, 2022). Gas chromatography–mass spectrometry (GC–MS) emerges as a pivotal technique for the effective separation and characterization of plant metabolites, contributing significantly to medicinal plant analysis and herbal drug validation (Iordache et al., 2009; Al-rubaye et al., 2017).

Chronic diseases such as diabetes mellitus (DM) continue to be a burden on millions of people worldwide in the face of global health challenges (Singab et al., 2014). Due to the drawbacks and adverse effects of current antidiabetic drugs, researchers are looking into alternative approaches. Medicinal plants have emerged as one such option for supplemental treatment that may have fewer side effects (Tafesse et al., 2017). However, in the case of gastrointestinal disorders, diarrhea poses a significant health concern, particularly in developing countries, leading to elevated rates of sickness and mortality (Bahekar and Kale, 2015). Traditional herbal medicine, endorsed by the World Health Organization (WHO), offers a viable approach to managing diarrheal disorders, presenting a bridge between traditional and modern healthcare (Atta and Mouneir, 2004). The unveiling of cancer’s molecular foundations over the last two decades has revolutionized treatment approaches, with recognition of the remarkable similarity in the fundamental processes across diverse tumor types (Weinberg, 1996). However, neurotoxicity associated with chemotherapy remains a critical limitation, necessitating a deeper understanding to guide appropriate therapeutic strategies (Schiff et al., 2009). Shifting to mental health, depression stands out as a predominant global disorder, affecting a substantial portion of the population (Santosh et al., 2011). The continuous difficulties in treating this serious medical issue are reflected in the search for safe and efficient antidepressant medications (Yu et al., 2002).

Despite the availability of synthetic drugs, the call for new therapeutics with fewer side effects resonates (Nisar et al., 2018). Clinical trials, grounded in the alignment between animal and clinical studies, play a pivotal role in advancing these discoveries (Alam et al., 2021b). In this all-encompassing approach, the investigation of plant-derived compounds stands as a continuum, advertising a potential worldview move in tending to changed wellbeing challenges over diabetes, gastrointestinal clutters, cancer, and mental wellbeing.

Exploring the therapeutic possibilities of *Baccaurea motleyana* Müll. Arg., an understudied plant with a rich history of traditional applications, this study aims to thoroughly examine the medicinal attributes of its seeds. The focus is on unraveling the historical uses and traditional applications of the plant to unlock its full medicinal potential. The study also intends to aid in the creation of new drugs by examining its medicinal qualities, locating bioactive components, and carrying out preclinical research. The investigation emphasizes the unrealized potential of compounds derived from plants and is in line with the world's dependence on conventional healthcare. Preclinical studies with mice and *in silico* analyses will be conducted to validate and explore the pharmacological properties, laying the groundwork for the development of novel medications from this plant. Ultimately, this research has the noble goal of advancing natural sources for innovative treatments, addressing health challenges with potentially fewer side effects, and broadening pharmaceutical options.

Materials and methods

Collection of the plant

In July 2022, seeds of *Baccaurea motleyana* were gathered from Narsingdi District, Dhaka Division, Bangladesh (Figure 1). The plant's identification was validated by experts at the Bangladesh National Herbarium in Mirpur, Dhaka. A voucher specimen of the plant, assigned the accession number 84584, has been archived in the herbarium for future reference.

Extraction of plant materials

Baccaurea motleyana seeds were obtained from the wild, subjected to shade drying, and subsequently pulverized using a mechanical grinder. The required quantity of leaf powder was accurately weighed, placed in a flask, completely immersed in methanol, incubated for the duration of 15 days, and then subjected to filtration. Subsequently, the filtered extract underwent concentration using a rotary evaporator (Islam et al., 2020).

Partition into different fractionated extractives

The modified Kupchan partitioning method (VanWagenen et al., 1993) was employed for solvent-solvent partitioning. The crude methanolic extract (CME) of *B. motleyana* seeds (BMS) underwent fractionation with petroleum ether (PET), dichloromethane (DCM), ethyl acetate (EA), and distilled water,

respectively, with an increasing relative polarity index. Subsequent to this process, rotary evaporation was utilized to obtain the petroleum ether-soluble fraction (PSF, 2.38 g), dichloromethane-soluble fraction (DSF, 2.75 g), ethyl acetate-soluble fraction (ESF, 2.18 g), and aqueous-soluble fraction (ASF, 1.6 g).

Phytochemical analysis

GC–MS analysis

The seeds of *Baccaurea motleyana* were used to obtain a crude methanolic extract, and electron impact ionization (EI) was employed to extract beneficial compounds. The analysis was carried out utilizing a SHIMADZU GC–MS QP-2020 instrument equipped with an auto-sampler (AOC-20s) and auto-injector (AOC-20i). The analysis utilized a SH Rxi 5MS Sill column (30 m × 0.25 mm; 0.25 µm), and helium was employed as the carrier gas with a flow pressure of 1.72 mL/min. The temperature of the oven followed a programmed sequence, starting at 80°C (held for 2.00 min and raised at 5°C/min), reaching 150°C (held for 5.00 min), and concluding at a final temperature of 280°C (held for 5.00 min). The injector operated at 220°C, the ion source at 280°C, and a 5.0 µL injection volume was used with a 50:1 split ratio in the splitless injection mode. Ionization mass spectrometric analysis was performed at 70 eV, covering the mass range from 45 m/z to 350 m/z over a 50.0-min period. The solvent cut time was 5.0 min, and the total run time was 55.0 min. Identification of the bioactive compounds relied on the retention time, MS fragment ions, and the percentage of these compounds calculated from the total peak area. Phytochemicals were identified by comparing their mass spectra with entries in NIST08s, NIST08, and NIST14 libraries. This approach facilitated the determination of the chemical names, structures, and molecular masses of the bioactive components (Kim et al., 2016; Obaidullah et al., 2021).

Biological activity study

Evaluation of *in vitro* cytotoxicity

The cytotoxic activity of the seeds of *B. motleyana* was evaluated by the brine shrimp lethality method (Meyer et al., 1982). In brief, 4 mg of the test sample was dissolved in dimethyl sulfoxide (DMSO), and serial dilution was performed to obtain variable concentrations (400.0–0.781 µg/mL) of the solutions. Ten living nauplii (*Artemia salina*) present in simulated seawater were taken in each test tube having tested solutions. After incubation at 24°C at room temperature in the presence of light, the number of surviving nauplii was calculated. For this experiment, vincristine sulfate was used as a positive control, and the solvent dimethyl sulfoxide (DMSO) served as a negative control. The percent (%) mortality was calculated for each dilution by using the following formula:

$$\% \text{ of mortality} = \frac{\text{Number of the nauplii death}}{\text{Number of nauplii taken}} \times 100 \%$$

The cytotoxic activity of the plant extract was assessed as the median lethal concentration value (LC₅₀ value), which was calculated from a plot of the % of non-living nauplii against the



FIGURE 1
Plant and plant parts of *B. motleyana*.

log concentration of plant extracts using the standard curve of the reference drug lapatinib.

Antimicrobial screening

The crude plant samples were tested for antimicrobial susceptibility by following the disc diffusion method (Bauer et al., 1996). Based on Rashid et al. (2023), the most prevalent pathogenic microorganisms have been selected for this screening. They include five Gram-positive bacteria (*Bacillus cereus*, *Bacillus megaterium*, *Bacillus subtilis*, *Staphylococcus aureus*, and *Sarcina lutea*), eight Gram-negative bacteria (*Salmonella paratyphi*, *Salmonella typhi*, *Vibrio parahaemolyticus*, *Escherichia coli*, *Vibrio mimicus*, *Shigella dysenteriae*, *Pseudomonas aeruginosa*, and *Shigella boydii*), and three fungi (*Saccharomyces cerevisiae*, *Candida albicans*, and *Aspergillus niger*). Ciprofloxacin (5 µg/disc) and fluconazole (5 µg/disc) were used as reference drugs for antibacterial and antifungal activities, respectively. Shortly, nutrient agar plates were inoculated with a standardized inoculum of the test microorganisms. PDA media was used to influence the growth of fungi. Discs of approximately 6 mm diameter made of filter paper were loaded with test samples named BMS CME, BMS ASF, BMS PSF, BMS DSF, and BMS ESF and were evenly distributed on the surface of the nutrient media. The blank disc containing the solvent was used as the negative control. Approximately 24 h after the incubation at 37 °C (for bacteria) and 25 °C (for fungi) in the upright position, the zone of inhibition was recorded in millimeters, which shows the effectiveness of the plant samples against the microorganisms. The test was repeated three times, and the average diameter was taken.

Experimental animal

For the *in vivo* biological study, Swiss albino mice aged 4–5 weeks were collected from the Animal Resource Branch of the International Center for Diarrheal Diseases and Research, Bangladesh (ICDDR'B). They were fed ICDDR'B formulated rodent food and water (*ad libitum*) and kept in standard polypropylene cages under a regular laboratory environment with a 12-h light–dark cycle. Food was withdrawn before 12 h of the experiment. The experimental procedure conducted on the animals was approved by the Institutional Animal Ethics Committee (Zimmermann, 1983).

Experimental design for *in vivo* studies

Five mice groups were assigned for *in vivo* biological studies, with four mice in each group. Group I served as the negative control, receiving 1% Tween 80 in normal saline (10 mL/kg body weight). Group II served as the positive control and was administered with standard drugs for the respective experiments. Groups III, IV, and V received a crude methyl extract of *Baccaurea motleyana* at doses of 200 mg/kg, 400 mg/kg, and 600 mg/kg body weight of mice, respectively.

Hypoglycemic effect

The plant samples were subjected to tests to evaluate the hypoglycemic effect of the methanolic extract of the seeds of *Baccaurea motleyana* by the oral glucose tolerance test in mice (Islam et al., 2019). During the experiment, test samples at 200 mg/kg, 400 mg/kg, and 600 mg/kg doses were administered orally at 0 minute to all tested groups of mice. Glibenclamide

(10 mg/kg of body weight) was used as the reference drug. After 30 min, all the mice were treated with a 10% glucose solution. The blood glucose level was recorded at 0 min and then at 30, 60, and 120 min using a glucometer. The percent reduction in the blood glucose level of *B. motleyana* was calculated by the equation below:

$$\% \text{ reduction in blood glucose} = \frac{BG_{\text{control}} - BG_{\text{test}}}{BG_{\text{control}}} \times 100\%,$$

where the average blood glucose level is expressed by BG_{test} for the test group and BG_{control} for the control group.

Antidiarrheal effect

The crude methanolic extract of *B. motleyana* seeds was subjected to tests to assess the antidiarrheal activity. The study was conducted by the method of castor oil-induced diarrhea in mice (Sisay et al., 2017). In brief, crude plant samples were administered at the respective doses (200, 400, and 600 mg per kg of body weight), and after 30 min, 0.5 mL of castor oil was injected to induce diarrhea in each mouse. Loperamide (50 mg/kg body weight) was used as the standard drug, and 1% Tween 80 in normal saline was used as the negative control. The antidiarrheal effect of the crude methanolic extract was observed for 4 h by a reduction in the frequency of defecation by the test samples. To evaluate the antidiarrheal activity, the following formula was used:

$$\% \text{ reduction in diarrhea} = \frac{D_{\text{control}} - D_{\text{test}}}{D_{\text{control}}} \times 100\%.$$

The average number of diarrheal defecation was expressed by D_{test} for the test group and D_{control} for the control group in the same duration.

CNS antidepressant activity

A diazepam-induced sleeping time test was carried out in Swiss albino mice to assess the CNS antidepressant activity of *B. motleyana* with a slight modification of the reference study (Akter et al., 2022). Fluoxetine (30 mg/kg body weight) was used as the reference drug. At first, plant samples at doses of 200, 400, and 600 mg per kg of body weight and standard were administered orally to each group of mice. After 30 min, each mouse was injected with diazepam (25 mg/kg body weight) through the intraperitoneal route to induce sleep. To evaluate the CNS antidepressant activity, the onset of sleeping time and the duration of sleeping time of each mouse were recorded.

Molecular docking

Software

Utilizing a computer-based methodology, we evaluated the binding affinities of the compounds derived from the methanolic seed extract of *B. motleyana* against diverse target proteins. The analysis was conducted employing a range of software applications, including PyRx, PyMOL 2.3, Discovery Studio 4.5, and Swiss-PDB viewer, to comprehensively assess the molecular interactions.

Ligand preparation

The compounds listed in the table had their 3D SDF structures searched for and downloaded from PubChem (<https://pubchem.ncbi.nlm.nih.gov/>, accessed on 30 November 2023). Simultaneously, the 3D SDF structures of the five standard compounds lapatinib

(PubChem CID_208,908), ciprofloxacin (PubChem CID_2764), glibenclamide (PubChem CID_3488), loperamide (PubChem CID_3955), and diazepam (PubChem CID_3016) were obtained from PubChem. A ligand library was then systematically generated by importing both the compounds and the standards into Discovery Studio 4.5. Subsequently, all the compounds were optimized using the PM6 semiempirical method, enhancing the precision of the docking process (Mahmud et al., 2021).

Target selection

We conducted computerized docking analysis on 15 compounds isolated from the methanolic extract of seeds of *B. motleyana* to investigate their potential cytotoxic, antimicrobial, hypoglycemic, antidiarrheal, and antidepressant properties. For cytotoxicity assessment, the 3D crystal structure of the epidermal growth factor receptor (EGFR) [PDB ID: 1XKK] (El Azab et al., 2021) was obtained from the Protein Data Bank (<https://www.rcsb.org/> accessed on 30 November 2023). Similarly, the 3D structures of dihydrofolate reductase (DHFR) [PDB ID: 4M6J] (Khatun et al., 2021), glucose transporter 3 (GLUT3) [PDB ID: 4ZWB] (Mojica et al., 2017), kappa-opioid receptor (KOR) [PDB ID: 6VI4] (Alam et al., 2021b), and human monoamine oxidase A (MOA) [PDB: 2Z5X] (Rahman et al., 2020) were downloaded from the same source to evaluate their antimicrobial, hypoglycemic, antidiarrheal, and antidepressant activities, respectively.

Ligand–protein binding

The evaluation of affinities and potential binding patterns between the phytocompounds and target molecules was conducted through a computer-aided ligand–protein interaction diagram. The docking process utilized semi-flexible modeling, employing the advanced software application PyRx AutoDock Vina. Specific amino acids with their corresponding IDs were meticulously selected from the literature for individual receptors to ensure precise target docking. The protein underwent preparation by loading and formatting as the required macromolecule, ensuring exclusive binding of ligands to the intended targets.

To optimize docking against the selected macromolecules, SD files of ligands were imported and converted into pdbqt format using the Open Babel tool in PyRx AutoDock Vina software. Grid mapping defined active amino sites within grid boxes, maintaining a specified center and dimension axes, as detailed in Table 1. Default supportive functions were retained during this stage. Subsequently, a conclusive docking analysis was performed using AutoDock Vina (version 1.1.2) to ascertain the ligands' affinity for the respective macromolecule. The final step involved result interpretation and the utilization of BIOVIA Discovery Studio version 4.5 to predict the most suitable 2D and 3D models.

ADME/T study

In the field of computer-based drug design, there is a growing focus on conducting comprehensive pharmacokinetic studies that encompass absorption, distribution, metabolism, excretion, and toxicology. Evaluating drug-likeness through bioavailability studies has become integral to drug discovery efforts. ADMET analyses, crucial for deciphering pharmacological structures, can be accessed through resources like <http://biosig.unimelb.edu.au/pkcsmprediction>. Widely utilized online platforms such as

TABLE 1 Selection of the target site and grid mapping of target receptors.

Receptor	Standard	Target binding sites	Reference	Grid box	
EGFR	Lapatinib	Leu 718, Val 726, Ala 743, Lys 745, Met 766, Lys 775, Arg 776, Leu 777, Leu 788, Thr 790, Gln 791, Leu 792, Met 793, Gly 796, Cys 797, Leu 799, Asp 800, Arg 803, Leu 844, Thr 854, Asp 855, and Phe 856	El Azab et al. (2021)	Center	x = 15.825187532
					y = 34.5721399187
					z = 35.800825226
				Dimension	x = 24.7838429695
					y = 19.8421893519
					z = 32.2648120992
DHFR	Ciprofloxacin	Ala 9, Ile 16, Lys 54, Lys 55, Thr 56, Leu 75, Ser 76, Arg 77, Glu 78, Arg 91, Ser 92, Leu 93, Gly 117, Ser 118, Ser 119, and Val 120	Khatun et al. (2021)	Center	x = 3.20608769545
					y = -3.56914211401
					z = -18.542188786
				Dimension	x = 20.3141281273
					y = 27.7715179138
					z = 27.0093471133
GLUT-3	Glibenclamide	Tyr 26, Thr 28, Gly 29, Val 30, Leu 167, Thr 191, Pro 194, Gln 198, Ile 309, Gly 312, Val 313, Thr 347, Trp 410, Leu 418, and Phe 42	Mojica et al. (2017)	Center	x = 111.281206841
					y = 14.4902327905
					z = 64.1163891831
				Dimension	x = 31.7208242373
					y = 35.5013767913
					z = 26.1685012591
KOR	Loperamide	Leu 103, Leu 107, Ser 136, Ile 137, Try 140, Ile 180, Trp 183, Leu 184, Ser 187, Ile 191, Leu 192 Ile 194, and Val 195	Alam M M et al. (2021)	Center	x = 54.1738452613
					y = -50.3649144833
					z = -16.3287029589
				Dimension	x = 15.1353410377
					y = 27.9195765234
					z = 17.9248494605
MOA	Diazepam	Ala 111, Phe 112, Pro 113, Tyr 121, Tyr 124, Asn 125, Trp 128, Arg 129, Thr 203, Thr 205, His 488, and Glu 492	Jendele et al. (2019)	Center	x = 50.7734380822
					y = 18.3788968615
					z = -22.1018219056
				Dimension	x = 17.607308401
					y = 19.3090003103
					z = 19.889121004

SwissADME (<http://www.sib.swiss>) predict drug-likeness based on the Lipinski rules and pharmacokinetic parameters. According to Lipinski, compounds meeting specific criteria, including a molecular weight below 500 amu, fewer than five hydrogen bond donor sites, fewer than 10 hydrogen bond acceptor sites, and a lipophilicity value (LogP) of ≤ 5 , are considered orally accessible (Hasnat et al., 2023). The detailed results of ADMET and drug-likeness for these compounds are outlined in the provided table.

Statistical analysis

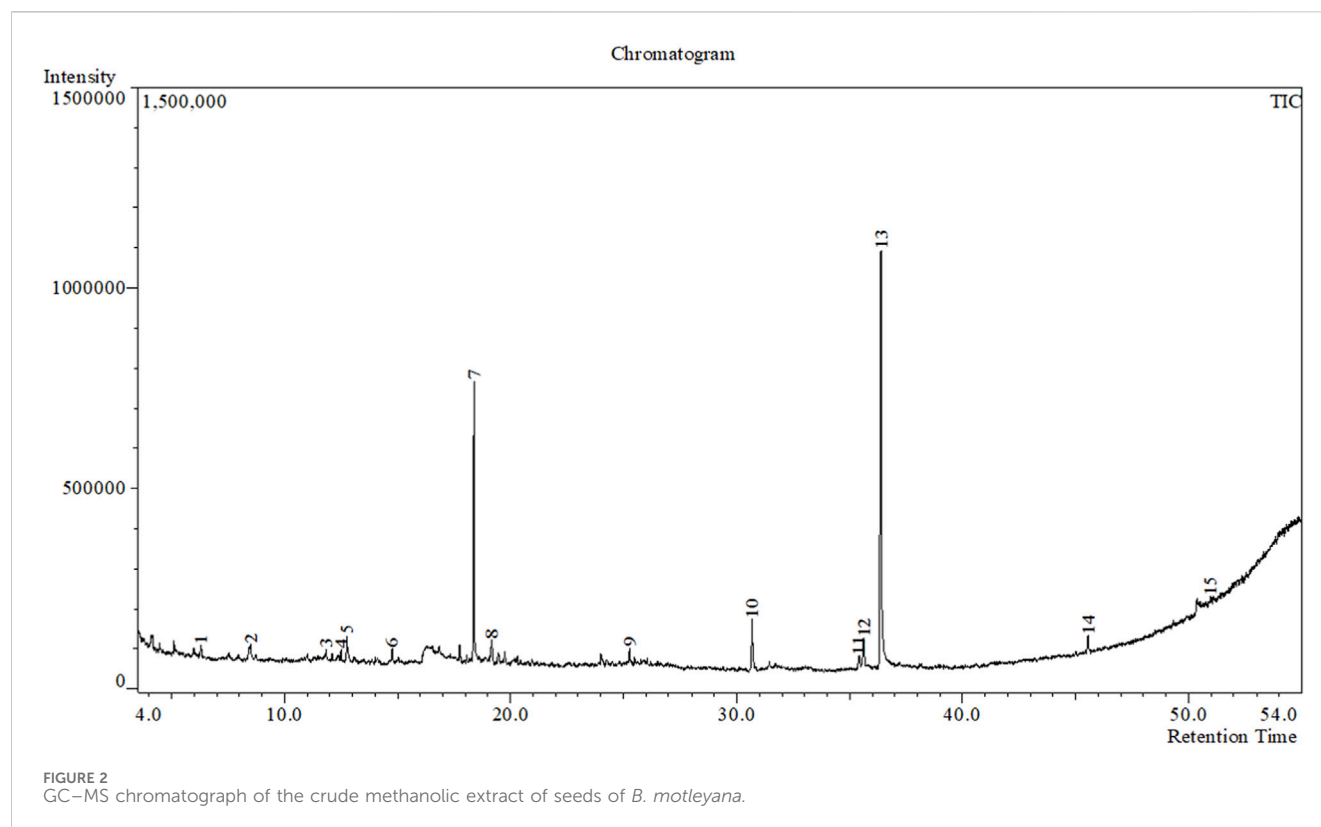
Statistical analysis was conducted utilizing GraphPad Prism 5.2 (GraphPad Software, Inc., La Jolla, CA, United States). The

outcomes were presented as mean \pm standard error (SEM). To assess statistical significance, one-way analysis of variance (ANOVA) and Dunnett’s test were employed. Significance levels were denoted as * $p < 0.5$, ** $p < 0.01$, and *** $p < 0.001$.

Result

GC–MS

In the GC–MS investigation, the examination of the crude methanolic extract from the seeds of *B. motleyana* uncovered 15



peaks, each signaling the presence of a bioactive molecule (Figure 2). The identification of these molecules involved a comparison of their molecular mass, chemical formula, and retention time with compounds acknowledged in the NIST library. This comprehensive analysis seeks to elucidate the diverse bioactive components found in the crude methanol seed extract of *B. motleyana*, offering valuable insights to augment the existing body of knowledge.

The distribution of compounds in the sample was quantified by representing their relative concentrations as peak area percentages. Predominant compounds, characterized by their high abundance, included phenol, 3,5-bis(1,1-dimethylethyl)- (45.257%), methyl stearate (21.251%), hexadecanoic acid, methyl ester (10.193%), dodecane, 2,6,11-trimethyl- (2.833%), cyclobarbitol (2.711%), 9-octadecenoic acid (Z), methyl ester (2.697%), diisooctyl phthalate (2.491%), and benzaldehyde dimethyl acetal (2.486%). The remaining compounds were present in concentrations below 2%. Additional details, such as retention time, mass/charge ratio, and peak area, are provided in Table 2.

Cytotoxic effect

The ethyl acetate (EA) fraction exhibited the most significant activity, displaying an LC_{50} value of 6.01 $\mu\text{g/mL}$, followed by the petroleum ether (PET) and dichloromethane (DCM) fractions with LC_{50} values of 9.92 and 8.40 $\mu\text{g/mL}$, respectively. In contrast, the crude methanolic extract (CME) and aqueous soluble fraction (ASF) demonstrated relatively weaker activity, with LC_{50} values of 27.00 and 35.51 $\mu\text{g/mL}$, respectively (Figure 3).

Antimicrobial effect

In this study, the antimicrobial assay was performed to evaluate the capacity of crude extracts to fight against the pathogenic microbes. The crude methanolic extract (BMS CSF), dichloromethane-soluble fraction (BMS DSF), and ethyl acetate-soluble fraction (BMS ESF) of seeds of *B. motleyana* showed mild-to-moderate antibacterial activity against both Gram-positive and Gram-negative bacteria compared with standard ciprofloxacin (Figure 4, Table 3).

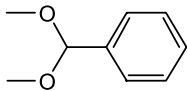

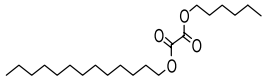
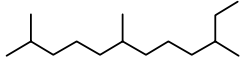
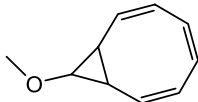
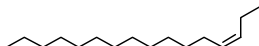
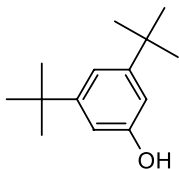
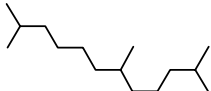
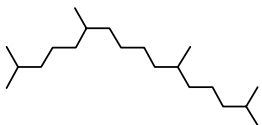
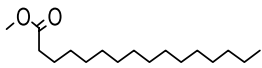
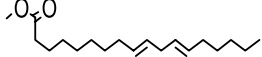
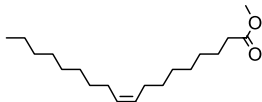
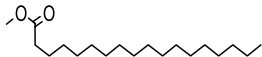
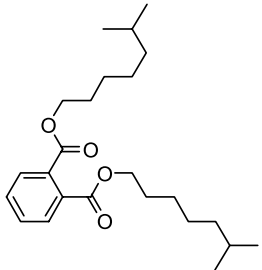
Hypoglycemic effect

The hypoglycemic activity of seeds of *B. motleyana* in mice is summarized in Table 4. The most substantial reduction in glucose levels was noted with the administration of BMS CME at a dose of 600 mg/kg, showing a value of $23.58\% \pm 0.18\%$, in comparison to the standard, which exhibited a reduction of $49.53\% \pm 0.58\%$. Both demonstrated highly significant results with a p -value less than 0.01. Particularly noteworthy was the extremely significant glucose level reduction of $36.42\% \pm 0.24\%$ observed 1 hour after the administration of BMS CME at a dose of 600 mg/kg.

Antidiarrheal effect

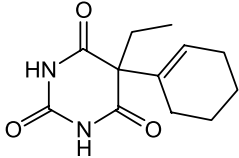
The methanolic extract of seeds of *B. motleyana* was subjected to a castor oil-induced antidiarrheal test, and the data are shown in Table 5. Castor oil administered orally influenced the episode of

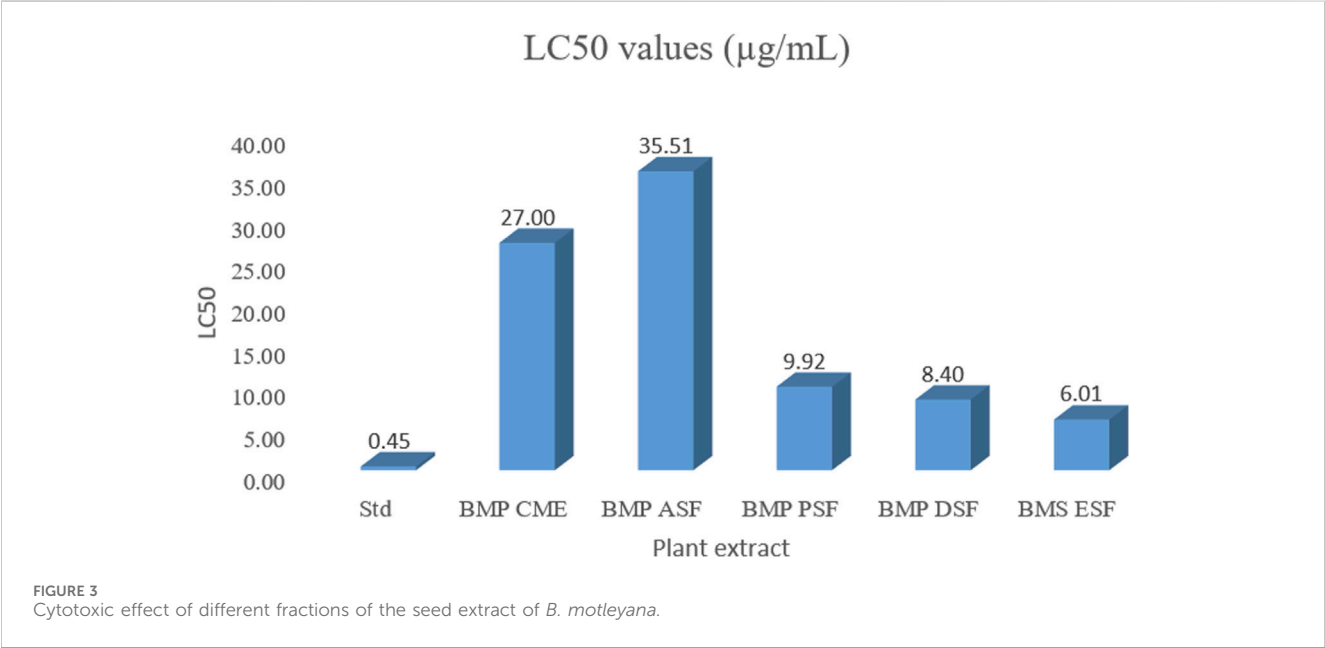
TABLE 2 GC–MS analysis of the methanolic extract of seeds of *B. motleyana*.

ID	Name	R.Time	m/z	Area	Concentration	Figure
1	Benzaldehyde dimethyl acetal	6.304	121.00	30424	2.486	
2	3-Tetradecene, (E)-	8.502	69.00	9807	0.801	
3	Oxalic acid, hexyl tridecyl ester	11.848	57.00	21828	1.783	
4	Dodecane, 2,6,10-trimethyl-	12.494	71.00	22750	1.859	
5	9-Methoxybicyclo[6.1.0]nona-2,4,6-triene	12.754	115.00	23846	1.948	
6	3-Hexadecene, (Z)-	14.763	69.00	16053	1.312	
7	Phenol, 3,5-bis(1,1-dimethylethyl)-	18.370	191.00	553919	45.257	
8	Dodecane, 2,6,11-trimethyl-	19.158	71.00	34671	2.833	
9	Hexadecane, 2,6,11,15-tetramethyl-	25.254	57.00	20521	1.677	
10	Hexadecanoic acid, methyl ester	30.675	74.00	124757	10.193	
11	9,12-Octadecadienoic acid, methyl ester, (E,E)-	35.414	67.00	8595	0.702	
12	9-Octadecenoic acid (Z)-, methyl ester	35.624	55.00	33009	2.697	
13	Methyl stearate	36.378	55.00	260098	21.251	
14	Diisooctyl phthalate	45.539	149.00	30488	2.491	

(Continued on following page)

TABLE 2 (Continued) GC–MS analysis of the methanolic extract of seeds of *B. motleyana*.

ID	Name	R.Time	m/z	Area	Concentration	Figure
15	Cyclobarbitol	50.949	207.00	33181	2.711	



diarrhea, which continued for the following 4 h in the control mice. The methanolic extract of seeds of *B. motleyana* displayed remarkable antidiarrheal activity by reducing the number of diarrheal feces in test animals. Regarding the reduction of diarrheal episodes, the most pronounced activity was observed with the 200 mg/kg extract, achieving a suppression percentage of 55.56 ± 0.71 . In comparison, the standard exhibited a slightly higher suppression of $61.11\% \pm 0.63\%$, while the 600 mg/kg and 400 mg/kg doses demonstrated suppressions of $50.00\% \pm 0.48\%$ and $22.22\% \pm 1.19\%$, respectively. Furthermore, after 4 h, both the standard and the 600 mg/kg dose showed highly significant results, whereas the 200 mg/kg dose exhibited a significant outcome.

Antidepressant effect

The methanolic extract of seeds of *B. motleyana* at 200, 400, and 600 mg/kg doses were subjected to a diazepam-induced sleeping time test to observe the delay of the onset of sleeping time and reduction of sleep duration induced by diazepam in Swiss albino mice. The data found from the study are displayed in Figure 5. Surprisingly, the seed extract displayed a significant delay in sleep onset at 200 and 400 mg/kg doses, while the 600 mg/kg dose showed minimal impact (Table 6). However, doses of 200 and 400 mg/kg demonstrated an extended duration

of sleeping time, suggesting dose-dependent effects on sleep Patterns (Table 7).

Molecular docking

The binding affinity of the identified compounds from the methanolic seed extract of *B. motleyana* against selected targets is shown in Table 8. Compound 14 displayed the lowest binding affinity toward EGFR, with a score of -7.3 kcal/mol, followed by compounds 7 and 15, which exhibited potential binding scores of -7 kcal/mol. However, when compared to the standard lapatinib with an affinity of -10.9 kcal/mol, seven other compounds scored lower than -6 kcal/mol. For DHFR, compound 15 demonstrated the highest activity, showing a notable binding affinity of -7.1 kcal/mol compared to the standard ciprofloxacin score of -8.2 kcal/mol. Additionally, compounds 7, 9, and 14 showed promising activity toward the receptor, with binding affinities of -6.3 , -6 , and -6.1 kcal/mol, respectively. In the case of GLUT-3, compounds 7 and 14 exhibited very prominent binding affinities of -7.6 and -7.9 kcal/mol, respectively, compared to the standard glibenclamide, with an affinity of -10.9 kcal/mol. Compounds 9 and 11 also showed satisfactory binding scores of -6.7 kcal/mol. Regarding KOR, compounds 7 and 14 approached the affinity score of the standard (-9.3 kcal/mol), demonstrating affinity scores of -7.1 and -7.6 kcal/mol, respectively. Additionally, compounds

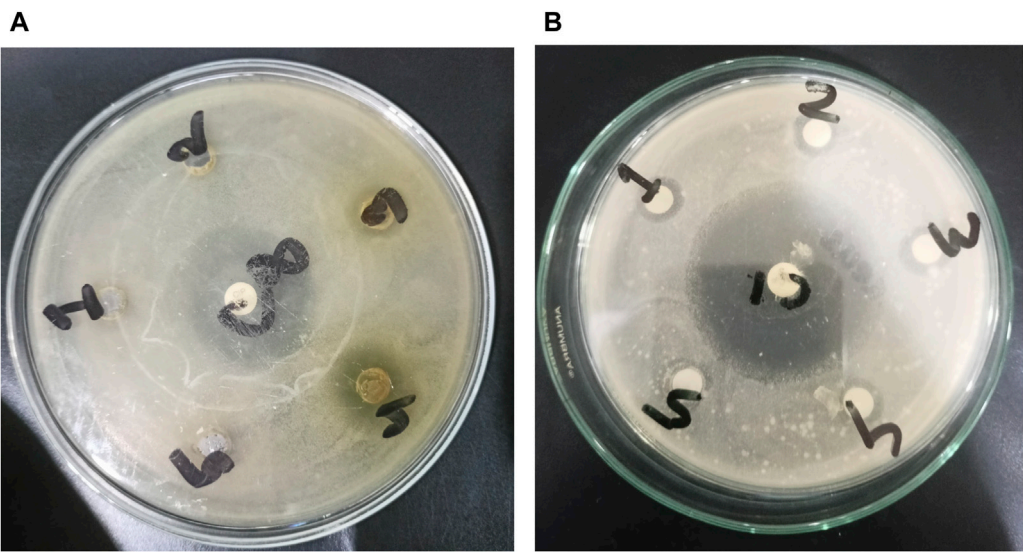


FIGURE 4 Development of zones of inhibition against microorganisms. In the case of Gram-negative *Escherichia coli*, activities are represented by (A), with 1, 2, 3, 4, and 5 corresponding to BMS ASF, BMS PSF, BMS ESF, BMS CME, and BMS DSF, respectively. For Gram-positive *Staphylococcus aureus*, (B) represents the activity, where 1, 2, 3, 4, and 5 correspond to BMS CME, BMS DSF, BMS ESF, BMS ASF, and BMS PSF, respectively.

TABLE 3 Antimicrobial activity displayed by different solvent soluble fractions of seeds of *B. motleyana*.

Test microorganism	Diameter of the zone of inhibition (mean ± SEM; mm)					
	BMS CME	BMS ASF	BMS PSF	BMS DSF	BMS ESF	Ciprofloxacin
Gram-positive bacteria						
<i>Bacillus cereus</i>	9 ± 0.05	0	0	0	7 ± 0.05	42 ± 0.08
<i>Bacillus megaterium</i>	6.99 ± 0.06	0	0	8 ± 0.05	8.99 ± 0.03	30 ± 0.08
<i>Bacillus subtilis</i>	10.98 ± 0.09	0	0	0	7 ± 0.04	41 ± 0.09
<i>Staphylococcus aureus</i>	12 ± 0.08	0	0	10 ± 0.12	8 ± 0.06	44 ± 0.05
<i>Sarcina lutea</i>	7.98 ± 0.1	0	0	0	9 ± 0.08	40 ± 0.09
Gram-negative bacteria						
<i>Salmonella paratyphi</i>	11 ± 0.05	0	0	8 ± 0.08	12 ± 0.05	43 ± 0.12
<i>Salmonella typhi</i>	9 ± 0.08	0	0	8 ± 0.04	11.98 ± 0.07	43 ± 0.06
<i>Vibrio parahaemolyticus</i>	9.97 ± 0.04	0	0	7 ± 0.08	11 ± 0.06	42 ± 0.04
<i>Escherichia coli</i>	13 ± 0.08	0	0	0	8 ± 0.06	41 ± 0.1
<i>Vibrio mimicus</i>	11 ± 0.08	0	0	0	9 ± 0.03	38 ± 0.06
<i>Shigella dysenteriae</i>	9 ± 0.06	0	0	8.99 ± 0.05	11 ± 0.06	40 ± 0.05
<i>Pseudomonas aeruginosa</i>	12 ± 0.08	0	0	0	10 ± 0.06	35 ± 0.08
<i>Shigella boydii</i>	11 ± 0.05	0	0	9.98 ± 0.09	8 ± 0.02	40 ± 0.06
Fungi						
<i>Saccharomyces cerevisiae</i>	8 ± 0.09	0	0	6.98 ± 0.01	8 ± 0.06	38 ± 0.05
<i>Candida albicans</i>	12 ± 0.05	0	0	0	11 ± 0.05	42 ± 0.06
<i>Aspergillus niger</i>	8.98 ± 0.07	0	0	8 ± 0.02	10 ± 0.08	52 ± 0.08

TABLE 4 Hypoglycemic activity of seeds of *B. motleyana*.

Treatment	% Reduction of the blood glucose level			
	Hour after administration of the plant sample/drug			
	0 h	.5 h	1 h	2 h
Standard (2 mg/kg)	28.85 ± 0.32*	3.49 ± 2.99	7.95 ± 1.73	49.53 ± 0.58**
BMS 200 mg/kg	17.31 ± 0.35	3.99 ± 0.71	22.85 ± 0.34**	6.13 ± 0.44
BMS 400 mg/kg	11.54 ± 0.32	23.19 ± 0.67*	23.84 ± 0.58*	11.79 ± 0.38
BMS 600 mg/kg	10.58 ± 0.18	13.47 ± 2.27	36.42 ± 0.24***	23.58 ± 0.18**

Values are expressed as mean ± SEM (n = 5); CTL, negative control; STD, positive control; ***p < 0.001, **p < 0.01, and *p < 0.05 compared to negative control.

TABLE 5 Antidiarrheal activity of the methanolic extract of seeds of *B. motleyana*.

Treatment	% Reduction in the frequency of the diarrheal episode			
	Hour after administration of the plant sample/drug			
	1 h	2 h	3 h	4 h
BMS 200 mg/kg	100.00 ± 0.00*	77.78 ± 0.50*	66.67 ± 0.25	55.56 ± 0.71*
BMS 400 mg/kg	50.00 ± 0.50	55.56 ± 0.41	55.56 ± 0.41	22.22 ± 1.19
BMS 600 mg/kg	100.00 ± 0.00*	100.00 ± 0.00**	100.00 ± 0.00**	50.00 ± 0.48**
BMS (50 mg/kg)	100.00 ± 0.00*	66.67 ± 0.25*	44.44 ± 0.48	61.11 ± 0.63**

Values are expressed as mean ± SEM (n = 5); Standard = positive control; ***p < 0.001, **p < 0.01, and *p < 0.05 compared to negative control.

TABLE 6 Delay of the onset of sleeping time exhibited by the methanolic extract of seeds of *B. motleyana*.

Group	Onset of sleep (minutes)						
	M1	M2	M3	M4	Avg	SD	SEM
Control	28.000	32.000	30.000	70.000	40	20.067	10.033
BMS 200 mg/kg	20.000	6.000	18.000	21.000	16.25	6.946	3.473
BMS 400 mg/kg	24.000	29.000	28.000	15.000	24	6.377	3.189
BMS 600 mg/kg	17.000	118.000	24.000	24.000	45.75	48.280	186.000
STD	18.000	20.000	20.000	20.000	19.5	1.000	0.500

9 and 15 conveyed prominent scores of −6.7 kcal/mol against the receptor. In comparison to the standard diazepam’s binding affinity toward MOA, which was −6.7 kcal/mol, compound 15 showed a very promising binding affinity of −6.6 kcal/mol. However, compounds 7, 9, and 14 demonstrated very promising affinities toward the receptor, with binding scores of −6.5, −6.3, and −6.4 kcal/mol, respectively.

Discussion

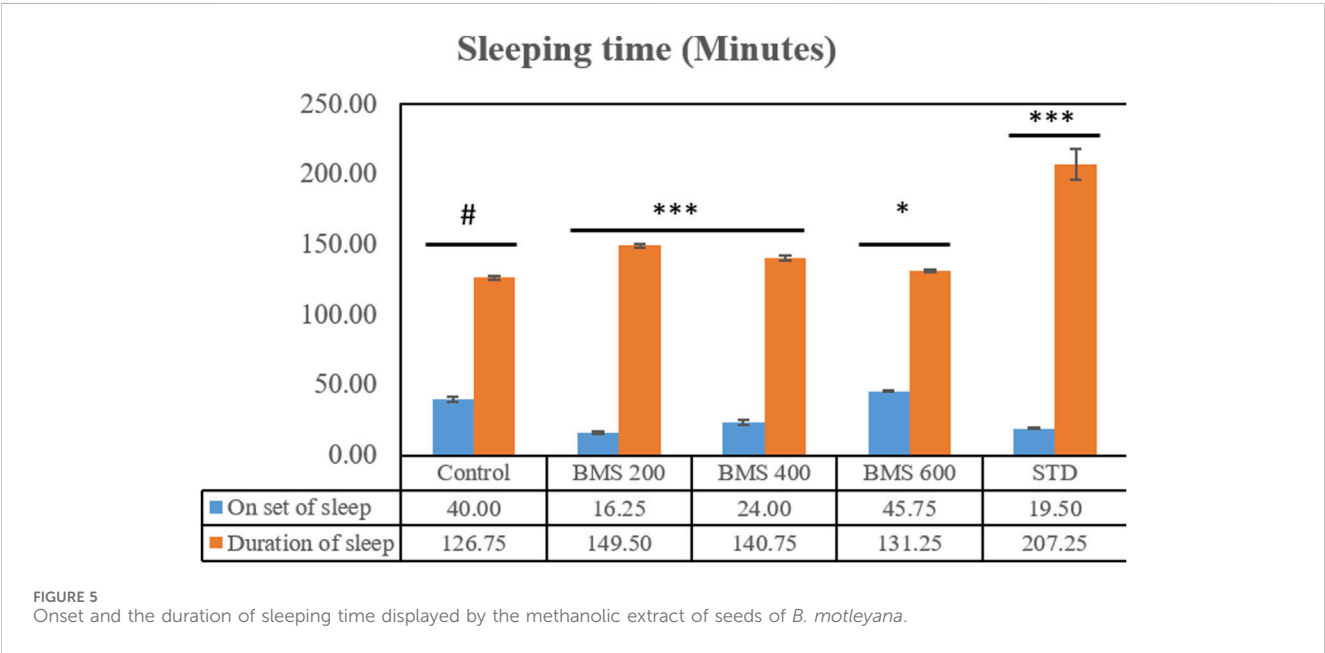
The search for innovative bioactive compounds with potential applications in emerging therapies places medicinal plants at the

forefront. Consequently, there is a growing emphasis on the extensive utilization of plant-based natural remedies in developing nations, attracting considerable attention due to their multifaceted protective benefits and positive influences on human health. Traditional medicines, enjoying widespread popularity, are relied upon by approximately 80% of individuals, even in underdeveloped regions (Alam et al., 2020). Medicinal plant extracts constitute complex amalgamations of secondary metabolites derived from plants, animals, and microorganisms. Typically containing 10 to 60 ingredients in varying concentrations, these extracts often hinge on 2–4 key molecules for their biological features (Rahman et al., 2013). The exploration of the chemical composition and structure of samples reveals a myriad of biological potentials inherent in medicinal plant extracts.

Interestingly, there is a conspicuous lack of published research utilizing GC–MS/MS for the characterization of bioactive chemicals in the seeds of *Baccaurea motleyana*. In response to this gap, a meticulously planned investigation, involving GC–MS/MS evaluation, was initiated. In the crude methanolic seed extract of *B. motleyana*, the phenolic compound 3,5-bis(1,1-dimethylethyl) emerged as the most abundant. Recent studies have revealed that this compound, also known as 3,5-di-tert-butylphenol, possesses antifungal properties against *Candida* strains. It effectively hinders biofilm formation and impacts the viability of planktonic cells, inducing significant morphological changes in both planktonic and biofilm cells, particularly affecting the cell membrane integrity. Moreover, 3,5-di-tert-butylphenol demonstrated synergistic effects with sodium dodecyl sulfate, leading to further

TABLE 7 Duration of sleeping time displayed by the methanolic extract of seeds of *B. motleyana*.

Group	Duration of sleep (minutes)						
	M1	M2	M3	M4	Avg	SD	SEM
Control	147	101	132	127	126.75	19.155	9.578
BMS 200 mg/kg	70	235	108	185	149.5	74.416	37.208
BMS 400 mg/kg	190	178	105	90	140.75	50.553	25.276
BMS 600 mg/kg	60	117	152	196	131.25	57.454	28.727
STD	222	218	176	213	207.25	21.156	10.578



disruption of membrane integrity. The compound also initiates the production of endogenous radical oxygen species in *Candida*, contributing to its anti-biofilm activity (Vijayakumar and MuhilVannan, 2021). Additionally, this compound, along with its analogous 2,6-ditert-butylphenol or phenol, 2,6-bis(1,1-dimethylethyl), has been reported to exhibit a range of activities, including antioxidant, cytotoxic, insecticidal, and nematocidal, as well as antibacterial and antiviral properties (Zhao et al., 2020).

In our study, a high amount of methyl stearate, around 21.251%, was found in the BMC CME, which was previously known for its medicinal potency. For instance, methyl stearate, identified as a bioactive compound in the fermentation broth, plays a crucial role in inhibiting nematode infection. Through reducing egg hatching, repelling J2s from plant roots, and regulating essential parasitic nematode genes (Mi-flp-18 and 16D10), methyl stearate demonstrates significant efficacy in controlling *Meloidogyne incognita*. Moreover, its positive impact on promoting banana plant growth at lower concentrations highlights its potential as an eco-friendly strategy for nematode control, providing a promising alternative to conventional pesticides and contributing to sustainable agricultural practices (Lu et al., 2020).

Hexadecanoic acid methyl ester, the third most abounded bioactive compound (10.193%) from the extract, displayed significant antibacterial efficacy against *Staphylococcus aureus* W35, *Pseudomonas aeruginosa* D31, *Klebsiella pneumoniae* DF30, and *K. pneumoniae* B45. Also research identified volatile compounds in *Imperata cylindrica*, including hexadecanoic acid methyl ester with antibacterial effects against *P. aeruginosa*, *Bacillus subtilis*, and *K. pneumoniae* (Lalthanpuui and Lalchhandama, 2019). Studies on *Scenedesmus intermedius* also highlighted the inhibitory impact of the hexadecanoic acid methyl ester against Gram-positive and Gram-negative bacteria (Davoodbasha et al., 2018). As a fatty acid ester, the hexadecanoic acid methyl ester acts on bacterial cell membranes, disrupting energy production, inhibiting enzyme activity, and causing direct lysis, making it a promising antibacterial agent with both safety and efficacy (Shaaban et al., 2021). The wide range of bioactive substances found in our study, such as methyl stearate, hexadecanoic acid methyl ester, and 3,5-ditert-butylphenol, highlights the enormous potential of medicinal plants. These compounds exhibit a wide range of activities, including antifungal, antibacterial, and nematode-inhibiting properties. As we combine conventional treatments with novel therapeutic

TABLE 8 Binding affinities of identified compounds from the methanolic extract of *B. motleyana* seeds against EGFR, DHFR, GLUT-3, KOR, and MOA.

No.	Compound name	PubChem ID	Molecular weight (g/mol)	Binding affinities (kcal/mol)				
				EGFR (1xkk)	DHFR (4M6J)	GLUT3 (4ZWB)	KOR(6VI4)	MOA (2Z5X)
1	Benzaldehyde dimethyl acetal	62375	152.19	−5.6	−5	−5.5	−5.2	−5.2
2	3-Tetradecene, (E)-	5352802	196.37	−5.8	−4.8	−5.9	−5.7	−5.3
3	Oxalic acid, hexyl tridecyl ester	6420365	356.50	−5.9	−5.8	−6.5	−6.1	−5.9
4	Dodecane, 2,6,10-trimethyl-	19773	212.41	−6.1	−5.2	−6	−6.4	−5.5
5	9-Methoxybicyclo[6.1.0] nona-2,4,6-triene	5370526	148.20	−5.6	−5.5	−6.2	−6	−5.5
6	3-Hexadecene, (Z)-	5364494	224.42	−6	−4.8	−5.6	−6	−5.1
7	Phenol, 3,5-bis(1,1-dimethylethyl)-	70825	206.32	−7	−6.3	−7.6	−7.1	−6.5
8	Dodecane, 2,6,11-trimethyl-	35768	212.41	−6	−5.2	−6	−6.2	−6.1
9	Hexadecane, 2,6,11,15-tetramethyl-	136331	282.50	−6.7	−6	−6.7	−6.7	−6.3
10	Hexadecanoic acid, methyl ester	8181	270.50	−6.1	−5	−6.1	−5.8	−5.4
11	9,12-Octadecadienoic acid, methyl ester, (E,E)-	5362793	294.50	−6.5	−5.5	−6.7	−6.4	−5.8
12	9-Octadecenoic acid (Z)-, methyl ester	5364509	296.50	−6.4	−5.2	−6.2	−6.3	−5.8
13	Methyl stearate	8201	298.50	−6.1	−5	−5.9	−6	−5.6
14	Diisooctyl phthalate	33934	390.60	−7.3	−6.1	−7.9	−7.6	−6.4
15	Cyclobarbitol	5,838	236.27	−7	−7.1	−6.2	−6.7	−6.6
Standards	Lapatinib	208908	581.10	−10.9	-	-	-	-
	Ciprofloxacin	2764	331.34	-	−8.2	-	-	-
	Glibenclamide	3488	494.00	-	-	−10.2	-	-
	Loperamide	3955	477.00	-	-	-	−9.3	-
	Diazepam	3016	284.74	-	-	-	-	−6.7

approaches, these compounds offer exciting prospects for future research in the pharmaceutical domains.

The presence of cytotoxic compounds in plant material is often assessed through cytotoxicity assays, with brine shrimp serving as a common zoological specimen for such studies. The brine shrimp lethality test is validated for assessing cytotoxicity in human solid tumors and essential oils, identifying potent anticancer compounds (Niksic et al., 2021). In this assay, a lower LC₅₀ value indicates higher toxicity. Extracts with LC₅₀ values over 1,000 µg/mL are considered non-toxic, while those with LC₅₀ between 500 and 1,000 µg/mL are weakly toxic (Apu et al., 2013). The ethyl acetate (EA) fraction from the *B. motleyana* seed extract demonstrated significant cytotoxic activity, presenting the lowest LC₅₀ value of 6.01 µg/mL compared to the standard 0.45 µg/mL. Notably, PET and DCM fractions also exhibited promising activity with LC₅₀ values of 9.92 and 8.40 µg/mL, respectively. However, it is essential to comment on the relatively poor activity observed in the remaining fractions when

compared to the standard. These results establish the EA fraction from the *B. motleyana* seed extract as a viable candidate for additional investigation in the development of cytotoxic agents by highlighting its notable cytotoxic potential. The significant activity found in the dichloromethane DCM and PET fractions points to more research directions. For a thorough understanding of the extract’s cytotoxic qualities, it is crucial to isolate and characterize particular bioactive compounds, as highlighted by the relatively lower activity in other fractions.

The rise of infectious diseases poses a growing global threat, escalating the risk of antimicrobial resistance. This increasing trend not only endangers public health but also exacerbates the challenges associated with antimicrobial resistance on a global scale (Dhingra et al., 2020). WHO reported that Antimicrobial resistance (AMR) will cause approximately 10 million deaths 2050 (Murray et al., 2022). Therefore, it will be beneficial to develop new antibacterial drugs from nature that decrease the incidence of

AMR by controlling the growth of bacteria. The result showed significant inhibitory effects against both Gram-positive and Gram-negative bacteria. The different fractions of plant samples displayed the most promising result with a range of zone of inhibition of 8–13 mm. The crude methanolic extract of seeds of *B. motleyana* exhibited the highest zone of inhibition against that of *E. coli* (13 mm), followed by *S. aureus* (12 mm). However, *C. albicans* was also found to be sensitive to the crude methanolic extract by displaying a zone of inhibition of 12 mm compared with standard fluconazole. The plant extracts exhibited antifungal properties that are comparable with the standard antifungal drug. However, this study might be helpful in studying the antimicrobial effect of the plant constituents more extensively and against other microorganisms so that they could be used to develop effective antimicrobial agents.

Diabetes is a chronic medical condition that is a global health challenge. As traditional plant sources are thought to have minimum side effects and are cost effective, various studies recommend them for the effective treatment of diabetes mellitus (Lee et al., 2021). In this experiment, the crude methanolic extract of plant samples at 600 mg/kg body wt. dose shows high hypoglycemic activity (36.42%) as compared to the standard drug glibenclamide (7.95%) 1 h later, as shown in Table 4. In comparison to *Baccaurea motleyana*, other plants like *Berberis aristata* and *Bixa orellana* have demonstrated significant hypoglycemic effects, attributed to compounds like berberine and bixin, respectively. *Catharanthus roseus* displayed dose-dependent blood sugar-lowering activity, with isolated alkaloids showing potential for type 2 diabetes management (Alam et al., 2022). These findings highlight the diverse mechanisms and bioactive compounds present in different plant extracts, suggesting their potential in diabetes treatment.

Following castor oil ingestion, ricinoleic acid induces gut irritation and inflammation, disrupting gastrointestinal motility, secretions, and epithelial permeability. This disrupts the re-absorption of Na⁺, K⁺, and water, leading to the release of inflammatory mediators, such as prostaglandins, histamine, and nitric oxide (Alam et al., 2021b). In the present investigation, the methanolic extract of *B. motleyana* seeds demonstrated significant antidiarrheal effects at doses of 200 mg/kg and 600 mg/kg in a castor oil-induced diarrhea model, surpassing the efficacy of the reference drug loperamide. The study substantiates the notion that the extract effectively alleviates diarrhea by inhibiting hypersecretion and enteropooling, presenting potential therapeutic advantages (Billah et al., 2013). The antidiarrheal property of the tested plant samples could be due to phytochemicals like glycosides, alkaloids, tannins, terpenes, flavonoids, and other phenolic compounds present in *B. motleyana* (Gutiérrez et al., 2014). The extract demonstrated substantial reduction in intraluminal fluid accumulation, comparable to the widely prescribed antidiarrheal drug loperamide, suggesting its potential in managing diarrhea, possibly by inhibiting hypersecretion and enteropooling in the gut (Alam M M et al., 2021).

Although several treatment modalities have been developed for coronary artery disease, depression, and anxiety, full symptom relief without adverse effects is still unattainable. The imperfect pharmacokinetics and related side effects of current medications make it difficult to use them in clinical settings. As a result, there are now serious concerns about the safety, effectiveness, duration of

action, and side effects of current medications. It is now essential to research new medications. Herbal medicine has emerged as a promising treatment option for these diseases because of the numerous neural targets that are involved (Fajemiroye et al., 2016). CNS stimulants have been used as a treatment option for depression (Avois et al., 2006). CNS stimulants generally alter sleep patterns by either shortening the duration of sleep, prolonging the onset of sleep, or affecting both aspects simultaneously (Rao and Tripathi, 2022). Among the three doses, the 600 mg/kg body weight dose exhibits the highest delay of onset of sleep (minutes), as shown in Figure 3, and the same dose displayed the lowest duration of sleeping time (Figure 5). Due to a significant correlation between reduced immobility and clinical potency in assessing antidepressants, the rat model is prioritized. Although the antidepressant test used in rats lacks symptomatology similar to human depression, it effectively distinguishes antidepressants from neuroleptics and anxiolytics. Determining the absolute effects of dopaminergic, anticholinergic, and GABAergic moieties as antidepressants is challenging (Emon et al., 2020). The methanolic extract of *B. motleyana* seeds demonstrates antidepressant-like effects, potentially restoring brain monoamines and reducing reserpine-induced depression in rats. Additional research has revealed the potential cytotoxic activity of the methanolic extract from *Baccaurea ramiflora* (Lour), suggesting a possible impact on the central nervous system through enhanced GABAergic inhibition. This effect parallels the actions of drugs with sedative-hypnotic, anxiolytic, and muscle relaxant properties, operating via the primary inhibitory neurotransmitter, gamma-aminobutyric acid (Nesa et al., 2018). However, the antidepressant action observed by plant extracts suggested the existence of a phytochemical constituent's flavonoid (Hossain et al., 2009).

EGFR plays a pivotal role in cancer management, particularly in the context of lung cancer. Overexpression of EGFR is implicated in various malignancies, including non-small-cell lung cancer. Upon ligand binding, EGFR undergoes conformational changes and phosphorylation, activating downstream pathways such as Raf1-extracellular signal-regulated kinase, PI3K/AKT, and STAT transcription factors. This activation contributes to uncontrolled cell proliferation and inhibits apoptosis, promoting cancer phenotypes (Ongko et al., 2022). Compound 14 demonstrated a significant binding affinity toward EGFR, forming one carbon-hydrogen, two conventional hydrogen, one pi-sigma, and five alkyl bonds with a potential binding score of -7.3 kcal/mol. Similarly, compounds 7 and 15 exhibited binding affinities of -7 kcal/mol. Compound 7 interacted through one pi-sigma and three pi-alkyl bonds, while compound 15 engaged through one carbon-hydrogen, two conventional hydrogens, and four alkyl bonds (Figure 6; Table 9).

DHFR, crucial in thymidylate biosynthesis, emerges as a promising target for infection treatment, with inhibitors potentially causing bacterial death (He et al., 2020). Additionally, DHFR-mediated disruptions in the folate pathway are implicated in uncontrolled cell growth, influencing cellular development and proliferation in malignancies (Kodidela et al., 2016). In computational docking studies, compound 15 displayed the highest binding affinity toward DHFR, disrupting two conventional hydrogens, one pi-sigma, and two alkyl bonds, resulting in a binding affinity score of -7.1 kcal/mol. This surpassed the standard ciprofloxacin (-8.2 kcal/mol), which formed one conventional hydrogen, three carbon-hydrogen, and two pi-alkyl



FIGURE 6

In diabetes, the regulation of glucose transporter isoforms, including GLUT-3, in retinal endothelial cells is pivotal. Elevated glucose levels lead to increased GLUT-3 mRNA expression,

TABLE 9 Bond and the binding site of highly active compounds against different targets, including EGFR, DHFR, GLUT-3, KOR, and MOA.

Receptor	Compound	Binding affinity (kcal/mol)	Bond type	Amino acids
EGFR	7	−7	Pi-sigma	Leu 844
			Pi-alkyl	Leu 718, Val 726, and Ala 743
	9	−6.7	Alkyl	Leu 718, Val 726, Ala 743, Lys 745, Met 766, Cys 775, Leu 777, Leu 788, and Leu 844
	14	−7.3	Carbon-hydrogen bond	Asp 855
			Conventional hydrogen bond	Lys 745 and Thr 854
			Pi-sigma	Phe 856
			Alkyl	Leu 718, Val 726, Ala 743, Met 766, and Leu 844
	15	−7	Carbon-hydrogen bond	Gly 721
			Conventional hydrogen bond	Asn 842 and Asp 855
			Alkyl	Val 726, Ala 743, Cys 797, and Leu 844
	Lapatinib	−10.9	Carbon-hydrogen bond	Ser 720 and Asp 855
			Conventional hydrogen bond	Lys 745 and Thr 790
			Pi-sigma	Met 766
			Alkyl	Leu 718, Val 726, Ala 743, Leu 777, and Leu 844
			Halogen(fluorine)	Cys 775 and Arg 776
			Unfavorable donor-donor	Met 793
			Pi-Pi T-shaped	Phe 856
DHFR	7	−6.3	Conventional hydrogen bond	Arg 91
			Pi-carbon	Arg 77
			Pi-alkyl	Leu 75
	9	−6	Alkyl	Val 8, Ala 9, Ile 16, Leu 22, Phe 34, and Tyr 121
	14	−6.1	Carbon-hydrogen bond	Ile 16, Gly 116, and Gly 117
			Conventional hydrogen bond	Thr 56 and Sern118
			Pi-pi T-shaped	Tyr 121
			Alkyl	Val 8, Leu 22, and Lys 55
	15	−7.1	Conventional hydrogen bond	Ile 7 and Glu 30
			Pi-sigma	Phe 34
			Alkyl	Ile 16 and Leu 22
	Ciprofloxacin	−8.2	Conventional hydrogen bond	Ala 9
			Carbon-hydrogen bond	Val 8, Thr 56, and Ser 118
			Pi-alkyl	Ile 16 and Leu 22
GLUT3	7	−7.6	Conventional hydrogen bond	Asn 315 and Glu 378
			Pi-pi T-shaped	Phe 289
			Alkyl	Ile 162, Ile 166, Ile 285, and Trp 386

(Continued on following page)

TABLE 9 (Continued) Bond and the binding site of highly active compounds against different targets, including EGFR, DHFR, GLUT-3, KOR, and MOA.

Receptor	Compound	Binding affinity (kcal/mol)	Bond type	Amino acids
	9	−6.7	Alkyl	Phe 24, Ile 166, Ile 285, Phe 289, Phe 377, and Trp 386
	11	−6.7	Conventional hydrogen bond	Asn 286
			Alkyl	Phe 24, Val 67, Ile 162, Ile 166, Ile 285, Phe 289, and Phe 377
	14	−7.9	Conventional hydrogen bond	Gln 281 and Asn 413
			Pi-pi T-shaped	Phe 289 and Phe 377
			Alkyl	Phe 24, Phe 70, Ile 166, Ile 285, and Trp 410
	Glibenclamide	−10.2	Conventional hydrogen bond	Asn 32, Val 67, and Asn 286
			Pi-sigma	Tyr 290
			Amide pi-stacked	Gly 417
			Alkyl	Ala 68, Ile 285, Phe 414, and Leu 418
KOR	C7	−7.1	Conventional hydrogen bond	Ile 180
			Pi-sigma	Trp 183 and Ile 191
			Alkyl	Val 195
	9	−6.7	Pi-sigma	Trp 183
			Alkyl	Phe 99, Ile 180, Leu 184, Ile 191, and Val 195
	14	−7.6	Conventional hydrogen bond	Ser 187
			Pi-pi stacked	Trp 183
			Alkyl	Phe 99, Tyr 140, Ile 180, Leu 184, Ile 191, and Val 195
	15	−6.7	Conventional hydrogen bond	Ser 187
			Carbon-hydrogen bond	SER 187
			Alkyl	Trp 183 and Ile 191
	Loperamide	−9.3	Pi-donor hydrogen bond	Ser 136
			Pi-sigma	Trp 183, Leu 184, and Ile 191
			Pi-pi T-shaped	Tyr 140
			Alkyl	Ile 180 and Val 195
MOA	7	−6.5	Pi-anion	Glu 492
			Pi-sigma	Phe 112
			Pi-alkyl	Trp 128 and His 488
	9	−6.3	Pi-sigma	His 488
			Alkyl	Phe 112, Tyr 121, Tyr 124, Trp 128, Arg 129, and Arg 493
	14	−6.4	Carbon-hydrogen bond	Asn 125 and His 488
			Conventional hydrogen bond	Thr 205
			Pi-anion	Glu 492
			Alkyl	Arg 129 and Arg 493

(Continued on following page)

TABLE 9 (Continued) Bond and the binding site of highly active compounds against different targets, including EGFR, DHFR, GLUT-3, KOR, and MOA.

Receptor	Compound	Binding affinity (kcal/mol)	Bond type	Amino acids
	15	−6.6	Conventional hydrogen bond	Phe 112 and Tyr 121
			Pi-alkyl	Tyr 124 and Trp 128
	Diazepam	−6.7	Pi-anion	Glu 492
			Pi-alkyl	Phe 112, Tyr 121, Trp 128, and His 488

potentially enhancing the efficient utilization of glucose by retinal endothelial cells. Conversely, excessively high glucose concentrations result in the downregulation of glucose transporters, contributing to diabetic retinopathy by mediating damage in the retinal microvasculature. Understanding the regulatory mechanisms of GLUT-3 in response to varying glucose levels provides valuable insights for potential intervention therapies in diabetes-related complications (Knott et al., 1996). When interacting with GLUT-3, glibenclamide engaged the receptor through three conventional hydrogen bonds, a single pi-sigma, amide pi stacked, along with four alkyl bonds, resulting in a binding score of −10.2 kcal/mol. In contrast, compound 14 interacted with GLUT-3 through two conventional hydrogens, two pi-pi, and five alkyl bonds, showing a binding score of −7.9 kcal/mol. Similarly, compounds 7, 9, and 11 formed three, one, and two different types of interactions, respectively (Figure 8; Table 9).

Opioid receptors, including μ , κ , and δ receptors, modulate gastrointestinal signaling by inhibiting enteric nerve activity and suppressing the neurotransmitter release, affecting excitatory and inhibitory motor pathways. This cascade results in delayed colonic transit, reduced enteric nerve excitability, and changes in secretion and fluid transport, ultimately impacting GI motility and stool consistency (Pannemans and Corsetti, 2018). Certain identified compounds, particularly compounds 7, 9, 14, and 15, demonstrated potential antioxidant activity by forming bonds with KOR. Compound 14 bound with a single conventional hydrogen, one pi-pi, and six alkyl bonds, resulting in a binding score of −7.6 kcal/mol compared to the standard score of −9.3 kcal/mol. Additionally, compounds 7, 9, and 15 formed three, two, and three different types of bonds, respectively, showing binding scores of −7.1, −6.7, and −6.7 kcal/mol (Figure 9; Table 9).

A study posits that monoamine oxidase A (MOA) density is likely elevated throughout the brain in individuals with major depressive disorder during untreated depressive episodes. This elevation is hypothesized as a potential mechanism contributing to the pathophysiology of depression as increased MOA activity could excessively lower brain monoamine levels, including serotonin, norepinephrine, and dopamine (Meyer et al., 2006). Regarding MOA, compounds 7, 9, 14, and 15 exhibited very strong binding affinities compared to the standard diazepam (−6.7 kcal/mol). Specifically, compound 15 formed two conventional hydrogen and two pi-alkyl bonds with the receptor, demonstrating the highest binding affinity of −6.6 kcal/mol. Meanwhile, diazepam formed one pi-anion and four pi-alkyl bonds (Figure 10; Table 9).

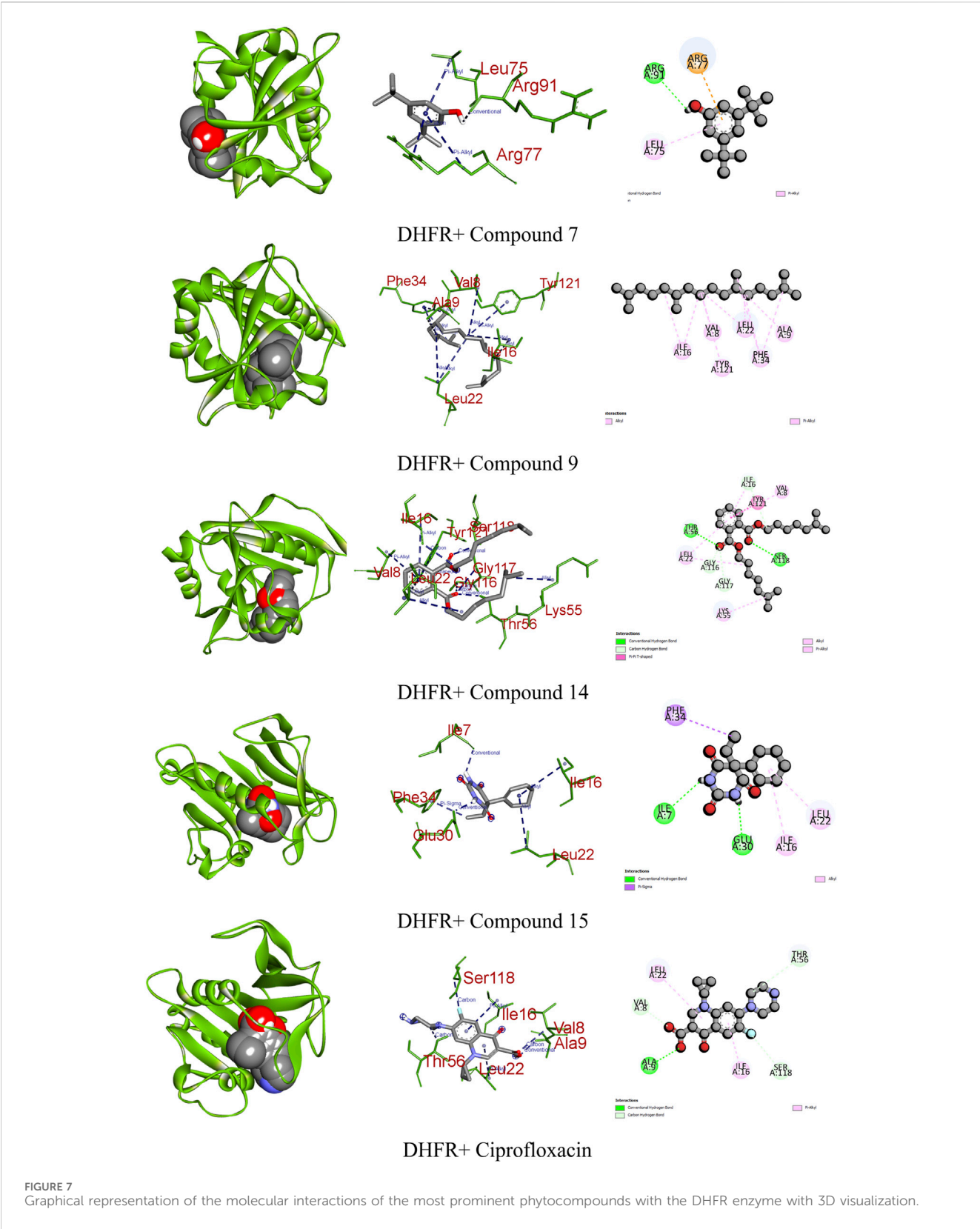
Surprisingly, our study revealed that various compounds identified from the methanolic extract of *B. motleyana* seeds displayed activity against multiple targets. This suggests a substantial involvement in mediating the diverse biological effects of the seed extract. This emphasizes the potential significance of these compounds in the overall pharmacological activity of the extract. Additionally, it is advisable to delve deeper into the exploration of these compounds in future research to gain a better understanding of their individual contributions and explore potential therapeutic applications.

The compounds with the highest binding affinities for the specified targets, as detailed in Table 10, underwent rigorous ADME/T screening. Notably, all these compounds exhibit robust intestinal absorptivity, coupled with negative water solubility, indicating their inherently lipophilic nature. In the term of the Rule of Five, compound 14 violates three rules, suggesting a limitation in terms of oral bioavailability. Conversely, compound 15 only violates a single rule, raising its candidacy as a potential oral drug. The remaining compounds each violate two rules. Despite these rule violations, all the compounds boast a remarkable bioavailability score of 0.55. Importantly, none of the compounds demonstrate AMES toxicity, underscoring their safety with respect to carcinogenicity. Similarly, all compounds test negative for hepatotoxicity. This comprehensive study strongly suggests that these compounds hold promising potential for future drug development.

The presence of the identified phytoconstituents in the seed extract of *B. motleyana* is implicated as a likely cause for a spectrum of biological effects, notably, antimicrobial, cytotoxic, antidiarrheal, anti-depressant, and antidiabetic activities. These findings underscore the multifaceted therapeutic potential of the plant's seed extract. Furthermore, the ADME/T (absorption, distribution, metabolism, excretion, and toxicity) study strongly advocates for the plausible drug-like qualities of these phytochemicals. This points toward their potential candidacy as therapeutic agents with reduced side effects. These promising results suggest the necessity for more comprehensive research to unravel the full therapeutic potential of these phytoconstituents and explore their suitability for drug development.

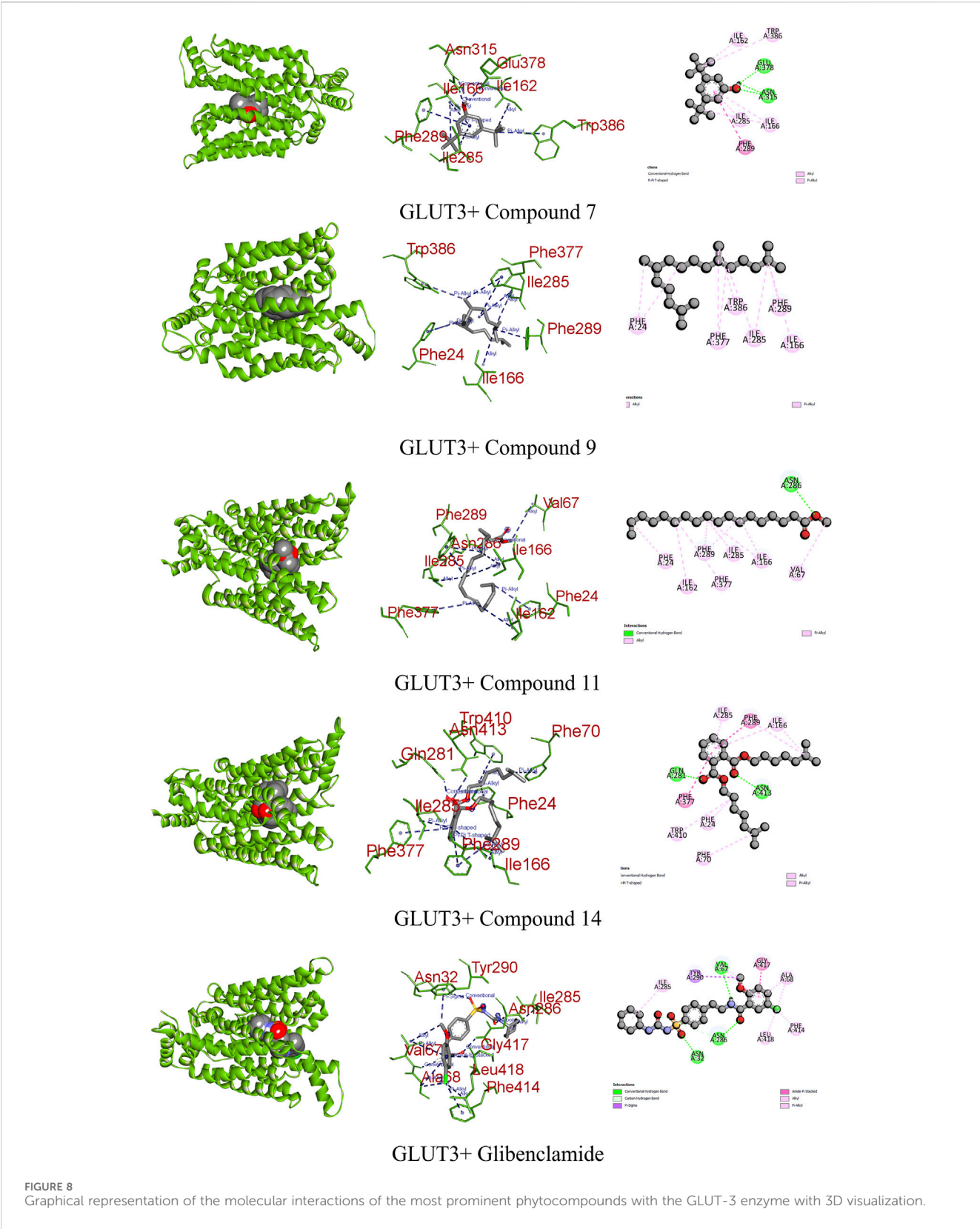
Limitation

Although this research has yielded promising findings, it is crucial to acknowledge the inherent limitations and approach them with a constructive perspective. First, the reliance on



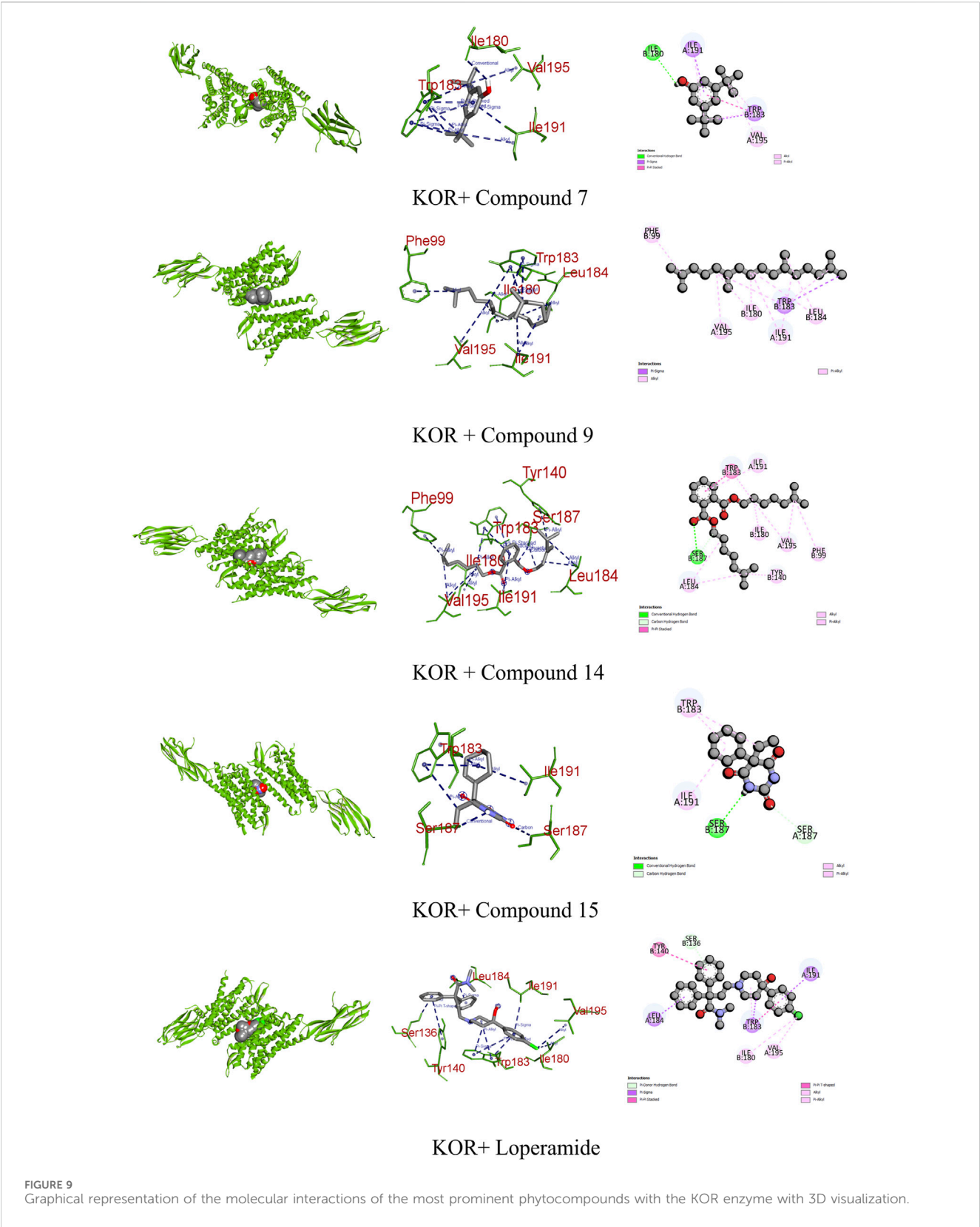
animal models, particularly rats, for assessing the antidepressant-like effects of the *B. motleyana* seed extract is a common and valuable starting point in preclinical studies. However, it is

essential to recognize that animal models may not perfectly mirror human responses, emphasizing the need for cautious extrapolation to human applications. Exploring potential

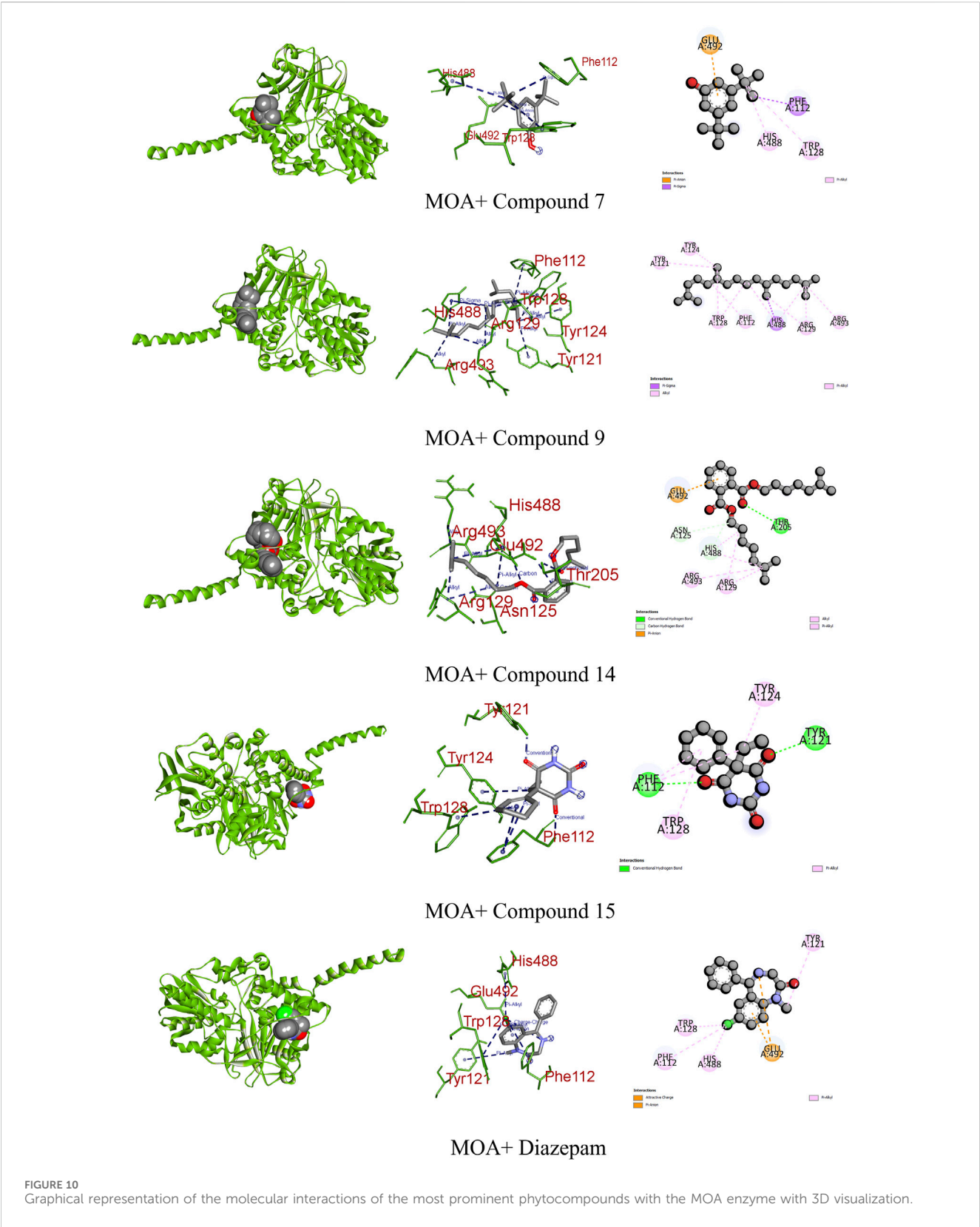


synergistic effects among the various compounds in the extract could enhance our understanding of the observed pharmacological activities. The observed antidiarrheal and hypoglycemic effects in

animal models provide valuable insights, yet it is recognized that animal responses may not perfectly mirror human reactions. To address this, the call for rigorous human clinical trials is emphasized,



ensuring a thorough evaluation of the extract's efficacy, safety profiles, and optimal dosage regimens for potential therapeutic applications. The cytotoxicity assay using brine shrimp larvae, while being a widely used method, is acknowledged for its limitations in accurately predicting human cytotoxic responses. Recognizing this constraint highlights the importance of



incorporating diverse cytotoxicity assays to obtain a more comprehensive understanding of the plant extract's safety profile. In conclusion, while these limitations are acknowledged, they present opportunities for further research and refinement. Addressing these considerations will contribute to a more nuanced understanding of the potential therapeutic applications

TABLE 10 ADME/T study of best bounded compounds from the methanol seed extract of *B. motleyana* against EGFR, DHFR, GLUT-3, KOR, and MOA.

Property	Model name (Unit)	Compound 7	Compound 9	Compound 11	Compound 14	Compound 15
Absorption	Water solubility (log mol/L)	−3.876	−8.667	−7.343	−6.757	−2.636
	CaCo ₂ permeability (log Papp in 10−6 cm/s)	1.668	1.426	1.612	1.425	0.491
	Intestinal absorption (human) (% absorbed)	92.254	91.681	92.66	91.448	80.555
	Skin permeability (log Kp)	−2.364	−2.621	−2.719	−2.656	−3.78
	P-glycoprotein substrate	No	No	No	No	No
	P-glycoprotein I inhibitor	No	No	No	Yes	No
	P-glycoprotein II inhibitor	No	Yes	Yes	Yes	No
Distribution	VDss (human) (log L/kg)	0.545	0.595	0.272	0.194	0.009
	Fraction unbound (human) (Fu)	0.042	0	0.028	0	0.598
	BBB permeability	0.47	0.981	0.767	−0.184	0.052
	CNS permeability	−0.858	−0.982	−1.463	−2.169	−3.002
Metabolism	CYP2D6 substrate	No	No	No	No	No
	CYP3A4 substrate	Yes	Yes	Yes	Yes	No
	CYP1A2 inhibitor	Yes	Yes	Yes	No	No
	CYP2C19 inhibitor	No	No	No	No	No
	CYP2C9 inhibitor	No	No	No	No	No
	CYP2D6 inhibitor	No	No	No	No	No
	CYP3A4 inhibitor	No	No	No	No	No
Excretion	Total clearance (log mL/min/kg)	0.781	1.546	2.032	1.652	0.149
	Renal OCT2 substrate	No	No	No	No	No
Toxicity	AMES toxicity	No	No	No	No	No
	Max. tolerated dose (human) (log mg/kg/day)	0.409	0.062	−0.019	1.112	0.623
	hERG I inhibitor	No	No	No	No	No
	hERG II inhibitor	No	Yes	No	Yes	No
	Oral rat acute toxicity (LD ₅₀) (mol/kg)	2.346	1.522	1.617	1.249	2.569
	Oral rat chronic toxicity (LOAEL) (log mg/kg_bw/day)	1.736	1.273	3.004	2.695	1.022
	Hepatotoxicity	No	No	No	No	No
	Skin sensitization	Yes	Yes	Yes	No	No
	<i>T. pyriformis</i> toxicity (log ug/L)	1.667	1.322	1.603	0.664	0.257
	Minnow toxicity (log mM)	−0.108	−2.211	−1.6	−3.429	1.782
Drug-likeness	Bioavailability score (%)	0.55	0.55	0.55	0.55	0.55
	Lipinski's Rule of Five	No; 2 violations: MW < 250, XLOGP3>3.5	No; 2 violations: Rotors>7, XLOGP3>3.5	No; 2 violations: Rotors>7, XLOGP3>3.5	No; 3 violations: MW > 350, Rotors>7, XLOGP3>3.5	No; 1 violation: MW < 250

of the *B. motleyana* seed extract, laying the groundwork for future advancements in natural medicine. Additionally, the *in silico* data will help in boosting up the finding of potential leads for further deeper experiments to prove their drug candidacy. Overall, while the study provides valuable insights into the pharmacological potential of the *B. motleyana* seed extract, further research involving diverse experimental models, including human clinical trials, is necessary to validate and extend these findings.

Conclusion

In summary, this comprehensive investigation elucidates the remarkable pharmacological versatility of *B. motleyana* seeds. The study underscores their substantial therapeutic potential, revealing significant bioactivities encompassing antidiarrheal, antimicrobial, antioxidant, hypoglycemic, and antidepressant properties. The identification of bioactive compounds through meticulous GC–MS analysis, coupled with insightful *in silico* studies, provides valuable insights into their potential molecular interactions with diverse therapeutic targets. Despite some rule violations in terms of oral bioavailability, the compounds exhibit promising ADME/T profiles, highlighting their candidacy for drug development. The multi-target activities of these compounds not only emphasize their integral role in the overall pharmacological effects of the seed extract but also open promising avenues for future research and pharmaceutical applications. This study contributes to the growing body of knowledge on plant-based remedies, emphasizing their potential as sources for novel and effective therapeutic agents.

Data availability statement

The raw data supporting the conclusions of this article will be made available by the authors, without undue reservation.

Ethics statement

The animal study was approved by the Department of Pharmacy, School of Pharmaceutical Sciences, State University of Bangladesh, 77, Satmasjid Road, Dhanmondi, Dhaka-1207, Bangladesh. The study was conducted in accordance with the local legislation and institutional requirements.

References

- Akter, A., Islam, F., Bepary, S., Al-Amin, M., Begh, M. Z. A., Islam, M. A. F. U., et al. (2022). CNS depressant activities of Averrhoa carambola leaves extract in thiopental-sodium model of Swiss albino mice: implication for neuro-modulatory properties. *Biologia* 77 (5), 1337–1346. doi:10.1007/s11756-022-01057-z
- Alam, M. M., Emon, N. U., Alam, S., Rudra, S., Akhter, N., Mamun, M. M. R., et al. (2021). Assessment of pharmacological activities of Lygodium microphyllum Cav. leaves in the management of pain, inflammation, pyrexia, diarrhea, and helminths: *in vivo*, *in vitro* and *in silico* approaches. *Biomed. Pharmacother.* 139, 111644. doi:10.1016/j.biopha.2021.111644
- Alam, S., Emon, N. U., Shahriar, S., Richi, F. T., Haque, M. R., Islam, M. N., et al. (2020). Pharmacological and computer-aided studies provide new insights into Millettia puguensis Ali (Fabaceae). *Saudi Pharm. J.* 28 (12), 1777–1790. doi:10.1016/j.jsps.2020.11.004
- Alam, S., Rashid, M. A., Sarker, M. M. R., Emon, N. U., Arman, M., Mohamed, I. N., et al. (2021a). Antidiarrheal, antimicrobial and antioxidant potentials of methanol

Author contributions

SS: conceptualization, investigation, methodology, validation, visualization, writing–original draft, and writing–review and editing. HH: conceptualization, formal analysis, investigation, methodology, visualization, writing–original draft, and writing–review and editing. SR: conceptualization, formal analysis, investigation, writing–original draft, and writing–review and editing. MI: data curation, methodology, software, and writing–review and editing. FN: data curation, methodology, software, validation, and writing–review and editing. SA: data curation, formal analysis, software, validation, visualization, and writing–review and editing. CS: data curation, formal analysis, software, validation, visualization, and writing–review and editing. SW: data curation, formal analysis, software, validation, visualization, and writing–review and editing. PG: data curation, formal analysis, software, validation, visualization, and writing–review and editing. AM: formal analysis, funding acquisition, investigation, project administration, resources, supervision, visualization, writing–original draft, and writing–review and editing.

Funding

The author(s) declare that financial support was received for the research, authorship, and/or publication of this article. This study was partially supported by the Post-Doctoral Research Start-up Fund of Lishui People's Hospital, Zhejiang, China (2023bsh001).

Conflict of interest

The authors declare that the research was conducted in the absence of any commercial or financial relationships that could be construed as a potential conflict of interest.

Publisher's note

All claims expressed in this article are solely those of the authors and do not necessarily represent those of their affiliated organizations, or those of the publisher, the editors, and the reviewers. Any product that may be evaluated in this article, or claim that may be made by its manufacturer, is not guaranteed or endorsed by the publisher.

extract of Colocasia gigantea Hook. f. leaves: evidenced from *in vivo* and *in vitro* studies along with computer-aided approaches. *BMC Complementary Med. Ther.* 21 (1), 119–212. doi:10.1186/s12906-021-03290-6

Alam, S., Sarker, M. M. R., Afrin, S., Richi, F. T., Zhao, C., Zhou, J. R., et al. (2021b). Traditional herbal medicines, bioactive metabolites, and plant products against COVID-19: update on clinical trials and mechanism of actions. *Front. Pharmacol.* 12, 671498. doi:10.3389/fphar.2021.671498

Alam, S., Sarker, M. M. R., Sultana, T. N., Chowdhury, M. N. R., Rashid, M. A., Chaity, N. I., et al. (2022). Antidiabetic phytochemicals from medicinal plants: prospective candidates for new drug discovery and development. *Front. Endocrinol.* 13, 800714. doi:10.3389/fendo.2022.800714

Al-rubaye, A. F., Hameed, I. H., and Kadhim, M. J. (2017). A review: uses of gas chromatography-mass Spectrometry (GC-MS) technique for analysis of bioactive

natural compounds of some plants. *Nat. Compd. Some Plants* 9 (1), 81–85. doi:10.25258/ijtp.v9i01.9042

Apu, A. S., Bhuyan, S. H., Khatun, F., Liza, M. S., Matin, M., and Hossain, M. F. (2013). Assessment of cytotoxic activity of two medicinal plants using brine shrimp (*Artemia salina*) as an experimental tool. *Int. J. Pharm. Sci. Res.* 4 (3), 1125.

Atta, A. H., and Mouneir, S. M. (2004). Anti-diarrhoeal activity of some Egyptian medicinal plant extracts. *J. Ethnopharmacol.* 92 (2–3), 303–309.

Avois, L., Robinson, N., Saudan, C., Baume, N., Mangin, P., and Saugy, M. (2006). Central nervous system stimulants and sport practice. *Br. J. Sports Med.* 40 (1), i16–i20. doi:10.1136/bjsm.2006.027557

Bahekar, S. E., and Kale, R. S. (2015). Anti-diarrheal activity of ethanolic extract of *Manihot esculenta* Crantz leaves in Wistar rats. *J. Ayurveda Integr. Med.* 6 (1), 35.

Bauer, A. W., Kirby, W. M., Sherris, J. C., and Turck, M. (1996). Antibiotic susceptibility testing by a standardized single disk method. *Am. J. Clin. Pathol.* 45 (4), 493–496. doi:10.1093/ajcp/45.4.ts.493

Billah, M. M., Islam, R., Khatun, H., Parvin, S., Islam, E., Islam, S. A., et al. (2013). Antibacterial, anti-diarrhoeal, and cytotoxic activities of methanol extract and its fractions of *Caesalpinia bonducella* (L.) Roxb leaves. *BMC complementary Altern. Med.* 13, 101–107. doi:10.1186/1472-6882-13-101

Davoodbasha, M., Edachery, H. S., Nooruddin, T., Lee, S. Y., and Kim, J. W. (2018). An evidence of C16 fatty acid methyl esters extracted from microalgae for effective antimicrobial and antioxidant property. *Microb. Pathog.* 115, 233–238. doi:10.1016/j.micpath.2017.12.049

Debnath, P., Ahmad, S. K., Mahedi, R. A., Ganguly, A., and Sarker, K. K. (2022). Bioactive compounds and functional properties of Rambai (*Baccaea motleyana* Müll. Arg.) fruit: a comprehensive review. *Food Sci. Nutr.* 10 (1), 218–226. doi:10.1002/fsn3.2661

Dhingra, S., Rahman, N. A. A., Peile, E., Rahman, M., Sartelli, M., Hassali, M. A., et al. (2020). Microbial resistance movements: an overview of global public health threats posed by antimicrobial resistance, and how best to counter. *Front. Public Health* 8, 535668.

El Azab, I. H., El-Sheshtawy, H. S., Bakr, R. B., and Elkanzi, N. A. (2021). New 1, 2, 3-triazole-containing hybrids as antitumor candidates: design, click reaction synthesis, DFT calculations, and molecular docking study. *Molecules* 26 (3), 708. doi:10.3390/molecules26030708

Elshafie, H. S., Camele, I., and Mohamed, A. A. (2023). A comprehensive review on the biological, agricultural and pharmaceutical properties of secondary metabolites based-plant origin. *Int. J. Mol. Sci.* 24, 3266. doi:10.3390/ijms24043266

Emon, N. U., Alam, S., Rudra, S., Chowdhury, S., Rajbangshi, J. C., and Ganguly, A. (2020). Evaluation of pharmacological potentials of the aerial part of *Achyranthes aspera* L.: *in vivo*, *in vitro* and *in silico* approaches. *Adv. traditional Med.* 22, 141–154. doi:10.1007/s13596-020-00528-5

Fajemiroye, J. O., da Silva, D. M., de Oliveira, D. R., and Costa, E. A. (2016). Treatment of anxiety and depression: medicinal plants in retrospect. *Fundam. Clin. Pharmacol.* 30 (3), 198–215. doi:10.1111/fcp.12186

Gutiérrez, S. P., Mendoza, D. Z., Peredo, C. S., Sánchez, O. S., and Sánchez, M. A. Z. (2014). Evaluation of the anti-diarrheal activity of *Salvia connivens*. *Pharm. Biol.* 52, 1467–1470. doi:10.3109/13880209.2014.898076

Hasnat, H., Shompa, S. A., Richi, F. T., Islam, M. M., Suman, M. H., Ahmed, N. U., et al. (2023). Bioactive secondary metabolites to combat diabetic complications: evidenced from *in silico* study. *Bangladesh Pharm. J.* 26 (2), 167–184. doi:10.3329/bpj.v26i2.67807

He, J., Qiao, W., An, Q., Yang, T., and Luo, Y. (2020). Dihydrofolate reductase inhibitors for use as antimicrobial agents. *Eur. J. Med. Chem.* 195, 112268. doi:10.1016/j.ejmech.2020.112268

Hossain, M. M., Biva, I. J., Jahangir, R., and Vhuiyan, M. M. I. (2009). Central nervous system depressant and analgesic activity of *Aphanamixis polystachya* (Wall.) parker leaf extract in mice. *Afr. J. Pharm. Pharmacol.* 3 (5), 282–286.

Iordache, A., Culea, M., Gherman, C., and Cozar, O. (2009). Characterization of some plant extracts by GC–MS. *Nucl. Instrum. methods Phys. Res. Sect. B* 267 (2), 338–342. doi:10.1016/j.nimb.2008.10.021

Islam, M., Jannat, T., Kuddus, M. R., Rashid, M. A., and Haque, M. R. (2019). *In vitro* and *in vivo* evaluation of pharmacological potentials of *Campsis radicans* L. *Clin. Phytoscience* 5, 1–9. doi:10.1186/s40816-019-0144-9

Islam, M., Kuddus, M. R., Rashid, M. A., and Haque, M. R. (2020). Phytochemical investigations of *Campsis radicans* L. *J. Appl. Pharm. Res.* 8 (3), 55–59. doi:10.18231/j. joapr.2020.v.8.i.3.55.59

Islam, M. A., Alam, S., Saha, T., Akter, F., Hasnat, H., Zaman, A., et al. (2022). Evaluation of biological activities of methanolic extract of leaves of *Bruguiera gymnorhiza* (L.) Lam.: *in vivo* studies using Swiss albino mice model. *Bangladesh Pharm. J.* 25 (1), 26–31. doi:10.3329/bpj.v25i1.57837

Jain, C., Khatana, S., and Vijayvergia, R. (2019). Bioactivity of secondary metabolites of various plants: a review. *Int. J. Mol. Sci.* 20 (2), 494–504.

Jendele, L., Krivak, R., Skoda, P., Novotny, M., and Hoksza, D. (2019). PrankWeb: a web server for ligand binding site prediction and visualization. *Nucleic acids Res.* 47 (W1), W345–W349. doi:10.1093/nar/gkz424

Khatun, M. C. S., Muhit, M. A., Hossain, M. J., Al-Mansur, M. A., and Rahman, S. A. (2021). Isolation of phytochemical constituents from *Stevia rebaudiana* (Bert.) and

evaluation of their anticancer, antimicrobial and antioxidant properties via *in vitro* and *in silico* approaches. *Heliyon* 7 (12), e08475. doi:10.1016/j.heliyon.2021.e08475

Kim, S., Thiessen, P. A., Bolton, E. E., Chen, J., Fu, G., Gindulyte, A., et al. (2016). PubChem substance and compound databases. *Nucleic acids Res.* 44 (D1), D1202–D1213. doi:10.1093/nar/gkv951

Knott, R. M., Robertson, M., Muckersie, E., and Forrester, J. V. (1996). Regulation of glucose transporters (GLUT-1 and GLUT-3) in human retinal endothelial cells. *Biochem. J.* 318 (1), 313–317. doi:10.1042/bj3180313

Kodidela, S., Pradhan, S. C., Muthukumar, J., Dubashi, B., Santos-Silva, T., and Basu, D. (2016). Genotype distribution of dihydrofolate reductase variants and their role in disease susceptibility to acute lymphoblastic leukemia in Indian population: an experimental and computational analysis. *J. Leuk.* 4 (209), 2. doi:10.4172/2329-6917.1000209

Lalthanpuui, P. B., and Lalthandama, K. (2019). Chemical profiling, antibacterial and antiparasitic studies of *Imperata cylindrica*. *J. Appl. Pharm. Sci.* 9 (12), 117–121.

Lee, M. M., Brooksbank, K. J., Wetherall, K., Mangion, K., Roditi, G., Campbell, R. T., et al. (2021). Effect of empagliflozin on left ventricular volumes in patients with type 2 diabetes, or prediabetes, and heart failure with reduced ejection fraction (SUGAR-DM-HF). *Circulation* 143 (6), 516–525.

Lim, T. K., and Lim, T. K. (2012). *Baccaea motleyana*. *Edible Med. Non-Medicinal Plants* 4, 239–242. doi:10.1007/978-94-007-4053-2_33

Lu, Q., Liu, T., Wang, N., Dou, Z., Wang, K., and Zuo, Y. (2020). Nematicidal effect of methyl palmitate and methyl stearate against *Meloidogyne incognita* in bananas. *J. Agric. food Chem.* 68 (24), 6502–6510. doi:10.1021/acs.jafc.0c00218

Mahmud, S., Rafi, M. O., Paul, G. K., Promi, M. M., Shimu, M. S. S., Biswas, S., et al. (2021). Designing a multi-epitope vaccine candidate to combat MERS-CoV by employing an immunoinformatics approach. *Sci. Rep.* 11 (1), 15431. doi:10.1038/s41598-021-92176-1

Meyer, B. N., Ferrigni, N. R., Putnam, J. E., Jacobsen, L. B., Nichols, D. E. J., and McLaughlin, J. L. (1982). Brine shrimp: a convenient general bioassay for active plant constituents. *Planta medica*. 45 (05), 31–34. doi:10.1055/s-2007-971236

Meyer, J. H., Ginovart, N., Boovariwala, A., Sagrati, S., Hussey, D., Garcia, A., et al. (2006). Elevated monoamine oxidase levels in the brain: an explanation for the monoamine imbalance of major depression. *Archives general psychiatry* 63 (11), 1209–1216. doi:10.1001/archpsyc.63.11.1209

Mohamed, S., Hassan, Z., and Hamid, N. A. (1994). Antimicrobial activity of some tropical fruit wastes (guava, starfruit, banana, papaya, passionfruit, langsat, duku, rambutan and rambai). *Pertanika* 17, 219.

Mojica, L., de Mejia, E. G., Granados-Silvestre, M. Á., and Menjivar, M. (2017). Evaluation of the hypoglycemic potential of a black bean hydrolyzed protein isolate and its pure peptides using *in silico*, *in vitro* and *in vivo* approaches. *J. Funct. Foods* 31, 274–286. doi:10.1016/j.jff.2017.02.006

Murray, C. J., Ikuta, K. S., Sharara, F., Swetschinski, L., Aguilar, G. R., Gray, A., et al. (2022). Global burden of bacterial antimicrobial resistance in 2019: a systematic analysis. *Lancet* 399 (10325), 629–655. doi:10.1016/S0140-6736(21)02724-0

Nesa, M. L., Karim, S. S., Api, K., Sarker, M. M. R., Islam, M. M., Kabir, A., et al. (2018). Screening of *Baccaea ramiflora* (Lour.) extracts for cytotoxic, analgesic, anti-inflammatory, neuropharmacological and anti-diarrheal activities. *BMC Complement Altern. Med.* 18, 1–9.

Niksic, H., Becic, F., Koric, E., Gusic, I., Omeragic, E., Muratovic, S., et al. (2021). Cytotoxicity screening of *Thymus vulgaris* L. essential oil in brine shrimp nauplii and cancer cell lines. *Sci. Rep.* 11 (1), 13178.

Nisar, B., Sultan, A., and Rubab, S. L. (2018). Comparison of medicinally important natural products versus synthetic drugs—a short commentary. *Nat. Prod. Chem. Res.* 6 (2), 308. doi:10.4172/2329-6836.1000308

Nurmayani, S., Widodo, W. D., and Matra, D. D. (2021). Characterization of rambai (*Baccaea motleyana*) genes putatively involved in sugar metabolism. *IOP Conf. Ser. Earth Environ. Sci.* 694 (1), 012067. doi:10.1088/1755-1315/694/1/012067

Obaidullah, A. J., Alanazi, M. M., Alsaif, N. A., Mahdi, W. A., Fantoukh, O. I., Tareq, A. M., et al. (2021). Deeper insights on *Cnesmone javanica* blume leaves extract: chemical profiles, biological attributes, network pharmacology and molecular docking. *Plants* 10 (4), 728. doi:10.3390/plants10040728

Ongko, J., Setiawan, J. V., Feroniytha, A. G., Juliana, A., Effraim, A., Wahjudi, M., et al. (2022). In-silico screening of inhibitor on protein epidermal growth factor receptor (EGFR). *IOP Conf. Ser. Earth Environ. Sci.* 1041 (1), 012075. doi:10.1088/1755-1315/1041/1/012075

Pannemans, J., and Corsetti, M. (2018). Opioid receptors in the GI tract: targets for treatment of both diarrhea and constipation in functional bowel disorders? *Curr. Opin. Pharmacol.* 43, 53–58. doi:10.1016/j.coph.2018.08.008

Prodhan, A. S. U., and Mridu, F. S. (2021). *Baccaea motleyana* (Rambai): nutritional, phytochemical, and medicinal overview. *Adv. Traditional Med.* 23, 11–35. doi:10.1007/s13596-021-00555-w

Rahman, J., Tareq, A. M., Hossain, M. M., Sakib, S. A., Islam, M. N., Ali, M. H., et al. (2020). Biological evaluation, DFT calculations and molecular docking studies on the antidepressant and cytotoxicity activities of *Cycas pectinata* buch.-ham. Compounds. *Buch.-Ham. Compd. Pharm.* 13 (9), 232. doi:10.3390/ph13090232

- Rahman, M. A., Sultana, R., Bin Emran, T., Islam, M. S., Rahman, M. A., Chakma, J. S., et al. (2013). Effects of organic extracts of six Bangladeshi plants on *in vitro* thrombolysis and cytotoxicity. *BMC complementary Altern. Med.* 13, 25–27. doi:10.1186/1472-6882-13-25
- Ramayani, P., and Fitmawati, (2020). Keanekaragaman rambai (*Baccaurea motleyana* (müll. arg.) di pulau bengkalis berdasarkan karakter morfologi. *Bul. Kebun Raya* 23 (1), 46–58. doi:10.14203/bkr.v23i1.5
- Rao, R., and Tripathi, R. (2022). “Stimulants and sleep, in *Sleep and Neuropsychiatric Disorders*”. Singapore: Springer Nature Singapore, 811–833.
- Rashid, P. T., Hossain, M. J., Zahan, M. S., Hasan, C. M., Rashid, M. A., Al-Mansur, M. A., et al. (2023). Chemico-pharmacological and computational studies of *Ophiorrhiza fasciculata* D. Don and *Psychotria silhetensis* Hook. f. focusing cytotoxic, thrombolytic, anti-inflammatory, antioxidant, and antibacterial properties. *Heliyon* 9 (9), e20100. doi:10.1016/j.heliyon.2023.e20100
- Santosh, P., Venugop, R., Nilakash, A. S., Kunjibihari, S., and Mangala, L. (2011). Antidepressant activity of methanolic extract of *Passiflora foetida* leaves in mice. *Int. J. Pharm. Pharm. Sci.* 3 (1), 112–5.
- Schiff, D., Wen, P. Y., and Van Den Bent, M. J. (2009). Neurological adverse effects caused by cytotoxic and targeted therapies. *Nat. Rev. Clin. Oncol.* 6 (10), 596–603. doi:10.1038/nrclinonc.2009.128
- Shaaban, M. T., Ghaly, M. F., and Fahmi, S. M. (2021). Antibacterial activities of hexadecanoic acid methyl ester and green-synthesized silver nanoparticles against multidrug-resistant bacteria. *J. basic Microbiol.* 61 (6), 557–568. doi:10.1002/jobm.202100061
- Singab, A. N., Youssef, F. S., and Ashour, M. L. (2014). Medicinal plants with potential antidiabetic activity and their assessment. *Med. Aromat. Plants* 3 (151), 2167–0412. doi:10.4172/2167-0412.1000151
- Sisay, M., Engidawork, E., and Shibeshi, W. (2017). Evaluation of the antidiarrheal activity of the leaf extracts of *Myrtus communis* Linn (Myrtaceae) in mice model. *BMC complementary Altern. Med.* 17, 103–111. doi:10.1186/s12906-017-1625-3
- Sisillia, L. (2009). *Aktivitas antibakteri zat ekstraktif kulit kayu Rambai (Baccaurea motleyana Muell. Arg.)*.
- Tafesse, T. B., Hymete, A., Mekonnen, Y., and Tadesse, M. (2017). Antidiabetic activity and phytochemical screening of extracts of the leaves of *Ajuga remota* Benth on alloxan-induced diabetic mice. *BMC complementary Altern. Med.* 17 (1), 243–249. doi:10.1186/s12906-017-1757-5
- Taher, M. A., Laboni, A. A., Shompa, S. A., Rahman, M. M., Hasan, M. M., Hasnat, H., et al. (2023). Bioactive compounds extracted from leaves of *G. cyanocarpa* using various solvents in chromatographic separation showed anti-cancer and anti-microbial potentiality in *in silico* approach. *Chin. J. Anal. Chem.* 51 (12), 100336. doi:10.1016/j.cjac.2023.100336
- Twaij, B. M., and Hasan, M. N. (2022). Bioactive secondary metabolites from plant sources: types, synthesis, and their therapeutic uses. *Int. J. Plant Biol.* 13 (1), 4–14. doi:10.3390/ijpb13010003
- VanWagenen, B. C., Larsen, R., Cardellina, J. H., Randazzo, D., Lidert, Z. C., and Swithenbank, C. (1993). Ulosantoin, a potent insecticide from the sponge *Ulosa ruetzleri*. *J. Org. Chem.* 58 (2), 335–337. doi:10.1021/jo00054a013
- Vijayakumar, K., and MuhilVannan, S. (2021). 3, 5-Di-tert-butylphenol combat against *Streptococcus mutans* by impeding acidogenicity, aciduranc and biofilm formation. *World J. Microbiol. Biotechnol.* 37 (12), 202. doi:10.1007/s11274-021-03165-5
- Weinberg, R. A. (1996). How cancer arises. *Sci. Am.* 275 (3), 62–70. doi:10.1038/scientificamerican0996-62
- Yu, Z. F., Kong, L. D., and Chen, Y. (2002). Antidepressant activity of aqueous extracts of *Curcuma longa* in mice. *J. Ethnopharmacol.* 83(1–2), 161–165.
- Zaman, A., Hasnat, H., Al Noman, Z., Islam, M. M., Al Nakib, A., Mukherjee, S., et al. (2023). Exploring pharmacological potentials of p-coumaric acid: a prospective phytochemical for drug discovery. *Bangladesh Pharm. J.* 26 (2), 185–194. doi:10.3329/bpj.v26i2.67808
- Zhao, F., Wang, P., Lucardi, R. D., Su, Z., and Li, S. (2020). Natural sources and bioactivities of 2, 4-di-tert-butylphenol and its analogs. *Toxins* 12 (1), 35. doi:10.3390/toxins12010035
- Zimmermann, M. (1983). Ethical guidelines for investigations of experimental pain in conscious animals. *Pain* 16, 109–110. doi:10.1016/0304-3959(83)90201-4



OPEN ACCESS

EDITED BY

Saša Đurović,
Institute of General and Physical Chemistry,
Serbia

REVIEWED BY

Darko Micić,
Institute of General and Physical Chemistry,
Serbia
Snežana Filip,
University of Novi Sad, Serbia

*CORRESPONDENCE

Safaet Alam,
✉ safaet.du@gmail.com
Abdullah Al Mamun,
✉ pharmaalmamun@yahoo.com

RECEIVED 30 November 2023

ACCEPTED 10 January 2024

PUBLISHED 01 March 2024

CITATION

Shahriar S, Shermin SA, Hasnat H, Hossain F,
Han A, Geng P, Alam S and Mamun AA (2024),
Chemico-pharmacological evaluation of the
methanolic leaf extract of *Catharanthus ovalis*:
GC–MS/MS, *in vivo*, *in vitro*, and *in*
silico approaches.
Front. Pharmacol. 15:1347069.
doi: 10.3389/fphar.2024.1347069

COPYRIGHT

© 2024 Shahriar, Shermin, Hasnat, Hossain,
Han, Geng, Alam and Mamun. This is an open-
access article distributed under the terms of the
Creative Commons Attribution License (CC BY).
The use, distribution or reproduction in other
forums is permitted, provided the original
author(s) and the copyright owner(s) are
credited and that the original publication in this
journal is cited, in accordance with accepted
academic practice. No use, distribution or
reproduction is permitted which does not
comply with these terms.

Chemico-pharmacological evaluation of the methanolic leaf extract of *Catharanthus ovalis*: GC–MS/MS, *in vivo*, *in vitro*, and *in silico* approaches

Saimon Shahriar ¹, Samia Akter Shermin¹, Hasin Hasnat ¹,
Faisal Hossain¹, Aixia Han², Peiwu Geng², Safaet Alam ^{3*} and
Abdullah Al Mamun ^{2*}

¹Department of Pharmacy, School of Pharmaceutical Sciences, State University of Bangladesh, Dhaka, Bangladesh, ²Central Laboratory of The Sixth Affiliated Hospital of Wenzhou Medical University, Lishui People's Hospital, Lishui, Zhejiang, China, ³Drugs and Toxins Research Division, BCSIR Laboratories Rajshahi, Bangladesh Council of Scientific and Industrial Research, Rajshahi, Bangladesh

Introduction: Natural plant-based medicines have gained popularity recently as a major source of inventive, risk-free, and more potent secondary bioactive compounds with medicinal potential. *Catharanthus ovalis* is a perennial shrub containing various indole alkaloids cultivated extensively for local medical purposes.

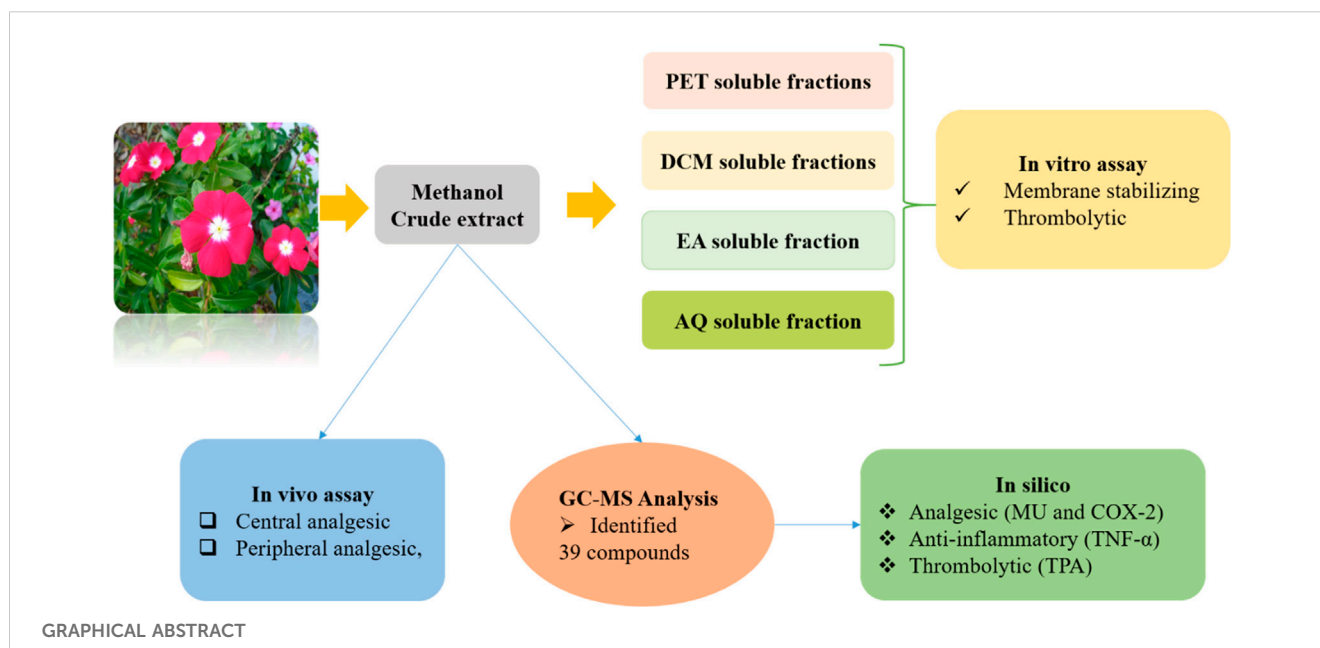
Methods: This research is conducted to identify the phytochemicals present in the leaves of *C. ovalis* and its central and peripheral analgesic, thrombolytic, and membrane-stabilizing activities through tail immersion, acetic acid-induced writhing, human blood clot lysis, and erythrocyte lysis by heat and hypotonic solution methods, respectively.

Results and discussion: A total of 39 compounds were identified using GC–MS/MS techniques, including hexadecanoic acid, methyl ester (56.749%), methyl stearate (29.782%), carvacrol and its TBDMS derivative (12.586%), and 9-octadecenoic acid, methyl ester, (E)- (9.297%) presented in high quantity. The highest tail immersion latency was observed for the 600 mg/kg extract of *C. ovalis* crude extract. Both 400 and 600 mg/kg doses of *C. ovalis* crude extract exhibited prominent peripheral analgesic activity. The maximum thrombolytic effect was observed by DCM soluble fraction extract by inhibiting 54.87% of the clot. However, the aqueous-soluble fraction of this extract manifested an excellent membrane-stabilizing effect by showing 73.98% and 87.51% hemolysis against heat- and hypotonic-induced hemolysis, respectively. Some of the compounds were identified as active agents against different receptors related to these diseases, which supported the findings of *in vitro* and *in vivo* tests.

Conclusion: Further investigation needs to be conducted to specify and identify the exact mechanism of action of these compounds.

KEYWORDS

phytochemical, GC–MS/MS, *Catharanthus ovalis*, membrane stabilizing, analgesic, thrombolytic, *in silico*, *in vitro*



1 Introduction

Since ancient times, plants have been used as excellent sources of medicines to treat many illnesses. Recently, natural plant-based products have drawn attention as a key source of creative, safer, and more potent secondary bioactive metabolites with therapeutic potential. Nearly 80% of all pharmaceuticals are either wholly or partially derived from plants (Obonti et al., 2021). According to the World Health Organization (WHO), 80% of people utilize herbal medicines as part of their primary healthcare. Plant-based treatments are anticipated to make up to 25% of all drugs in developed nations such as the United States while making up to 80% of all drugs in rapidly growing nations such as India and China. Even in the modern period, plants are still a potential source of medication for serious illnesses such as cancer, oxidative stress, cancer, diarrhea, depression, fever, and thrombosis (Islam et al., 2022). It has been demonstrated that *in vitro* screening techniques can offer essential initial observations required to choose crude plant extracts with potentially beneficial features for additional chemical and pharmacological research (Mathekg and Meyer, 1998).

Catharanthus is a genus of flowering plants of the Apocynaceae (dogbane) family (Tolambiya and Mathur, 2016). It has glossy opposing leaves, and its stunning five-petaled flowers come in a range of pink, white, and purple hues and can be distinguished by its evergreen, herbaceous, or subshrubby habit (Mishra and Verma et al., 2017). Typically, there are eight species in this genus, seven of which are native to Madagascar, namely, *Catharanthus coriaceus*, *Catharanthus lanceus*, *Catharanthus longifolius*, *C. ovalis*, *Catharanthus roseus*, *Catharanthus scitulus*, and *Catharanthus trichophyllus*, and one of which, namely, *Catharanthus pusillus*, has been reported from India (Alam et al., 2017). Historically, the Caribbean native plant family Apocynaceae has been utilized for a variety of medical conditions; especially, European herbalists used plants of these

families for diabetes and illnesses as diverse as headaches, as well as for wound healing (Kabesh et al., 2015).

However, the *Catharanthus* genus is well known for its diverse phytochemical composition, especially for the high concentrations of alkaloids, terpenoids, and flavonoids. Vinblastine and vincristine are two of the most noteworthy alkaloids and have received much attention for their powerful anticancer properties. In addition, several other bioactive substances have been discovered, contributing to a variety of pharmacological actions (Pham et al., 2020). *Catharanthus roseus*, the most common species of the *Catharanthus* genus rooted in traditional folklore, is revered for its diverse applications in treating burns, rheumatism, and menstrual disorders and its potential in managing hypertension, diabetes, and cancer and supporting uterine contractions (Chaturvedi et al., 2022; De et al., 2022).

Catharanthus ovalis Markgr., a perennial plant, typically grows in dry shrubland or desert biomes and can grow up to 40 cm in height (Tropical Plants Database, 2023). Although indigenous to southern Madagascar and Africa, it is cultivated extensively for local medical purposes. Historically, the plant's pure extract was consumed as a trial poison. Additionally, worms are expelled using an extract of the aerial sections. Indole alkaloids, including many bisindole alkaloids, are abundant in this species. On the other hand, it comprises several pharmacologically effective chemicals such as leurosine, vindoline, vindolinine, coronaridine, catharanthine, and vinblastine (Tropical Plants Database, 2023). Despite its recognized medicinal potency, there is a notable absence of comprehensive pharmacological research on this species, limiting our understanding of its full therapeutic potential and applications. The purpose of this investigation was to identify the phytochemicals present in the *C. ovalis* leaf tissue through GC-MS/MS techniques. Additionally, this study used *in vivo* and *in vitro* methodologies to examine several biological functions of the leaf extract. However, the *in silico* approach was adopted for the preliminary screening of the

identified phytochemicals responsible for those biological activities.

2 Materials and methods

2.1 Plant material

Catharanthus ovalis Markgr. was collected from Sylhet, Bangladesh, and was identified by the Bangladesh National Herbarium with an accession number of DACB 88049. The plant is prepared and preserved in the phytochemical research laboratory of the Department of Pharmacy at the State University of Bangladesh.

2.2 Preparation of extract and subsequent fractions

The *C. ovalis* leaf material was taken from the wild, shade-dried, and turned into a powder using a mechanical grinder. The needed amount of leaf powder was weighed, transferred to a flask, totally submerged in methanol, incubated for 15 days, and then, filtered. Following that, a rotary evaporator was used to concentrate the filtered extract (Islam et al., 2020). The concentrated extract contains both polar and nonpolar plant material components, and 2 μ L of the sample solution was used in GC–MS/MS for chemical analysis.

Solvent–solvent partitioning was conducted using the process described by VanWagenen et al. (1993). A measure of 5 g of the crude methanolic extract of *C. ovalis* (COCME) was dissolved in 10% aqueous methanol and then extracted sequentially with petroleum ether, dichloromethane, ethyl acetate, and finally, water to obtain four respective fractions: petroleum ether-soluble fraction (COPESEF), dichloromethane-soluble fraction (CODMSF), ethyl acetate-soluble fraction (COEASF), and aqueous-soluble fraction (COASF). All the fractions were evaporated to dryness and were used for further analysis.

2.3 Phytochemical analysis

2.3.1 GC–MS/MS analysis and the identification of phytochemicals

A GCMS-TQ8040 GC–MS/MS (Shimadzu, Japan) system with an Elite-5MS (5% diphenyl/95% dimethyl polysiloxane) and a fused capillary column (30 0.25 m ID 0.25 m df) was used to conduct the GC–MS/MS analysis of the methanolic extract of *C. ovalis*. The electron ionization system employed for GC–MS/MS detection operated in an electron impact mode with an ionization energy of 70 eV. An electron ionization system with an ionization energy of 70 eV was run in an electron impact mode for GC–MS/MS detection. As a carrier gas, helium gas (99.999%) was used with an injection volume of 2 μ L and a constant flow rate of 1 mL/min (a split ratio of 10:1). The oven temperature was programmed to start at 50°C (isothermal for 1 min), increase by 15°C/min to 200°C, then 5°C/min to 300°C, and end with a 7 min isothermal at 300°C. The injector temperature was kept at 250°C. At a scan speed of 2000,

mass spectra were collected at 70 eV. The entire running time for the GC/MS was 36 min, and the solvent delay was 3.50 min. The spectrum was measured between 50 and 600 m/z. Comparing each component's average peak area to the total areas allowed us to determine the proportional percentage amount of each component. The identification of compounds using GC–MS spectra involved leveraging the National Institute of Standards and Technology (NIST) database, which contains approximately 62,000 patterns. The spectra of the unknown components were compared against both the known components stored in the NIST collection and the database's extensive collection of patterns. The NIST database, which contains more than 62,000 patterns, was used for the GC–MS/MS experiment. A comparison was made between the spectra of the unknown components and the spectrum of known components kept in the NIST collection. The components of the test materials' names, molecular weights, and structures were determined and listed in Table 1 (Sermakkani and Thangapandian, 2012).

2.4 In vitro test

2.4.1 In vitro thrombolytic activity

Streptokinase (SK) was used as the reference standard for the evaluation of the thrombolytic activity of crude methanolic extract (COCME), petroleum ether soluble fraction (COPESEF), dichloromethane soluble fraction (CODMSF), ethyl acetate soluble fraction (COEASF), and aqueous-soluble fraction (COASF) of the leaf extract of *C. ovalis* using the technique developed by Prasad et al. (2006).

At first, six Eppendorf tubes were weighed, and then, 500 μ L of the volunteers' venous blood was placed in each tube and incubated for 45 min at 37°C. After the coagulation formed, the serum was removed from this tube. To confirm the weight of the clot, each tube was reweighed. Then, 100 μ L of aforementioned fractions and standard streptokinase were correctly added to each Eppendorf tube. Each tube underwent a further 90-min incubation at 37°C for coagulation. After incubation, the fluid was removed, and the tubes were weighed again to measure the weight change following clot disruption. The final percentage of clot lysis was determined by measuring the weight difference before and after the clot lysis process.

The ultimate percentage of clot lysis was calculated using the weight difference between before and after clot lysis.

$$\% \text{ clot lysis} = \frac{\text{Weight of the lysis clot}}{\text{Weight of the clot before lysis}} \times 100\%.$$

2.4.2 In vitro membrane-stabilizing activity

The approach published in the work of Sikder et al. (2012) was used to assess the membrane-stabilizing ability of the plant samples. This method involves hemolysis brought on by heat and hypotonic solution. The blood was collected, and ethylenediaminetetraacetic acid was used as an anticoagulant. Then, the blood was washed with an isotonic solution (0.9% NaCl) and centrifuged for 10 min at 3,000 rpm speed. This washing was carried out three times, and finally, the stock erythrocyte was collected.

TABLE 1 A total number of 39 compounds identified by GC–MS/MS analysis from the leaf extract of *C. ovalis* with their molecular weight and PubChem ID.

Serial	Retention time	% concentration	Compound	Molecular weight	Formula	PubChem ID
1	3.526	12.59	Carvacrol, TBDMS derivative	264.48	C ₁₆ H ₂₈ OSi	13581204
2	3.7	4.50	3,3-Dimethoxy-2-butanone	132.16	C ₆ H ₁₂ O ₃	140871
3	3.815	5.29	3,5-Octadienedioic acid, dimethyl ester	398.5	C ₁₆ H ₁₄ O ₄ S ₄	11502178
4	3.895	2.86	3-Methylbenzyl alcohol, TBDMS derivative	384.7	C ₁₇ H ₃₂ O ₄ Si ₃	22967275
5	4.18	2.46	Cyclopentene, 1-ethenyl-3-methylene-	68.12	C ₅ H ₈	8882
6	4.369	1.25	p-Xylene	106.16	C ₈ H ₁₀	7809
7	4.379	2.82	Dibenzo[b,f][1,4]diazocine, 5,6,11,12-tetrahydro-5-methyl-	206.24	C ₁₄ H ₁₀ N ₂	11969075
8	8.655	0.46	2,6-Dihydroxyacetophenone, 2TMS derivative	296.51	C ₁₄ H ₂₄ O ₃ Si ₂	91740707
9	10.817	1.82	Phenol, 3,5-bis(1,1-dimethylethyl)-	206.32	C ₁₄ H ₂₂ O	70825
10	10.901	2.28	3-Hydroxymandelic acid, 3TMS derivative	384.7	C ₁₇ H ₃₂ O ₄ Si ₃	522304
11	14.232	1.12	2,6-Dihydroxybenzoic acid, 3TMS derivative	370.66	C ₁₆ H ₃₀ O ₄ Si ₃	520869
12	15.661	56.75	Hexadecanoic acid, methyl ester	270.5	C ₁₇ H ₃₄ O ₂	8181
13	15.885	1.55	10-Hydroxydecanoic acid, methyl ester	202.29	C ₁₁ H ₂₂ O ₃	520259
14	15.9	1.99	Tetradecanoic acid, 12-methyl-, methyl ester	256.42	C ₁₆ H ₃₂ O ₂	21206
15	15.94	1.99	Tridecanoic acid, 4,8,12-trimethyl-, methyl ester	270.5	C ₁₇ H ₃₄ O ₂	560155
16	17.68	0.42	Cyclooctasiloxane, hexadecamethyl-	593.2	C ₁₆ H ₄₈ O ₈ Si ₈	11170
17	18.377	9.30	9-Octadecenoic acid, methyl ester, (E)-	296.5	C ₁₉ H ₃₆ O ₂	5280590
18	18.806	29.78	Methyl stearate	298.5	C ₁₉ H ₃₈ O ₂	8201
19	18.96	5.58	Heneicosanoic acid, methyl ester	340.6	C ₂₂ H ₄₄ O ₂	22434
20	19.06	2.44	Methyl 9-methyltetradecanoate	256.42	C ₁₆ H ₃₂ O ₂	554137
21	19.105	0.94	Tetradecanoic acid, 5,9,13-trimethyl-, methyl ester	284.5	C ₁₈ H ₃₆ O ₂	554056
22	21.613	1.35	Heneicosane	296.6	C ₂₁ H ₄₄	12403
23	23.241	1.59	Eicosane	282.5	C ₂₀ H ₄₂	8222
24	24.829	3.96	2-Methylhexacosane	380.7	C ₂₇ H ₅₆	150931
25	24.903	5.37	9-Hexadecenoic acid, methyl ester, (Z)-	268.4	C ₁₇ H ₃₂ O ₂	643801
26	29.28	0.44	3,7-Dimethyl-6-nonen-1-ol	212.33	C ₁₃ H ₂₄ O ₂	5363308
27	30.859	0.63	Distearin	625	C ₃₉ H ₇₆ O ₅	102615
28	31.23	0.28	2-Naphthalenemethanol, 1-(dimethylamino)-1,2,3,4,4a,5,6,8a-octahydro- $\alpha,\alpha,\alpha,\alpha$ -tetramethyl-	265.4	C ₁₇ H ₃₁ NO	558550
29	31.343	0.28	4,5-Dichloro-2-nitrobenzoic acid	236.01	C ₇ H ₃ Cl ₂ NO ₄	583642
30	32.13	0.53	Trispiro[4.2.4.2.4.2.]heneicosane	288.5	C ₂₁ H ₃₆	566316
31	32.505	0.35	Methyl 9-heptadecenoate or 9–17:1	282.5	C ₁₈ H ₃₄ O ₂	10902087
32	32.95	1.30	3-Methylsalicylic acid, 2TMS derivative	296.51	C ₁₄ H ₂₄ O ₃ Si ₂	624536
33	33.575	0.38	Traumatic acid, (E)-, 2TMS derivative	372.6	C ₁₈ H ₃₆ O ₄ Si ₂	5463675
34	34.44	1.03	Dihydroartemisinin, 10-O-(t-butyloxy)-	356.5	C ₁₉ H ₃₂ O ₆	537898

2.4.2.1 Hemolysis induced by a hypotonic solution

A hypotonic solution was used during the experimentation. The test material, including COCME, COPESF, CODMSF, COEASF, and COASF at a dose of 2.0 mg/mL and aspirin (standard) at a dose of 0.10 mg/mL, was mixed separately with 0.5 mL stock erythrocyte suspension, 4.5 mL hypotonic solution (0.3% NaCl), and 10 mM

sodium phosphate buffer (pH 7.4). For the negative control group, water is used in place of the test material. The mixes underwent a 10-min incubation at room temperature, followed by a 10-min centrifugation at 3,000 rpm.

Finally, the supernatant's absorbance [optical density (OD)] was taken at 540 nm using a UV spectrophotometer.

The hemolysis percentage was calculated using the following equation:

$$\% \text{ hemolysis} = 1 - \frac{OD2}{OD1} \times 100\%.$$

Here, OD1 is the optical density of the hypotonic-buffered saline solution alone (control group); OD2 is the optical density of the test sample in the hypotonic solution.

2.4.2.2 Hemolysis induced by heat

At first, 4.5 mL of isotonic solution and 10 mM sodium phosphate buffer solution and the standard aspirin at a dose of 0.10 mg/mL or the abovementioned samples at a dose of 1 mg/mL were poured into two sets of different centrifugal tubes. Then, 30 μ L of stock erythrocytes were mixed with each of the tubes. One set of tubes was incubated in a water bath at 54°C for 20 min. The second pair was kept in an ice bath at 0°C–50°C for the same time. After that, these mixtures were centrifuged for 3 min at 3,000 rpm speed, and then, UV spectrophotometric absorbance was taken at 540 nm.

The hemolysis percentage was calculated using the following equation:

$$\% \text{ hemolysis} = 1 - \frac{OD2 - OD1}{OD3 - OD1} \times 100\%.$$

Here, OD 1 is the test sample unheated, OD 2 is test sample heated, and OD 3 is the control sample heated.

2.5 In vivo test

2.5.1 Test animal

Swiss albino mice aged 4–5 weeks of either sex were procured from the International Center for Diarrheal Disease and Research in Bangladesh for use in *in vivo* biological experiments (ICDDR, B). They received free access to rodent chow and water while being housed at a constant room temperature of 24°C \pm 2°C and relative humidity levels of 60%–70% for 12 h of light and darkness. However, food was withheld 12 h prior to the experiment and throughout its duration. The care and use of experimental animal guidance were followed in conducting the studies. The institution's ethics committee gave its approval to the procedures for using animals in the tests.

2.5.2 Study design for the *in vivo* test

The experimental models consisted of five groups of Swiss albino mice, with each group containing four mice, and the assignment to the groups was performed randomly. For the various experimental models, five groups of three Swiss albino mice were randomly assigned, where each group contained four mice. The negative control group, serving as the first group, received 10 mL/kg of distilled water. The first group acted as

the negative control and received 10 mL/kg of distilled water. The second group acted as the experiment's positive control and was administered normal medications. The third, fourth, and fifth groups received 200, 400, and 600 mg/kg b.w dose of COCME, respectively.

2.5.3 In vivo central analgesic activity

The tail immersion method described by Ezeja et al. (2011) was used to determine the central analgesic activity of COCME. Diclofenac sodium (50 mg/kg bw) solution was administered as standard. COCME (200, 400, and 600 mg/kg bw) for test groups and distilled water for the negative control group were administered orally. In order to conduct the test, 1–2 cm of the mouse's tail was dipped into a water bath filled with warm water that was kept at a constant temperature of 55°C. The mouse's tail deflection time was timed at 0, 30, 60, and 90 min after the treatments were administered.

The following equation was used to calculate the % time elongation, which was then compared to the reference value to assess the central analgesic action.

The central analgesic action of the group increases with group elongation %.

$$\% \text{ time elongation} = \frac{T_{\text{test}} - T_{\text{control}}}{T_{\text{control}}} \times 100\%.$$

Here, T_{test} is the average time of tail deflection in the test group, and T_{control} is the average time of tail deflection in the control group.

2.5.4 In vivo peripheral analgesic activity

To ascertain the peripheral analgesic effect of *C. ovalis* in albino mice, the acetic acid-induced writhing test was carried out as previously reported (Satyanarayana et al., 2004). Diclofenac sodium (50 mg/kg bw) solution was injected intraperitoneally as standard. Test groups were given three different doses including 200, 400, and 600 mg/kg bw of COCME, and the negative control group was given only distilled water. After 30 min of sample administration, glacial acetic acid (0.1 mL/30 mg bw) was injected through the intraperitoneal route. For each group of mice, the number of abdominal constrictions, or writhes, was measured from 5 min after the injection of acetic acid until 10 min later, and the percentage inhibition of writhing was calculated using the following formula to assess the peripheral analgesic activity:

$$\% \text{ inhibition of writhing} = \frac{W_{\text{test}} - W_{\text{control}}}{W_{\text{control}}} \times 100\%.$$

Here, W_{test} refers to the average number of writhing in the test group, and W_{control} refers to that in the control group.

2.6 In silico study

2.6.1 Docking software

The molecules were subjected to computational docking analysis, employing widely recognized software applications such as PyRx, PyMOL 2.3, Discovery Studio 4.5, and Swiss-PdbViewer, to explore their molecular interactions and binding affinities in a virtual environment (Hasnat et al., 2023).

2.6.2 Molecular docking: ligand preparation

The structures of 39 isolated compounds of the *C. ovalis* leaf extract and aspirin (PubChem CID- 2,244), diclofenac sodium (PubChem CID- 3,033), and streptokinase (PubChem CID- 9815560) were downloaded from the PubChem database and are presented in Table 1 (<https://pubchem.ncbi.nlm.nih.gov/>). In order to obtain the best possible hit rate against the aforementioned targets, the ligands were downloaded in the 3DSDF format. These ligands, along with their PubChem CIDs, were serially loaded in the Discovery Studio 4.5. It should be mentioned that the Pm6 semiempirical technique was used to optimize all phytochemicals in order to improve docking accuracy (Bikadi and Hazai, 2009).

2.6.3 Molecular docking: protein preparation

Three-dimensional crystal structures, including the mu-opioid receptor (PDB ID: 5C1M) for central analgesic activity (Ahmed *et al.*, n.d.), cyclooxygenase-2 (COX-2) [PDB ID: 1CX2] for peripheral analgesic activity (Muhammad *et al.*, 2015), tumor necrosis factor alpha (TNF- α) [PDB ID: 2AZ5] for membrane-stabilizing activity (Kumar *et al.*, 2021), and tissue plasminogen activator (TPA) [PDB ID: 1A5H] for thrombolytic activity (Emon *et al.*, n.d.), were collected from the RCSB Protein Data Bank (<https://www.rcsb.org/structure>) in the PDB format. Using Discovery Studio 2020, all of the water and the heteroatoms were taken out of the proteins. Then, using the Swiss-PdbViewer's energy reduction software, all the biomolecules were organized by adding nonpolar hydrogen atoms and kept in their lowest energy state for future research.

2.6.4 Ligand–protein interaction

To forecast potential binding profiles of isolated compounds with their binding affinities to the target molecules, the present computer-aided ligand–protein interaction was drawn (Bikadi and Hazai, 2009). Regarding the process of linking molecular drugs to proteins, for this molecular drug–protein linking procedure, highly sophisticated PyRxAutodock Vina was used, and semi-flexible modeling was used for the molecular docking. Initially, the protein was loaded and prepared to interact with the target macromolecule. To ensure specific ligand binding to the target, we selected amino acids with their respective IDs from the literature. The protein was first loaded and formatted to the target macromolecule, and the literature-based amino acids with their ID were chosen to ensure target-specific ligand binding.

For the 5C1M target, Asp 147, Tyr 148, Met 151, Lys 233, Trp 293, Ile 296, His 297, Val 300, Ile 322, Gly 325, and Tyr 326 amino acids from A chain were selected for site-targeted docking (Ahmed *et al.*, 2021). However, His 90, Gln 192, Val 349, Leu 352, Ser 353, Tyr 355, Tyr 385, Ala 516, Phe 518, Val 523, Ala 527, and Ser 530 amino acids of 1CX2 were selected (Muhammad *et al.*, 2015). As standard, diclofenac sodium was used to check its affinity with these receptors. Additionally, TYR 59, TYR 119, LEU 120, GLY 121, and TYR 151 amino acids of the A chain and TYR 59, SER60, GLN 61, TYR 119, LEU 120, and GLY 121 amino acids of the B chain of 2AZ5 were picked for site-specific docking (Kumar *et al.*, 2021). Here, aspirin was used as standard. Using PrankWeb, Arg 39, Leu 41, Cys 42, His 57, Cys 58, Gln 60, Glu

60A, Phe 60C, Tyr 99, Tyr 151, Asp 189, Ala 190, Cys 191, Gln 192, Gly 193, Ser 195, Ile 213, Ser 214, Trp 215, Gly 216, Leu 217, Gly 219, Val 224, Pro 225, Gly 226, Val 227, and Tyr 228 amino acids of 1A5H were chosen for site-specific docking (Jendele *et al.*, 2019). Streptokinase was employed as a reference and as a thrombolytic drug to determine the binding affinity with 1A5H and compare it to the identified compounds' affinity toward the receptor.

Next, in order to find the most optimal binding interactions with the selected macromolecules, all the ligands' PDB files were imported and then converted to the pdbqt format using the Open Babel tool within the PyRxAutoDock Vina software. Subsequently, the minimized ligand structures were employed for docking simulations.

Second, to match the best optimal hit during the docking against these selected macromolecules, all the PDB files of the ligands were imported and afterward minimized into the pdbqt format with the Open Babel tool in the PyRxAutoDock Vina software.

Finally, the grid box was created by maintaining the protein's active binding sites inside the box's center, which was designated as the grid mapping center. For the mu receptor center, X = −0.8683, Y = 14.0586, and Z = −57.3660, with dimensions X = 19.0100, Y = 18.1292, and Z = 19.8212, were maintained for the grid box. For the COX-2 grid mapping center, X = 22.5615, Y = 21.2666, and Z = 15.7556, with dimensions X = 22.59057, Y = 17.8973, and Z = 24.1880. However, for the TNF-alpha receptor grid mapping center, X = −19.8828, Y = 73.8134, and Z = 37.9172, with dimensions X = 19.7402, Y = 22.1537, and Z = 13.7094. Finally, for the 1A5H center, X = 5.5242, Y = 35.06182, and Z = 49.2687, with dimensions X = 26.8695, Y = 23.9366, and Z = 30.8053 for the grid box, were maintained.

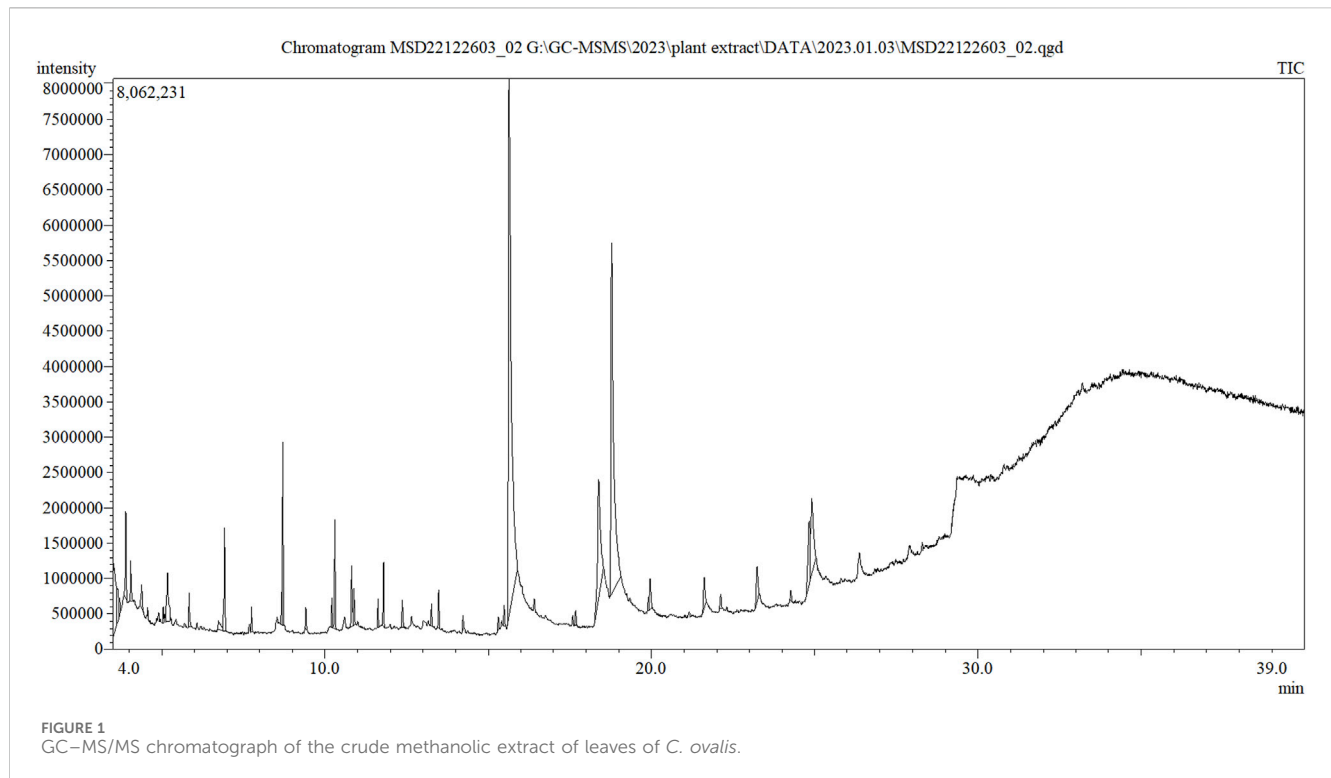
Upon docking, the remaining parameters were set to their default values. Subsequently, using AutoDock Vina (version 1.1.2), computer-based-aided molecular docking of the ligand compounds was carried out while maintaining all essential conditions default (Ahmed *et al.*, 2021). Finally, BIOVIA Discovery Studio version 4.5 was used to conceptualize all docking analyses for extrapolating and concluding the best-fitted figures using 2D and 3D configurations.

2.6.5 ADME/T study

pkCSM (<http://structure.bioc.cam.ac.uk/Pkcsms>) was used to evaluate the absorption, distribution, metabolism, excretion, and toxicological (ADME/T) parameters (Pires *et al.*, 2015). Meanwhile, Swiss ADME (<http://www.swissadme.ch>) was used to determine the drug-likeness and bioavailability score of selected compounds (Daina *et al.*, 2017).

2.7 Statistical analysis

The data were presented as a standard error mean (SEM). Statistical analyses using one-way ANOVA were conducted followed by Dunnett's multiple comparison tests. The observed values were compared to the control group and were considered statistically significant at $p < 0.05$, $p < 0.01$, and $p < 0.001$ (Miah *et al.*, 2018).



3 Results

3.1 GC–MS/MS analysis

The sample produced 39 peaks on the GC–MS/MS chromatogram (Figure 1), indicating 39 different phytochemical components. Following a comparison of the mass spectra of the constituents in the NIST library with those of the picks, 39 phytocompounds were defined and identified (Table 1).

The maximum peak area was found for hexadecanoic acid [methyl ester] (56.749%), methyl stearate (29.782%), carvacrol [TBDMS derivative] (12.586%), 9-octadecenoic acid [methyl ester, (E)-] (9.297%), heneicosanoic acid [methyl ester] (5.580%), 9-hexadecenoic acid [methyl ester, (Z)-] (5.372%), 3,5-octadiynedioic acid [dimethyl ester] (5.291%), 3,3-dimethoxy-2-butanone (4.496%), 2-methylhexacosane (3.963%), 3-methylbenzyl alcohol, TBDMS derivative (2.856%), dibenzo[b,f][1,4]diazocine, 5,6,11,12-tetrahydro-5-methyl- (2.817%), cyclopentene, 1-ethenyl-3-methylene- (2.456%), methyl 9-methyltetradecanoate (2.438%), 3-hydroxymandelic acid [3TMS derivative] (2.275%), [1,3,5]triazine-2-carboxylic acid, 4-ethylamino-6-morpholin-4-yl-, amide (2.131%), etc. The remaining compounds have a peak area of less than 2%.

3.2 Thrombolytic activity

In this investigation, the CODMSF exhibited an extremely strong thrombolytic impact by inhibiting 54.87% of the clot, which is close to the standard streptokinase (66.66%) (Figure 2). Additionally, COCME and COAQSF fractions demonstrated noteworthy anti-thrombosis effects through suppressing clots by

37.65% and 45.32%, respectively, while the control group only showed 7.06% clot lysis. This result signifies that there is a huge opportunity to develop new thrombolytic drugs from *C. ovalis*.

3.3 Membrane-stabilizing activity

Our study demonstrated that the COAQSF has manifested remarkable membrane-stabilizing activities exceeding aspirin (standard) activities with twice its value. Figure 3 illustrates that COAQSF inhibited 73.98% and 87.51% hemolysis against heat and hypotonic solution-induced hemolysis, respectively, while the values were 3.08% and 22.26%, respectively, for the standard streptokinase. However, CODMSF exhibited prominent activity followed by COEASF, where the inhibition of hemolysis was measured at 27.27% and 17.67% for COSMSF and 13.81% and 12.17% for COEASF against heat- and hypotonic solution-induced hemolysis, respectively. This finding enhanced the probability of developing new remedies against inflammation.

3.4 Central analgesic activity

By extending the experimental mice's tail immersion period, the various dosages of the crude methanolic extract of *C. ovalis* (200, 400, and 600 mg/kg) demonstrated considerable central analgesic efficacy. A dose- and time-dependent increase in the activity was observed. The highest activity was observed for 600 mg/kg extract which increased the tail emerged time to approximately 139.75 ± 0.23 , 222.34 ± 0.07 , and $381.14 \pm 0.55\%$, respectively, after 30, 60, and 90 min of dose ingestion (Table 2).

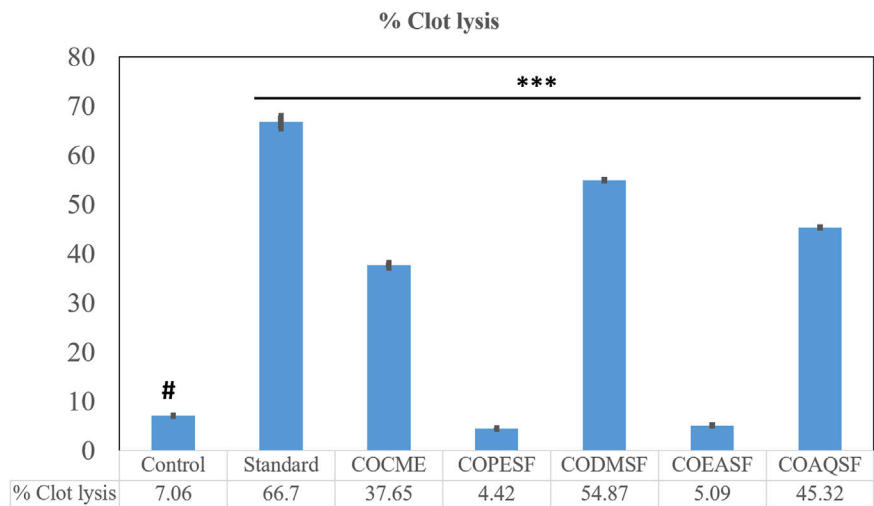


FIGURE 2 Thrombolytic effect of different fractions of the *C. ovalis* leaf extract. Each value is expressed as mean percentage (n = 3), *p < 0.05, **p < 0.01, and ***p < 0.001, and compared with the control group.

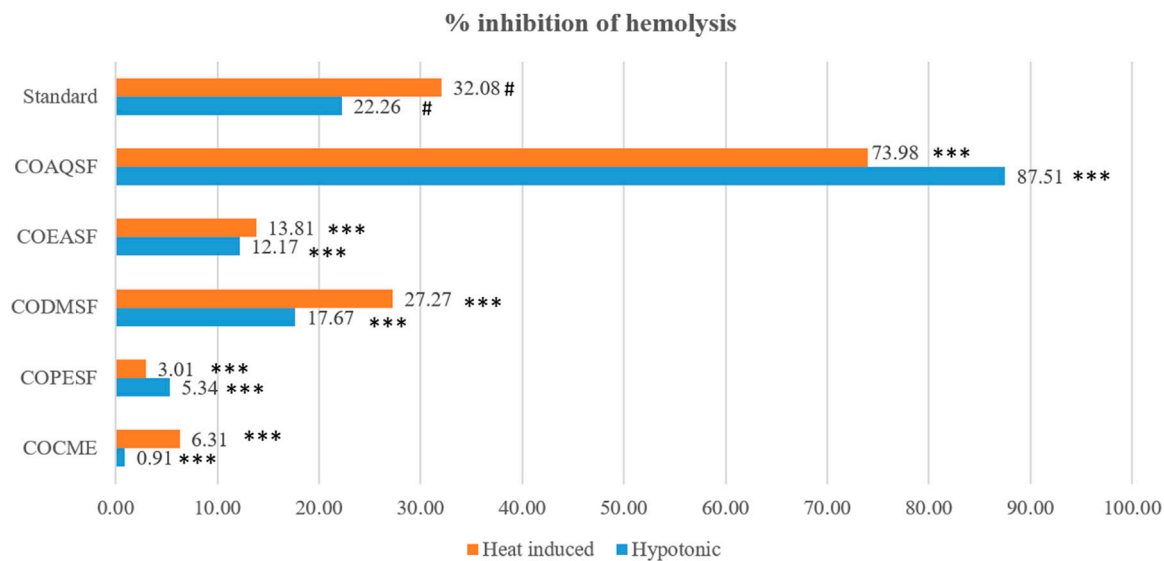


FIGURE 3 Membrane-stabilizing effect of different fractions of the *C. ovalis* leaf extract. Each value is expressed as mean percentage (n = 3), *p < 0.05, **p < 0.01, and ***p < 0.001, and compared with the standard group.

3.5 Peripheral analgesic activity

A remarkable peripheral analgesic activity was observed for different dosages of the COCME, especially for the dose of 400 mg/kg and 600 mg/kg. In comparison to the control (34.5 mean writhings), an average of 16.5 mean writhings was witnessed in the 200 mg/kg dose group, and 9.5 mean writhings were noted in the 400 and 600 mg/kg extract groups (Table 3). This indicates that the 200, 400, and 600 mg/kg COCMEs reduced writhing by approximately 32.65 ± 1.19 , 61.22 ± 1.04 , and $61.22 \pm 1.85\%$, respectively. All of the data were significantly justified.

3.6 Molecular docking study

The lowermost activity was observed by C30 with a binding affinity of -8.8 kcal/mol followed by C34, C7, C36, C28, and C39, which exhibited binding affinities of -8.5 , -8.1 , -7.7 , -7.3 , and -7.2 kcal/mol, respectively, against the Mu receptor compared to the standard diclofenac sodium, which scored -7.6 kcal/mol (Table 4). Figure 4 shows that C30 attached to eight amino acids of Mu receptors, namely, HIS 54, MET 151, LYS 233, VAL 236, TRP 293, ILE 296, VAL 300, and TYR 326, while C34 attached to nine amino acids, namely, HIS 54, TYR 148, MET

TABLE 2 Central analgesic effect of different doses of the crude methanolic extract of the leaves of *C. ovalis* in the mice model. Each value is expressed as mean \pm SEM (n = 4). * $p < 0.05$, ** $p < 0.01$, *** $p < 0.001$ and compared with the control group (only distilled water).

Treatment	% time elongation (mean \pm SEM)		
	At 30 min	At 60 min	At 90 min
Standard	146.75 \pm 0.16	345.66 \pm 0.25**	683.12 \pm 0.34**
Control	35.67 \pm 0.11	24.92 \pm 0.64	24.30 \pm 0.91
COCME 200	45.34 \pm 0.26*	102.92 \pm 0.22**	203.14 \pm 0.15**
COCME 400	132.58 \pm 0.23**	193.92 \pm 0.16**	309.37 \pm 0.21**
COCME 600	139.75 \pm 0.23**	222.34 \pm 0.07**	381.14 \pm 0.55**

151, VAL 236, TRP 293, ILE 296, HIS 297, and VAL 300. In comparison, the standard diclofenac is bound through six amino acids, namely, MET 151, ILE 296, HIS 297, ILE 322, VAL 300, and VAL 236.

Table 4; Figure 5 illustrate that C27 exhibited the highest efficacy against the COX-2 receptor through a series of bonds with the amino acids including MET 113, VAL 116, LEU 117, GLN 192, VAL 349, LEU 352, GLY 354, LEU 359, TYR 385, TRP 387, PHE 518, VAL 523, ALA 527, and LEU 531 with a binding score of -9.5 kcal/mol. However, C7 is bound to six amino acids of COX-2, namely, ARG 120, LEU 531, VAL 349, LEU 352, VAL 523, and ALA 527, and shows a binding affinity of -9 kcal/mol. Comparably, the standard diclofenac sodium exhibited a binding affinity of -7.9 kcal/mol and interacted with LEU 531, VAL 349, LEU 352, TYR 355, GLY 526, and ALA 527 of COX-2. Additionally, C39, C36, C21, C15, and C22 showed notable binding affinity of -8.4 , -7.8 , -7.2 , -7.1 , and -7 kcal/mol against COX-2, respectively. In addition, approximately 16 compounds exhibited a binding affinity ranging from -6.9 to -6.3 kcal/mol against the receptor.

When compared to regular aspirin (-5.3 kcal/mol), C30 had a binding affinity for TNF- α (PDB ID: 2AZ5) of -9.3 kcal/mol. C7, C27, C28, and C39 all had binding affinities of -7.5 kcal/mol, whereas C34 had a binding affinity of -7.9 kcal/mol. However, with binding affinities ranging from -6.5 to -5.8 kcal/mol, C3, C9, C21, C26, C29, and C36 scored higher affinities compared to aspirin. In the case of active amino acid residue, C30 was found to bind against TYR 59 TYR 119 of the A chain and TYR 59 of the B chain. Similarly, C39 bound to TYR 59 TYR 119 of the A chain and LEU 57 of the B chain, whereas aspirin bound to HIS 57, TYR 99, ALA 190, CYS 191, GLN 192, GLY 193, TRP 215, and GLY 216 of the A chain (Figure 6).

In the case of TPA (PDB ID: 1A5H), the most prominent affinity was witnessed in C7 and C30 with a binding affinity of -7.4 kcal/mol. On the other hand, C6, C27, C29, C34, and C26 manifested promising affinities with values of -6.1 , -6.9 , -6.1 , -6.7 , and -6.9 kcal/mol, respectively, compared to a value of -6.3 kcal/mol of the standard streptokinase. While C30 bound to TYR 99, ARG 174, and TRP 215 amino acids of the TPA receptor in Figure 7, C7 bound to ALA 190, CYS 191, SER 195, SER 214, GLY 216, and GLY 219 amino acids. The active amino acid residues for the streptokinase were HIS 57, TYR 99, ALA 190, CYS 191, GLN 192, GLY 193, TRP 215, and GLY 216, as shown in Figure 7.

4 Discussion

The best place to find novel bioactive compounds with new treatments is in medicinal plants. As a result, plant-based natural remedies are widely used in developing nations and given special attention because of their multiple protective benefits and beneficial effects on human health. Approximately 80% of people use traditional medicines, even in underdeveloped nations (Alam et al., 2020a). Oils contained by plant extract are typically intricate blends of vital secondary metabolites that have been extracted from plants, animals, and microorganisms. These mixes contain between 10 and 60 ingredients in varying concentrations, but often just 2–4 main molecules are responsible for the biological features (Rahman et al., 2013). The goal of the current research was to identify the chemical components and assess their biological and pharmacological potential in order to understand the significance of the methanolic crude extract of *C. ovalis*. The study will provide an update, confirm the value of aromatherapy, and add a new bearing on biopotency.

The GC–MS/MS analysis was carried out to identify the various volatile matter components found in the methanolic crude extract of *C. ovalis* leaves, such as alcohols, acids, amides, amines, esters, and hydrocarbons, both in quantitative and qualitative ways. A quantitative measurement of each component's quantity can be found in peak heights or regions beneath the peaks. This study identified 39 phytocompounds from the methanolic crude extract of leaves of *C. ovalis* while the maximum peak was acquired for hexadecanoic acid [methyl ester], which is approximately 56.749%, indicating the presence of a large quantity of this compound in this extract.

Hexadecanoic acid has been reported for potential antioxidant activity as well as anticancer potential against human colon cancer cells (Bharath et al., 2021). In addition, the compound exhibited

TABLE 3 Peripheral analgesic effect of different doses of the crude methanolic extract of the leaves of *C. ovalis* in the mice model. Each value is expressed as mean \pm SEM (n = 4), * $p < 0.05$, ** $p < 0.01$, and *** $p < 0.001$, and compared with the control group (only distilled water).

Test groups	Mean writhing	% inhibition of writhing (mean \pm SEM)
Control	24.5	
Standard	4	83.67 \pm 0.41**
COCME 200	16.5	32.65 \pm 1.19*
COCME 400	9.5	61.22 \pm 1.04**
COCME 600	9.5	61.22 \pm 1.85*

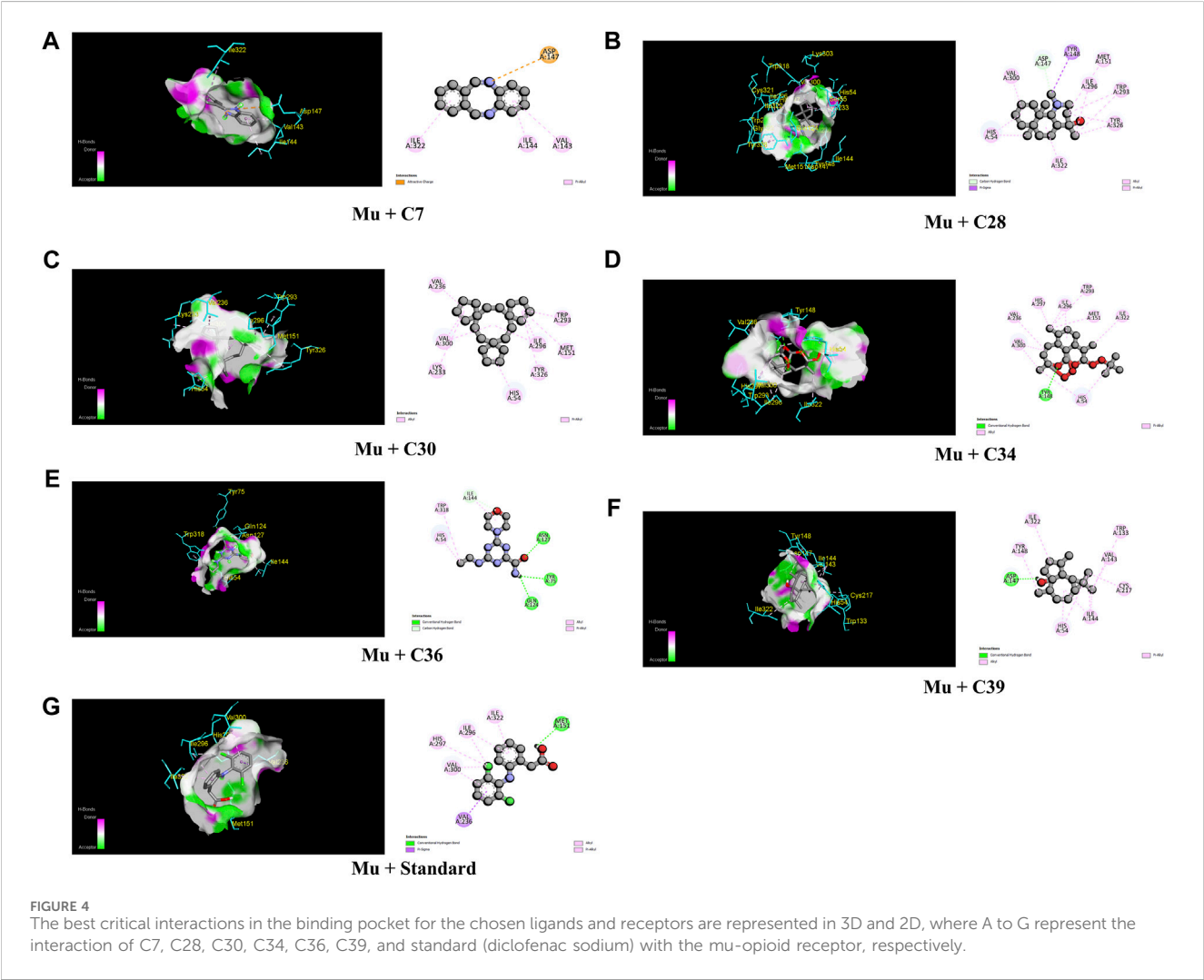
TABLE 4 Binding affinities of the identified compounds and standards against four receptors representing central and peripheral analgesic, membrane-stabilizing, and thrombolytic activities.

Compound	Binding affinity			
	Central analgesic	Peripheral analgesic	Membrane stabilizing	Thrombolytic
	Mu	COX-2	TNF-α	TPA
C1	−3	−3.1	−3	−3.3
C2	−4	−4.4	−4.2	−4.2
C3	−6.4	−4.9	−6.1	−5.8
C4	−3.1	−3.1	−3	−3.3
C5	−3.5	−3.8	−3.5	−4.1
C6	−5	−5.4	−4.7	−6.1
C7	−8.1	−9	−7.5	−7.4
C8	−1.2	−1.1	−0.9	−1.1
C9	−6.6	−6.6	−6.5	−5.2
C10	−1.2	−1	−0.9	−1.1
C11	−1.2	−1	−0.9	−1.1
C12	−5.4	−6.3	−5.4	−5.5
C13	−5.1	−5.7	−4.7	−5.2
C14	−5.6	−6.3	−5.1	−5.4
C15	−6.1	−7.1	−5.6	−6
C16	−1.5	−1.5	−1.1	−1.6
C17	−6	−6.7	−5.4	−5.5
C18	−5.9	−6.8	−5.1	−5.7
C19	−5.7	−6.9	−5.4	−5.3
C20	−5.8	−6.3	−5.5	−5.8
C21	−6.1	−7.2	−5.8	−5.7
C22	−6	−7	−5.4	−5.4
C23	−5.3	−6.7	−4.9	−5.6
C24	−6.4	−6.6	−5.2	−5.5
C25	−5.5	−6.5	−5	−5.8
C26	−5.8	−6.4	−5.8	−5.9
C27	−6.9	−9.5	−7.5	−6.9
C28	−7.3	−5.5	−7.5	−5.7
C29	−6.1	−6.5	−6.4	−6.1
C30	−8.8	−6.3	−9.3	−7.4
C31	−5.8	−6.7	−5.2	−5.3
C32	−1.2	−1.1	−0.9	−1.1
C33	−1.2	−1	−0.9	−1.1
C34	−8.5	−6.5	−7.9	−6.7
C35	−6.3	−6.3	−5.3	−5.6

(Continued on following page)

TABLE 4 (Continued) Binding affinities of the identified compounds and standards against four receptors representing central and peripheral analgesic, membrane-stabilizing, and thrombolytic activities.

Compound	Binding affinity			
	Central analgesic	Peripheral analgesic	Membrane stabilizing	Thrombolytic
	Mu	COX-2	TNF- α	TPA
C36	−7.7	−7.8	−6.5	−6.9
C37	−1.2	−1	−0.9	−1.1
C38	−1.2	−1	−0.9	−1.1
C39	−7.2	−8.4	−7.5	−5.9
Aspirin	-	-	−5.8	-
Diclofenac sodium	−7.6	−7.9	-	-
Streptokinase	-	-	-	−6.3



significant antibacterial activity against several antibiotic-resistant bacteria including *Staphylococcus aureus* W35, *Pseudomonas aeruginosa* D31, *Klebsiella pneumoniae* DF30, and *K. pneumoniae* B40 (Shaaban et al., 2021). Furthermore, methyl ester of hexadecanoic acid isolated from *Annona muricata* Linn. has been found promising antifungal potential against *Alternaria solani*, *Aspergillus erythrocephalus*, and *Aspergillus albicans* (Abubacker and Deepalakshmi, 2013). However, the presence of a significant

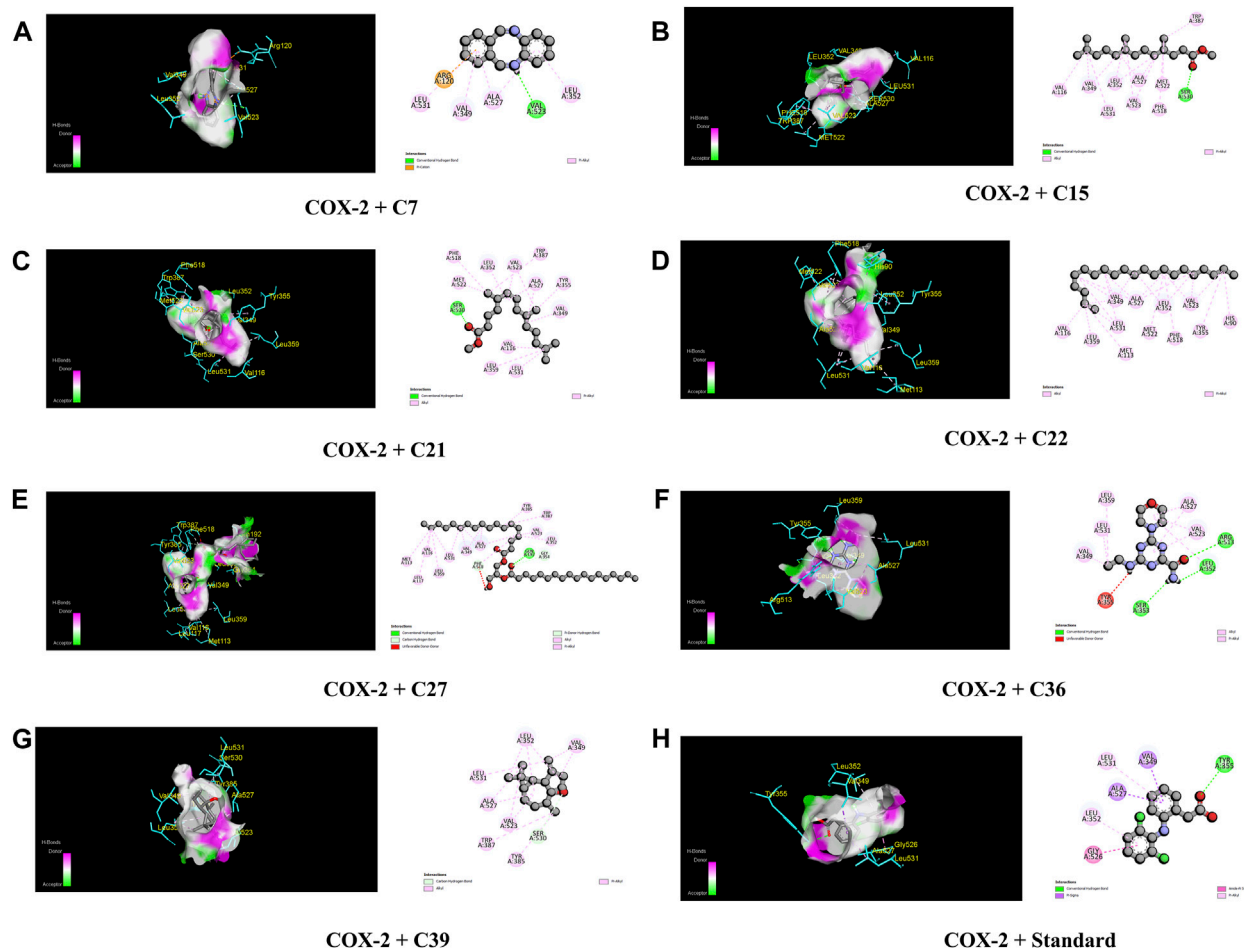


FIGURE 5
The best critical interactions in the binding pocket for the chosen ligands and receptors are represented in 3D and 2D, where A to H represent the interaction of C7, C15, C21, C22, C27, C36, C39, and standard (diclofenac sodium) with the COX-2 receptor, respectively.

amount of hexadecanoic acid in *C. ovalis* leaf extract increases the possibility that it has natural cytotoxic, antibacterial, and antifungal properties.

Our investigation revealed a substantial presence of methyl stearate, constituting approximately 29.782%, known for its medicinal properties. Notably, as a bioactive compound identified in the fermentation broth, methyl stearate plays a pivotal role in inhibiting nematode infection. Its efficacy is demonstrated through actions such as reducing egg hatching, repelling J2s from plant roots, and modulating key parasitic nematode genes (Mi-flp-18 and 16D10). This compound shows promise in effectively controlling *Meloidogyne incognita*. Additionally, its positive influence on enhancing banana plant growth at lower concentrations suggests its potential as an environmentally friendly approach to nematode control. This presents a viable alternative to conventional pesticides, contributing to sustainable agricultural practices (Lu et al., 2020).

Blood flow in the circulatory system is impeded if a thrombus forms inside blood arteries, which can lead to a number of fetal cardiovascular illnesses including hypertension, stroke, and anoxia. Thrombolites are substances that prevent thrombus formation, hence managing and treating embryonic cardiovascular disorders (Islam et al., 2019). Several studies have been conducted in the past

using medicinal plants from Bangladesh to identify natural chemicals having anti-thrombolytic potential (Rahman et al., 2013). The research discovered that the dichloromethane (DCM) fraction of the methanolic leaf extract from *C. ovalis* exhibited notable thrombolytic activity. Moreover, both the crude methanolic extract and the aqueous fraction demonstrated encouraging properties in dissolving blood clots, which increases the potential for developing novel preparations derived from this plant to mitigate cardiovascular diseases.

Inflammation causes lysosome lysis, which releases enzymes that cause different types of tissue damage. Inflammation causes lysosome lysis, which releases enzymes that cause different types of tissue damage. When an RBC is exposed to adverse circumstances or substances such as hypotonic medium or heat, the membranes break due to hemolysis and hemoglobin oxidation. In times of enhanced permeability brought on by inflammatory mediators, the stability of the membrane limits the passage of proteins from the blood and fluids into the RBC (Kosala et al., 2018). Thus, by stabilizing RBC induced by both hypotonic solution as well as heat, the aqueous fractions illustrated extremely potent anti-inflammatory activity compared to the standard aspirin. Furthermore, the crude methanolic extract from the leaves of *C. ovalis* demonstrated a

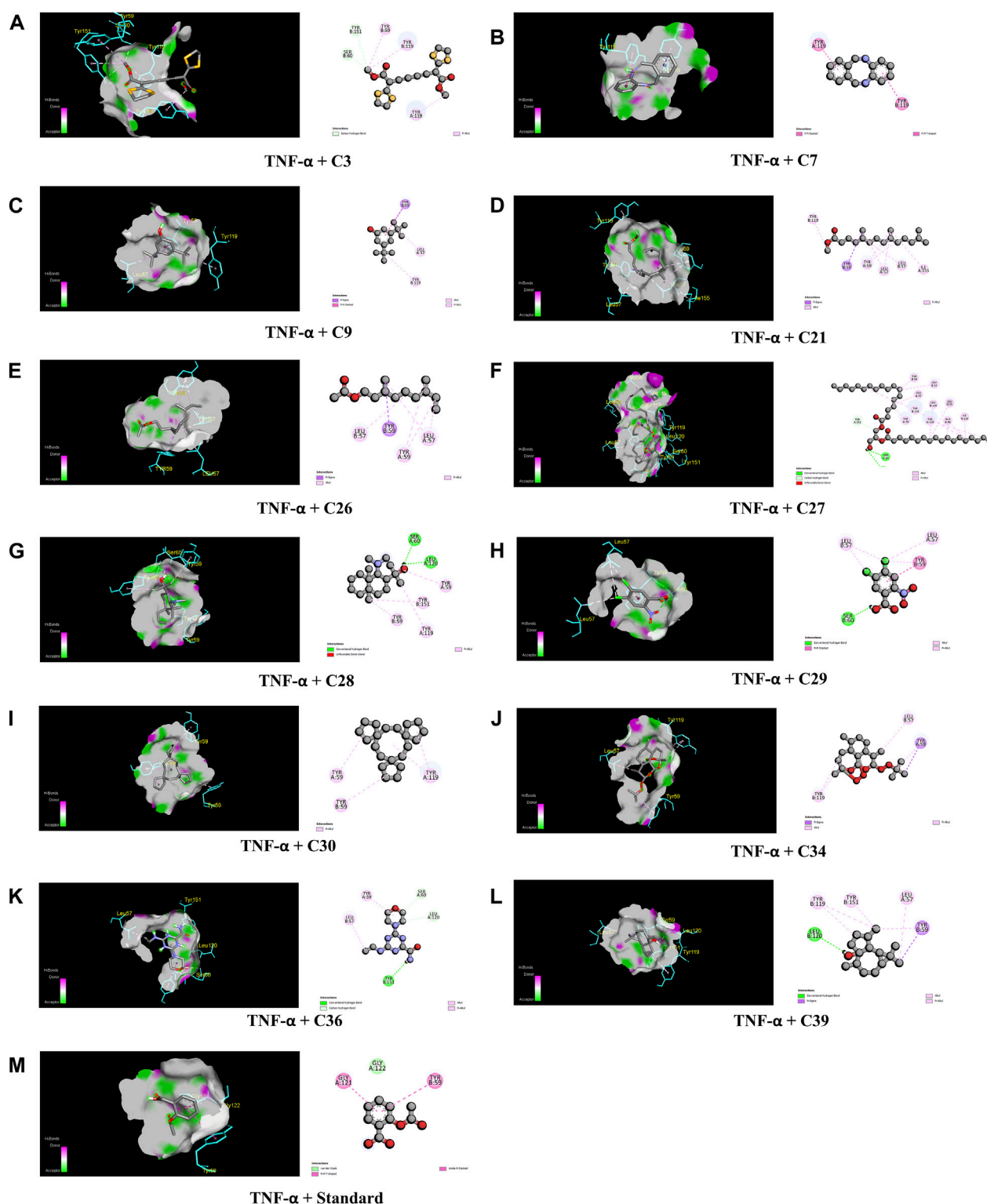
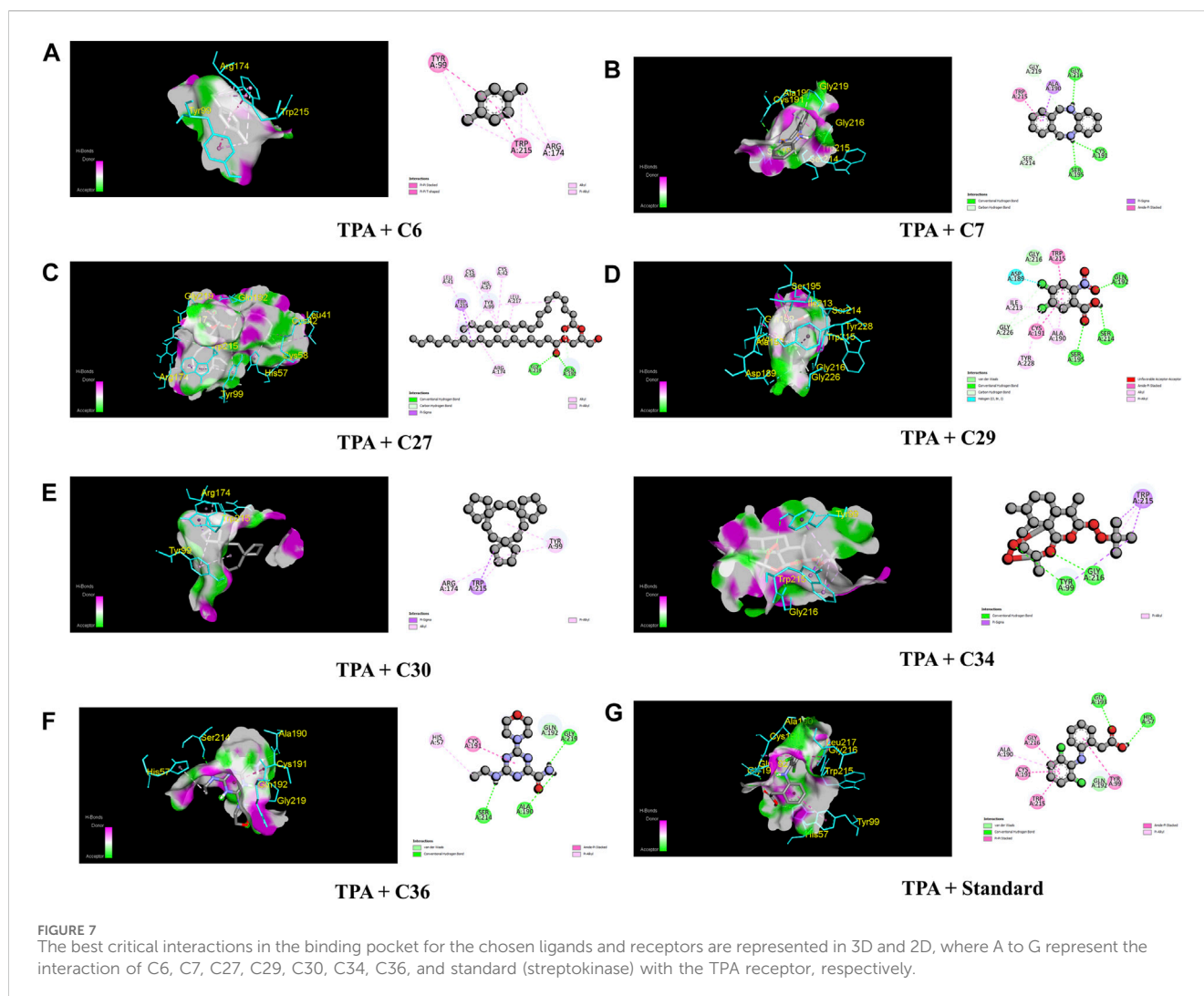


FIGURE 6

The best critical interactions in the binding pocket for the chosen ligands and receptors are represented in 3D and 2D, where A to M represent the interaction of C3, C7, C9, C21, C26, C27, C28, C29, C30, C34, C36, C39, and standard (aspirin) with the TNF- α receptor, respectively.

remarkable ability to prevent hemolysis, approaching the efficacy of the standard. A study represented that hexadecanoic acid, as evidenced by its stable binding within the active site of phospholipase A2 (PLA2), demonstrates a potential anti-

inflammatory effect by impeding substrate entry and hindering catalytic residues. Understanding its interaction with PLA2 may contribute to the development of drugs targeting chronic inflammatory conditions such as rheumatoid arthritis and asthma



(Aparna et al., 2012). So, our finding suggests that the presence of high amount of hexadecanoic acid is the reason for the extract potential membrane-stabilizing effect.

Using the tail immersion test, we assessed the central analgesic ability of the crude extract of *C. ovalis*. This procedure results in supra-spinal pain that is centrally mediated. While it is generally established that acetic acid somehow triggers the release of endogenous pain mediators, activating the pain-sensing neurons (Arslan and Bektas, 2010), in this study, the peripheral analgesic activity of the crude methanolic extract from the leaves of *C. ovalis* was determined by inducing writhing on mice with acetic acid.

This study unveiled a statistically significant and noteworthy central analgesic effect from the crude methanol leaf extract of *C. ovalis*, which was both dose- and time-dependent. Interestingly, the moderate dose (400 mg/kg) exhibited the most potent peripheral analgesic activity, with statistically significant results, followed by the highest dose (600 mg/kg). This finding could serve as an initial avenue for further investigation aimed at uncovering more precise insights into the plant's pain-relieving properties.

To better understand the biological roles of substances from nature and to estimate ligand–receptor interactions, molecular

docking studies were widely used. It offers further details on potential methods of action and binding style in the binding sites of certain proteins (Alam et al., 2020b).

As a matter of fact, a molecular docking investigation was carried out to clarify and validate the experimental findings from biological research. This technique confirms the experimental results. In order to find the central and peripheral analgesic properties, the identified compounds docked against Mu (PDB ID: 5C1M) and COX-2 (PDB ID: 1CX2) receptors, respectively, while TNF- α (PDB ID: 2AZ5) and TPA (PDB ID: 1A5H) receptors were selected for screening the anti-inflammatory and thrombolytic activities of identified compounds from the crude methanolic extract of leaves of *C. ovalis*.

The strongest affinity toward the Mu receptor was observed by C30 or trispiro[4.2.4.2.4.2.]heneicosane (−8.8 kcal/mol), followed by C34 or dihydroartemisinin, 10-O-(t-butyloxy)- (−8.5 kcal/mol). Meanwhile, distearin (C27), dibenzo[b,f][1,4]diazocine, 5,6,11,12-tetrahydro-5-methyl- (C7), and 4aH-cycloprop[e]azulen-4a-ol, decahydro-1,1,4,7-tetramethyl-, [1aR-(1a.alpha.,4.beta.,4a.beta.,7.alpha.,7a.beta.,7b.alpha.)]- (C39) suppressed the activity of standard (−7.9 kcal/mol) against the COX-2 receptor with binding affinities of −9.3, −9, and 8.4 kcal/mol, respectively. Subsequently, trispiro[4.2.4.2.4.2.]heneicosane (C30) and dibenzo

TABLE 5 Absorption and distribution profile of the selected compounds which showed the best interaction against these receptors.

Properties	Absorption							Distribution			
Model name (unit)	Water solubility (log mol/L)	Caco2 permeability (log Papp in 10–6 cm/s)	Intestinal absorption (human) (%) absorbed)	Skin permeability (log Kp)	P-glycoprotein substrate	P-glycoprotein I inhibitor	P-glycoprotein II inhibitor	VDss (human) (log L/kg)	Fraction unbound (human) (fu)	BBB permeability	CNS permeability
C3	–4.36	1.513	97.394	–2.654	No	Yes	No	–0.762	0.048	–0.106	–2.05
C6	–2.522	1.547	95.713	–1.236	No	No	No	0.325	0.362	0.409	–1.677
C7	–2.331	1.506	74.539	–2.061	No	No	No	0.49	0.19	0.169	–1.336
C9	–3.876	1.668	92.254	–2.364	No	No	No	0.545	0.042	0.47	–0.858
C15	–6.455	1.644	93.941	–2.255	No	No	No	0.311	0.07	0.725	–1.672
C21	–6.849	1.643	94.049	–2.434	No	No	No	0.333	0.031	0.744	–1.621
C22	–8.558	1.37	89.328	–2.793	No	No	Yes	0.579	0	1.033	–1.144
C26	–4.141	1.625	94.593	–1.662	No	No	No	0.183	0.336	0.606	–2.201
C27	–3.907	–0.108	84.821	–2.735	Yes	No	Yes	–0.956	0.171	–1.044	–3.112
C28	–3.195	1.482	93.208	–3.125	Yes	No	No	0.563	0.552	0.585	–3.228
C29	–2.009	1.39	89.429	–2.735	No	No	No	0.012	0.807	0.276	–3.186
C30	–7.358	1.441	93.087	–2.546	No	No	Yes	0.73	0	0.797	–1.366
C34	–3.651	1.271	83.834	–2.735	Yes	No	No	–1.374	0.209	0.672	–1.239
C36	–2.8	0.108	66.393	–3.045	No	No	No	–0.294	0.67	–0.819	–3.198
C39	–3.98	1.496	93.979	–2.247	No	No	No	0.571	0.326	0.617	–2.536

TABLE 6 Metabolism and excretion profile of the selected compounds which showed the best interaction against these receptors.

Properties	Metabolism							Excretion	
Model name (unit)	CYP2D6 substrate	CYP3A4 substrate	CYP1A2 inhibitor	CYP2C19 inhibitor	CYP2C9 inhibitor	CYP2D6 inhibitor	CYP3A4 inhibitor	Total clearance (log mL/min/kg)	Renal OCT2 substrate
C3	No	Yes	No	No	No	No	No	0.409	No
C6	No	No	No	No	No	No	No	0.254	No
C7	No	Yes	Yes	No	No	No	No	0.498	Yes
C9	No	Yes	Yes	No	No	No	No	0.781	No
C15	No	No	Yes	No	No	No	No	1.563	No
C21	No	Yes	Yes	No	No	No	No	1.594	No
C22	No	Yes	Yes	No	No	No	No	2.033	No
C26	No	No	No	Yes	No	No	No	1.645	No
C27	No	Yes	No	No	No	No	No	2.239	No
C28	No	No	No	No	No	No	No	0.419	No
C29	No	No	No	No	No	No	No	−9.401	No
C30	No	Yes	Yes	No	No	No	No	0.841	No
C34	No	No	Yes	Yes	No	No	No	0.518	No
C36	No	No	No	No	No	No	No	0.32	No
C39	No	No	No	Yes	Yes	No	No	0.856	No

TABLE 7 Toxicology and drug-likeness profile of the selected compounds which showed the best interaction against these receptors.

Properties		Toxicity									Drug-likeness	
Model name (unit)	AMES toxicity	Max. tolerated dose (human) (log mg/kg/day)	hERG I inhibitor	hERG II inhibitor	Oral rat acute toxicity (LD50) (mol/kg)	Oral rat chronic toxicity (LOAEL) (log mg/kg_bw/day)	Hepatotoxicity	Skin sensitization	<i>Tetrahymena pyriformis</i> toxicity (log ug/L)	Minnow toxicity (log mM)	Lipinski's rule of five	Bioavailability score (%)
C3	No	-0.62	No	No	2.531	0.87	No	No	0.534	-0.262	No; 1 violation: MW > 350	0.55
C6	No	0.921	No	No	1.841	2.168	No	No	-0.022	1.31	Yes	0.55
C7	Yes	0.096	No	No	1.702	0.769	No	No	1.678	1.101	No; 1 violation: MW < 250	0.55
C9	No	0.409	No	No	2.346	1.736	No	Yes	1.667	-0.108	No; 2 violations: MW < 250, XLOGP3>3.5	0.55
C15	No	0.432	No	No	1.643	2.76	No	Yes	2.302	-1.221	No; 2 violations: rotors>7, XLOGP3>3.5	0.55
C21	No	0.386	No	No	1.633	2.833	No	Yes	2.172	-1.536	No; 2 violations: rotors>7, XLOGP3>3.5	0.55
C22	No	-0.06	No	Yes	1.611	1.146	No	Yes	0.748	-2.613	No; 2 violations: rotors>7, XLOGP3>3.5	0.55
C26	No	0.43	No	No	1.693	2.392	No	Yes	1.629	0.192	No; 3 violations: MW < 250, rotors>7, XLOGP3>3.5	0.55
C27	No	0.142	No	No	3.105	0.496	No	No	0.285	-6.303	No; 3 violations: MW > 350, rotors>7, XLOGP3>3.5	0.17
C28	No	0.184	No	No	2.027	0.754	No	Yes	0.286	1.5	No; 1 violation: XLOGP3>3.5	0.55
C29	Yes	0.319	No	No	2.482	5.273	No	No	0.285	6.004	No; 1 violation: MW < 250	0.56

(Continued on following page)

TABLE 7 (Continued) Toxicology and drug-likeness profile of the selected compounds which showed the best interaction against these receptors.

Properties	Toxicity									Drug-likeness			
	Model name (unit)	AMES toxicity	Max. tolerated dose (human) (log mg/kg/day)	hERG I inhibitor	hERG II inhibitor	Oral rat acute toxicity (LD50) (mol/kg)	Oral rat chronic toxicity (LOAEL) (log mg/kg_bw/day)	Hepatotoxicity	Skin sensitization	Tetrahymena pyriformis toxicity (log ug/L)	Minnow toxicity (log mM)	Lipinski's rule of five	Bioavailability score (%)
	C30	No	-0.25	No	Yes	1.631	1.562	No	No	1.021	-1.112	No; 1 violation: XLOGP3>3.5	0.55
	C34	Yes	1.375	No	No	2.482	0.188	No	No	0.285	4.787	No; 2 violations: MW > 350, XLOGP3>3.5	0.55
	C36	No	1.065	No	No	2.389	1.784	Yes	No	0.252	2.593	Yes	0.55
	C39	No	0.215	No	No	1.698	1.185	No	Yes	1.118	1.105	No; 2 violations: MW < 250, XLOGP3>3.5	0.55

Lipinski's five principles, but C3, C7, C28, C29, and C30 were determined to have violated one of Lipinski's laws. Additionally, C9, C15, C21, C22, C34, and C39 each had two violations. Finally, C26 and C27 demonstrated three violations of Lipinski's law. The results indicate that the compounds adhere to Lipinski's criteria, which means they are safe for oral use and may function as promising medication candidates.

However, all of the substances in Table 7 with the exception of C27, which had a bioavailability value of 0.17%, showed a bioavailability score of 0.55%. Consequently, pkCSM is a unique method for predicting pharmacokinetic and toxicological effects that use graph-based signatures to reflect the chemistry and topology of small molecules (Pires et al., 2015). None of these compounds except C34 was found to be hepatotoxic. However, none of these compounds inhibits hERG I, and except for C22 and C30, none of them inhibits hERG II, indicating these compounds may not have cardiotoxicity (Muster et al., 2008). In addition, all of these compounds displayed negative values for water solubility (log mol/L), indicating their lipophilic nature, which facilitates efficient absorption (Table 5).

All these assumptions from the ADME/T study influenced the idea of treating these compounds, particularly which exhibited prominent binding affinities toward the abovementioned receptors, for their drug-like candidacy and further investigation.

In this study, the presence of the aforementioned substances, which showed potential binding affinities against those four receptors, supported the outcomes of biological activities such as thrombolytic and membrane-stabilizing as well as peripheral and central analgesic effects of the *C. ovalis* leaf extract. In addition, this docking suggested that those compounds may become potential drug candidates for these four disease states. However, in order to identify and develop the pharmaceutically active constituent from the extracts of *C. ovalis*, extensive investigations are needed to investigate the real mechanism of action and drug safety concerns.

5 Conclusion

According to the findings of this study, *C. ovalis* leaves can be a notable source of analgesic and membrane-stabilizing potentials as well as a viable candidate for thrombolytic potential. In

[b,f][1,4]diazocine, 5,6,11,12-tetrahydro-5-methyl (C7) illustrated remarkable binding affinities toward TNF- α and TPA (Table 4).

The fact that C7 and C36 have higher binding affinities than projections for each of these four receptors suggests that they could be future therapeutic options for these various disorders. However, C27 exhibited strong affinity against COX-2, TNF- α , and TPA receptors, while C30 and C34 manifested lower binding affinity against Mu, TNF- α , and TPA receptors. In addition, C39 was found to have strong binding activities against Mu, COX-2, and TNF- α receptors.

Tables 5–7 show the various ADME/T parameters of the most prominent compounds found through the *in silico* study. According to Lipinski, a substance will be orally accessible if it meets the following requirements: molecular weight <500 amu, hydrogen bond donor sites <5, hydrogen bond acceptor sites <10, and lipophilicity value LogP \leq 5 (Zhang and Wilkinson, 2007). The above data demonstrated that C6 and C36 did not violate any of Lipinski's five principles, but C3, C7, C28, C29, and C30 were determined to have violated one of Lipinski's laws. Additionally, C9, C15, C21, C22, C34, and C39 each had two violations. Finally, C26 and C27 demonstrated three violations of Lipinski's law. The results indicate that the compounds adhere to Lipinski's criteria, which means they are safe for oral use and may function as promising medication candidates.

However, all of the substances in Table 7 with the exception of C27, which had a bioavailability value of 0.17%, showed a bioavailability score of 0.55%. Consequently, pkCSM is a unique method for predicting pharmacokinetic and toxicological effects that use graph-based signatures to reflect the chemistry and topology of small molecules (Pires et al., 2015). None of these compounds except C34 was found to be hepatotoxic. However, none of these compounds inhibits hERG I, and except for C22 and C30, none of them inhibits hERG II, indicating these compounds may not have cardiotoxicity (Muster et al., 2008). In addition, all of these compounds displayed negative values for water solubility (log mol/L), indicating their lipophilic nature, which facilitates efficient absorption (Table 5).

All these assumptions from the ADME/T study influenced the idea of treating these compounds, particularly which exhibited prominent binding affinities toward the abovementioned receptors, for their drug-like candidacy and further investigation.

In this study, the presence of the aforementioned substances, which showed potential binding affinities against those four receptors, supported the outcomes of biological activities such as thrombolytic and membrane-stabilizing as well as peripheral and central analgesic effects of the *C. ovalis* leaf extract. In addition, this docking suggested that those compounds may become potential drug candidates for these four disease states. However, in order to identify and develop the pharmaceutically active constituent from the extracts of *C. ovalis*, extensive investigations are needed to investigate the real mechanism of action and drug safety concerns.

5 Conclusion

According to the findings of this study, *C. ovalis* leaves can be a notable source of analgesic and membrane-stabilizing potentials as well as a viable candidate for thrombolytic potential. In

addition, several bioactive potential constituents showed favorable binding affinity to particular proteins in molecular docking analysis, and the ADME/T investigation demonstrated their pharmacokinetics and drug-like characteristics. As a result, the computational work has confirmed the biological activity testing data and offered encouraging insight for evaluating *C. ovalis* as a noteworthy therapeutic candidate. Further investigation needs to be carried out to isolate these compounds and establish their mechanism of action against these specific receptors in a broad setup.

Data availability statement

The raw data supporting the conclusion of this article will be made available by the authors, without undue reservation.

Ethics statement

The animal study was approved by the Department of Pharmacy, School of Pharmaceutical Sciences, State University of Bangladesh, 77, Satmasjid Road, Dhanmondi, Dhaka-1207, Bangladesh. The study was conducted in accordance with the local legislation and institutional requirements.

Author contributions

SS: data curation, formal analysis, investigation, methodology, project administration, resources, validation, and writing—original draft. SAS: data curation, investigation, software, and writing—review and editing. HH: formal analysis, methodology, software, validation, and writing—original draft, writing—review

and editing. FH: data curation, investigation, methodology, resources, visualization, and writing—review and editing. AH: software, visualization, writing—review and editing, and data curation. PG: visualization, writing—review and editing, data curation, formal analysis, and software. SA: formal analysis, investigation, project administration, resources, software, supervision, visualization, and writing—review and editing. AM: conceptualization, funding acquisition, project administration, supervision, visualization, writing—original draft, and writing—review and editing.

Funding

The author(s) declare financial support was received for the research, authorship, and/or publication of this article. This study was partially supported by the Post-Doctoral Research Start-up Fund of Lishui People's Hospital, Zhejiang, China (2023bsh001).

Conflict of interest

The authors declare that the research was conducted in the absence of any commercial or financial relationships that could be construed as a potential conflict of interest.

Publisher's note

All claims expressed in this article are solely those of the authors and do not necessarily represent those of their affiliated organizations, or those of the publisher, the editors, and the reviewers. Any product that may be evaluated in this article, or claim that may be made by its manufacturer, is not guaranteed or endorsed by the publisher.

References

- Abubacker, M. N., and Deepalakshmi, T. (2013). *In vitro* antifungal potentials of bioactive compound methyl ester of hexadecanoic acid isolated from *Annona muricata* Linn. (Annonaceae) leaves. *Biosci. Biotechnol. Res. ASIA* 10, 879–884. doi:10.13005/bbra/1211
- Ahmed, T., Rahman, S. A., Asaduzzaman, M., Islam, A. B. M. M. K., and Chowdhury, A. A. (2021). Synthesis. *in vitro* bioassays, and computational study of heteroaryl nitazoxanide analogs. *Pharmacol. Res. Perspect.* 9, e00800. doi:10.1002/prp2.800
- Alam, M. M., Naeem, M., Khan, M. M. A., and Uddin, M. (2017). "Vincristine and vinblastine anticancer catharanthus alkaloids: pharmacological applications and strategies for yield improvement," in *Catharanthus roseus: current research and future prospects*. (Cham, Switzerland: Springer), 277–307. doi:10.1007/978-3-319-51620-2_11
- Alam, S., Emon, N. U., Rashid, M. A., Arman, M., and Haque, M. R. (2020a). Investigation of biological activities of *Colocasia gigantea* Hook. f. leaves and PASS prediction. *in silico* molecular docking with ADME/T analysis of its isolated bioactive compounds. *BioRxiv*. doi:10.1101/2020.05.18.101113
- Alam, S., Emon, N. U., Shahriar, S., Richi, F. T., Haque, M. R., Islam, M. N., et al. (2020b). Pharmacological and computer-aided studies provide new insights into *Milletia puguensis* Ali (Fabaceae). *Saudi Pharm. J.* 28 (12), 1777–1790. doi:10.1016/j.jsps.2020.11.004
- Aparna, V., Kalarickal, V., Mandal, P. K., and Sadasivan, C. (2012). Anti-inflammatory property of n -hexadecanoic acid: structural evidence and kinetic assessment. *Chem. Biol. Drug Des.* 2, 434–439. doi:10.1111/j.1747-0285.2012.01418.x
- Arslan, R., and Bektas, N. (2010). Antinociceptive effect of methanol extract of *Capparis ovata* in mice. *Pharm. Biol.* 48 (10), 1185–1190. doi:10.3109/13880201003629323
- Bharath, B., Perinbam, K., Devanesan, S., AlSalhi, M. S., and Saravanan, M. (2021). Evaluation of the anticancer potential of Hexadecanoic acid from brown algae *Turbinaria ornata* on HT29 colon cancer cells. *J. Mol. Struct.* 1235 (13022), 130229. doi:10.1016/j.molstruc.2021.130229
- Bikadi, Z., and Hazai, E. (2009). Application of the PM6 semi-empirical method to modeling proteins enhances docking accuracy of AutoDock. *J. Cheminformatics.* 1, 15–16. doi:10.1186/1758-2946-1-15
- Chaturvedi, V., Goyal, S., Mukim, M., Meghani, M., and Patwekar, F. (2022). A comprehensive review on *catharanthus roseus* L. (G.) don: clinical Pharmacology, Ethnopharmacology and Phytochemistry. *J. Ethnopharmacol.* 2 (2), 17–36. doi:10.46610/jpr.2022.v04i02.003
- Daina, A., Michielin, O., and Zoete, V. (2017). SwissADME: a free web tool to evaluate pharmacokinetics, drug-likeness and medicinal chemistry friendliness of small molecules. *Sci. Rep.* 7 (1), 42717. doi:10.1038/srep42717
- De, N., Bhowmik, S., and Saha, B. (2022). Medicinal uses of *Catharanthus roseus*. *J. adv. microbiol.*, 9.
- Ezeja, M. I., Omeh, Y. S., Ezeigbo, I. I., and Ekechukwu, A. (2011). Evaluation of the analgesic activity of the methanolic stem bark extract of *Dialium guineense* (Wild). *Ann. Med. health Sci. Res.* 1 (1), 55–62.
- Hasnat, H., Shompa, S. A., Richi, F. T., Islam, M. M., Suman, M. H., Ahmed, N. U., et al. (2023). Bioactive secondary metabolites to combat diabetic complications: evidenced from *in silico* study. *Bangladesh Pharm. J.* 26 (2), 167–184. doi:10.3329/bpj.v26i2.67807
- Islam, M., Jannat, T., Kuddus, M. R., Rashid, M. A., and Haque, M. R. (2019). *In vitro* and *in vivo* evaluation of pharmacological potentials of *Campsis radicans* L. *Clin. Phytoscience.* 5, 42–49. doi:10.1186/s40816-019-0144-9
- Islam, M., Kuddus, M. R., Rashid, M. A., and Haque, M. R. (2020). Phytochemical investigations of *Campsis radicans* L. *J. Appl. Pharm. Res.* 8 (3), 55–59. doi:10.18231/j.joapr.2020.v.8i.3.55.59
- Islam, M. A., Alam, S., Saha, T., Akter, F., Hasnat, H., Zaman, A., et al. (2022). Evaluation of biological activities of methanolic extract of leaves of *Bruguiera*

- gymnorhiza (L.) lam.: *in vivo* studies using Swiss albino mice model. *Bangladesh Pharmacol. J.* 25 (1), 26–31. doi:10.3329/bpj.v25i1.57837
- Jendele, L., Krivak, R., Skoda, P., Novotny, M., and Hoksza, D. (2019). PrankWeb: a web server for ligand binding site prediction and visualization. *Nucleic Acids Res.* 47, W345–W349. doi:10.1093/nar/gkz424
- Kabesh, K., Senthilkumar, P., Ragunathan, R., and Kumar, R. R. (2015). Phytochemical analysis of *Catharanthus roseus* plant extract and its antimicrobial activity. *Int J.* 3 (2), 162–172.
- Kosala, K., Widodo, M. A., Santoso, S., and Karyono, S. (2018). *In vitro* and *in vivo* anti-inflammatory activities of *Coptosapelta flavescens* Korth Roots methanol extract. *J. Appl. Pharm. Sci.* 8 (9), 42–48. doi:10.7324/JAPS.2018.8907
- Kumar, P. S., Krishnaswamy, G., Desai, N. R., Sreenivasa, S., and Kumar, D. A. (2021). Design, synthesis, PASS prediction, in-silico ADME and molecular docking studies of substituted-(Z)-3-benzylidene-5-aza-2-oxindole derivatives (Part-1). *Chem. Data Collect.* 31, 100617. doi:10.1016/j.cdc.2020.100617
- Lu, J., Meng, Z., Chen, Y., Yu, L., Gao, B., Zheng, Y., et al. (2020). Apigenin induced autophagy and stimulated autophagic lipid degradation. *Food Funct.* 11 (10), 9208–9215. doi:10.1039/d0fo00949k
- Mathekga, A. D. M., and Meyer, J. J. M. (1998). Antibacterial activity of South African *Helichrysum* species. *S. Afr.* 64 (5), 293–295. doi:10.1016/S0254-6299(15)30903-0
- Miah, M. M., Das, P., Ibrahim, Y., Shajib, M. S., and Rashid, M. A. (2018). *In vitro* antioxidant, antimicrobial, membrane stabilization and thrombolytic activities of *Dioscorea hispida* Dennst. *Eur. J. Integr. Med.* 19, 121–127. doi:10.1016/j.eujim.2018.02.002
- Mishra, J. N., and Verma, N. K. (2017). A brief study on *Catharanthus roseus*: a review. *Intern. J. Res. Pharmacy Pharmaceut. Sci.* 2 (2), 20–23.
- Muhammad, N., Shrestha, L., Wadood, A., Khan, H., De Feo, V., Khan, A. Z., et al. (2015). First evidence of the analgesic activity of govaniadine, an alkaloid isolated from *Corydalis govaniana* Wall. *Nat. Prod. Res.* 29 (5), 430–437. doi:10.1080/14786419.2014.951933
- Muster, W., Breidenbach, A., Fischer, H., Kirchner, S., Mller, L., and Phler, A. (2008). Computational toxicology in drug development. *Drug Discov. Today* 13 (7–8), 303–310. doi:10.1016/j.drudis.2007.12.007
- Obonti, A. T., Alam, S., Kamal, T. B., Zaman, A., Hasnat, H., Saha, T., et al. (2021). Prospective plants with corroborated antimalarial actions: a review. *Bangladesh Pharmacol. J.* 24 (2), 180–193. doi:10.3329/bpj.v24i2.54716
- Pham, H. N. T., Vuong, Q. V., Bowyer, M. C., and Scarlett, C. J. (2020). Phytochemicals derived from *Catharanthus roseus* and their health benefits. *Technologies* 8, 80. doi:10.3390/technologies8040080
- Pires, D. E., Blundell, T. L., and Ascher, D. B. (2015). pkCSM: predicting small-molecule pharmacokinetic and toxicity properties using graph-based signatures. *J. Med. Chem.* 58 (9), 4066–4072. doi:10.1021/acs.jmedchem.5b00104
- Prasad, S., Kashyap, R. S., Deopujari, J. Y., Purohit, H. J., Taori, G. M., and Daginawala, H. F. (2006). Development of an *in vitro* model to study clot lysis activity of thrombolytic drugs. *Thromb. J.* 4, 14–4. doi:10.1186/1477-9560-4-14
- Rahman, M. A., Sultana, R., Bin Emran, T., Islam, M. S., Rahman, M. A., Chakma, J., et al. (2013). Effects of organic extracts of six Bangladeshi plants on *in vitro* thrombolysis and cytotoxicity. *BMC Complement Altern. Med.* 13, 1–7. doi:10.1186/1472-6882-13-25
- Satyannarayana, P. S., Jain, N. K., Singh, A., and Kulkarni, S. K. (2004). Isobolographic analysis of interaction between cyclooxygenase inhibitors and tramadol in acetic acid-induced writhing in mice. *Prog. Neuropsychopharmacol. Biol.* 28 (4), 641–649. doi:10.1016/j.pnpbp.2004.01.015
- Sermakkani, M., and Thangapandian, V. (2012). GC-MS analysis of *Cassia italica* leaf methanol extract. *Asian J. Pharm. Clin. Res.* 5 (2), 90–94.
- Shaaban, M. T., Ghaly, M. F., and Fahmi, S. M. (2021). Antibacterial activities of hexadecanoic acid methyl ester and green-synthesized silver nanoparticles against multidrug-resistant bacteria. *J. Basic Microbiol.* 61 (6), 557–568. doi:10.1002/jobm.202100061
- Sikder, M. A. A., Millat, M. S., Sultana, A., Kaiser, M. A., and Rashid, M. A. (2012). *In vitro* membrane stabilizing activity, total phenolic content, cytotoxic, thrombolytic and antimicrobial activities of *Calliandra surinamensis* (Wall.). *J. Pharmacogn. Phytochem.* 1 (3), 40–44.
- Tolambiya, P., and Mathur, S. (2016). A study on potential phytopharmaceuticals assets in *Catharanthus roseus* L.(Alba). *Int. J. Life Sci. Biotechnol. Pharm. Res.* 5 (1), 1–6.
- Tropical Plants Database (2023). Prota. Available at: <http://www.prota.org>.
- VanWagenen, B. C., Larsen, R., Cardellina, J. H., Randazzo, D., Lidert, Z. C., and Swithenbank, C. (1993). Ulosantoin, a potent insecticide from the sponge *Ulosa ruetzleri*. *J. Org. Chem.* 58 (2), 335–337. doi:10.1021/jo00054a013
- Zhang, M. Q., and Wilkinson, B. (2007). Drug discovery beyond the rule-of-five. *Curr. Opin. Biotechnol.* 18 (6), 478–488. doi:10.1016/j.copbio.2007.10.005



OPEN ACCESS

EDITED BY

Tomislav Tosti,
University of Belgrade, Serbia

REVIEWED BY

Jinghong Zhang,
Huaqiao University, China
Zivoslav Lj Tesic,
University of Belgrade, Serbia
Uros Babic,
University of Belgrade, Serbia

*CORRESPONDENCE

Xiaofeng Zhang,
✉ zhangxiaofeng1962@163.com
Xilin Xu,
✉ hlj542833@sina.com

RECEIVED 27 December 2023

ACCEPTED 04 March 2024

PUBLISHED 02 April 2024

CITATION

Du J, Wang Y, Wu C, Zhang X, Zhang X and Xu X (2024), Targeting bone homeostasis regulation: potential of traditional Chinese medicine flavonoids in the treatment of osteoporosis. *Front. Pharmacol.* 15:1361864. doi: 10.3389/fphar.2024.1361864

COPYRIGHT

© 2024 Du, Wang, Wu, Zhang, Zhang and Xu. This is an open-access article distributed under the terms of the [Creative Commons Attribution License \(CC BY\)](https://creativecommons.org/licenses/by/4.0/). The use, distribution or reproduction in other forums is permitted, provided the original author(s) and the copyright owner(s) are credited and that the original publication in this journal is cited, in accordance with accepted academic practice. No use, distribution or reproduction is permitted which does not comply with these terms.

Targeting bone homeostasis regulation: potential of traditional Chinese medicine flavonoids in the treatment of osteoporosis

Jiazhe Du¹, Yincang Wang¹, Chengliang Wu², Xinyu Zhang¹, Xiaofeng Zhang^{3*} and Xilin Xu^{4*}

¹Graduate School, Heilongjiang University of Traditional Chinese Medicine, Harbin, China, ²Institute of Orthopedics and Traumatology, The First Affiliated Hospital of Zhejiang Chinese Medical University, Hangzhou, China, ³Teaching and Research Section of Orthopedics and Traumatology, Heilongjiang University of Chinese Medicine, Harbin, China, ⁴Department of Orthopedics, The Third Affiliated Hospital of Heilongjiang University of Traditional Chinese Medicine, Harbin, China

Osteoporosis is a systemic metabolic disease characterized by disrupted bone formation/resorption and homeostasis. Flavonoids extracted from traditional Chinese medicinal plants regulate bone homeostasis by intervening in differentiating bone marrow mesenchymal stem cells, balancing the bone immune system, inhibiting oxidative stress response, and reversing iron overload. The target molecules and signaling pathways, such as Wnt/ β -catenin and OPG/RANKL/RANK, directly affect osteoblast/osteoclast activity, exhibiting significant potential in the treatment of OP. Therefore, this study presents a systematic review of the recent literature to provide comprehensive information on the traditional Chinese medicine flavonoids involved in the regulation of bone homeostasis. Also, the molecular mechanisms and pharmacological uses of these metabolites are summarized, and their clinical translation and development potential are discussed.

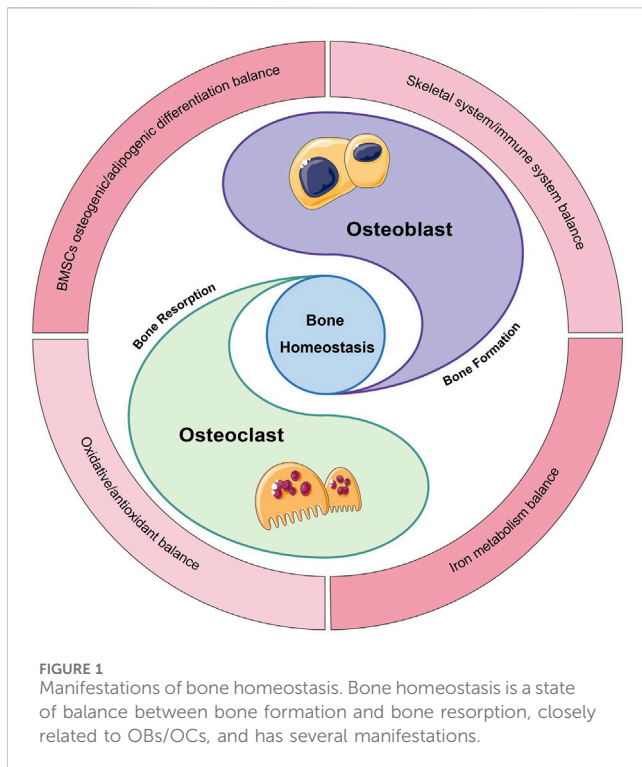
KEYWORDS

flavonoids, osteoporosis, traditional Chinese medicine, bone homeostasis, flavonols

1 Introduction

Osteoporosis (OP) is a systemic bone metabolism disease characterized by decreased bone mineral density, destruction of bone microstructure, and an increased risk of fractures. The incidence of the disease is closely related to age, and primary OP is most common in postmenopausal and senile conditions. As the global population ages, the incidence of this disease is increasing (Zhu et al., 2023).

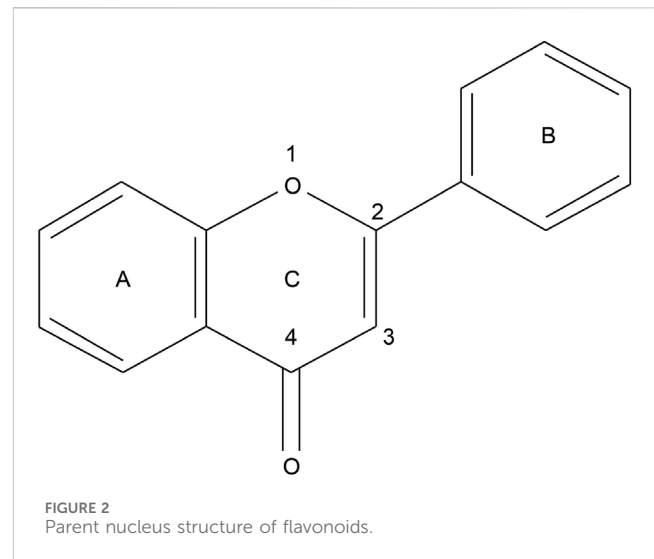
Regarding the mechanism of occurrence, the bone remodeling imbalance theory suggests that the bone resorption rate is greater than the rate of bone formation, which disrupts the body's normal homeostasis, ultimately leading to the development of OP. This process is effected by multicellular bone, the basic functional unit. Also, the damaged bone is resorbed, forming new bone to fill the holes. The unit is mainly composed of osteoblast (OB) and osteoclast (OC) (Loundagin and Cooper, 2022). OB produces new bone, and OC dissolves old bone to mediate bone formation and resorption, respectively, maintaining a dynamic balance for the stability of the skeletal system. Therefore, optimal bone homeostasis is regarded as the balance between OB and OC activities. Literature review identified several manifestations of homeostasis, such as bone marrow mesenchymal



stem cells (BMSCs) osteogenic/adipogenic differentiation balance, skeletal system/immune system balance, oxidative/antioxidative balance, and iron metabolism balance (Figure 1).

Over the years, numerous therapeutic drugs have been developed for OP to improve bone metabolism. Bisphosphonates, calcitonin, oestrogens, their receptor modulators, monoclonal antibodies, and tissue protease inhibitors are used to inhibit bone resorption, while parathyroid hormone and active vitamin D are employed to promote bone formation (Morin et al., 2023). These drugs, whether used alone or in sequential combination, have demonstrated efficacy in regulating bone homeostasis. However, their clinical use is limited due to high costs, adverse effects, and potential carcinogenicity. For instance, bisphosphonates, the most common first-line therapy for OP, work by binding to bone to prevent resorption. Alendronate and zoledronic acid are notable examples. Alendronate often causes esophageal discomfort and gastric dyspepsia, whereas zoledronic acid typically leads to flu-like symptoms and fever in its acute phase (Lu et al., 2020). In addition, hormone therapy is frequently employed during early menopause to counteract bone loss caused by estrogen deficiency. Large doses of exogenous estrogen therapy can increase the risks of breast and endometrial cancer, cardiovascular events, and thromboembolism (Rozenberg et al., 2020). So long-term use of this is discouraged. In recent years, there has been a gradual increase in basic research on the use of traditional Chinese medicine (TCM) for the treatment of OP. TCM exhibits fewer adverse effects compared to conventional first-line drugs, making it suitable for prolonged use. Studies have shown that TCM, either alone or combined with first-line drugs, offers superior clinical efficacy.

Several studies have screened many active metabolites from Chinese herbal plants; flavonoids comprise a significant category.



In terms of avoiding adverse drug reactions, citrus bioflavonoids seem to be safe, without causing side effects even during pregnancy; naringin-derived drugs are used in traditional medicine because of their non-addictive and non-toxic properties (Bampidis et al., 2022); isoflavones not only help reduce the risk of breast and endometrial cancer but also alleviate hot flushes associated with menopause (Gómez-Zorita et al., 2020). Yong et al. (2021) conducted a double-blind experiment on 58 healthy postmenopausal women, administering a daily dose of Epimedium prenylflavonoid extract (740 mg) or a placebo for 6 weeks. Based on verifying the association between the drug and bone synthesis metabolic markers, they further demonstrated that taking the drug was not associated with adverse symptoms, with no observed changes in liver, hematological, and renal parameters. Compared to first-line medications, natural flavonoid metabolites are mostly similar to estrogens, possessing anti-inflammatory, antibacterial, anticancer, antioxidant, osteogenic, osteoclast, and estrogen-like effects (Cushnie and Lamb, 2005). They can regulate disease and body health from a variety of perspectives, not just limited to regulating bone metabolism. This is one of the advantages of these metabolites. In addition, there is a growing body of research demonstrating the superiority of flavonoids alone or in combination with first-line drugs (Oršolić et al., 2014; Liu et al., 2015; Oršolić et al., 2022). This type of research is still scarce, mostly based on animal experiments, and involving clinical evidence is even more rare. Some researchers conducted a randomised double-blind trial among healthy late postmenopausal women (Zhang et al., 2007). They found a significant reduction in bone loss in the intervention group (a daily dose of 60 mg of icariin, 15 mg of daidzein, and 3 mg of genistein). In another clinical study of 360 osteoporosis patients, Epimedium total flavone capsule showed higher efficacy in back pain, leg pain scores, and BMD enhancement rates compared to Gusongbao capsule (Lu et al., 2013). Though there are some flavonoid supplements currently sold as TCM products, wellcharacterised extracts studied through rigorously designed clinical trials are still rare. In addition, a growing body of evidence is suggesting that TCM flavonoids can modulate OB and OC activities to regulate bone homeostasis. Herein, we

conducted a comprehensive systematic review on the potential of TCM flavonoids in treating OP by restoring bone homeostasis.

2 Characterization of flavonoids

As a subclass of polyphenols, flavonoids possess unique chemical structures and biological functions. They, also known as bioflavonoids or plant flavonoids, are predominantly present in food-borne plants, such as vegetables, fruits, legumes, and tea, either in bound or free form (Yonekura-Sakakibara et al., 2019). Structurally, flavonoids refer to a series of compounds in which two phenolic hydroxyl benzene rings (A- and B-ring) are linked to each other by the three central carbon atoms. The basic parent nucleus is 2-phenylchromanone (Figure 2). Approximately, 10,000 types of flavonoids can be categorized based on their structures into flavones, flavonols, flavanones, flavanonols, isoflavones, and others (Yonekura-Sakakibara et al., 2019). Among these, flavones do not have oxygen-containing groups at the “3” position, but if there is an “-OH” or other oxygen-containing groups at the “3” position, they are known as flavonols. Flavanones and flavanonols are based on flavones and flavonols, respectively. The double bond at the C2-C3 position of the C ring is hydrogenated and saturated and hence, termed as dihydroflavones and dihydroflavonols. In the case of isoflavones, the B ring position is connected to the “3” position rather than the “2” position. Regarding stability, it is now generally accepted that flavonoids enhance stability through the conjugation of the C2-C3 double bonds and acyl groups, as well as electronic delocalization. The α and β unsaturated pyranones at the centre of the molecule are the key to their various biological activities. In general, the strength of antioxidant and other biological activities of flavonoids is determined by the number of phenolic hydroxyl groups. The higher the number of substituents, the stronger the activity of scavenging oxygen radicals, especially the neighbouring hydroxyl substitution can greatly increase the activity. Regarding reactivity, the reactivity of flavonoids towards specific targets is dependent on the bioactive hydroxyl group in the structure (He et al., 2021). The Fukui index confirms this by identifying molecule regions susceptible to nucleophilic, electrophilic, and radical attacks (Ayers and Parr, 2000). Regarding drug activity, the broad-spectrum pharmacological activities of flavonoids have been a hotspot for researchers. Demonstrated pharmacological activities include antitumor, antioxidant, anti-inflammatory, antibacterial, and antiviral effects, among others (Guan and Liu, 2016; Shen N. et al., 2022). They can also alleviate cardiovascular diseases such as hyperlipidaemia and myocardial ischaemia. Their mild phytoestrogenic properties render them promising for treating menopausal syndrome in women (Miksicek, 1993).

Up to now, more than 9,000 flavonoids have been isolated from plants. As key constituents of many TCMs, some flavonoids can be extracted directly from TCM plants. However, these metabolites exhibit low solubility, poor stability, and limited bioavailability. Additionally, plant extracts typically comprise complex mixtures. To enhance flavonoids' bioavailability, recent years have seen the adoption of new extraction techniques, including ultrasound and supercritical fluid extraction. Moreover, enhancing activity through the synergistic effects of metabolites extracted from the same plant

has garnered attention. Tomofumi et al. (Shimizu et al., 2018) demonstrated that baicalein, wogonin, and oroxylin A, extracted from scutellaria root, synergistically potentiate LPS-induced PGE2 and NO. Further, these metabolites uniquely inhibit various steps in the NF- κ B signaling pathway. This synergistic effect also extends to the interaction between flavonoids and minerals. Bone minerals like calcium and phosphorus form hydroxyapatite, a crucial bone component also reflected in blood levels. Trace minerals, including magnesium, silicon, and zinc, directly influence bone metabolism. At this stage, some studies have proved that flavonoids can form metal complexes with metal ions or combine with metal nanomaterials to enhance antioxidant and anticancer activities (Matsia et al., 2022; Sysak et al., 2023; Zangade et al., 2023). This process also somewhat enhances the bioavailability of flavonoids.

In the treatment of OP, the anti-OP activity of flavonoids makes them safe and ideal natural therapeutic agents. They offer cost-effectiveness with minimal adverse effects (Guan and Liu, 2016). Previously, there have been a large number of herbal single drugs and compound preparations containing flavonoids that have been shown to have significant therapeutic effects on OP (Zhang et al., 2016). Over the years, a large number of active metabolites have been screened from them, especially total flavonoids of *Rhizoma drynariae* (Shen Z. et al., 2022), total flavonoids of *Epimedium*, and soy isoflavone (Ming et al., 2013). These flavonoids' active metabolites include naringin, icariin, and daidzein. Figure 3 illustrates common TCM flavonoids, highlighting their structural formulas.

3 TCM flavonoids modulate bone homeostasis

Bone homeostasis can manifest in various forms, and the balance disruption can cause OP. The addition of TCM flavonoids can specifically regulate this process by intervening in the differentiation of BMSCs, balancing the bone immune system, inhibiting oxidative stress response, and reversing iron overload. The specific pathways are illustrated in Figure 4.

3.1 Intervention in the differentiation of BMSCs

Bone homeostasis is regulated by BMSCs' osteogenic/adipogenic differentiation balance. In addition, BMSCs can differentiate into OBs and other cells, promote bone marrow tissue repair, and influence the activities of OBs and OCs. This provides a stable internal environment for bone growth and development. Typically, the bone regeneration process is closely related to the balance in osteogenic and adipogenic progenitor cell activities. An imbalance in osteogenic/adipogenic differentiation may arise if the number, proliferative capacity, and differentiation potential of bone progenitor cells decrease due to aging or specific physiological conditions. As a result, the bone homeostatic system regulated by BMSCs will be broken. In terms of mechanism, the classical Wnt signaling pathway, consisting of Wnt/ β -catenin, has been found to be closely linked to bone formation. This pathway regulates OB

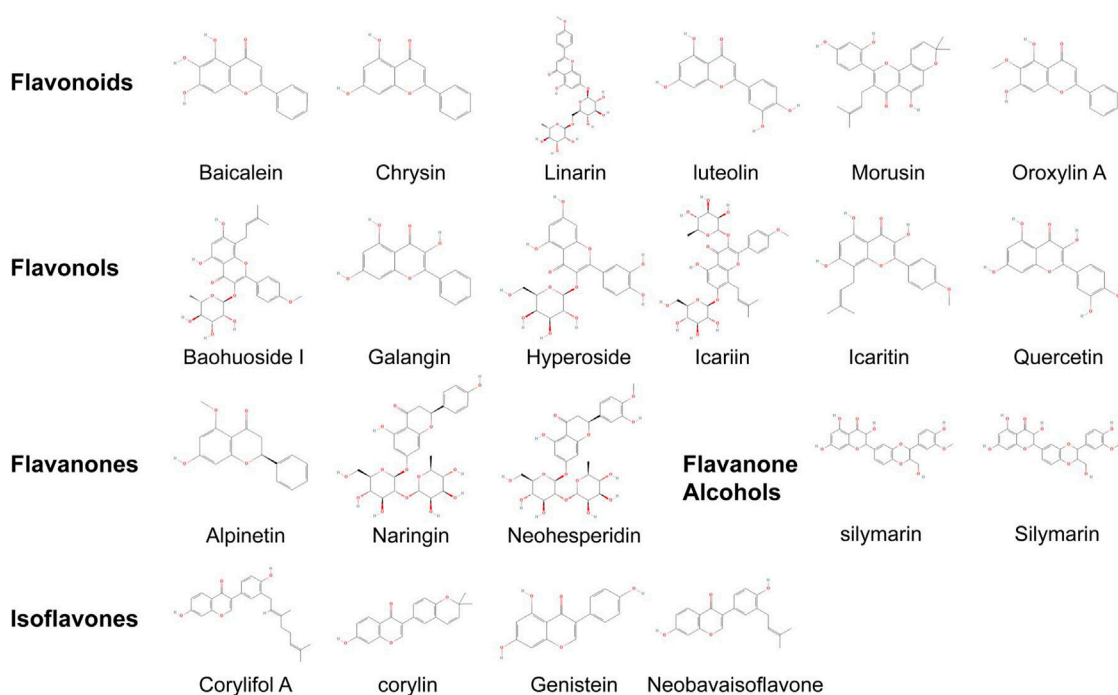


FIGURE 3
Structural formulas and classification of common TCM flavonoids. The compounds listed in this paper can be classified according to the presence or absence of oxygen-containing group substitution at the "3" position, whether the double bond is hydrogenated or not, and the position of the B-ring connection. They can be mainly divided into flavones, flavonols, flavanones, flavanonols and isoflavones.

differentiation and also acts as an inhibitor of adipocyte differentiation. The β -catenin protein in this pathway effectuates differentiation into OBs by inhibiting the adipogenic differentiation of BMSCs (Mei et al., 2022). Recent studies have focused on non-coding RNAs, including miRNAs, lncRNAs, and circRNAs, of which some regulate OP through the Wnt/ β -catenin pathway (Liu et al., 2021; Wang Y. et al., 2022; An F. et al., 2023). They serve as diagnostic markers for disease and help expand the research on related target genes to further clarify the pathogenesis.

Nowadays, the study of TCM has advanced to the protein and gene level of pathways, elaborating the regulation of bone homeostasis via BMSCs' osteogenic/adipogenic differentiation balance with respect to signaling pathway. Among the pathways closely related to the directional differentiation of BMSCs, Wnt/ β -catenin has become a key target for OP intervention using botanical drug extracts. TCM flavonoids, such as neohesperidin, icariin, and morusin, regulate the differentiation of BMSCs into OB through this pathway (Chang et al., 2021; Chen et al., 2021; Gao et al., 2021). Icariin, a pentenyl flavonol glycoside isolated from *Epimedium brevicornu Maxim.* [Berberidaceae; *epimedium folium*], is one of the active metabolites in the treatment of OP and has been studied in depth more than others. One study suggested that the inhibition of BMSC differentiation may be associated with the overexpression of *sclerostin* gene or the transfection treatment of knockdown constructs, and treatment with icariin can reverse this process through the Wnt/ β -catenin pathway (Gao et al., 2021). In addition to the investigation of the classical pathway, Wnt proteins activate non-classical signaling pathways through different receptors. However, these pathways are more complex and

involve a larger number of species compared to the Wnt/ β -catenin pathway. For example, Yuan et al. (2018) proposed that the NF- κ B/ β -catenin signaling pathway regulates BMSCs' osteogenic/adipogenic differentiation balance. Quercetin, a flavonols, reversed these effects by inhibiting this signaling, significantly improving ovariectomized rats' bone structure and function. Similar studies have been conducted based on other signaling pathways (for example, PKA/mTOR/ULK1, JAK2/STAT3, and PKA/CREB) that have elucidated the mechanism of action of some TCM flavonoids in the intervention of BMSCs' differentiation (Wang W. et al., 2022; Zeng et al., 2023a; Zeng et al., 2023b). Among these, alpinetin and galangin attenuated dexamethasone-induced bone loss in mice with OP. Meanwhile, the osteogenic differentiation-inducing effects of these two drugs are related to enhanced autophagic signaling. Alpinetin enhanced the PKA/mTOR/ULK 1 autophagy signaling pathway, while galangin enhanced the PKA/CREB-mediated autophagy flux. In the study on the former, researchers first constructed a mouse model of OP and used parathyroid hormone as a positive control to verify that alpinetin significantly attenuated dexamethasone-induced OP symptoms. The study showed that a daily dose of 40 mg/kg body weight caused no toxic side effects, had negligible effects on OC activity, and initially alleviated OP symptoms. Next, to quantify the expression of osteogenic markers after alpinetin stimulation, osteocalcin (OCN), alkaline phosphatase (ALP), and Runx2 were measured. Combined with the previous experience they finally came to a conclusion that the preventive effect of alpinetin against OP was mediated by augmenting PKA/autophagy signaling because it was suppressed by co-treatment with a PKA inhibitor or autophagy

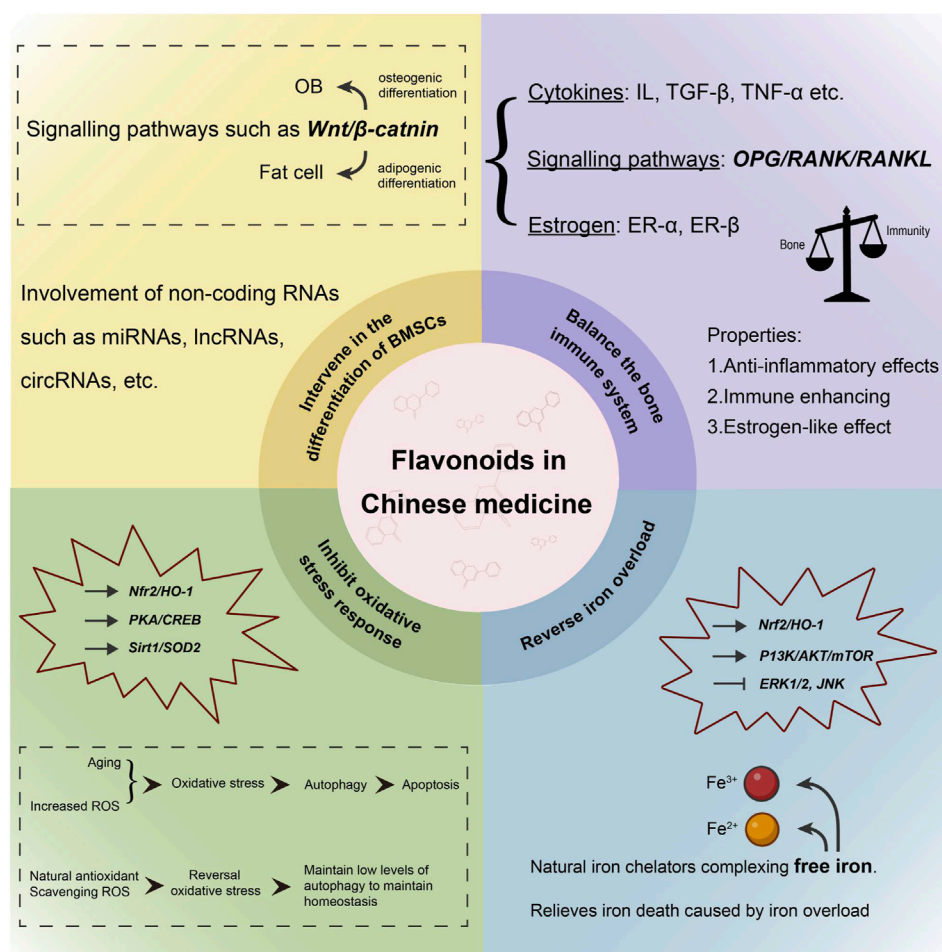


FIGURE 4
Pathways of TCM flavonoids regulating bone homeostasis.

inhibitor. In addition to pathway-specific studies, it was proposed that icariin promotes BMSC differentiation by upregulating miR-335-5p, suggesting that specific miRNAs can also be used as targets for the drug treatment of OP (Teng et al., 2022). This finding has expanded the scope for subsequent research. In addition, there have also been studies comparing TCM flavonoids with first-line drugs in terms of efficacy. For example, compared with the antiresorptive drug, alendronate, and an anabolic drug, PTH1-34, icarrin possessed the positive effects on the co-culture by increasing ALP activity, estradiol production and decreasing acid phosphatase (TRAP) activity (Liu et al., 2015). This goes some way to affirming the need to target flavonoids for R&D at this stage. The relevant studies on the intervention of TCM flavonoids in BMSCs differentiation are summarized in Table 1.

In this part, the mechanisms through which TCM flavonoids intervene in BMSCs are clarified and the outcomes mainly involve promoting differentiation towards OBs to regulate bone homeostasis. BMSCs proliferate and differentiate into osteoblastic precursor cells and further differentiate into mature OBs. The classical Wnt signaling pathway plays an important role in the survival and differentiation of OB. Therefore, this classical pathway

will be the primary entry point in the study of TCM flavonoids for regulating BMSCs differentiation. Based on this pathway, extending to other related signaling pathways (such as NF-κB/β-catenin) or investigating the effects of flavonoids as dietary supplements [such as soy isoflavones (Ge et al., 2023)] on the pathway would be meaningful. Additionally, it has been reported that Wnt signaling pathway, as a key signaling pathway for osteogenic differentiation of BMSCs, is also closely related to the development of hypoxia-induced diseases (Chavali et al., 2020). Bone injuries are usually accompanied by tissue oedema and haematoma, leading to the formation of a local hypoxic environment. Thus, the potential of TCM flavonoids to preserve the osteogenic differentiation capability of BMSCs in hypoxic conditions warrants further research. In addition to this, leveraging existing results and knowledge of relevant signal transduction, forthcoming inquiries could focus on optimizing flavonoid compounds' effectiveness on target cells, introducing other functional proteins or non-coding RNAs into the pathway, facilitating cytokine transmission and controlling cell activation, improving biomarker sensitivity and specificity, and using special medications to mitigate stem cell transplant rejection reactions, which may constitute new avenues of research.

TABLE 1 Studies related to the intervention in the differentiation of BMSCs by TCM flavonoids.

Compound	Source	Model	Mechanism	Result	References
Icariin	<i>Epimedium brevicornu Maxim.</i>	12-week-old female SD rats	Activate the Wnt/ β -catenin pathway; Regulate sclerostin; Enhance ALP activity	Promote <i>in situ</i> proliferation and osteogenic differentiation of BMSCs	Gao et al. (2021)
		Mouse MC3T3-E1 cells and RAW 264.7 cells	Enhance OPG and RANKL gene and protein expression and decrease NF- κ B and RANK expression; Increase ALP and TGF- β 1 levels	Promote osteogenic differentiation and inhibit adipogenic differentiation of BMSCs; Promote OB differentiation and inhibit OC differentiation	Zhang et al. (2017)
		7-week-old female ovariectomized SD rats	Upregulate miR-335-5p to inhibit PTEN	Promote osteogenic differentiation of BMSCs	Teng et al. (2022)
		Human BMSCs	Enhance GLI-1 expression	Promote proliferation and osteogenic differentiation of BMSCs	Xia et al. (2023)
		6-week-old female ovariectomized SD rats	Induce the IGF-1 pathway; Interaction with ER- α to phosphorylate downstream AKT	Promote osteogenic differentiation of BMSCs	Zhou et al. (2021)
Neohesperidin	<i>Citrus \times aurantium f. aurantium</i>	Human BMSCs	Activate the Wnt/ β -catenin pathway	Promote osteogenic differentiation of BMSCs	Chang et al. (2021)
Morusin	<i>Morus alba L.</i>	16-week-old female ovariectomized Wistar rats	Activate the Wnt/ β -catenin pathway	Promote proliferation and osteogenic differentiation of BMSCs	Chen et al. (2021)
Quercetin	<i>Styphnolobium japonicum (L.) Schott</i>	Adult female ovariectomized SD rats	Antagonize the TNF- α -induced NF- κ B/ β -catenin signaling pathway	Promote osteogenic differentiation of BMSCs	Yuan et al. (2018)
Alpinetin	<i>Alpinia hainanensis K.Schum.</i>	Human BMSCs; mouse BMSCs	Enhance the PKA/mTOR/ULK1 autophagy signaling	Promote osteogenic differentiation of BMSCs	Zeng et al. (2023a)
Galangin	<i>Alpinia officinarum Hance</i>	3-month-old hormone-treated female C57BL/6 mice; human BMSCs	Enhance PKA/CREB autophagy signaling	Promote osteogenic differentiation of BMSCs	Zeng et al. (2023b)
Naringin	<i>Citrus \times aurantium f. aurantium</i>	Female Lewis rats	Inhibit activation of the JAK2/STAT3 pathway	Promote osteogenic differentiation of BMSCs	Wang et al. (2022a)
Total flavonoids of <i>Rhizoma drynariae</i>	<i>Drynaria roosii Nakaike</i>	20-week-old male SD rats	Enhance angiogenic-osteogenic coupling by promoting angiogenesis through the PDGF-BB/VEGF/RUNX2/OSX signaling axis	Improve angiogenic capacity and osteogenic capacity of BMSCs	Shen et al. (2022b)
Baohuoside I	<i>Epimedium brevicornu Maxim.</i>	Mouse BMSCs cells	Increase ALP activity in OB; Inhibit IL-1b, IL-6, IL-8, and TNF- α secretion	Stimulate differentiation of BMSCs toward OB and inhibit lipid formation; Modulate immune function	Xi et al. (2019)
Luteolin	<i>Lonicera japonica Thunb.</i>	1.5-month-old SPF-grade female ovariectomized SD rats	Regulate PI3K-Akt signaling pathway activity	Promote differentiation of BMSCs to OB	Liang et al. (2022)

3.2 Balancing the bone immune system

Bone homeostasis is associated with the regulation of skeletal system/immune system balance. The concept of osteoimmunology, first introduced in 2000, highlights the close connection between the two systems (Arron and Choi, 2000). Both bone tissue and immune cells originate from the bone marrow, with bone tissue and immune microenvironment influencing each other in physiological and pathological conditions (Lorenzo et al., 2008). The abnormal activation of the immune system can alter the coupling balance of OB and OC, leading to imbalanced bone homeostasis.

Concurrently, bone metabolism also regulates the immune system through cytokines, signaling pathways, and estrogen (Terashima and Takayanagi, 2018).

Immune cells produce a variety of cytokines that regulate the production and activity of OB and OC through RANKL-dependent or -independent pathways, influencing bone homeostasis. These cytokines include interleukin-8 (IL-8) (Niu et al., 2019), IL-18 (Mansoori et al., 2016), IL-33 (De Martinis et al., 2020a), IL-34 (Xu et al., 2021), IL-37 (Ye et al., 2019), transforming growth factor- β (TGF- β) (Cao et al., 2022) (bone protective factors), IL-1 α (Zheng et al., 2021), IL-1 β (Otsuka et al., 2023), IL-6 (Wang

et al., 2021), IL-17 (Roberts et al., 2022), IL-31 (De Martinis et al., 2020b), TNF- α (Yao et al., 2021), macrophage-stimulating factor (M-CSF) (Inoue et al., 2023), interferon- γ (IFN- γ) (Biros et al., 2022) (bone resorptive factors), and IL-10, IL-27 (Shukla et al., 2017) (pleiotropic factors). TGF- β is a well-studied cytokine that participates in the production of regulatory cells and exerts immunosuppressive functions to maintain immune homeostasis. In maintaining bone homeostasis, it regulates the replication and differentiation of chondrocytes, OBs and OCs, which play crucial roles in bone formation and mineralization. Furthermore, the TGF- β superfamily has a significant impact on the bone structure (Omosule et al., 2023). OPG/RANKL/RANK is a major signaling pathway mediating bone resorption/bone formation. The equilibrium of RANKL and OPG determines the balance of bone homeostasis. RANKL, expressed by BMSCs and OB, binds to RANK, promoting OC differentiation and enhancing bone resorption activity. On the other hand, OPG, produced by B lymphocytes and OB, competes with RANKL to bind RANK. Therefore, the extent to which OPG interferes with the binding between RANKL and RANK determines the rate of bone resorption. Several lymphocytes are involved throughout the production process and pathway regulation (Song et al., 2020; Frase et al., 2023). Thus, it can be deemed that the signaling pathway serves as a link between various OBs, immune cells, and cytokines, influencing the formation and differentiation of OBs and OCs. Similarly, estrogen also affects the skeletal system/immune system balance. Estrogen receptor (ER) is located on the surface of both OBs and OCs and stimulates OBs directly to regulate differentiation and proliferation, matrix mineralization, and mechanical stress response. In addition to affecting receptors, estrogen also contributes to the development of OP by influencing the body's inflammation level (Alippe and Mbalaviele, 2019). Chronic inflammatory factors promote bone resorption while inhibiting bone formation. Low estrogen is predisposed toward a low-level chronic inflammatory state, resulting in elevated TNF- α , IL-1, IL-6, IL-17 and decreased expression of IFN- γ , IL-4, and IL-10 (Cheng C. H. et al., 2022; Azam et al., 2023). Previous studies have examined estrogen and inflammation separately with respect to OP; however, accumulating evidence suggests an interrelation between these two mechanisms. Estrogen may also influence OC activity by regulating inflammatory factors, providing a new theoretical basis for the development of OP.

Furthermore, it could be speculated that the essence of bone immune system balance is that different immune cells and cytokines regulate OBs and OCs through classic pathways, such as OPG/RANKL/RANK to promote or inhibit bone resorption and ultimately achieve bone homeostasis. Many TCM flavonoids possess anti-inflammatory and immune-enhancing properties and directly regulate bone immune homeostasis. This process is closely associated with the targets mentioned above. Icariin is the most common among the numerous TCM and active metabolites that promote bone formation (Wang Z. et al., 2018). A previous study designated icariin-treated bone microvascular endothelial cells (BMECs) as the experimental group and used ultracentrifugation to isolate extracellular vesicles from this group and the blank control group (Zhang et al., 2022). The results revealed significantly increased expression of vascular endothelial growth factor (VEGF) and TGF- β 1, and these contents packaged within the

vesicles were proposed to promote angiogenesis. The assay also detected differential expression of up to 29 inflammatory factors, primarily involved in OC generation, indicating a dual role of icariin in regulating bone homeostasis through the immune pathway. In addition, epimedium plants contain other flavonoids, including icariin A, B, C, and baohuoside I (BHS I), that exhibit anti-OP activity. In one study, Xi et al. (2019) conducted experiments on BHSI. *In vitro*, the positive control group was treated with genistein, a drug that has been shown to be effective, and the experimental group was treated with different concentrations of BHSI. ALP and TRAP staining revealed that a low concentration (1 μ mol/L) of BHSI promoted osteogenic differentiation and inhibited adipogenic differentiation. Meanwhile, *in vivo*, they examined serum inflammatory factor levels in the BHSI-treated de-ovulated rat model and found significant reductions in IL-1 β , TNF- α , IL-6 and IL-8. This indicates that BHSI modulates abnormal immune functions. In addition, they critically verified the estrogen-like effects of BHSI due to its structural similarity to icariin. However, it turned out that BHSI did not react with ER- α and ER- β *in vitro*. In terms of inhibiting inflammatory system responses, linarin, a key metabolite of TCM *Chrysanthemum indicum* L. [Asteraceae; *chrysanthemi indici* flos] and *Buddleja officinalis* Maxim. [Scrophulariaceae; *buddlejae* flos], was identified by Yang et al. (2022) to reduce the levels of NF- κ B, p65, IKK β , IL-6, and TNF- α . And among the studies on signalling pathways, OPG/RANK/RANKL is undoubtedly the most representative. Hyperoside is present in many botanical drugs and can be extracted from quercetin. Experimental evidence suggests that hyperoside promotes bone formation and reduces bone resorption by inactivating the Traf 6-mediated RANKL/RANK/NF- κ B pathway, thereby increasing the OPG/RANKL ratio (Chen et al., 2018). In another study, Jiang et al. (2018) experimented with the epimedium-derived isomeric flavonoids CIT and IT. Validated by molecular docking and animal experiments, they found that the combination of isomeric flavonoids (CIT/IT) with OPG/RANKL targets attenuated the excitation effect of OPG or RANKL on RANK. Moreover, since CIT binds stronger to RANKL than IT, CIT has a more significant ability to inhibit bone resorption. Over all, these findings show the effects of TCM flavonoids on immune cells, cytokines, and signaling pathways. Introducing the variable “estrogen” in studies on flavonoids to regulate the bone immune system would aid in comprehending the effects of TCM on postmenopausal conditions characterized by low estrogen levels and decreased immune function. For instance, molecular docking was used to confirm that chrysin, an extract derived from *Oroxylum indicum* (L.) Kurz in the family Bignoniaceae, interacts with both α and β estrogen receptors with exothermic binding energies of 229.83 kcal/Mol and 252.72 kcal/Mol, respectively, and also fits perfectly into the active site of both α and β estrogen receptors (Ibrahim et al., 2021). The interaction between the drug and the receptor reversed the reduction in estradiol caused by ovariectomy. These metabolites have phytoestrogenic effects that act by binding to the estrogen receptor. Phytoestrogens are a good alternative to hormone replacement therapy. The use of natural phytoestrogens can, to some extent, avoid the adverse effects of long-term administration of exogenous oestrogens, such as breast cancer and endometrial cancer. These drugs are useful in the treatment of OP in postmenopausal women and deserve special attention. For

TABLE 2 Studies related to the balancing of skeletal immune system by TCM flavonoids.

Compound	Source	Model	Mechanism	Result	References
Icariin	<i>Epimedium brevicornu Maxim.</i>	Male SD rats	Inhibit the RANKL-p38/ERK-NFAT pathway	Inhibit OC differentiation	Cheng et al. (2022b)
		Bone marrow-derived macrophages; rat BMSCs	Promote macrophage polarization toward anti-inflammatory M2 type; Promote osteogenic differentiation of BMSCs and inhibit RANKL-induced OB formation by modulating macrophage cytokines	Modulate host immune response; promote osseointegration	Chai et al. (2022)
		Isolated BMECs in the femoral head of patients with primary and secondary OP	Promote VEGF and TGF- β 1 expression in isolated EVs; Differentially express 29 inflammatory factors	Enhance the role of EV in reversing glucocorticoid-induced injury in BMECs	Zhang et al. (2022)
Baohuoside I	<i>Epimedium brevicornu Maxim.</i>	Female ovariectomized SD rats	Downregulate IL-1 β , TNF- α , IL-6, and IL-8	Inhibit bone resorption	Xi et al. (2019)
Linarin	<i>Chrysanthemum indicum L.</i>	2-month-old C57BL/6 male mice	Downregulate MDA; Downregulate NF- κ B, p65, IKK β , IL-6, and TNF- α	Downregulate RANKL/RANK to reduce OC generation	Yang et al. (2022)
Hyperoside	<i>Hypericum perforatum L.</i>	68-week-old female ovariectomized Kunming mice	Inhibit TRAF-6-mediated RANKL/RANK/NF- κ B pathway and increase OPG/RANKL ratio	Increase bone density and restore bone trabecular microarchitecture	Chen et al. (2018)
		8-week-old female ovariectomized C57BL/6 mice	Downregulate miR-19a-5p-mediated IL-17A levels	Relieve bone resorption	An et al. (2023b)
Chrysin	<i>Oroxylum indicum (L.) Kurz</i>	3-month-old female ovariectomized Wistar rats	Interact with ER- α and ER- β	Reduce bone remodeling marker alterations and increase bone mineral content	Ibrahim et al. (2021)
Oroxylin A	<i>Oroxylum indicum (L.) Kurz</i>	6-week-old C57BL/6J mice	Reduce ROS levels through Nrf2-mediated antioxidant responses; Attenuate NFATc1 activity	Inhibit RANKL-induced OC activity; Prevent OVX-induced and LPS-induced bone loss	Xian et al. (2021)
Corylin	<i>Psoralea fructus</i>	8-week-old C57BL/6 mice	Inhibit P65 nuclear translocation; Attenuate NF- κ B and NFATc1 activity	Inhibit OC differentiation	Yu et al. (2021)
Total flavonoids of <i>Rhizoma drynariae</i>	<i>Cullen corylifolium (L.) Medik.</i>	Murine BMSCs, MC3T3-E1 cells subclone 14, IDG-SW3 cells, RAW 264.7 cells	Modulate Wnt/ β -catenin pathway and OPG/RANKL/RANK axis by combined metformin	Improve bone mineral density, bone trabecular microstructure, and mechanical properties	Jiang et al. (2023b)

example, among several soybean isoflavones, genistein has the most positive effects on bone cells without any significant adverse effects on the breast and uterus cells due to its high affinity for ER- β receptors compared to ER- α (Arcoraci et al., 2017). Specific studies related to TCM flavonoids balancing the bone immune system are summarized in Table 2.

The emergence of osteoimmunology emphasizes the involvement of the immune microenvironment in the pathological development of OP. This process is regulated by the immune system, which includes bone formation and resorption. TCM flavonoids regulate skeletal system/immune system homeostasis by interfering with cytokines, signalling pathways and estrogen. The OPG/RANK/RANKL pathway, recognized as a key pathway, has been the focus of some studies searching for flavonoids that can specifically regulate it. Flavonoids targeting RANKL or its receptor RANK could open new treatment avenues for OP, particularly in inhibiting excessive bone resorption. An example is the isomeric flavonoid (CIT/IT) mentioned above. Furthermore, it is worth noting that monoclonal antibodies (mAbs) generated by B cells play a considerable role in the treatment of OP. For instance, RANKL mAbs like denosumab inhibit bone resorption, whereas sclerostin

mAbs like romosozumab promote bone formation. In terms of the connection between flavonoids and mAbs, the hotspots of research at this stage mainly focus on “adding specific flavonoids to promote cell culture to increase the production of mAbs (Toronjo-Urquiza et al., 2020; Noguchi et al., 2023)” and “producing specific mAbs for flavonoids and establishing immunoassay methods (Zhang et al., 2023).” Although this research is in its early stages, it shows promising potential and merits further investigation.

3.3 Inhibiting oxidative stress response

The oxidative/antioxidative balance directly influences bone homeostatic regulation, while estrogen deficiency has been traditionally viewed as the primary cause of OP. Recent mechanistic studies suggested significant pathogenic roles of aging and elevated reactive oxygen species (ROS). Oxidative stress arises from an imbalance between oxidation and antioxidation within the body, wherein ROS production surpasses the buffering capacity of the antioxidant defense system, leading to cellular damage and apoptosis. In the regulation of bone homeostasis, oxidative stress reduces OB

activity, further decreasing bone mass and promoting OC production, which causes an imbalance in bone mass. The former may be related to P13K (Ding et al., 2016) and ERK5 (Xia et al., 2017) pathways; the latter might be closely linked to the high expression of NF- κ B (Li et al., 2018). In a recent study, *DDIT3* and *FOXO3* were identified as biomarkers of oxidative stress in postmenopausal OP by bioinformatics analysis (Liu et al., 2023). Subsequently, a TF-miRNA-mRNA network associated with these two characterized genes was constructed, offering potential biological targets for future clinical treatment. In addition, oxidative stress can also activate cellular autophagy signaling pathways. Under normal physiological conditions, cells maintain a basal level of autophagy to preserve homeostasis by eliminating damaged organelles. However, under stress conditions, autophagy is upregulated, leading to organelle degradation and induction of apoptosis. In bone tissue, autophagy influences the survival and differentiation of OBs and OCs, regulating oxidative/antioxidative balance and affecting bone homeostasis. In another study, OBs were treated with the autophagy blocker 3-MA and the autophagy activator RAP, respectively (Li et al., 2017). Flow cytometry analysis revealed that autophagy partially mitigated the damage induced by oxidative stress and promoted OB proliferation. However, excessive autophagy activated the apoptotic pathway, leading to OB apoptosis. Apparently, not only oxidative stress has a bidirectional regulatory effect on autophagy, but also autophagy has a bidirectional regulatory effect on bone metabolism.

The mutual antagonism between oxidative/antioxidative responses and the activation of autophagy in senescent cells directly affects the balance of bone homeostasis. Flavonoids, such as soy isoflavones, icariin, silymarin, and other botanical drug extracts, are well-known natural antioxidants with potent anti-inflammatory properties as well as strong antioxidant activity and reducibility. Compared to clinical first-line use, studies have shown that chrysin and quercetin are superior to alendronate as preventive agents on a number of criteria (Oršolić et al., 2014). Several years later they further found that treatment with chrysin or naringenin improved bone quality, reduced bone resorption, and bone mineral deposition, although with a lower efficacy compared with alendronate (Oršolić et al., 2022). However, flavonoids exhibited more pronounced antioxidative, anti-inflammatory and phytoestrogenic activities. These metabolites inhibit the production of ROS radicals by directly blocking free radical chain reactions through the phenolic hydroxyl groups in their structure and promote the decomposition of accumulated free radicals by enhancing the activity of endogenous antioxidant enzymes. Therefore, studies have also investigated the regulation of bone homeostasis by TCM flavonoids through this pathway. Additionally, the studies on dihydroflavone compound silymarin demonstrated its ability to enhance serum total antioxidant capacity (TAC) and SOD2 production while reducing MDA production, thereby decreasing ROS levels and restoring bone homeostasis (Tao et al., 2022). SOD is an antioxidant enzyme that scavenges free oxygen radicals, while MDA is a cytotoxic lipid oxidation product. Naringenin and chrysin, two commonly occurring flavonoids, are also derived from natural TCM plants. The former is widely detected in *Citrus × aurantium* f. *aurantium* of the Rutaceae family, and the latter is most common in *Oroxylum indicum* (L.) Kurz of the Bignoniaceae family. These two drugs can be extracted through

alcohol extraction, chromatography and crystallization. Overall, the regulatory system of bone homeostasis can be considered an interconnected network, wherein individual balances interact and influence each other. In addition to studying the effects of TCM flavonoids on oxidative stress and autophagy alone, recent studies have combined this balance with skeletal system/immune system balance and iron metabolism balance. For instance, a Chinese study assessed the widely used drug icariin in autophagy (Bai et al., 2023). The researchers incubated BMSCs with 100 μ M H₂O₂ to construct a model of senescence state and used 3-MA as a control. They found that icariin at a concentration of 0.1 μ M significantly enhanced the expression of autophagic-related genes and activated autophagy in senescent macrophages and rejuvenates osteogenesis of senescent BMSCs. The study also provided insights into the transcriptomic analysis, revealing the significant association of the TNF- α signaling pathway with the level of autophagy, further supporting the concrete data on the mechanism of action of icariin in regulating autophagy and reducing inflammation.

Additionally, a study reported for the first time the mechanism of quercetin in treating OP caused by iron overload (Xiao et al., 2023). In this experiment, quercetin characteristically reduced apoptosis and ROS production induced by ferric ammonium citrate (FAC). It upregulated Bcl-2 while downregulated the expression of caspase 3 and Bax. These effects were achieved through activating the Nrf2/HO-1 signaling pathway and attenuating FAC-induced oxidative stress damage. In addition to conventional drug intervention targets, recent studies have also focused on combining flavonoid metabolites with other materials to create novel coatings. Based on mussels, Yang et al. (2023) loaded baicalein (BAI) onto bovine serum albumin (BSA) and added tannic acid (TA) to prepare a TA/BAI-BSA composite protein that scavenges ABTS⁺ and DPPH[•] + free radicals, exhibiting significant antioxidant effects. Tao et al. (2022) modified hydroxyapatite coatings with silybin, a major component of silymarin, to study the effects of interfering with oxidative/antioxidant balance on osteogenic differentiation under high glucose conditions. The findings indicated that silybin restores OB function by activating the SIRT1/SOD2 pathway. The specific studies related to TCM flavonoids for inhibiting oxidative stress response are summarized in Table 3.

The pathological mechanisms of OP are complex, encompassing oxidative stress and autophagy. Therefore, whether flavonoid botanical drugs should be used as antioxidants alone or in combination with other treatments requires further investigation. Besides understanding the mechanisms through which flavonoids influence oxidative/antioxidant balance and autophagy homeostasis, current research is focused on the impact of external factors such as estrogen, glucocorticoids, hyperglycemia, and hypoxia. Additionally, in the field of biomaterials preparation, the application of TCM flavonoids composite implants in bone restoration and the development of novel coatings and scaffolds provide research directions for the future.

3.4 Reversing iron overload

Iron overload disrupts iron metabolic homeostasis, leading to death and risk of bone homeostatic imbalance. Iron death is

TABLE 3 Studies related to the inhibition of oxidative stress by TCM flavonoids.

Compound	Source	Model	Mechanism	Result	References
Genistein	<i>Glycine max (L.) Merr.</i>	12-week-old female ovariectomized SD rats	Target ER- α to inhibit p16 ^{INK4a} expression; upregulate SIRT3 and PGC-1 α expression	Rescue BMSCs from premature senescence; Elevate ROS levels and mitochondrial dysfunction	Li et al. (2023)
Icariin	<i>Epimedium brevicornu Maxim.</i>	12-week-old female ovariectomized BALB/c mice	Upregulate autophagy-related genes <i>LC3B/A</i> , <i>Atg5</i> , <i>Atg7</i> expression and downregulate autophagy marker P62 expression; Activate the TNF pathway	Activate senescent macrophage autophagy and OC differentiation	Bai et al. (2023)
Quercetin	<i>Styphnolobium japonicum (L.) Schott</i>	MC3T3-E1 cells	Activate the Nrf2/HO-1 pathway	Counteract iron overload-induced oxidative stress damage	Xiao et al. (2023)
Silymarin	<i>Silybum marianum (L.) Gaertn.</i>	12-week-old female ovariectomized SD rats	Promote serum TAC and SOD2 production, reduce MDA production and lower ROS levels	Promote SIRT1 and SOD2 transcription in iron-overloaded MC3T3-E1 to restore bone metabolic homeostasis	Tao et al. (2022)
Baicalein	<i>Scutellaria baicalensis Georgi</i>	MC3T3-E1 cells	Remove ABTS+ and DPPH free radicals	Reduce H ₂ O ₂ oxidation-induced intracellular ROS to maintain oxidative stress viability	Yang et al. (2023)
Silibinin	<i>Silybum marianum (L.) Gaertn.</i>	3-month-old female SD rats; MC3TE-E1 cells	Activate the SIRT1/SOD2 pathway and reduce ROS levels	Improve OB activity and enhance osseointegration	Tao et al. (2022)
Corylifol A	<i>Cullen corylifolium (L.) Medik.</i>	9-week-old female ovariectomized SPF mice	Enhance the expression of antioxidant enzyme genes <i>Cat</i> , <i>Hmox1</i> , and <i>Nqo1</i> ; Promote the production of antioxidant enzymes CAT and NQO1	Clear ROS and inhibit OC differentiation	Xu et al. (2023)
Galangin	<i>Alpinia officinarum Hance</i>	3-month-old male C57BL/6 mice; human BMSCs	Enhance the PKA/CREB signaling	Induce autophagy; Enhance osteogenic differentiation	Zeng et al. (2023b)
Neobavaisoflavone	<i>Cullen corylifolium (L.) Medik.</i>	Mouse MC3T3-E1 cells	Activate the CRNDE-mediated Nrf2/HO-1 pathway	Reverse hormonal effects on apoptosis; Affect ROS, MDA, LDH, and Nrf2 levels to protect OB from oxidative stress	Zhu et al. (2021)
Total flavonoids of Rhizoma dryariae	<i>Drynaria roosii Nakaike</i>	Aged female ovariectomized SPF rats	Increase SOD and GSH-Px activity and reduce ROS and MDA production	Improve antioxidant defenses; Increase bone density and reduce bone mineral loss	Mu et al. (2021)

characterized by iron-dependent lipid peroxidation, ROS-induced cell membrane rupture, and mitochondrial miniaturization. A correlation has been established between iron metabolic homeostasis and the oxidative/antioxidant balance. Excessive free Fe²⁺ reacts with lipid peroxides through Fenton reaction, resulting in high levels of ROS accumulation that lead to bone loss (Stockwell et al., 2017; Agidigbi and Kim, 2019). In terms of bone homeostasis, iron overload can inhibit OB activity, interfering with its differentiation and mineralization processes and activating OC activation, causing bone loss and leading to OP. The degree of iron overload is positively correlated with the development of OP (Balogh et al., 2018). In a study on OB, Cen et al. (Luo et al., 2022) concluded that iron death caused by iron overload inhibits OB differentiation via FAC. Mechanistically, this process is achieved by downregulating the expression of Wnt target genes, interfering with the transcription of the Wnt reporter gene *TopFlash* and inhibiting the classical Wnt signaling. A study on OC revealed that iron stimulates OC production in bone marrow-derived macrophages, which is mechanistically dependent on ROS production and activation of the NF- κ B signaling pathway (Wang X. et al., 2018). In addition to the effects of iron overload, iron deficiency can also

lead to bone loss. Some studies established an iron-deficient environment by chelating iron in the medium using desferrioxamine. These also showed that the effect on OB exhibits a biphasic response. Specifically, cell metabolism is enhanced in mild iron deficiency, while in severe iron deficiency, cell activity is greatly suppressed (Zhao et al., 2012).

Iron death directly affects bone homeostasis, primarily caused by iron overload, which is often treated with iron chelators that facilitate iron excretion, eliminate free iron, reduce iron accumulation in tissues, and alleviate bone loss (Bordbar et al., 2019). The approved iron chelators, deferoxamine, deferiprone, and deferasirox, are effective but have some side effects. Flavonoids have gained increasing attention due to their exceptional iron chelation, antioxidant, and low toxicity properties; hence, several studies have investigated their potential as plant-based iron chelators. As an example, quercetin-treated dendritic cells exhibit gene activation that enhances extracellular iron export and mitigates inflammatory response, thereby reducing intracellular iron levels. Another study proposed that quercetin affects hepcidin expression via the BMP6/SMAD4 signaling pathway, mitigating ethanol-induced iron overload-induced liver injury. In the treatment of orthopedic

TABLE 4 Studies related to reversal of iron overload by TCM flavonoids.

Compound	Source	Model	Mechanism	Result	References
Icariin	<i>Epimedium brevicornu Maxim.</i>	MC3TE-E1 cells; 5-week-old C57BL/6 mice	Promote OB survival; Reverse iron overload-induced decrease in Runx2, alkaline phosphatase and bone-bridging protein expression	Reverse excess iron ion-induced bone loss	Jing et al. (2019)
		Male SD rats	Regulate mitochondrial fusion and division; Activate the PI3K/AKT/mTOR pathway and inhibit the ERK1/2 and JNK pathways	Reduce damage to BMSCs from iron overload	Yao et al. (2019)
Icaritin	<i>Epimedium brevicornu Maxim.</i>	Female Kunming mice, female SD rats; zebrafish embryos	Complex-free iron to construct AIP	Reduce iron overload and low-bone density promotes osteogenesis	Jiang et al. (2023a)
Quercetin	<i>Styphnolobium japonicum (L.) Schott</i>	MC3TE-E1 cells	Increase ALP activity to promote bone mineralization nodule formation; Upregulate Runx2, Osterix, and Bcl-2 expression; Downregulate caspase 3 and Bax expression; Activate the Nrf2/HO-1 pathway	Attenuates FAC-induced oxidative stress damage, iron deposition, and bone loss	Xiao et al. (2023)
Silymarin	<i>Silybum marianum (L.) Gaertn.</i>	12-week-old female ovariectomized SD rats	Promote OB proliferation and differentiation and increase OB ability to secrete ALP and mineralization; Enhance the transcription and expression levels of target genes, such as <i>Runx-2</i> , <i>SOD2</i> , and <i>SIRT1</i>	Improve bone metabolism and oxidative stress status	Tao et al. (2022)

diseases, naringenin and icariin have been proven to attenuate cartilage damage and promote chondrocyte proliferation and differentiation in the iron overload state (Wang et al., 2016; Pan et al., 2022). Evidently, specific flavonoids from TCM positively regulate iron homeostasis, with research extending to orthopedic conditions, such as arthropathy. Table 4 provides specific information on regulating OP by reversing iron overload. The research in this field is yet in the early stages, with limited publications and depth of exploration compared to other balances. Icariin is one of the most popular medications that has been shown in numerous trials to relieve OP and promote bone regeneration. Yao et al. (2019) used a 100 μ M FAC-treated model to simulate iron overload and observed that epimedium glycosides at concentrations of 0.1, 1, and 10 μ M significantly enhanced the expression of Runx2, OPN, and β -catenin proteins, identifying 1 μ M as the optimal concentration. Meanwhile, icariin safeguarded BMSCs against the collapse in mitochondrial membrane potential (MMP) due to iron overload and mitigated FAC's inhibitory impact on JC-1 aggregate formation. In addition, icaritin, the glycosidic ligand of the other two metabolites (icariin, baohuoside I) of the *Epimedium brevicornu Maxim.* plant, has adequate musculoskeletal permeability and iron complexing properties. It can also utilize unstable plasma iron to construct artificial iron pools that would reverse the iron overload and promote osteogenesis (Jiang J. et al., 2023). Icaritin was hypothesized to act as a potential natural phytochelator in this experiment. The regulatory processes of TCM flavonoids are directly related to the balance of oxidative/antioxidative systems. Iron overload leads to an excess of lipid ROS free radicals, leading to the accumulation of lipid hydroperoxides and disruption of cell membrane structure, which ultimately triggers iron death.

In conclusion, iron chelators constitute a potential therapeutic strategy in animal models. Iron overload and the phenomenon of iron death causing OP have also become a hot topic of research. Nonetheless, in-depth studies would utilize the unique advantages of

TCM flavonoids in addition to their chelating, oxidizing, and low side effects. For instance, future research would focus on investigating the role of various hormones (EPO and iron modulators) and the impact of external factors, such as inflammation, acidosis, and anemia. Notably, in recent years, our understanding of the mechanism of iron death has improved, and another theory known as “copper death” has gained significant attention. Copper death is distinct from iron death and oxidative stress in terms of the underlying mechanism that triggers OP. The phenomenon is closely related to immune factors and directly mediates the skeletal system/immune system balance (Xu et al., 2018; Liu et al., 2022). Similarly, TCM plants have significant potential for the study of copper death on OP. For instance, copper oxide quantum dots were successfully synthesized on chitosan with the aid of *Angelica sinensis*, resulting in enhanced OB activity and alleviating OP(Hu et al., 2019).

4 Conclusion and future perspectives

TCM has a long history in the treatment of OP. Presently, bone-active metabolites contained in TCM have become the focus of OP research, with pharmacologists exploring their mechanisms of action. The treatment of OP is complex, with equal importance placed on inhibiting bone destruction and enhancing bone formation. In clinical practice, combining multiple drugs, including sequential therapy, is commonplace. With its unique multi-target and multi-pathway advantages, TCM can effectively treat complex diseases with lower dosages. At the same time, TCM can also be taken in the form of dietary therapy, which can overcome the drawbacks and adverse effects of long-term administration of conventional drugs. Human diets not only contain six major nutrients but also non-nutrient components such as flavonoids. Flavonoids play a therapeutic and regulatory role in bone health by affecting the body's absorption of minerals such as calcium and

magnesium, as well as the synthesis of collagen (a major component of the bone matrix). Moreover, from the perspective of TCM, it is common to use of several herbal plants' mixtures or drug pair as a therapeutic option. So using flavonoids as a dietary supplement has great potential and it will help to avoid the damage caused by first line drugs' side effects. However, we must also recognize that current research is still largely focused on cellular and animal experiments. Screening for efficient TCM flavonoids for new drug development and their early clinical validation and use is greatly beneficial for the advancement of this field.

Herein, this paper categorises and summarises four different types of balance affecting bone homeostasis, each of which is independent but interrelated. The closest connections were skeletal system/immune system balance, oxidative/antioxidant system balance, and iron metabolism balance, whereas the BMSCs osteogenic/adipogenic differentiation appeared more as a consequence. The therapeutic mechanism of TCM flavonoids for OP also unfolds based on balance. It is through "intervening in the differentiation of BMSCs," "balancing the bone immune system," "inhibiting oxidative stress response," and "reversing iron overload" that drugs characteristically target OBs or OCs, and ultimately re-establish a new bone homeostasis. Exploring pathogenesis from the perspective of bone metabolic homeostasis offers fresh insights into the mechanisms of drug action and the development of new therapeutic targets. Similarly, many balancing systems, such as copper metabolism balance and intestinal flora balance, have homeostatic properties, which have not yet been studied and may be a potential hot spot in the future. In copper metabolism, copper and iron are trace elements in the human body, which can be investigated by analogy based on the existing results of iron metabolism balance, while the intestinal flora balance can be linked to the gut-bone and other balance axes. These phenomena would aid in studying the effects of intestinal flora, microorganisms, and endocrinology on bone homeostasis. Additionally, in terms of signalling pathways, it is not difficult to find that Wnt/ β -catenin and OPG/RANKL/RANK are deservedly the star pathways in the study of flavonoids in treating OP, and many recent studies are based on these two. Further research could identify targeted agonists or inhibitors for these pathways. Besides this, the research process on other pathways must be accelerated.

Despite the potential of TCM flavonoids in regulating bone homeostasis, the experimental research faces limitations. 1) The chemical composition of flavonoids extracted from different TCM sources varies considerably, which can affect their biological activity and efficacy in treating OP. Future research could focus on characterizing flavonoid profiles of TCM more precisely to establish standardized extracts for clinical evaluation. 2) Many flavonoids have low bioavailability due to poor absorption, rapid metabolism, and elimination. It is necessary to enhance the bioavailability of flavonoids through means such as biotransformation and novel drug delivery systems to exert their biological activity. 3) Indicators such as therapeutically effective dose, dietary recommendations and maximum tolerable intake are uncertain, and side effect manifestations require long-term follow-up studies. 4) The current studies on flavonoids remain at the level of animal experiments, with only a few clinical experiments, due to the bidirectional regulatory effect and multi-targeting properties of

TCM. 5) Apart from studies on single drugs, studies on multi-targets and multi-pathways for the combined use of multiple TCM are still at a low level. There is a need to improve the design of trials and expand the samples of clinical studies. 6) Besides the in-depth research on well-known phytoestrogenic ingredients such as soy isoflavones and corylin, controversies persist regarding phytoestrogen concentrations and the regulation of estrogen receptor genes in OB and BMSCs. Subsequently, estrogen-like activity screening and comparisons of TCM metabolites are needed. 7) Progress in translating research into innovative applications is limited. Future efforts should explore using TCM flavonoids to develop new cellular scaffolds and coatings. These findings expand our understanding of various diseases, such as OP, leading to fractures and bone defects.

In conclusion, TCM flavonoids have promising prospects for development and application with advancing technology. The research in this field will provide new insights for finding effective and safe natural medicines. At the same time we have identified limitations and offered some practical solutions. It is necessary to utilize the advantages of TCM in treating OP, and explore the integration of Chinese and Western medicine. At the same time, focusing on the innovation the dietary therapies and development of new drugs from TCM flavonoids is of great significance for the prevention and treatment of OP.

Author contributions

JD: Writing—original draft. YW: Data curation, Formal Analysis, Writing—review and editing. CW: Methodology, Writing—review and editing. XnZ: Conceptualization, Writing—original draft. XaZ: Conceptualization, Supervision, Writing—review and editing. XX: Investigation, Writing—original draft.

Funding

The author(s) declare that financial support was received for the research, authorship, and/or publication of this article. National Natural Science Foundation of China (No. 82374496).

Conflict of interest

The authors declare that the research was conducted in the absence of any commercial or financial relationships that could be construed as a potential conflict of interest.

Publisher's note

All claims expressed in this article are solely those of the authors and do not necessarily represent those of their affiliated organizations, or those of the publisher, the editors and the reviewers. Any product that may be evaluated in this article, or claim that may be made by its manufacturer, is not guaranteed or endorsed by the publisher.

References

- Agidighi, T. S., and Kim, C. (2019). Reactive oxygen species in osteoclast differentiation and possible pharmaceutical targets of ROS-mediated osteoclast diseases. *Int. J. Mol. Sci.* 20 (14), 3576. doi:10.3390/ijms20143576
- Alippe, Y., and Mbalaviele, G. (2019). Omnipresence of inflammasome activities in inflammatory bone diseases. *Semin. Immunopathol.* 41 (5), 607–618. doi:10.1007/s00281-019-00753-4
- An, F., Meng, X., Yuan, L., Niu, Y., Deng, J., Li, Z., et al. (2023a). Network regulatory mechanism of ncRNA on the Wnt signaling pathway in osteoporosis. *Cell Div.* 18 (1), 3. doi:10.1186/s13008-023-00086-7
- An, H., Chu, C., Zhang, Z., Zhang, Y., Wei, R., Wang, B., et al. (2023b). Hyperoside alleviates postmenopausal osteoporosis via regulating miR-19a-5p/IL-17A axis. *Am. J. Reprod. Immunol.* 90 (1), e13709. doi:10.1111/aji.13709
- Arcoraci, V., Atteritano, M., Squadrito, F., D'Anna, R., Marini, H., Santoro, D., et al. (2017). Antiosteoporotic activity of genistein aglycone in postmenopausal women: evidence from a post-hoc analysis of a multicenter randomized controlled trial. *Nutrients* 9 (2), 179. doi:10.3390/nu9020179
- Arron, J. R., and Choi, Y. (2000). Bone versus immune system. *Nature* 408 (6812), 535–536. doi:10.1038/35046196
- Ayers, P. W., and Parr, R. G. (2000). Variational principles for describing chemical reactions: the fukui function and chemical hardness revisited. *J. Am. Chem. Soc.* 122 (9), 2010–2018. doi:10.1021/ja9924039
- Azam, Z., Sapra, L., Baghel, K., Sinha, N., Gupta, R. K., Soni, V., et al. (2023). Cissus quadrangularis (hadjod) inhibits RANKL-induced osteoclastogenesis and augments bone health in an estrogen-deficient preclinical model of osteoporosis via modulating the host osteoimmune system. *Cells* 12 (2), 216. doi:10.3390/cells12020216
- Bai, L., Liu, Y., Zhang, X., Chen, P., Hang, R., Xiao, Y., et al. (2023). Osteoporosis remission via an anti-inflammatory effect by icariin activated autophagy. *Biomaterials* 297, 122125. doi:10.1016/j.biomaterials.2023.122125
- Balogh, E., Paragh, G., and Jeney, V. (2018). Influence of iron on bone homeostasis. *Pharm. (Basel)* 11 (4), 107. doi:10.3390/ph11040107
- Bampidis, V., Azimonti, G., Bastos, M. L., Christensen, H., Dusemund, B., Fašmon Durjava, M., et al. (2022). Assessment of the feed additive consisting of naringin for all animal species for the renewal of its authorisation (HealthTech Bio Actives, S.L.U. (HTBA)). *Efsa J.* 20 (4), e07267. doi:10.2903/j.efsa.2022.7267
- Biros, E., Malabu, U. H., Vangaveti, V. N., Birosova, E., and Moran, C. S. (2022). The IFN- γ /miniTrpRS signaling axis: an insight into the pathophysiology of osteoporosis and therapeutic potential. *Cytokine Growth Factor Rev.* 64, 7–11. doi:10.1016/j.cytogfr.2022.01.005
- Bordbar, M., Haghpasand, S., Zekavat, O. R., Saki, F., Bazrafshan, A., and Bozorgi, H. (2019). Effect of different iron chelation regimens on bone mass in transfusion-dependent thalassemia patients. *Expert Rev. Hematol.* 12 (11), 997–1003. doi:10.1080/17474086.2019.1662721
- Cao, Z., Liu, G., Zhang, H., Wang, M., and Xu, Y. (2022). Nox4 promotes osteoblast differentiation through TGF- β signal pathway. *Free Radic. Biol. Med.* 193 (Pt 2), 595–609. doi:10.1016/j.freeradbiomed.2022.11.016
- Chai, H., Sang, S., Luo, Y., He, R., Yuan, X., and Zhang, X. (2022). Icariin-loaded sulfonated polyetheretherketone with osteogenesis promotion and osteoclastogenesis inhibition properties via immunomodulation for advanced osseointegration. *J. Mater. Chem. B* 10 (18), 3531–3540. doi:10.1039/d1tb02802b
- Chang, Y. W., Zhu, W. J., Gu, W., Sun, J., Li, Z. Q., and Wei, X. E. (2021). Neohesperidin promotes the osteogenic differentiation of bone mesenchymal stem cells by activating the Wnt/ β -catenin signaling pathway. *J. Orthop. Surg. Res.* 16 (1), 334. doi:10.1186/s13018-021-02468-5
- Chavali, M., Ulloa-Navas, M. J., Pérez-Borredá, P., García-Verdugo, J. M., McQuillen, P. S., Huang, E. J., et al. (2020). Wnt-dependent oligodendroglial-endothelial interactions regulate white matter vascularization and attenuate injury. *Neuron* 108 (6), 1130–1145.e5. doi:10.1016/j.neuron.2020.09.033
- Chen, M., Han, H., Zhou, S., Wen, Y., and Chen, L. (2021). Morusin induces osteogenic differentiation of bone marrow mesenchymal stem cells by canonical Wnt/ β -catenin pathway and prevents bone loss in an ovariectomized rat model. *Stem Cell Res. Ther.* 12 (1), 173. doi:10.1186/s13287-021-02239-3
- Chen, Y., Dai, F., He, Y., Chen, Q., Xia, Q., Cheng, G., et al. (2018). Beneficial effects of hyperoside on bone metabolism in ovariectomized mice. *Biomed. Pharmacother.* 107, 1175–1182. doi:10.1016/j.biopha.2018.08.069
- Cheng, C. H., Chen, L. R., and Chen, K. H. (2022a). Osteoporosis due to hormone imbalance: an overview of the effects of estrogen deficiency and glucocorticoid overuse on bone turnover. *Int. J. Mol. Sci.* 23 (3), 1376. doi:10.3390/ijms23031376
- Cheng, L., Jin, X., Shen, H., Chen, X., Chen, J., Xu, B., et al. (2022b). Icariin attenuates thioacetamide-induced bone loss via the RANKL-p38/ERK-NFAT signaling pathway. *Mol. Med. Rep.* 25 (4), 126. doi:10.3892/mmr.2022.12642
- Cushnie, T. P., and Lamb, A. J. (2005). Antimicrobial activity of flavonoids. *Int. J. Antimicrob. Agents* 26 (5), 343–356. doi:10.1016/j.ijantimicag.2005.09.002
- De Martinis, M., Ginaldi, L., Sirufo, M. M., Bassino, E. M., De Pietro, F., Pioggia, G., et al. (2020a). IL-33/Vitamin D crosstalk in psoriasis-associated osteoporosis. *Front. Immunol.* 11, 604055. doi:10.3389/fimmu.2020.604055
- De Martinis, M., Sirufo, M. M., Suppa, M., and Ginaldi, L. (2020b). IL-33/IL-31 Axis in osteoporosis. *Int. J. Mol. Sci.* 21 (4), 1239. doi:10.3390/ijms21041239
- Ding, G., Zhao, J., and Jiang, D. (2016). Allicin inhibits oxidative stress-induced mitochondrial dysfunction and apoptosis by promoting PI3K/AKT and CREB/ERK signaling in osteoblast cells. *Exp. Ther. Med.* 11 (6), 2553–2560. doi:10.3892/etm.2016.3179
- Frase, D., Lee, C., Nachiappan, C., Gupta, R., and Akkouch, A. (2023). The inflammatory contribution of B-lymphocytes and neutrophils in progression to osteoporosis. *Cells* 12 (13), 1744. doi:10.3390/cells12131744
- Gao, J., Xiang, S., Wei, X., Yadav, R. L., Han, M., Zheng, W., et al. (2021). Icariin promotes the osteogenesis of bone marrow mesenchymal stem cells through regulating sclerostin and activating the wnt/ β -catenin signaling pathway. *Biomed. Res. Int.* 2021, 6666836. doi:10.1155/2021/6666836
- Ge, J., Yu, Y. J., Li, J. Y., Li, M. Y., Xia, S. M., Xue, K., et al. (2023). Activating Wnt/ β -catenin signaling by autophagic degradation of APC contributes to the osteoblast differentiation effect of soy isoflavone on osteoporotic mesenchymal stem cells. *Acta Pharmacol. Sin.* 44 (9), 1841–1855. doi:10.1038/s41401-023-01066-x
- Gómez-Zorita, S., González-Arceo, M., Fernández-Quintela, A., Eseberri, I., Trepiana, J., Portillo, M. P., et al. (2020). Anti-obesity effects of macroalgae. *Nutrients* 12 (12), 2378. doi:10.3390/nu12082378
- Guan, L. P., and Liu, B. Y. (2016). Antidepressant-like effects and mechanisms of flavonoids and related analogues. *Eur. J. Med. Chem.* 121, 47–57. doi:10.1016/j.ejmech.2016.05.026
- He, H.-F., Wei, K., Yin, J., and Ye, Y. (2021). Insight into tea flavonoids: composition and Chemistry. *Food Rev. Int.* 37 (8), 812–823. doi:10.1080/87559129.2020.1721530
- Hu, Z., Tang, Y., Yue, Z., Zheng, W., and Xiong, Z. (2019). The facile synthesis of copper oxide quantum dots on chitosan with assistance of phyto-angelica for enhancing the human osteoblast activity to the application of osteoporosis. *J. Photochem Photobiol. B* 191, 6–12. doi:10.1016/j.jphotobiol.2018.11.009
- Ibrahim, S. O., Mada, S. B., Abarshi, M. M., Tanko, M. S., and Babangida, S. (2021). Chrysin alleviates alteration of bone-remodeling markers in ovariectomized rats and exhibits estrogen-like activity *in silico*. *Hum. Exp. Toxicol.* 40 (12_Suppl. 1), S125–s136. doi:10.1177/09603271211033777
- Inoue, K., Qin, Y., Xia, Y., Han, J., Yuan, R., Sun, J., et al. (2023). Bone marrow Adipoq-lineage progenitors are a major cellular source of M-CSF that dominates bone marrow macrophage development, osteoclastogenesis, and bone mass. *Elife* 12, e82118. doi:10.7554/eLife.82118
- Jiang, J., He, J., Xiao, S., Shenyan, J., Chen, T., and Pei, D. (2023a). Screening of superior anti-osteoporotic flavonoids from Epimedium Folium with dual effects of reversing iron overload and promoting osteogenesis. *Biomed. Chromatogr.* 37 (9), e5686. doi:10.1002/bmc.5686
- Jiang, J., Xiao, S., Xu, X., Ma, H., Feng, C., and Jia, X. (2018). Isomeric flavonoid aglycones derived from Epimedium Folium exerted different intensities in anti-osteoporosis through OPG/RANKL protein targets. *Int. Immunopharmacol.* 62, 277–286. doi:10.1016/j.intimp.2018.07.017
- Jiang, N., Jin, H., Yang, K., Zhang, Z., Xu, W., Chen, X., et al. (2023b). The mechanism of metformin combined with total flavonoids of Rhizoma Drynariae on ovariectomy-induced osteoporotic rats. *Biomed. Pharmacother.* 165, 115181. doi:10.1016/j.biopha.2023.115181
- Jing, X., Du, T., Chen, K., Guo, J., Xiang, W., Yao, X., et al. (2019). Icariin protects against iron overload-induced bone loss via suppressing oxidative stress. *J. Cell Physiol.* 234 (7), 10123–10137. doi:10.1002/jcp.27678
- Li, D. Y., Yu, J. C., Xiao, L., Miao, W., Ji, K., Wang, S. C., et al. (2017). Autophagy attenuates the oxidative stress-induced apoptosis of Mc3T3-E1 osteoblasts. *Eur. Rev. Med. Pharmacol. Sci.* 21 (24), 5548–5556. doi:10.26355/eurrev_201712_13991
- Li, M., Yu, Y., Xue, K., Li, J., Son, G., Wang, J., et al. (2023). Genistein mitigates senescence of bone marrow mesenchymal stem cells via ERRA-mediated mitochondrial biogenesis and mitophagy in ovariectomized rats. *Redox Biol.* 61, 102649. doi:10.1016/j.redox.2023.102649
- Li, Z., Chen, C., Zhu, X., Li, Y., Yu, R., and Xu, W. (2018). Glycyrrhizin suppresses RANKL-induced osteoclastogenesis and oxidative stress through inhibiting NF- κ B and MAPK and activating AMPK/Nrf2. *Calcif. Tissue Int.* 103 (3), 324–337. doi:10.1007/s00223-018-0425-1
- Liang, G., Zhao, J., Dou, Y., Yang, Y., Zhao, D., Zhou, Z., et al. (2022). Mechanism and experimental verification of luteolin for the treatment of osteoporosis based on network Pharmacology. *Front. Endocrinol. (Lausanne)* 13, 866641. doi:10.3389/fendo.2022.866641
- Liu, D., Hu, Z., Tang, Z., Li, P., Yuan, W., Li, F., et al. (2023). Identification of biomarkers associated with oxidative stress-related genes in postmenopausal osteoporosis. *Cell Mol. Biol. (Noisy-le-grand)* 69 (6), 186–192. doi:10.14715/cmb/2023.69.6.28

- Liu, H., Yue, X., and Zhang, G. (2021). Downregulation of miR-146a inhibits osteoporosis in the jaws of ovariectomized rats by regulating the Wnt/ β -catenin signaling pathway. *Int. J. Mol. Med.* 47 (3), 6. doi:10.3892/ijmm.2020.4839
- Liu, Y., Zhu, J., Xu, L., Wang, B., Lin, W., and Luo, Y. (2022). Copper regulation of immune response and potential implications for treating orthopedic disorders. *Front. Mol. Biosci.* 9, 1065265. doi:10.3389/fmolb.2022.1065265
- Liu, Y. Q., Han, X. F., Liu, T., Cheng, M. C., and Xiao, H. B. (2015). A cell-based model of bone remodeling for identifying activity of icarrin in the treatment of osteoporosis. *Biotechnol. Lett.* 37 (1), 219–226. doi:10.1007/s10529-014-1661-8
- Lorenzo, J., Horowitz, M., and Choi, Y. (2008). Osteoimmunology: interactions of the bone and immune system. *Endocr. Rev.* 29 (4), 403–440. doi:10.1210/er.2007-0038
- Loundagin, L. L., and Cooper, D. M. L. (2022). Towards novel measurements of remodeling activity in cortical bone: implications for osteoporosis and related pharmaceutical treatments. *Eur. Cell Mater* 43, 202–227. doi:10.22203/eCM.v043a15
- Lu, L., Lu, L., Zhang, J., and Li, J. (2020). Potential risks of rare serious adverse effects related to long-term use of bisphosphonates: an overview of systematic reviews. *J. Clin. Pharm. Ther.* 45 (1), 45–51. doi:10.1111/jcpt.13056
- Lu, M., Wang, L., Luo, Y., Ge, J., Gao, S., Chen, J., et al. (2013). Treatment of primary osteoporosis with epidural total flavone capsule: a multicenter clinical observation on 360 cases. *Chin. J. Osteoporos.* 19 (3), 279–282.
- Luo, C., Xu, W., Tang, X., Liu, X., Cheng, Y., Wu, Y., et al. (2022). Canonical Wnt signaling works downstream of iron overload to prevent ferroptosis from damaging osteoblast differentiation. *Free Radic. Biol. Med.* 188, 337–350. doi:10.1016/j.freeradbiomed.2022.06.236
- Mansoori, M. N., Shukla, P., Kakaji, M., Tyagi, A. M., Srivastava, K., Shukla, M., et al. (2016). IL-18BP is decreased in osteoporotic women: prevents Inflammasome mediated IL-18 activation and reduces Th17 differentiation. *Sci. Rep.* 6, 33680. doi:10.1038/srep33680
- Matsia, S., Tsave, O., Hatzidimitriou, A., and Salifoglou, A. (2022). Chromium flavonoid complexation in an antioxidant capacity role. *Int. J. Mol. Sci.* 23 (13), 7171. doi:10.3390/ijms23137171
- Mei, H., Li, X., Wu, Y., Feng, Q., Li, Z., Jiang, C., et al. (2022). Enhanced PDGFR/Wnt/ β -catenin activity of mesenchymal stem cells with high migration ability rescue bone loss of osteoporosis. *Cell Signal* 97, 110394. doi:10.1016/j.cellsig.2022.110394
- Miksicsek, R. J. (1993). Commonly occurring plant flavonoids have estrogenic activity. *Mol. Pharmacol.* 44 (1), 37–43. doi:10.3181/00379727-208-43830
- Ming, L. G., Chen, K. M., and Xian, C. J. (2013). Functions and action mechanisms of flavonoids genistein and icariin in regulating bone remodeling. *J. Cell Physiol.* 228 (3), 513–521. doi:10.1002/jcp.24158
- Morin, S. N., Feldman, S., Funnell, L., Giangregorio, L., Kim, S., McDonald-Blumer, H., et al. (2023). Clinical practice guideline for management of osteoporosis and fracture prevention in Canada: 2023 update. *Cmaj* 195 (39), E1333–e1348. doi:10.1503/cmaj.221647
- Mu, P., Hu, Y., Ma, X., Shi, J., Zhong, Z., and Huang, L. (2021). Total flavonoids of *Rhizoma Drynariae* combined with calcium attenuate osteoporosis by reducing reactive oxygen species generation. *Exp. Ther. Med.* 21 (6), 618. doi:10.3892/etm.2021.10050
- Niu, X., Chen, Y., Qi, L., Liang, G., Wang, Y., Zhang, L., et al. (2019). Hypoxia regulates angiogenic-osteogenic coupling process via up-regulating IL-6 and IL-8 in human osteoblastic cells through hypoxia-inducible factor-1 α pathway. *Cytokine* 113, 117–127. doi:10.1016/j.cyto.2018.06.022
- Noguchi, K., Imahori, D., Kido, Y., Nuntawong, P., Tanaka, H., Morimoto, S., et al. (2023). Quality assessment method for Chinpri, dried Citrus spp. peel and its derived Kampo medicines using specific monoclonal antibody against hesperidin. *Phytochem. Anal.* 34 (6), 652–660. doi:10.1002/pca.3255
- Omosule, C. L., Joseph, D., Weiler, B., Gremminger, V. L., Silvey, S., Lafaver, B. N., et al. (2023). Whole-body metabolism and the musculoskeletal impacts of targeting activin A and myostatin in severe osteogenesis imperfecta. *JBM R Plus* 7 (7), e10753. doi:10.1002/jbm4.10753
- Oršolić, N., Goluža, E., Dikić, D., Lisičić, D., Sašilo, K., Rodak, E., et al. (2014). Role of flavonoids on oxidative stress and mineral contents in the retinoic acid-induced bone loss model of rat. *Eur. J. Nutr.* 53 (5), 1217–1227. doi:10.1007/s00394-013-0622-7
- Oršolić, N., Nemrava, J., Jeleč, Ž., Kukolj, M., Odeh, D., Jakopović, B., et al. (2022). Antioxidative and anti-inflammatory activities of chrysin and naringenin in a drug-induced bone loss model in rats. *Int. J. Mol. Sci.* 23 (5), 2872. doi:10.3390/ijms23052872
- Otsuka, Y., Kondo, T., Aoki, H., Goto, Y., Kawaguchi, Y., Waguri-Nagaya, Y., et al. (2023). IL-1 β promotes osteoclastogenesis by increasing the expression of IGF2 and chemokines in non-osteoclastic cells. *J. Pharmacol. Sci.* 151 (1), 1–8. doi:10.1016/j.jpshs.2022.10.007
- Pan, Z., He, Q., Zeng, J., Li, S., Li, M., Chen, B., et al. (2022). Naringenin protects against iron overload-induced osteoarthritis by suppressing oxidative stress. *Phytomedicine* 105, 154330. doi:10.1016/j.phymed.2022.154330
- Roberts, J. L., Mella-Velazquez, G., Dar, H. Y., Liu, G., and Drissi, H. (2022). Deletion of IL-17ra in osteoclast precursors increases bone mass by decreasing osteoclast precursor abundance. *Bone* 157, 116310. doi:10.1016/j.bone.2021.116310
- Rozenberg, S., Al-Daghri, N., Aubertin-Leheudre, M., Brandi, M. L., Cano, A., Collins, P., et al. (2020). Is there a role for menopausal hormone therapy in the management of postmenopausal osteoporosis? *Osteoporos. Int.* 31 (12), 2271–2286. doi:10.1007/s00198-020-05497-8
- Shen, N., Wang, T., Gan, Q., Liu, S., Wang, L., and Jin, B. (2022a). Plant flavonoids: classification, distribution, biosynthesis, and antioxidant activity. *Food Chem.* 383, 132531. doi:10.1016/j.foodchem.2022.132531
- Shen, Z., Dong, W., Chen, Z., Chen, G., Zhang, Y., Li, Z., et al. (2022b). Total flavonoids of *Rhizoma Drynariae* enhances CD31(hi)Emcn(hi) vessel formation and subsequent bone regeneration in rat models of distraction osteogenesis by activating PDGF-BB/VEGF/RUNX2/OSX signaling axis. *Int. J. Mol. Med.* 50 (3), 112. doi:10.3892/ijmm.2022.5167
- Shimizu, T., Shibuya, N., Narukawa, Y., Oshima, N., Hada, N., and Kiuchi, F. (2018). Synergistic effect of baicalein, wogonin and oroxylin A mixture: multistep inhibition of the NF- κ B signalling pathway contributes to an anti-inflammatory effect of *Scutellaria root* flavonoids. *J. Nat. Med.* 72 (1), 181–191. doi:10.1007/s11418-017-1129-y
- Shukla, P., Mansoori, M. N., Kakaji, M., Shukla, M., Gupta, S. K., and Singh, D. (2017). Interleukin 27 (IL-27) alleviates bone loss in estrogen-deficient conditions by induction of early growth response-2 gene. *J. Biol. Chem.* 292 (11), 4686–4699. doi:10.1074/jbc.M116.764779
- Song, L., Guo, C., Liu, R., Ma, H., Li, Y., Shang, Q., et al. (2020). The critical role of T cells in glucocorticoid-induced osteoporosis. *Cell Death Dis.* 12 (1), 45. doi:10.1038/s41419-020-03249-4
- Stockwell, B. R., Friedmann Angeli, J. P., Bayir, H., Bush, A. I., Conrad, M., Dixon, S. J., et al. (2017). Ferroptosis: a regulated cell death nexus linking metabolism, redox biology, and disease. *Cell* 171 (2), 273–285. doi:10.1016/j.cell.2017.09.021
- Sysak, S., Czarzynska-Goslinska, B., Szyk, P., Koczorowski, T., Młynarczyk, D. T., Szczolko, W., et al. (2023). Metal nanoparticle-flavonoid connections: synthesis, physicochemical and biological properties, as well as potential applications in medicine. *Nanomater. (Basel)* 13 (9), 1531. doi:10.3390/nano13091531
- Tao, Z. S., Wang, H. S., Li, T. L., and Wei, S. (2022). Silibinin-modified Hydroxyapatite coating promotes the osseointegration of titanium rods by activation SIRT1/SOD2 signaling pathway in diabetic rats. *J. Mater. Sci. Mater. Med.* 33 (9), 62. doi:10.1007/s10856-022-06684-1
- Teng, J. W., Bian, S. S., Kong, P., and Chen, Y. G. (2022). Icariin triggers osteogenic differentiation of bone marrow stem cells by up-regulating miR-335-5p. *Exp. Cell Res.* 414 (2), 113085. doi:10.1016/j.yexcr.2022.113085
- Terashima, A., and Takayanagi, H. (2018). Overview of osteoimmunology. *Calcif. Tissue Int.* 102 (5), 503–511. doi:10.1007/s00223-018-0417-1
- Toronto-Urquiza, L., Acosta-Martin, A. E., James, D. C., Nagy, T., and Falconer, R. J. (2020). The use of catechins in Chinese hamster ovary cell media for the improvement of monoclonal antibody yields and a reduction of acidic species. *Biotechnol. Prog.* 36 (4), e2980. doi:10.1002/btpr.2980
- Wang, J., Chen, J., Zhang, B., and Jia, X. (2021). IL-6 regulates the bone metabolism and inflammatory microenvironment in aging mice by inhibiting Setd7. *Acta histochem.* 123 (5), 151718. doi:10.1016/j.acthis.2021.151718
- Wang, P., Zhang, F., He, Q., Wang, J., Shiu, H. T., Shu, Y., et al. (2016). Flavonoid compound icariin activates hypoxia inducible factor-1 α in chondrocytes and promotes articular cartilage repair. *PLoS One* 11 (2), e0148372. doi:10.1371/journal.pone.0148372
- Wang, W., Mao, J., Chen, Y., Zuo, J., Chen, L., Li, Y., et al. (2022a). Naringin promotes osteogenesis and ameliorates osteoporosis development by targeting JAK2/STAT3 signalling. *Clin. Exp. Pharmacol. Physiol.* 49 (1), 113–121. doi:10.1111/1440-1681.13591
- Wang, X., Chen, B., Sun, J., Jiang, Y., Zhang, H., Zhang, P., et al. (2018a). Iron-induced oxidative stress stimulates osteoclast differentiation via NF- κ B signaling pathway in mouse model. *Metabolism* 83, 167–176. doi:10.1016/j.metabol.2018.01.005
- Wang, Y., Zhou, X., and Wang, D. (2022b). Mesenchymal stem cell-derived extracellular vesicles inhibit osteoporosis via MicroRNA-27a-induced inhibition of DKK2-mediated wnt/ β -catenin pathway. *Inflammation* 45 (2), 780–799. doi:10.1007/s10753-021-01583-z
- Wang, Z., Wang, D., Yang, D., Zhen, W., Zhang, J., and Peng, S. (2018b). The effect of icariin on bone metabolism and its potential clinical application. *Osteoporos. Int.* 29 (3), 535–544. doi:10.1007/s00198-017-4255-1
- Xi, Y., Jiang, T., Yu, J., Xue, M., Xu, N., Wen, J., et al. (2019). Preliminary studies on the anti-osteoporosis activity of Baohuoside I. *Biomed. Pharmacother.* 115, 108850. doi:10.1016/j.biopha.2019.108850
- Xia, G., Li, X., Zhu, X., Yin, X., Ding, H., and Qiao, Y. (2017). Mangiferin protects osteoblast against oxidative damage by modulation of ERK5/Nrf2 signaling. *Biochem. Biophys. Res. Commun.* 491 (3), 807–813. doi:10.1016/j.bbrc.2017.06.184
- Xia, S. L., Ma, Z. Y., Wang, B., Gao, F., Guo, S. Y., and Chen, X. H. (2023). Icariin promotes the proliferation and osteogenic differentiation of bone-derived mesenchymal stem cells in patients with osteoporosis and T2DM by upregulating GLI-1. *J. Orthop. Surg. Res.* 18 (1), 500. doi:10.1186/s13018-023-03998-w
- Xian, Y., Su, Y., Liang, J., Long, F., Feng, X., Xiao, Y., et al. (2021). Oroxylin A reduces osteoclast formation and bone resorption via suppressing RANKL-induced ROS and NFATc1 activation. *Biochem. Pharmacol.* 193, 114761. doi:10.1016/j.bcp.2021.114761

- Xiao, J., Zhang, G., Chen, B., He, Q., Mai, J., Chen, W., et al. (2023). Quercetin protects against iron overload-induced osteoporosis through activating the Nrf2/HO-1 pathway. *Life Sci.* 322, 121326. doi:10.1016/j.lfs.2022.121326
- Xu, J., Fu, L., Bai, J., Zhong, H., Kuang, Z., Zhou, C., et al. (2021). Low-dose IL-34 has no effect on osteoclastogenesis but promotes osteogenesis of hBMSCs partly via activation of the PI3K/AKT and ERK signaling pathways. *Stem Cell Res. Ther.* 12 (1), 268. doi:10.1186/s13287-021-02263-3
- Xu, X., Lu, Y., Yang, X., Du, Z., Zhou, L., Li, S., et al. (2018). Copper-modified Ti6Al4 V suppresses inflammatory response and osteoclastogenesis while enhancing extracellular matrix formation for osteoporotic bone regeneration. *ACS Biomater. Sci. Eng.* 4 (9), 3364–3373. doi:10.1021/acsbomaterials.8b00736
- Xu, Y., Song, D., Lin, X., Peng, H., Su, Y., Liang, J., et al. (2023). Corylifol A protects against ovariectomized-induced bone loss and attenuates RANKL-induced osteoclastogenesis via ROS reduction, ERK inhibition, and NFATc1 activation. *Free Radic. Biol. Med.* 196, 121–132. doi:10.1016/j.freeradbiomed.2023.01.017
- Yang, S., Ni, G., Xia, M., Li, H., and Gao, Z. (2023). Mussel inspired multifunctional bovine serum albumin (BSA) coatings loaded with Baicalein (Bai) to enhance osteogenesis and resist oxidative stress for potential application on implant. *Int. J. Biol. Macromol.* 229, 752–765. doi:10.1016/j.ijbiomac.2022.12.285
- Yang, Y., Cheng, R., Liu, J., Fang, J., Wang, X., Cui, Y., et al. (2022). Linarin protects against cadmium-induced osteoporosis via reducing oxidative stress and inflammation and altering RANK/RANKL/OPG pathway. *Biol. Trace Elem. Res.* 200 (8), 3688–3700. doi:10.1007/s12011-021-02967-w
- Yao, X., Jing, X., Guo, J., Sun, K., Deng, Y., Zhang, Y., et al. (2019). Icarin protects bone marrow mesenchymal stem cells against iron overload induced dysfunction through mitochondrial fusion and fission, PI3K/AKT/mTOR and MAPK pathways. *Front. Pharmacol.* 10, 163. doi:10.3389/fphar.2019.00163
- Yao, Z., Getting, S. J., and Locke, I. C. (2021). Regulation of TNF-induced osteoclast differentiation. *Cells* 11 (1), 132. doi:10.3390/cells11010132
- Ye, C., Zhang, W., Hang, K., Chen, M., Hou, W., Chen, J., et al. (2019). Extracellular IL-37 promotes osteogenic differentiation of human bone marrow mesenchymal stem cells via activation of the PI3K/AKT signaling pathway. *Cell Death Dis.* 10 (10), 753. doi:10.1038/s41419-019-1904-7
- Yonekura-Sakakibara, K., Higashi, Y., and Nakabayashi, R. (2019). The origin and evolution of plant flavonoid metabolism. *Front. Plant Sci.* 10, 943. doi:10.3389/fpls.2019.00943
- Yong, E. L., Cheong, W. F., Huang, Z., Thu, W. P. P., Cazenave-Gassiot, A., Seng, K. Y., et al. (2021). Randomized, double-blind, placebo-controlled trial to examine the safety, pharmacokinetics and effects of Epimedium prenylflavonoids, on bone specific alkaline phosphatase and the osteoclast adaptor protein TRAF6 in post-menopausal women. *Phytomedicine* 91, 153680. doi:10.1016/j.phymed.2021.153680
- Yu, A. X., Xiao, J., Zhao, S. Z., Kong, X. P., Kwan, K. K., Zheng, B. Z., et al. (2021). Biological evaluation and transcriptomic analysis of corylin as an inhibitor of osteoclast differentiation. *Int. J. Mol. Sci.* 22 (7), 3540. doi:10.3390/ijms22073540
- Yuan, Z., Min, J., Zhao, Y., Cheng, Q., Wang, K., Lin, S., et al. (2018). Quercetin rescued TNF-alpha-induced impairments in bone marrow-derived mesenchymal stem cell osteogenesis and improved osteoporosis in rats. *Am. J. Transl. Res.* 10 (12), 4313–4321.
- Zangade, S. B., Dhulshette, B. S., and Patil, P. B. (2023). Flavonoid-metal ion complexes as potent anticancer metallodrugs: a comprehensive review. *Mini Rev. Med. Chem.* 24. doi:10.2174/0113895575273658231012040250
- Zeng, C., Wang, S., Chen, F., Wang, Z., Li, J., Xie, Z., et al. (2023a). Alpinetin alleviates osteoporosis by promoting osteogenic differentiation in BMSCs by triggering autophagy via PKA/mTOR/ULK1 signaling. *Phytother. Res.* 37 (1), 252–270. doi:10.1002/ptr.7610
- Zeng, C., Wang, S., Gu, H., Chen, F., Wang, Z., Li, J., et al. (2023b). Galangin mitigates glucocorticoid-induced osteoporosis by activating autophagy of BMSCs via triggering the PKA/CREB signaling pathway. *Acta Biochim. Biophys. Sin. (Shanghai)* 55 (8), 1275–1287. doi:10.3724/abbs.2023063
- Zhang, D., Qiu, J., Niu, Q. T., Liu, T., Gu, R., Zhang, X., et al. (2023). Effects of various pine needle extracts on Chinese hamster ovary cell growth and monoclonal antibody quality. *Prep. Biochem. Biotechnol.* 53 (9), 1081–1091. doi:10.1080/10826068.2023.2166959
- Zhang, G., Qin, L., and Shi, Y. (2007). Epimedium-derived phytoestrogen flavonoids exert beneficial effect on preventing bone loss in late postmenopausal women: a 24-month randomized, double-blind and placebo-controlled trial. *J. Bone Min. Res.* 22 (7), 1072–1079. doi:10.1359/jbmr.070405
- Zhang, N. D., Han, T., Huang, B. K., Rahman, K., Jiang, Y. P., Xu, H. T., et al. (2016). Traditional Chinese medicine formulas for the treatment of osteoporosis: implication for antiosteoporotic drug discovery. *J. Ethnopharmacol.* 189, 61–80. doi:10.1016/j.jep.2016.05.025
- Zhang, Q., Li, T., Li, Z., Lu, J., Wu, X., Gao, F., et al. (2022). Autocrine activity of extracellular vesicles induced by icariin and its effectiveness in glucocorticoid-induced injury of bone microvascular endothelial cells. *Cells* 11 (12), 1921. doi:10.3390/cells11121921
- Zhang, S., Feng, P., Mo, G., Li, D., Li, Y., Mo, L., et al. (2017). Icarin influences adipogenic differentiation of stem cells affected by osteoblast-osteoclast co-culture and clinical research adipogenic. *Biomed. Pharmacother.* 88, 436–442. doi:10.1016/j.biopha.2017.01.050
- Zhao, G. Y., Zhao, L. P., He, Y. F., Li, G. F., Gao, C., Li, K., et al. (2012). A comparison of the biological activities of human osteoblast hFOB1.19 between iron excess and iron deficiency. *Biol. Trace Elem. Res.* 150 (1–3), 487–495. doi:10.1007/s12011-012-9511-9
- Zheng, X., Wang, Q., Xie, Z., and Li, J. (2021). The elevated level of IL-1α in the bone marrow of aged mice leads to MSC senescence partly by down-regulating Bmi-1. *Exp. Gerontol.* 148, 111313. doi:10.1016/j.exger.2021.111313
- Zhou, L., Poon, C. C., Wong, K. Y., Cao, S., Dong, X., Zhang, Y., et al. (2021). Icarin ameliorates estrogen-deficiency induced bone loss by enhancing IGF-I signaling via its crosstalk with non-genomic ERα signaling. *Phytomedicine* 82, 153413. doi:10.1016/j.phymed.2020.153413
- Zhu, Z., Wang, X., Wang, Z., Zhao, Z., Zhou, P., and Gao, X. (2021). Neobavaisoflavone protects osteoblasts from dexamethasone-induced oxidative stress by upregulating the CRNDE-mediated Nrf2/HO-1 signaling pathway. *Drug Dev. Res.* 82 (7), 1044–1054. doi:10.1002/ddr.21811
- Zhu, Z., Yu, P., Wu, Y., Wu, Y., Tan, Z., Ling, J., et al. (2023). Sex specific global burden of osteoporosis in 204 countries and territories, from 1990 to 2030: an age-period-cohort modeling study. *J. Nutr. Health Aging* 27 (9), 767–774. doi:10.1007/s12603-023-1971-4

Glossary

AIP	artificial iron pools
ALP	alkaline phosphatase
BAI	baicalein
BHSI	baohuoside I
BMECs	Bone microvascular endothelial cells
BMSCs	Bone marrow mesenchymal stem cells
BSA	bovine serum albumin
ER	estrogen receptor
EVs	extracellular vesicles
FAC	ferric ammonium citrate
IFN-γ	interferon- γ
IL	interleukin
LDH	lactate dehydrogenase
LPS	lipopolysaccharide
M-CSF	macrophage-stimulating factor
MDA	malondialdehyde
OB	osteoblast
OC	osteoclast
OCN	osteocalcin
OP	osteoporosis
OPG	osteoclastogenesis inhibitory factor
OVX	ovariectomy
PKA	protein kinase A
ROS	reactive oxygen species
SOD	superoxide dismutase
TA	tannic acid
TAC	total antioxidant capacity
TCM	traditional Chinese medicine
TGF-β	transforming growth factor- β
TNF-α	tumour necrosis factor- α
TRAP	tartrate resistant acid phosphatase
VEGF	vascular endothelial growth factor

Frontiers in Nutrition

Explores what and how we eat in the context of health, sustainability and 21st century food science

A multidisciplinary journal that integrates research on dietary behavior, agronomy and 21st century food science with a focus on human health.

Discover the latest Research Topics

[See more →](#)

Frontiers

Avenue du Tribunal-Fédéral 34
1005 Lausanne, Switzerland
frontiersin.org

Contact us

+41 (0)21 510 17 00
frontiersin.org/about/contact

